2018 Tran-SET Conference

Welcome

Welcome to the 2018 Tran-SET Conference!

On behalf of the organizing committee, I am honored to welcome you to the inaugural Transportation Consortium of South Central States (Tran-SET) Conference held in the lively city of New Orleans, Louisiana.

Tran-SET is a University Transportation Center (UTC) comprising of 11 partnering institutions across Region 6 (AR, LA, NM, OK, and TX), with an aim to address the accelerated deterioration of our transportation infrastructure through the development, evaluation, and implementation of cutting-edge technologies, novel materials, and innovation construction management processes: from research to implementation. We believe that our focus on implementation makes us unique and our strong alliances with industry, academic, and government agencies will help us succeed and reach our goals.

The Tran-SET Conference will bring together academics, industry professionals, state DOTs, and other government agencies interested in solving transportation challenges facing Region 6. Participants will be introduced to Tran-SET's research, education, workforce development, and technology transfer activities. Attendees will see a variety of technical contributions covering multiple transportation fields, including pavements, asphalt and concrete materials, structures, geotechnical, safety, intelligent transportation systems, and policy and planning. The Tran-SET Conference will host an exhibition showing some of the technologies that have been developed/utilized in our research projects.

Please enjoy the exhibition and the conference! Your presence is an indication that you are committed to making a positive difference, not only to our transportation industry, but also throughout your state and the country. We hope you have a productive meeting and enjoy all that New Orleans has to offer!

Marwa Hassan, Ph.D., PE Civil (VA)
Director of Tran-SET

Table of Contents

Improving the Transportation System Performance in the Baton Rouge Area, LA, through Supply- and Demand-Oriented Measures for Mitigating Traffic Congestion

Samir Ahmed[1] and Osama Osman[2]

[1]Professor, School of Civil and Environmental Engineering, Oklahoma State University
[2]Postdoc, Department of Civil and Environmental Engineering, Louisiana State University

INTRODUCTION

Traffic congestion and the resulting unreliable transportation system performance are major impediment to sustainable economic growth, productivity and urban area vitality. Traffic congestion is caused by several factors including inadequate base capacity, increased demands, traffic control devices, traffic incidents, work zones, special events and weather. Unreliable travel times and delays to region-wide commuters, late deliveries, limited skilled labor markets, increased stress levels, and air pollution are examples of the impacts of congestion on commuters, shippers, just-in-time manufacturing processes and complex supply-chain networks. A 2009 study entitled “Gridlock and Growth” [1] found that a 10% reduction in travel times could boost production of goods and services by 1%, leading to tens of billions of dollars in higher income and output in urban areas.

According to the Texas A&M Transportation Institute’s (TTI) “2015 Annual Mobility Scoreboard” [2] and the Baton Rouge Area Capital Region Industry for Sustainable Infrastructure Solutions (CRISIS), the Baton Rouge area has been suffering from severe traffic congestion that threatens the economic development in the area. Baton Rouge is listed as the third worst midsized urban area in the category of average annual commuter traffic delay; second worst among midsized cities for the amount of annual excess fuel consumed per commuter, and near the top of the list for the amount of money congestion is costing the average commuter per year, at $1,262. Baton Rouge also ranks third worst for cities its size both for freeway travel unreliability, and total truck congestion costs per year, at $189 million. Reasons for this traffic congestion in Baton Rouge include the high freight demand associated with the oil and gas industry in the area [3], and the rapid growth in population density, currently about 700,000 residents, which generates around 3.2 million vehicle trips every day [4]. These high traffic demands cause severe delays and fast spreading breakdowns on the transportation infrastructures in Baton Rouge. One of the main facilities suffering from severe traffic congestion in Baton Rouge is the I-10 Mississippi River Bridge, possibly because of the chemical plants located on the west bank of the river.

The I-10 Mississippi River Bridge is a 6-lane facility that represents the main link between East and West Baton Rouge areas [5]. The only other link is an older bridge located 8-miles to the north of the Mississippi Bridge. Travelers choose to use the I-10 Mississippi Bridge because of the ease of access to several significant locations in Baton Rouge, in addition to the extra travel time and discomfort travelers may experience when rerouting through the city network to use the older bridge. According to Louisiana Department of Transportation and Development (LADOTD), the average annual daily traffic (AADT) on and around the I-10 Mississippi River Bridge exceeds 108,000 vehicle/day based on 2014 estimates. This figure represents 13% increase in AADT compared to the 2011 estimates [6]. The bridge is causing severe traffic congestion that affects the surrounding streets and intersections and extends over prolonged periods. Solving such an acute congestion problem is challenging especially that capacity expansion is an expensive solution. For instance, a recent study showed that a new Mississippi River bridge could significantly solve the current bridge's congestion problem; however, such bridge will cost around $1 billion [7]. Therefore, other congestion mitigation solutions such as Active Traffic Management (ATM) and the application of Intelligent Transportation Systems (ITS) must be investigated. As such, this study aims to perform network analysis to identify the extent of and find solution to the congestion problem at the I-10 Mississippi River Bridge.

METHODOLOGY

The research team performed a comprehensive review of the recently completed research projects and studies related to the congestion problem in Baton Rouge. Highlights and results of those projects were compiled to understand the extent of the congestion problem and identify the previously proposed solutions. Available roadway, traffic and control data for the I-10 Mississippi River bridge study area were collected from several sources including the Louisiana Department of Transportation and Development, the Baton Rouge Area Chamber, the Capital Region Planning Commission, and the Capital Regions Industry for Sustainable Infrastructure Solutions. The data included traffic volumes, travel times and speeds; albeit with low-resolution. High-resolution data were not readily available. Data related to existing traffic control systems, e.g., signal timing plans, were collected by the research team.

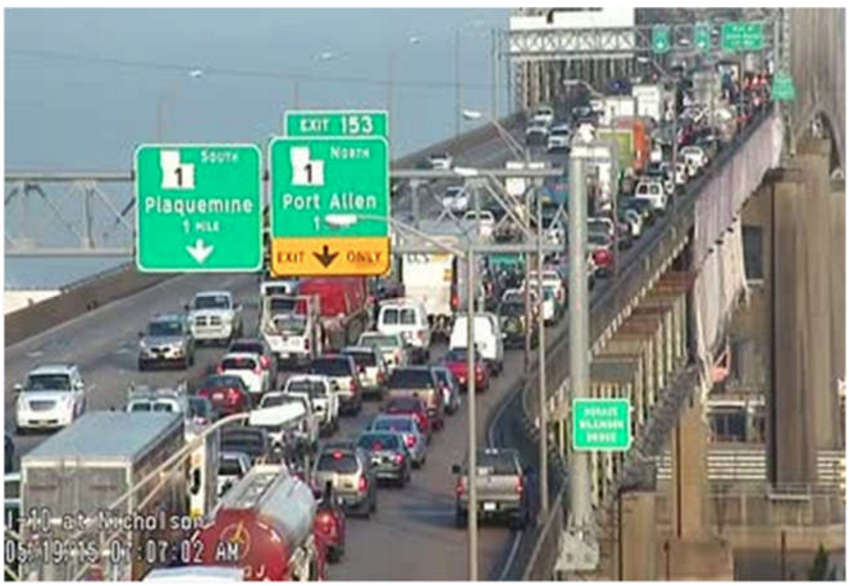

Figure 1. Crawling across the I-10 Mississippi River Bridge in Baton Rouge, LA

A computer simulation model of the roadway network around the I-10 Mississippi River Bridge has been developed and is being validated using available data. The model will be used to test alternative improvements and countermeasures to solve the congestion problem. Measures for mitigating congestion can be classified into two basic groups: supply-oriented measures and demand-oriented measures. Supply measures add capacity to the system or make the system operate more efficiently. Their focus is on the transportation system. Demand measures, on the other hand, focus on drivers and travelers and attempt to modify their trip-making behavior. Because of the interaction of supply and demand and the resulting equilibrium flows, actions that affect either supply or demand tend to influence both. A combination of measures is typically required to combat traffic congestion.

FINDINGS

Our review of past studies related to Baton Rouge traffic problems, specifically congestion at the I-10 Mississippi River bridge, concluded that the construction of a new bridge is the only solution that has been considered to address traffic congestion at the existing bridge site. However, given the limited revenue sources in the region, the $1 billion cost of a new bridge renders this alternative infeasible in the immediate future. Other solutions based on active traffic management (ATM) and the application of Intelligent Transportation Systems (ITS) must be considered.

The research team is currently finalizing the simulation model to test potential improvements at critical locations near the i-10 Mississippi river bridge. Additional high-resolution data may be required upon initial validation of the simulation results; however, the research team believes that the available data can help perform the required analysis to an acceptable accuracy.

REFERENCES

1. Hartgen, D.T., M.G. Fields, and A.T. Moore, Gridlock and growth: the effect of traffic congestion on regional economic performance. 2009, Reason Foundation Los Angeles, CA.
2. Schrank, D., et al., 2015 urban mobility scorecard. 2015.
3. Council, W.B.R.P. LA 1/ LA 415 CONNECTOR. 2017 [cited 2017; Available from: http://wbrcouncil.org/ProjectProposal.
4. Commission, C.R.P., Congestion Management Process. 2013, CRPC: Baton Rouge, Louisiana.
5. DOTD. Frequently Asked Questions. 2007 [cited 2017; Available from: http://wayback.archive.org/web/20070808151948/http://www.dotd.state.la.us/press/faq.asp#bridges.
6. DOTD. [cited 2017; Available from: http://wwwapps.dotd.la.gov/engineering/tatv/.
7. I-10 Corridor Study. 2016 [cited 2017; Available from: http://i10br.com/.

Relationship Between Road Network Characteristics and Traffic Safety

Hatim Sharif and Samer Dessouky
University of Texas at San Antonio

INTRODUCTION

Roadway and human factors, as well as other factors, affect the level of safety at intersections. Some of these factors have been identified while others still await identification. For instance, past research in Indiana (Savolainen and Tarko 2005), Iowa (Burchett and Maze 2005), and Nebraska (Khattak et al. 2006) has determined that intersections near horizontal or vertical curves tend to have a higher crash rate than those intersections located on tangent sections of highways. Some studies postulate that drivers may find it difficult to estimate the inter-vehicle gaps in high speed traffic flows coming from opposite directions. Burchett and Maze (2005) indicates that many drivers turning left onto the major road have more difficulty judging gaps in the far side of traffic coming from the right, compared to the near side of traffic coming from the left. This difficulty increases at intersections located on horizontal curves where drivers find it equally difficult to find a safe gap in either direction Road safety is typically defined in terms of the injuries and fatalities that occur on the roadway system. Therefore, definitions of road safety are often based on crash outcomes such as "…the number of accidents (crashes) (Many safety professionals and some in the media believe one should consistently use the term "crash" which implies these events are preventable as opposed to "accident" which implies the incidents are unintentional.), or accident consequences, by kind and severity, expected to occur on the entity during a specific period" (Hauer, 1997). The science of safety has evolved over the past several years and is focusing more on data and analysis, rather than solely adhering to standards. For example, it was commonly assumed when road safety improvements met the standards contained in the Manual of Uniform Traffic Control Devices (MUTCD) and the American Association of State Highway Transportation Officials (AASHTO) – A Policy on Geometric Design of Highway and Streets (also known as the "Green Book") they were considered safe. However, most of those standards have not been evaluated specifically for their impact on safety. Crashes may occur on a roadway designed to meet standards, and this does not necessarily mean the roadway is unsafe. Science-based road safety management is referred to as data-driven or evidence-based. This approach to road safety emphasizes estimates of the effect on safety (data and analysis), rather than adherence to standards based on personal experience, beliefs, and intuition. The safety metrics (e.g., fatalities and serious injuries) of a roadway are compared to roadways with similar characteristics to evaluate its safety performance. The goal of the evidence-based approach is to understand and quantify the expected consequences and outcomes of our actions (e.g., changes in the expected number of crashes/injuries/fatalities); the resulting calculations become the experience or evidence on which future decisions are made.

It has long been recognized that intersections are the element of the roadway system that experiences the greatest number and severity of crashes; at least one-third (Alexander et al. 2007) and as much as one-half (Kuciemba and Cirillo 1992) of all crashes occur at intersections. This is expected because different traffic streams meet and conflict with each other at intersections. Intersections involving high-speed multilane divided highways (also known as ''expressways'') and minor streets with two-way stop control (Burchett and maze 2005, Maze et al. 2016) are no exception. Although expressways are considered to be safer than two-lane roadways (Maze et al. 2016) any collision that occurs at an intersection on these types of roadways could potentially be very severe due to the high speeds. Intersection characteristics on these divided highways that contribute to more crashes need more detailed study in order to identify safety countermeasures.

Enforcement and Education

Nearly every city, region and country in the world enforces accurate use of traffic control measures designed to prevent collisions: stop signs, traffic lights, turning lanes, pedestrian crossings, etc. Differences in practices are much more noticeable when it comes to impaired and distracted driving, use of safety equipment, and driver education initiatives.

The best source of information on traffic law enforcement and education is the Governors Highway Safety Association (GHSA) website (http://www.ghsa.org/index.html), which documents laws and safety initiatives in the entire country. This site provides information by state and by specific issue. The three definitions underlined below describe some of the efforts recommended by GHSA.

Impaired driving can refer to operating a motor vehicle while under the influence of alcohol, drugs, or both. All states have laws to address impaired driving. The alcohol-impaired driving laws are better understood and easier to enforce than those for drug-impaired driving.

Zero tolerance laws make it illegal to drive with any measurable amount of specified substances in the body. These laws are best suited for illegal drugs: if it is illegal to possess or use a drug, then it is reasonable to prohibit driving after the drug has been used; 16 states have zero tolerance laws for one or more drugs.

Per se laws make it illegal to drive with amounts of specified drugs in the body that exceed set limits. Six states have per se laws in effect for one or more drugs. All states define driving with a blood alcohol concentration $\geq 0.08\%$ as a crime.

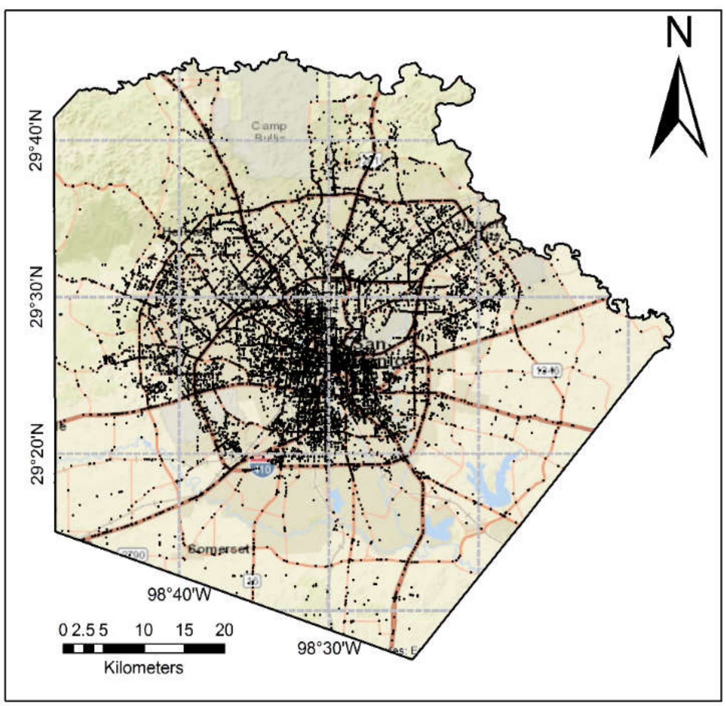

Figure 1. Spatial distribution of crashes in San Antonio for 2013.

METHODOLOGY

FHWA-SA-10-005 brief summarizes different estimates of the crash reduction that might be expected if a specific countermeasure or group of countermeasures is implemented with respect to intersection crashes. The crash reduction estimates are presented as crash reduction factors (CRFs), which are the percentage crash reduction that might be expected after implementing a given countermeasure. FHWA warns that a CRF should be regarded as a generic estimate of the effectiveness of a countermeasure. It says that a CRF estimate is a useful guide, but it remains necessary to apply engineering judgment and to consider site-specific environmental, traffic volume, traffic mix, geometric, and operational conditions that will affect the safety impact of a countermeasure. This publication has 11 pages with tables of CRFs for each countermeasure by type of crash (all or fatal/injury). Some but not all CRFs in these tables have standard errors, which helps evaluate their accuracy.

Several examples of CRFs are listed below. When available, the CRF standard error in the number in parenthesis. Some simple, low-cost solutions appear very effective in reducing crashes (see for example the first countermeasure listed below), while others have a negative impact. Increasing median width in intersections is an example of countermeasure with a negative impact (CRF<0, therefore crashes tend to increase).

- Convert two-way stop control to all-way stop control.
  CRF=48% (4%) for all crashes.
- Provide advanced dilemma zone detection for high speed approaches to four-leg signalized intersections.
  CFR=39% for fatal/injury crashes.
- Install signals.
  CFR=15% for all crashes.
- Install left turn lane at signalized intersections.
  CRF=15% for all crashes at three-leg intersections.
  CFR=18% for all crashes at four-leg intersections, one approach.
  CRF=33% for all crashes at four-leg intersections, 2 approaches.
- Install left turn lane at stop-controlled three-leg intersections.
  CRF=44% (6%) for all crashes
  CRF=62% for left turn crashes
  CRF=55% (10%) for all fatal/injury crashes
- Install left turn lane at stop-controlled four-leg intersections, one approach
  CFR=28% (3%) for all crashes
  CFR=37% all for left-turn crashes
  CFR=35% (3%) for all fatal/injury crashes.
- Install left turn lane at stop-controlled four-leg intersections, 2 approaches
  CFR=48% (3%) for all crashes
  CFR=60% for all left-turn crashes
  CFR=58% (4%) for all fatal/injury crashes.
- Convert two-way stop-controlled intersection to roundabout (1 lane road)
  CRF=71% (4%) for all crashes
  CRF= 87% (3%) for fatal/injury crashes.
- Install splitter islands on minor road approaches
  CRF=35% for all crashes.

What is an intersection crash?

The Texas Crash Records Information System (CRIS), the Police reports and most of the technical literature acknowledge that not all crashes related to an intersection occur at the intersection. Stephens (2004) defines an intersection-related crash as "a traffic crash in which (1) the first harmful event occurs on an approach to or exit from an intersection and (2) results from an activity, behavior or control related to the movement of traffic units through the intersection." It is generally accepted that an intersection area of influence in terms of traffic safety extends about 250ft away from the centerline in all directions. It is likely that many of the inconsistencies found are due to different interpretations of the variable value. Verifying such details would require manually checking variable values against crash narratives. Clearly, this is infeasible within this project schedule and manpower. On the other hand, the number of verified intersection crashes ensures sufficient data to obtain statistically valid conclusions.

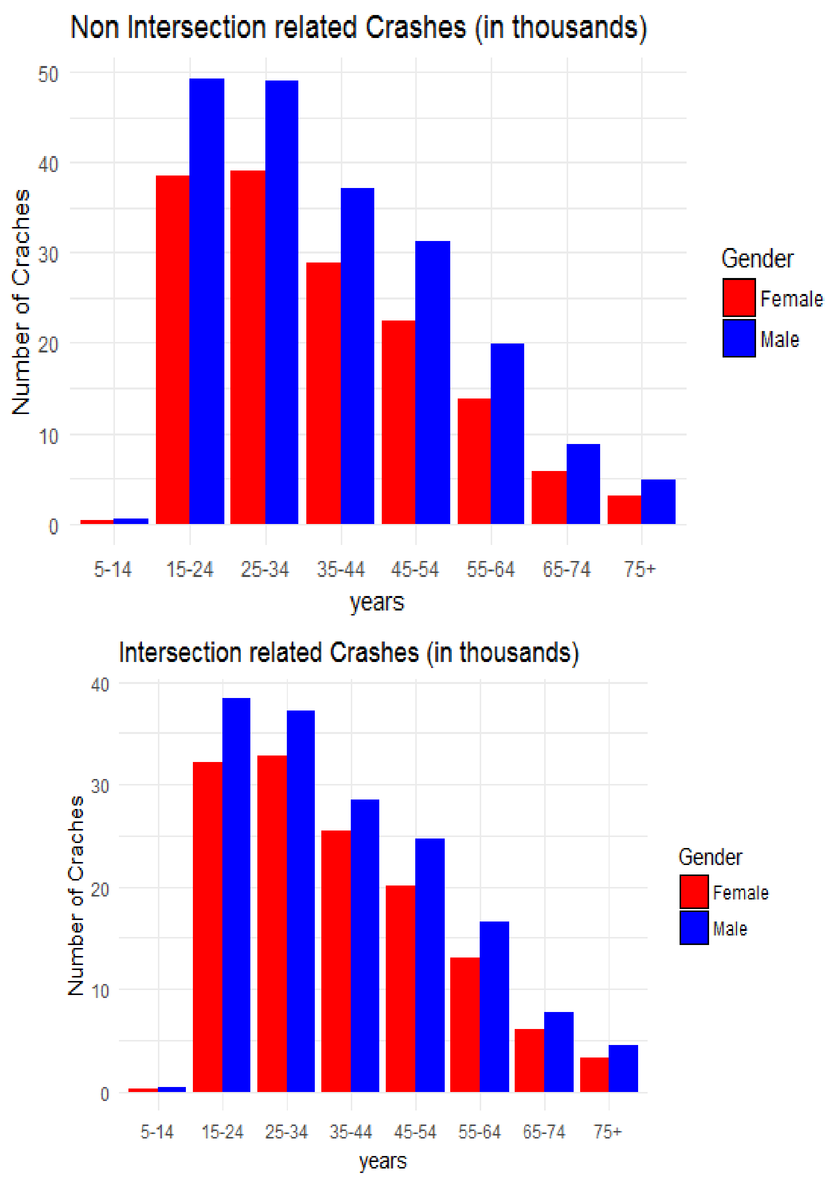

Figure 2. Difference between intersection and non-intersection crashes.

Figure 3. Images of the FM 78 and Walzem Rd. intersection

Intersection Characteristics

	FM 78	**Walzem Rd.**
Signs	10, 11 and 16	10, 11 and 16
Speed (mph)	45	45
Marking	Clear/visible	Clear/visible
Lighting	Yes	Yes
Traffic	Following signal lights	Following signal lights
Obstruction	90-degree angle intersection with no obstructions	

FINDINGS

The research team has been analyzing intersection crash data in San Antonio for the 2012-2016 period. Figure 2 shows the spatial distribution of crashes in San Antonio for 2013 while Figure 3 shows the difference between intersection and non-intersection crashes. Figure 4 shows an example of one of the problematic intersections in San Antonio. The FM 78 with Walzem rd. is a fully signalized urban intersection. FM 78 has two-lane in each direction in addition to a bike lane. The intersection seems to be in low elevation of a sag curve making it very visible from the approaches. All directions has a separate left turn lanes while only FM 78 has separate right turn lanes. The intersection history of crashes is shown in Figure 5.

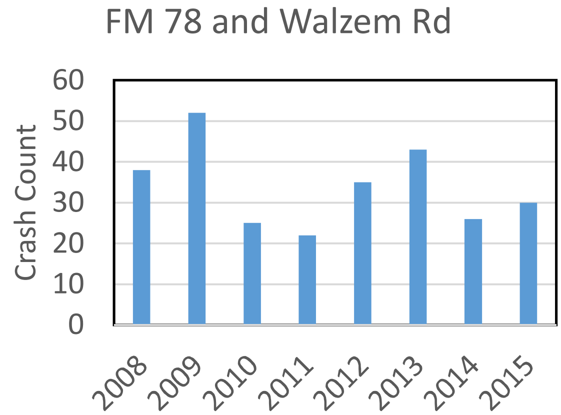

Figure 4. History of crashes at FM 78 and Walzem Rd., San Antonio.

CONCLUSION

Most of intersection-related crashes in San Antonio occurred in the downtown area. The number of intersection-related crashes increase in 2016. More male drivers are involved in such crashes in such crashes than females (a ratio of about 4:3). Age distribution of drivers follows the demographic composition of licensed drivers in the area. A significant proportion of intersection-related crashes occurred at feeder roads adjacent to major freeways in San Antonio.

REFERENCES

AASHTO. *A Policy on Geometric Design of Highways and Streets* (a.k.a. ''The Green Book''). American Association of State Highway and Transportation Officials (AASHTO), Washington, DC, 2004.

Alexander, Lee, Pi-Ming Cheng, Max Donath,Alec Gorjestani, Arvind Menon, and Craig Shankwitz. *Intersection Decision Support Surveillance System: Design, Performance, and Initial Driver Behavior Quantization*. Report # MN/RC-2007-30. Minnesota Department of Transportation (Mn/DOT), St. Paul, Minnesota, 2007.

Burchett, G., and T.Maze. ''Rural Expressway Intersections that Contribute to Reduced Safety Performance.'' Proc., 2005 *Mid-Continent Transportation Research Symposium*, Iowa State University, Ames, Iowa, 2005.

Khattak, A., L. Zhang, et al. ''Crash Analysis of Expressway Intersections in Nebraska.'' *TRB 85th Annual Meeting Compendium of Papers* (CD-ROM), Transportation Research Board, Washington, DC, 2006.

Kuciemba, S. R., and J. A. Cirillo. *Safety Effectiveness of Highway Design Features*. Report # FHWA ID 91 048, Federal Highway Administration (FHWA), McLean,Virginia, 1992.

Maze, T. H., Neal H. Hawkins, and Gary Burchett. *Rural Expressway Intersection Synthesis of Practice and Crash Analysis*. Center for Transportation Research and Education, Iowa State University, Ames, Iowa, 2004. http://www.ctre.iastate.edu/reports/expressway.pdf (Accessed

Stephen M., 2004, "What is the Effect of Driver Education Programs on Traffic Crash and Violation Rates?" Publication FHWA-AZ-04-546, developed for the Arizona Department of Transportation.

Savolainen, P., and A. Tarko. ''Safety Impacts at Intersections on Curved Segments.'' *Transportation Research Record*, No. 1908, 2005, pp.130–140, doi: 10.3141/1908-16.

Study the Impacts of Freight Consolidation and Truck Sharing on Freight Mobility

Tieming Liu, Devaraja Radha Krishnan, and Chaoyue Zhao
School of Industrial Engineering and Management, Oklahoma State University

INTRODUCTION

The trucking industry has become an indispensable part of U.S. economy. According to the American Trucking Associations, U.S. companies transport over 70 percent of their goods across the country using freight trucking services. The trucking industry contributes around $650 billion dollars of revenue to U.S. annually. This constitutes over 84% of revenue in the country's commercial transportation sector.

However, the trucking industry in the U.S. is very fragmented. According to the Department of Transportation, the 50 largest trucking companies handle just 30 percent of freight activities across the U.S. The trucking industry is composed of 110,000 carriers and 350,000 independent owner-operators. Around 97% of carriers in America own less than 20 trucks and around 90% of carriers own 6 or lesser trucks.

This fragmentation presents a big barrier to improve the efficiency of the trucking industry. It is difficult for small carriers to get enough shipping demand to fill the truckload for every trip. Some trucks travel emptily in the returning trip. It is estimated that around 20 percent of trucks on roads are traveling empty, which is a huge cost to the transportation companies. The low efficiency of the trucking industry causes high price to the shippers. Traveling empty trucks also contributed to traffic congestion and air pollution.

The newly established online freight-equipment matching marketplaces can help small carriers find shippers to fill the truckload quickly. Online freight matching marketplaces work like Uber, which connects drivers and passengers based on demand. In online freight matching marketplaces, a mobile application is used as communication platform between carriers and businesses needing transportation. The online market places help carriers find freight to fill the trucks quickly.

However, online freight consolidation is much more complicated than Uber's online driver-passenger matching. In passenger transportation, both cars and passengers are standard. Whereas, in freight transportation, there are many different types and sizes of freight, and every type of trucks has its own size and weight limits. Only certain types of freight may be shipped together in the same truck. It is very difficult and time-consuming for carriers to search shippers' demand information online to identify freight consolidation options. It will be very helpful if the online freight-matching marketplace could provide consolidation solutions to the carriers. As the number of trucking companies using online marketplaces increases, the demand for freight consolidation algorithms will also increase.

Although highly demanded, currently there are no online freight consolidation algorithms available, due to the complex nature of the problem itself. Most online freight-matching marketplaces are small start-up companies, and they lack the recourse and expertise to develop freight consolidation algorithms. The goal of this project is to show the impacts of online freight consolidation on freight mobility, congestion and emission reduction, and thus draw the attention of transportation authority and logistics companies to this problem. This project will lead to more resources and experts devoted to study online freight matching problems and thus further improve the efficiency of freight transportation.

There is considerable amount of literature on heterogeneous fleet of trucks and vehicle routing (please refer to [1,2,4,5] and the references therein). However, to our best knowledge, there is no research on online freight consolidation or the impacts of freight consolidation on environment and traffic congestion. We will study the impacts of online freight consolidation on greenhouse gas emissions and traffic congestion resulting in this project. We hope our results will lead to future studies on online freight consolidation algorithms for the trucking industry.

METHODOLOGY

In this project, we aim to examine the impacts of online freight consolidation on traffic and emission reduction. Toward this goal, we will first analyse the sample data of freight movement from our industrial partners to identify truck sharing opportunities. Then we will use the approach in [3] to develop mathematical models and evaluate the impacts of truck sharing on freight mobility and traffic reduction. We hope that the results would motivate logistics companies to pay attention to freight consolidation opportunities and design effective cost sharing structures. We hope this research will lead to the development of effective algorithms for online freight consolidation and the improvement of freight mobility. This project includes the following specific tasks:

- Task 1: Literature review of truck sharing initiatives in the U.S. Identification of new start-up companies, types of commodities, tonnage/volumes of commodities.
- Task 2: Identification of truck-sharing data available and letters of commitment from data owners agreeing to provide their data for research.
- Task 3: Develop and validate freight demand models for shared freight hauling.
- Task 4: Develop and validate models for quantifying the impacts of truck sharing on network capacity, congestion, environment, etc.
- Task 5: Apply the models in Tasks 3 & 4 to forecast freight moved by truck sharing by commodity type and estimate the resulting benefits of truck sharing.

FINDINGS

The project started in May 2017. So far, we have completed the first three tasks: literature review, data acquisition and the development of freight sharing models. We have co-signed the non-disclosure agreement with Transplace and obtained their shipment data for one sample month. Then we established two mathematical models to identify freight sharing opportunities. Both models try to identify effective routes for trucks to pick up and deliver shipments. Different shipments will be consolidated along a route, but will never be relayed over multiple trucks, hence reducing the loading / unloading time and cost. We will evaluate the efficiency of the two models with the industrial data in the next step.

CONCLUSION

Online freight-equipment matching market places are promising to provide freight consolidation solutions to small carriers, and thus improve the efficiency of the fragmented transportation industry in the U.S. This project aims to show the impacts of online freight consolidation on freight mobility, congestion and emission reduction. Some potential benefits from our research are the following:

1. Small and mid-level CPG shippers can have a better strategy for freight consolidation. This can help them to reduce the usage of LTL shipping. This can give them a competitive advantage over their large counterparts.

2. Even the large-scale shippers handle sudden demand fluctuations with LTL carriers. They can reduce the cost during fluctuations by freight consolidation.
3. Reducing unused capacity of trucks. Consequently, this reduces transportation cost for the companies.
4. Reducing number of empty trucks on the roads. This can reduce traffic congestion and greenhouse gas emission.
5. The driver shortage problem can be levitated, due to the reduction of the number of traveling empty trucks.
6. Customer satisfaction is another benefit, as customers prefer their freight being shipped by a single truck rather than transferring between multiple trucks.

This project will draw the attention of transportation authorities and logistics companies to online freight consolidation problems, and thus lead more resources and experts to study efficient freight-consolidation algorithms to further improve the efficiency of the fragmented freight transportation industry and reduce traffic congestion and emissions.

REFERENCES

1. Chu, C. (2005). A heuristic algorithm for the truckload and less-than-truckload problem. European Journal of Operational Research, 165(3), 657-667.
2. Hoff, A., Anderson, H., Christiansen, M., Hasle, G., & Løkketangen, A. (2010). Industrial aspects and literature survey: Fleet composition and routing. Computers & Operations Research, 37(9), 2041–2061.
3. Hwang, T. S. (2014). Freight demand modeling and logistics planning for assessment of freight systems' environmental impacts. PhD thesis. University of Illinois at Urbana-Champaign.
4. Tarantilis, C., & Kiranoudis, C. (2007). A flexible adaptive memory-based algorithm for real-life transportation operations: Two case studies from dairy and construction sector. European Journal of Operational Research, 179(3), 806-822.
5. Tavakkoli-Moghaddam, R., Safaei, N., Kah, M., & Rabbani, M. (2007). A new capacitated vehicle routing problem with split service for minimizing fleet cost by simulated annealing. Journal of the Franklin Institute, 344(5), 406-425.

Emission Analysis of Diesels Derived from Biomass used for Hybrid Transportation Fleet

Hongbo Du[1], Arndreya Howard[1,2], Raghava Kommalapati[1,2]

[1]Center for Energy and Environmental Sustainability
[2]Department of Civil and Environmental Engineering, Prairie View A&M University

INTRODUCTION

Heavy-duty vehicles (HDVs) account for 70% of all freight fleet, and most HDVs on roads are heavy duty diesel trucks [1]. Exhaust from these vehicles has been identified as major source of air pollution. Over the past two decades, researchers and vehicle manufactures have explored and implemented ways to improve fuel efficiency and reduce vehicle emissions, including the use of hybrid electric vehicles [2] and the development of new fuels [3]. Hybrid passenger cars fueled with gasoline and diesel are very popular in the world market, and hybrid HDVs are just emerging. Currently, the most used fuels for diesel vehicles in the world are low sulfur diesel (LSD) and ultra-low sulfur diesel (ULSD), even the conventional diesel is still used in some countries. Except the three popular diesels, there are new types of diesel, which have been developed and tested, such as ultra-low sulfur diesel, biodiesel (BD), ethanol-diesel (ED), and renewable diesel (RD). BD is a renewable fuel that can be produced from vegetable oils, animal fats, or recycled restaurant grease. BD is similar to the conventional diesel, and it can be blended into the standard diesel or low sulfur diesel up to 20% in volume with no, or only minor engine modifications. ED is a diesel fuel produced by blending the standard diesel with up to 15% of ethanol in volume using an additive package, where the additive can comprise from 0.2% to 5.0%. Typical ethanol used in the ED blends is bioethanol derived from corn, potato, sugar, starches, even from forestry residue, agriculture residue and algae. RD can be produced through biomass pyrolysis and transformed from bio-oil which can be soybean oil, rapeseed oil or algae oil with better cold and storage properties. ED and RD are also suitable for typical diesel engines without engine modification. The performances and vehicle emissions of ultra-low sulfur diesel and BD used in conventional diesel engines have been widely studied [4, 5], however, the reports of BD, ED and RD used in hybrid diesel vehicles are rare. Compared to the vehicle emissions of LSD, overall emissions of BD, ED and RD used in hybrid diesel vehicles including passenger cars and heavy heavy duty diesel trucks (HHDDTs) are evaluated by life cycle assessment (LCA) in our study.

METHODOLOGY

This study uses a life cycle analysis tool called the GREET model, to evaluate the overall emissions of different diesels used in hybrid diesel vehicles in 2017 and 2030. The biodiesel is BD20, which contains 20% biodiesel derived from soybean in volume. ED is the ethanol-diesel blend of 89% LSD, 10% bioethanol, and 1% additivities in volume. The bioethanol is produced from corn through a wet-milling process of ethanol conversion. In order to comprehensively study the effects of different feedstocks on the emissions, RD is detailed to deriving from forest residue and corn stover through pyrolysis, and from soybean and algae through bio-oil transformation. The availabilities of different feedstocks are investigated across the nation. The evaluation of emissions associated with the different diesels is classified into two stages of well-to-pump (WTP), and well-to-wheels (WTW). The energy and water use for fuel production is investigated during the WTP stage. The overall emissions are evaluated based on the most two popular types of hybrid diesel vehicles: passenger cars and heavy heavy duty diesel trucks (HHDDTs). The uncertainties of vehicle operations are elucidated based on available experimental data of fuel efficiencies and emission factors of different hybrid diesel vehicles.

RESULTS AND DISCUSSION

The energy use and emissions of the standard diesel and LSD during fuel production are the default values which are taken from the national statistical data in the USA. The availabilities of corn, soybeans, different biomass and algae vary in different states. Table 1 lists the energy and water use, and emissions associated with LSD, BD20, ED and RD during the WTP stage in 2017. In Table 1, RD-soybeans, RD-corn stover, RD-forest residue and RD-algae represents the diesels which are differently derived from soybeans, corn stover, forest residue and algae. RD-algae takes the greatest energy consumption and contributes to the highest emissions of GHGs, CO, NO_x, PM_{10}, $PM_{2.5}$ and SO_x except VOC because of the difficulty of algae separation from water. The negative energy value of RD-soybeans is attributed to the coproducts of soybean meals and propane fuel mix in the long pathway of RD production from soybeans. However, RD-soybeans consumes the highest volume of water mainly due to irrigation of soybean fields and contributes to the highest VOC emissions. The production of BD takes about half of the energy which is consumed by LSD production with slight increases of various emissions of GHGs, VOC, CO, NO_x, PM_{10}, $PM_{2.5}$ and SO_x. Predicting various emissions in 2030, some significant reductions will occur on the emissions of NO_x, PM_{10}, $PM_{2.5}$ and SO_x.

Table 1: The energy and water use, and emissions associated with LSD, BD20, ED and RD during the WTP stage in 2017.

Fuel	Energy (kJ/MJ)	Water (m^3/MJ)	GHGs (g_{CO2eq}/MJ)	VOC (mg/MJ)	CO (mg/MJ)	NOx (mg/MJ)	PM10 (mg/MJ)	$PM_{2.5}$ (mg/MJ)	SO_x (mg/MJ)
LSD	210	0.08	18.38	7.68	13.44	29.86	2.05	1.66	15.85
BD20	118	0.48	19.06	9.98	14.91	31.13	2.20	1.81	18.23
ED	236	0.18	20.80	10.60	15.09	33.7	2.90	1.91	19.92
RD-soybeans	-281	2.18	22.36	18.98	20.43	35.38	2.19	1.78	27.04
RD-corn stover	814	0.07	31.32	7.77	18.28	35.05	3.3	2.52	34.38
RD -forest residue	990	0.07	27.08	7.06	17.07	33.78	2.56	1.85	20.95
RD -algae	2431	0.15	60.30	15.94	65.41	57.22	7.83	5.66	70.57

The overall GHG emissions of passenger cars and HHDDTs using different diesels during the WTP stage are shown in Figure 1. The GHG emissions of both vehicle types fueled with RD-corn stover and RD-forest residue are much lower than those of the base fuel LSD used for their corresponding vehicles. The GHG emissions of passenger cars powered by LSD, BD20, RD-soybeans and ED are similar, and the GHG reductions of LSD, BD20 and ED would be significant in 2030 except RD-soybeans. The GHG emissions of HHDDTs powered by RD-soybeans are the highest, and the GHG reductions of HHDDTs fueled with LSD, BD20 and ED in 2030 are not as significant as the future passenger cars.

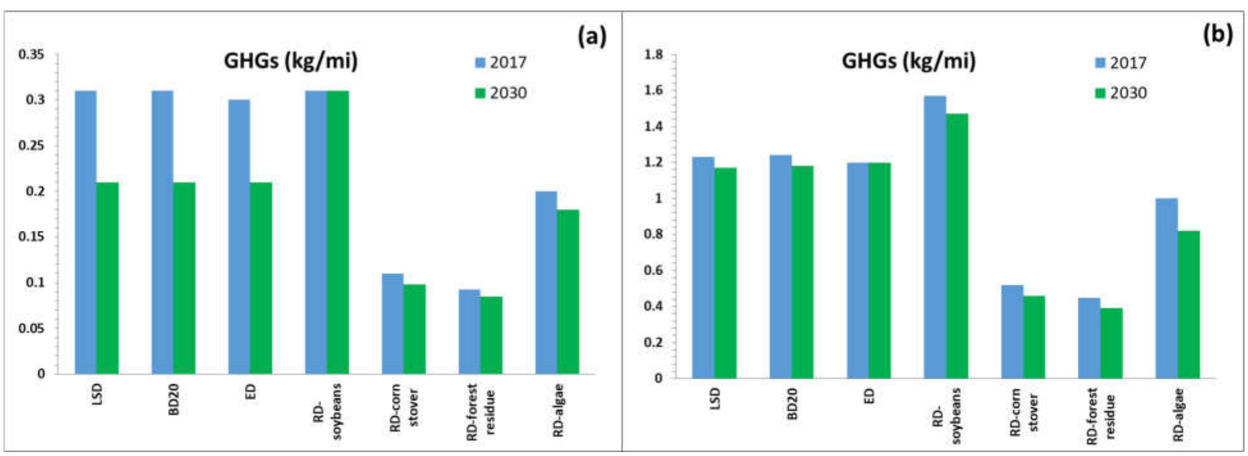

Figure 1: Overall GHG emissions of passenger cars (a) and HHDDTs (b) using various diesels in 2017 and 2030.

Other overall emissions such as VOC, CO, NO_x, PM10, PM2.5 and SO_x are also analyzed in 2017 and 2030 with LCA. The reductions of all the other emissions are significant in 2030. VOC emissions vary from different diesels for passenger cars, and the highest emissions occur on RD-soybeans. For HHDDTs, VOC emissions associated with RD-soybeans and RD-algae are much higher than those by fueling with other diesels. CO emissions of these diesels are similar for passenger cars, however, RD-algae contributes much more than other diesels for HHDDTs. The highest emissions of NO_x, PM10, PM2.5 and SO_x also occur on RD-algae for both vehicle types.

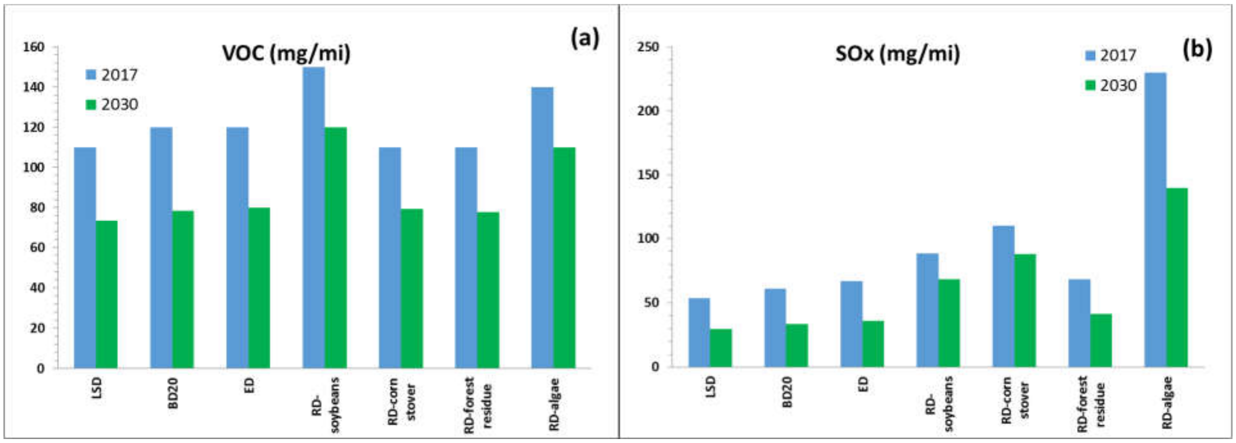

Figure 2: Overall VOC (a) and SO_x(b) emissions of passenger cars (a) and HHDDTs (b) using various diesels in 2017 and 2030.

CONCLUSION

The effects of different diesels and their derivation resources on vehicle emissions are evaluated with GREET model. The highest GHG reductions occur on RD-soybeans for passenger cars and HHDDTs, and RD-RD and RD-corn stover have a promising potential to alleviate the global warming. The fuel RD-algae needs a great technology breakthrough for future use in hybrid diesel vehicles on a large scale.

REFERENCES

1. Quiros, D.C., et al., *Greenhouse gas emissions from heavy-duty natural gas, hybrid, and conventional diesel on-road trucks during freight transport.* Atmospheric Environment, 2017. **168**: p. 36-45.
2. Guan, B., et al., *Review of state of the art technologies of selective catalytic reduction of NOx from diesel engine exhaust.* Applied Thermal Engineering, 2014. **66**(1-2): p. 395-414.
3. Gopalakrishnan, K., A. Mudgal, and S. Hallmark, *NEURO-FUZZY APPROACH TO PREDICTIVE MODELING OF EMISSIONS FROM BIODIESEL POWERED TRANSIT BUSES.* Transport, 2011. **26**(4): p. 344-352.
4. Bachmann, C., et al., *Life-Cycle Assessment of Diesel-Electric Hybrid and Conventional Diesel Trucks for Deliveries.* Journal of Transportation Engineering, 2015. **141**(4).
5. Lee, D.Y. and V.M. Thomas, *Parametric modeling approach for economic and environmental life cycle assessment of medium-duty truck electrification.* Journal of Cleaner Production, 2017. **142**: p. 3300-3321.

Non-Destruction Detection of Moisture Damage in Pavements Using Ground Penetrating Radar

Mohammad Z. Bashar[1], Mostafa A. Elseifi[2], Momen Mousa[1], and Zhongjie Zhang[3]

[1]GRA, Department of Civil and Environmental Engineering, Louisiana State University
[2]Professor, Department of Civil and Environmental Engineering, Louisiana State University
[3]Pavement Geotechnical Research Administrator, Louisiana Transportation Research Center

INTRODUCTION

Ground Penetrating Radar (GPR) is a highly versatile tool that transmits short pulses of electromagnetic waves into the pavement and the reflections from the material boundaries and subsurface anomalies are picked up by the receiver mounted on a survey vehicle. As the vehicle can operate at a normal driving speed, it gives GPR an extra edge over the other NDE techniques of pavement condition evaluation (*1*, *2*). GPR was found to be effective in a wide range of highway applications including but not limited to, the estimation of pavement layer thickness, detection of subsurface moisture, density variations, voids, and underground utility locations (*3*). Noninvasive, continuous, and high-speed evaluation of the pavement distresses such as delamination, stripping, rutting is essential for the transportation agencies in the planning phase of future maintenance and rehabilitation activities. This would also ensure adequate allocation of maintenance and rehabilitation funds by a state agency (*4*).

Stripping in asphalt pavement is a moisture related phenomenon that leads to the loss of bond between aggregates and asphalt binder. It propagates upward from the asphalt-base interface leaving a weak unstable layer at the bottom of the HMA layer (*3*, *5*). Historically, detection of stripping in HMA layers was carried out by coring followed by visual inspection. This process is not only time consuming and labor intensive, but also it does not allow the highway maintenance agencies to accurately quantify the area and severity of stripping in the existing pavements. GPR, on the other hand, has shown a good potential to be used as a non-destructive tool to detect moisture damages in in-service pavements (*4–6*).

The primary objective of this study was to develop a methodology that can be implemented to use GPR in detecting distresses in HMA. Field data and roadway cores were used to evaluate the capabilities of GPR in detecting the presence, extent, and severity of stripping and delamination in in-place pavement sections.

METHODOLOGY

To evaluate GPR capabilities in detecting distresses in flexible pavements, a field testing program was undertaken by Louisiana Department of Transportation and Development (LADOTD). Field data used in this study included cores samples, and GPR scans. GPR surveys were conducted on the entire length of most of the control sections in Louisiana in 2010. A GPR system manufactured by Geophysical Survey Systems, Inc. (GSSI) was utilized in this study to perform these surveys. This equipment comprises a control unit, monitor, and two bowtie (ground coupled) antennae operating at center frequencies of 900 MHz and 1.6 GHz.

LaDOTD performed pavement coring at most of the road segments. At least one core sample was extracted from each road segment to verify pavement thicknesses and to identify any material deteriorations below the pavement surface as well as bonding problems. The core thicknesses were measured in accordance with ASTM D3549. In this study, core samples were visually inspected to determine whether stripping was a problem for each road segment. Based on this inspection, 12 moderate to severely stripped and 12 non- stripped cores obtained from different road segments were selected and the corresponding GPR data at the core locations were investigated and analyzed.

FINDINGS

Although it is very difficult to draw any firm conclusions based on the results from a small set of data, a common pattern was observed among the dielectric values of the stripped and non-stripped HMA layers when surveyed during a dry season, i.e., after the water has drained out from the stripped layer. In general, sections with stripping had slightly lower dielectric values as compared to the sections without stripping, which is consistent with the findings from the past studies (*4*, *6*). After drainage of water from the pavement section, stripping induced voids creates a low-density inner layer which can be attributed to the lower dielectric values for the sections with stripping. To demonstrate the range of dielectric values obtained from different cores, the values were sorted in ascending order based on their respective core condition, as shown in Figure 1. The average dielectric value for the stripped cores was found to be 5.5 whereas the cores without any stripping had an average dielectric value of 6.3. It is worthy to mention that stripped cores number 10,11, and 12 had relatively high dielectric constant. Weather records indicated that these sections were exposed to rainfall ranging from 0.3-0.79 inch within 48 hours before the scanning of the sections. The saturated surface of the pavements resulted in a higher dielectric value for these sections.

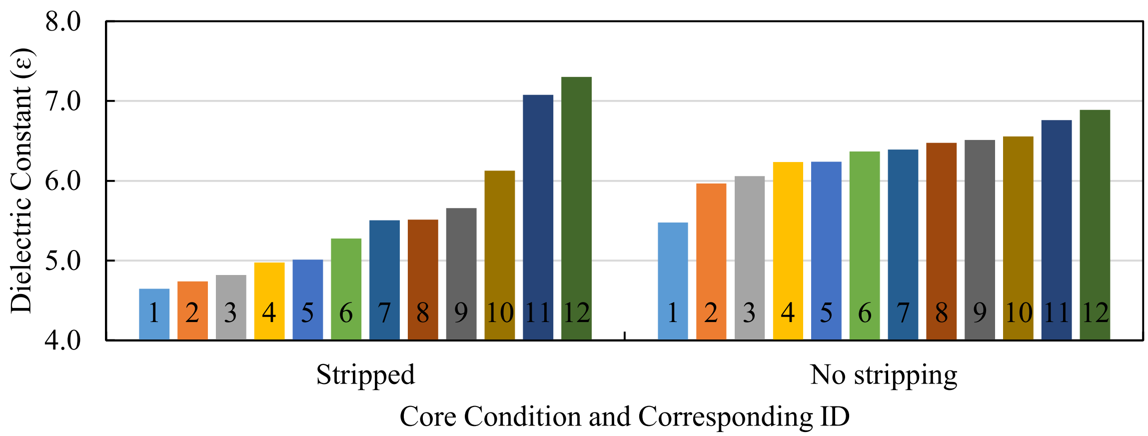

Figure 1 Surface dielectric constants for cores with and without stripping

While conducting the visual inspection of the traces, GPR images were found to be in reverse phase i.e., intermediate large negative peaks were observed in-between two regular positive peaks for the stripped sections. The same pattern was observed at all the stripped core locations, which is consistent with the findings of previous studies (*4*, *6*, *7*). Figure 2 shows a core collected from section 297-01 that had moderate stripping at a depth of 8 inches. A large negative peak was observed at the location of stripping. Therefore, careful visual inspection of the traces can help identifying the stripped locations in a pavement.

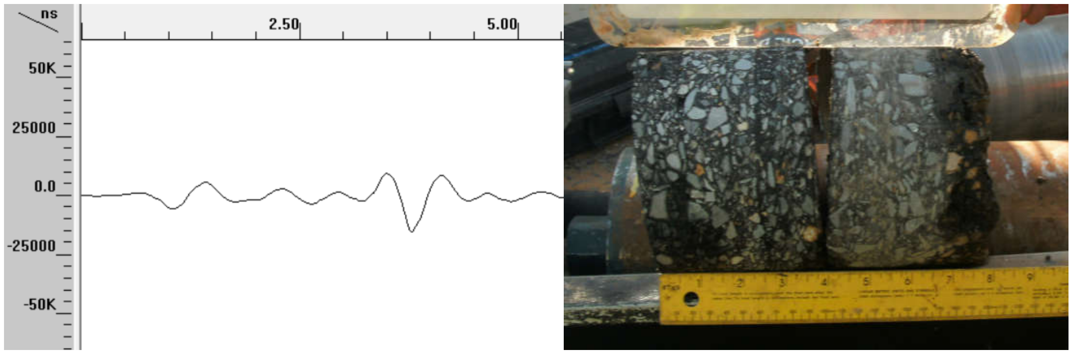

Figure 2 Visual inspection of the traces showing intermediate negative peaks at stripped depths

The accuracy of Uniformity Index (UI) in detecting potential stripping in HMA layers was tested by comparing the predicted stripping condition based on the UI profile with the actual stripping condition based on the extracted core. Therefore, the UI profiles for all 20 sections were plotted using the entire project length as the normalization length. The UI predicted conditions were compared with the actual core conditions.

The results indicated that the UI predictions were 88.9% accurate in detecting stripping for the sections having an HMA thickness greater than 7 inches. The accuracy dropped down to 73.3% when the core thicknesses ranged from 3 to 7 inches. However, one limitation of using UI in predicting stripping is that if the whole scanned section is equally stripped, UI profile will not show any variations in the values as it works based on the relative change in reflection activities.

GPR data for each segment was analyzed to identify the locations with delamination factors falling between the warning range. Both the reflection amplitude and travel time of the electromagnetic waves were used to compute the warning value ranges. Like other parameters estimated from GPR data, this technique only allows the users to preliminary narrow down the locations with potential delamination. In field tests, the identified locations must be validated with other techniques such as core drilling.

CONCLUSIONS

The primary objective of this study was to develop a methodology to detect distresses in HMA using GPR. GPR data for 20 flexible pavements along with the data obtained from the extracted cores were used to evaluate the capabilities of GPR in detecting distresses such as stripping and delamination. Based on the outcomes of this study, the following conclusions were drawn:

- Stripping was found to be associated with lower dielectric values of the HMA layers. The average dielectric constant value for the stripped cores was estimated as 5.5 whereas the sections without stripping exhibited a greater dielectric value of 6.3 on average.
- The saturated surfaces were found to have greater dielectric values ranging from 7 to 7.3 regardless of the stripping condition.
- Intermediate large negative peaks between the regular positive peaks were observed in the GPR traces for the stripped locations.
- The reflection amplitudes from the top of the base layer were found to be lower for the sections with stripping as compared with the sections without stripping.
- For homogenous sections, the UI varied around unity, whereas greater fluctuations in the UI values were observed for non-homogeneous sections.

- UI predicted stripping with 73.33% accuracy for stripping depths ranging from 3 to 7 inches and with 88.89% accuracy for stripping depths greater than 7 inches.
- GPR estimated delamination factor can primarily be used to locate the areas with potential inadequate compaction and delamination. However, these techniques are required to be accompanied by other methods such as core drilling for an accurate evaluation of the in-place pavements.

REFERENCES

1. Khamzin, A. K., A. V. Varnavina, E. V. Torgashov, N. L. Anderson, and L. H. Sneed. Utilization of air-launched ground penetrating radar (GPR) for pavement condition assessment. *Construction and Building Materials*, Vol. 141, 2017, pp. 130–139.
2. Al-Qadi, I. L., and S. Lahouar. Measuring layer thicknesses with GPR - Theory to practice. *Construction and Building Materials*, Vol. 19, No. 10, 2005, pp. 763–772.
3. Cao, Y., S. Dai, J. F. Labuz, and J. Pantelis. *Implementation of Ground Penetrating Radar*. Minnesota Department of Transportation, Maplewood, MN, 2007.
4. Rmeili, E., and T. Scullion. Detecting Stripping in Asphalt Concrete Layers Using Ground Penetrating Radar. *Transportation Research Record*, Vol. 1568, No. 1, 1997, pp. 165–174.
5. Hammons, M. I., K. Maser, and S. Nazarian. *Detection of Stripping in Hot Mix Asphalt*. Georgia Department of Transportation, Forest Park, GA, 2005.
6. Hammons, M., H. Von Quintus, G. Geary, P. Wu, and D. Jared. Detection of Stripping in Hot-Mix Asphalt. *Transportation Research Record*, Vol. 1949, 2006, pp. 20–31.
7. Maser, K. R., and T. Scullion. Automated Pavement Subsurface Profiling Using Radar: Case Studies of Four Experimental Field Sites. *TRANSPORTATION RESEARCH RECORD*, No. 1344, 1992, pp. 148–154.

Evaluation of Comparative Damaging Effects of Multiple Truck Axles for Flexible Pavements

Stefan Romanoschi[1], Athanassios T. Papagiannakis[2], Mohsen Talebsafa[1], Constantin Popescu[1], and Rajesh Kaphle[2]

[1]University of Texas, Arlington
[2]University of Texas at San Antonio

INTRODUCTION

The objective of this research is to evaluate the comparative damaging effects of multiple truck axles including overloaded axles for asphalt pavements in the South Central region of the United States, by investigating the response of the pavement structure to various truck loading configurations. This is needed in order to harmonize truck load limit regulations between US states as well as between the US and our NAFTA neighbors, Considerable work was recently done in revisiting truck weights and dimensions under MAP-21 funding. This was done using the state of the art AASHTOWare Pavement ME (ME) software that computes the damage caused by each axle based on the longitudinal strain at the bottom of the asphalt layer. It also assumes that each axle is acting independently.

Some previous work by the researchers indicated that there might be a cumulative effect of different axles on the transverse strain at the bottom of the asphalt layer, and that the cumulated transverse strain is bigger than the longitudinal strain. It seems that the accumulation of strain is due to the viscoelastic behavior of thick asphalt layers at high temperature during warm days, and the short distance between some axles. Therefore, this accumulation of transverse strain and thus, the increase in pavement damage, must be accurately determined. Moreover, this will be a major issue when automated trucks will use our roads and highways. Automated trucks will likely travel in platoons, with a driver needed only in the first truck and the other trucks following at very short distances.

A major limitation of current approaches to flexible pavement design is that all materials are considered linear elastic, homogeneous and isotropic. This assumption is made to simplify the response calculations. The effect of loading speed is considered only by adjusting the dynamic modulus of the asphalt concrete based on the master curve data provided. This assumption has a major consequence: when a truck passes over the pavement structure, the strains induced by an axle group are treated independently from those induce by subsequent axle groups (e.g., steering axle versus following tandems in a class 9 truck or 18-wheeler). In other words, there is no consideration of overlapping strain effects from the various axle groups of a truck. In-situ strain measurements from several instrumented pavement sections in the United States and overseas clearly proved that:

a) The transverse strain induced by the front axle of the truck does not completely recover before the strain induced by the following axles develops. Therefore, the transverse strains under the rear axles are much higher than those estimated by linear elastic models.
b) The strains under a multiple axle are much higher than those estimated by linear elastic models, even when the effect of the front axle(s) is removed.
c) The transverse horizontal strain at the bottom of the HMA layer is bigger that the longitudinal horizontal strain because of the compounding effects from multiple axles.

Most pavement structural models compute only the longitudinal strain because it is assumed to be the largest.

d) The compounding effect increases when the vehicle speed decreases and when the temperature in the HMA layers is high, as normally is in the South Central region of the United States.

Figure 1 shows an example of the signals for the longitudinal and transverse horizontal strains measured at the bottom of the asphalt layer of a thick pavement structure. The signals on the left side of the figure were recorded under the passing of a Class 5 vehicle (a truck with steering axle and dual tire single axle in the rear, like an UPS delivery truck). The signals on the right side were recorded under the passing of a Class 8 vehicle (a truck with steering axle and dual-tire tandem drive axles for the tractor and dual-tire single axle in the rear of the trailer). The trucks travelled at over 40 mph. The figure shows clearly that, for both trucks, the longitudinal strain caused by the steering axle does not recover completely before the arrival of the rear axle, causing strain signal overlap. It also shows that the transverse strains are larger than the longitudinal strains. These findings clearly indicate that the pavement response, and consequently the relative damage, caused by various truck and axle configurations need to be further studied through in-situ strain measurements on in-service pavements. Clearly, the effect of the strain signature overlap between consecutive axle groups needs to be considered, in order to establish the correct strain magnitude to be used for pavement design.

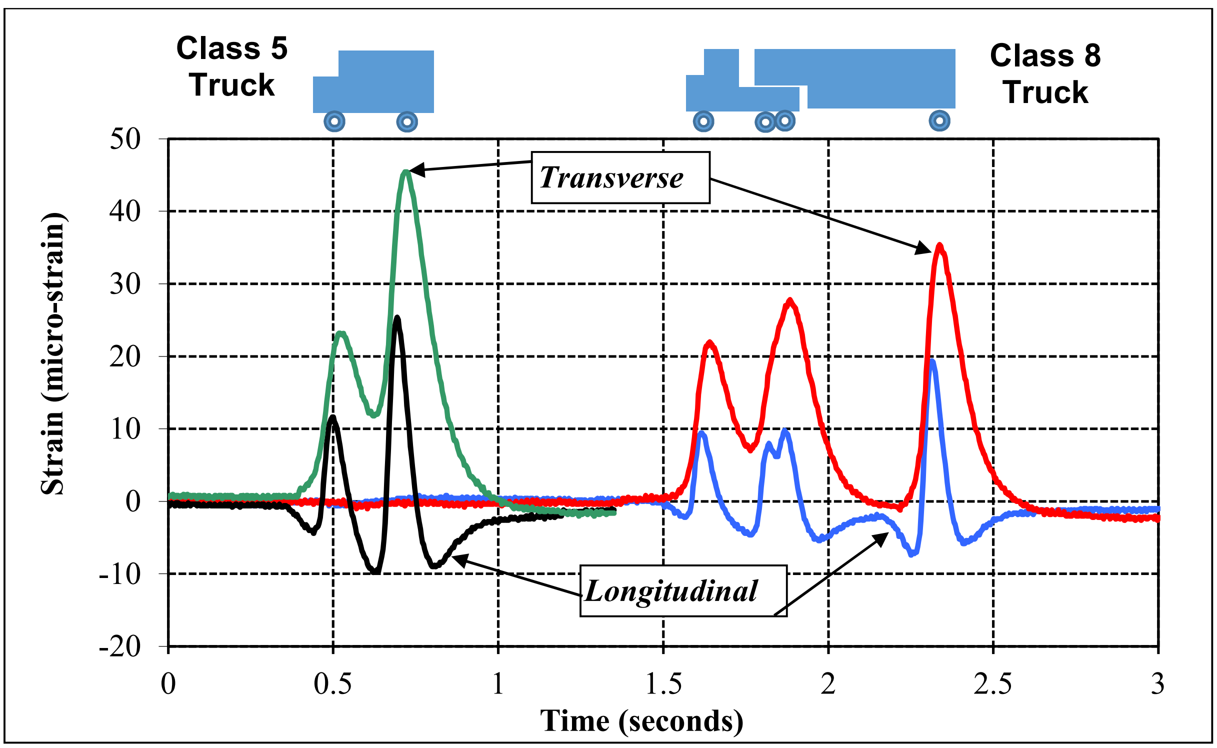

Figure 1. Transverse Strain at 60mph truck speed

Figure 1 illustrates well the importance of accurately computing the horizontal shear strain at the bottom of the asphalt concrete layer. For the class 5 vehicle, the maximum transverse under the rear axle is about 46 microstrain versus 26 microstrain for the maximum longitudinal strain. If the longitudinal strain is considered instead of the transverse strain in the computation of the fatigue damage caused by the passing of the rear axle, the fatigue damage is underestimated by $(46/26)^{3.92} = 9.36$ times. For the class 8 vehicle, the fatigue damage at the bottom of the asphalt layer caused by the passing of the rear axle is underestimated by $(28/10)^{3.92} = 56.6$ times. Clearly, the lack of considering the compounding effect of different axles on the magnitude of the transverse horizontal strain at the bottom of the asphalt layer leads to severe under-prediction of the fatigue damage and therefore, of the fatigue cracking initiation and development.

The compounding effect of the front and rear axles of the truck has not been observed before, or it has not been given a proper consideration. This is likely because most measurements of horizontal strains at the bottom of asphalt concrete layers under the passing of a truck have been done on thinner pavements, with the thickness of the asphalt concrete layers less than ten inches. For the same vehicle speed, the duration of the strain signal is considerably shorter for thinner pavements than for thicker pavements and therefore, the compounding effect is smaller.

METHODOLOGY

The aim of this project is to develop a strain measurement dataset that will allow revisiting pavement response under in-service traffic for the purpose of quantifying pavement damage under various truck/axle configurations. For this, a thick flexible pavement structure will be instrumented with sensors to measure the horizontal strains at the bottom of the asphalt layer in the longitudinal and transverse direction. This dataset will include complete strain signal data, not only the maximum strain values. The dataset will be supporting further development of mechanistic models for the calculation of strains in asphalt pavement structures.

In addition, the pavement layer properties from the instrumented pavement site will allow comparing the measured versus estimated strains using conventional layer visco-elastic techniques. The mechanical properties of pavement layers will be measured in the laboratory; the for the moisture This effort will support further improvements to any ME pavement design methods because it will provide measured data supporting the concept of compounding effects for the transverse strain at the bottom of the asphalt layers.

A literature review that aims to assemble information from previous pavement response monitoring projects has been conducted. The goal of the review was not only collect information on the methodology used for measuring horizontal strains at the bottom of the HMA layer, but to identify projects in which the compounding effect of different truck axles on the longitudinal and transverse strains at the bottom of the HMA layer has been observed.

The design the instrumentation to be used for the strain measurements when trucks with various axle loads and configurations pass over the pavement structure was also done. The instrumentation plan has been prepared. The strain gauges were purchased and their wires were extended to the desired length. The pressure relays to be used for the lateral position measurements have been ordered. The programming of the data acquisition system has been completed.

The project will significantly impact the process of computing the damaging effect of various truck configurations. It will better provide data to support the inclusion of visco-elastic models for asphalt materials, the inclusion of the entire truck when computing the damage and not treat each axle independently. This will improve significantly the quantification of relative pavement damage due to the load limit increase and the search for trucks with improved configurations. The project will lead to extension of the life of flexible pavement and an improved utilization of funds for the maintenance and rehabilitation of state and local roads.

FINDINGS

A literature review that aims to assemble information from previous pavement response monitoring projects has been conducted. The goal of the review was not only collect information on the methodology used for measuring horizontal strains at the bottom of the HMA layer, but to identify projects in which the compounding effect of different truck axles on the longitudinal and transverse strains at the bottom of the HMA layer has been observed.

The design the instrumentation to be used for the strain measurements when trucks with various axle loads and configurations pass over the pavement structure was also done. The instrumentation plan has been prepared. The strain gauges were purchased and their wires were extended to the desired length. The pressure relays to be used for the lateral position measurements have been ordered. The programming of the data acquisition system has been completed.

The design of the instrumentation was completed; the configuration of the in-situ instrumentation is presented in Figures 2. The strain gauges selected are model KM-100HAS manufactured by Tokyo Sokki in Japan. These are the only strain gauges specifically designed to measure strain in asphalt layers. They are robust to survive installation and can measure strains up to 5,000 macrostrains. The cable purchased for connecting the strain gauges to the acquisition system is model TX4-1000 shielded cable distributed by Omega Inc.

The sensor system for the determining the lateral position of the test vehicles is similar in concept to that used at NCAT (Figure 3). However, air hoses laid on the pavement surface will use as axle sensing strips. Two air hoses placed transversely to the direction of travel will help determine the speed of the vehicle and on a third air hose placed in diagonal will help determine the lateral position based on speed. Pressure switches, mounted and the ends of the three air hoses, become activated when the pressure in the respective air hose increases because of a vehicle wheel is on top of that hose.

The National Instruments data acquisition system (CompactDAQ) and I/O modules currently available at the University of Texas at Arlington (UTA) can accommodate the selected strain gauges and the number of sensors (8 strain gauges and three positioning relays) and sampling rates (1,000 Hz) required by the project.

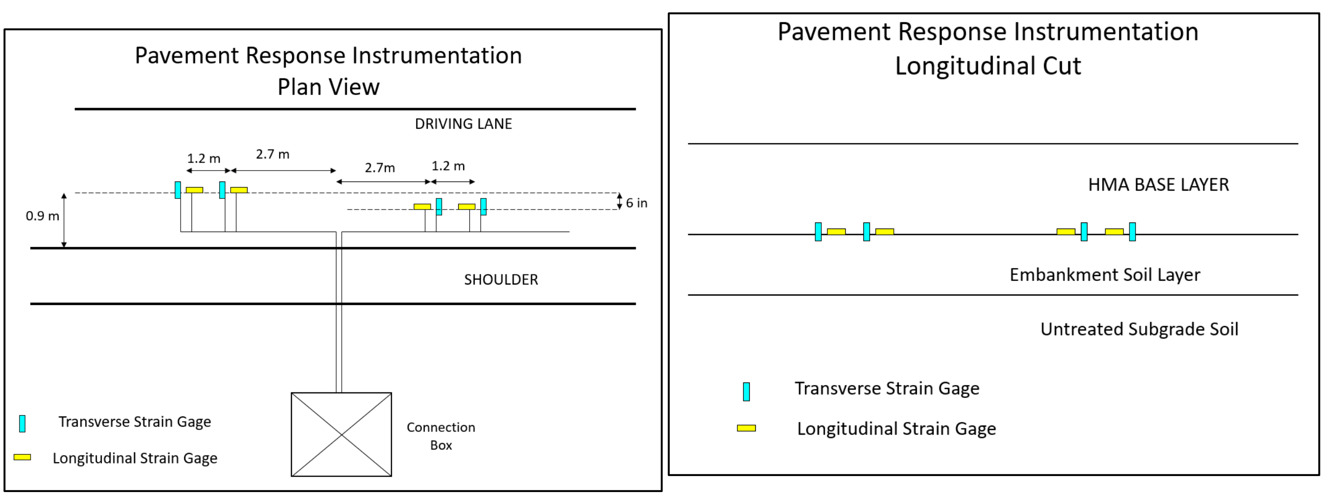

a) Plan view; b) Side view

Figure 2. Instrumentation Diagram.

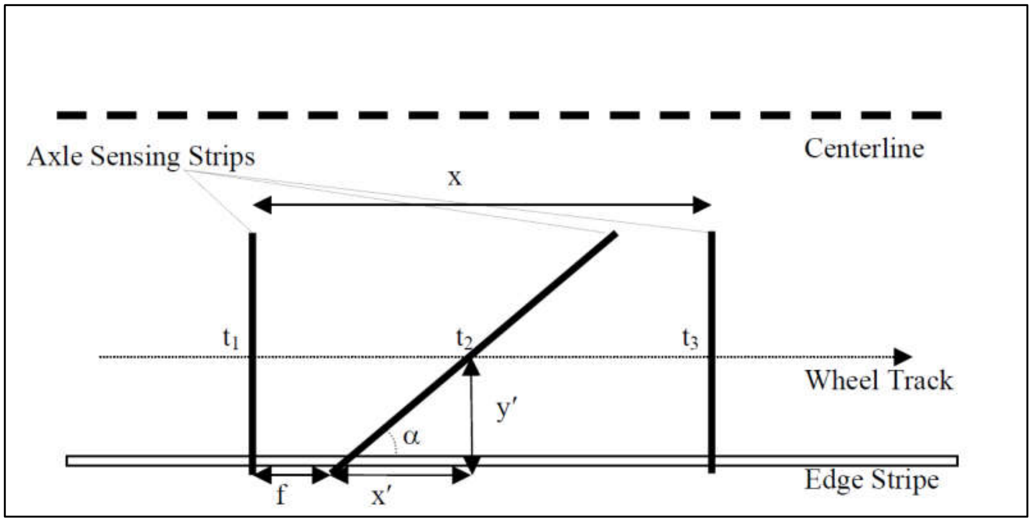

Figure 3. Plan view of the lateral positioning system used at NCAT

CONCLUSION

The project will significantly impact the process of computing the damaging effect of various truck configurations. It will better provide data to support the inclusion of visco-elastic models for asphalt materials, the inclusion of the entire truck when computing the damage and not treat each axle independently. This will optimize the quantification of relative pavement damage due to the load limit increase and the search for trucks with improved configurations. The project will lead to extension of the life of flexible pavements and an improved utilization of funds for the maintenance and rehabilitation of state and local roads.

Simplified Approach for Structural Evaluation of Flexible Pavements at The Network Level

Mena Souliman[1], Stefan Romanoschi[2], Samer Dessouky[3], Karthikeyan Loganathan[1], and Mayzan Isied[1]
[1]University of Texas at Tyler
[2]University of Texas, Arlington
[3]University of Texas at San Antonio

INTRODUCTION

Pavement deflection testing has been utilized widely as a nondestructive technique to evaluate the structural capacity of pavements at both network and project levels. By far the most popular deflection measuring device is the Falling Weight Deflectometer (FWD), which can record the deflection bowl shape. In this device, a load is applied on the pavement surface and deflections at several radial locations from the load are recorded. Complex backcalculation has been utilized to estimate layer moduli and determine overlay thickness at the project level analysis.

Based on the collected literature, it can be concluded that researchers have developed parameters, which include the difference between the central FWD deflection and deflection at a certain distance (Coetzee et al. (1989), Gedafa et al. (2010), Haas et al. (2001), Scullion (1988)), to evaluate the structural capacity of pavements. Deflection ratio is also one of the common parameters that are used by some of the highway agencies to estimate the pavement structural capacity (Zhang (2003)). Another parameter is the normalized area parameter, which is the total area of the deflection bowl normalized by the central deflection, which was found to be highly correlated to the pavement stiffness (Saleh (2015)). Although various transportation agencies use several methods, there is no standard acceptable method available to provide accurate estimate of the structural integrities of pavement layers and the subgrade.

It can be concluded that most of the up-to-date developed indices are exclusively based on either central deflections or one deflection point along FWD deflection bowl, and that there is no available comprehensive deflection or structural index that utilizes the entire FWD deflection bowl data.

Therefore, the proposed research study aims to achieve the following objectives:

(1) Introduce new comprehensive pavement layer deflection and deflection bowl area parameters which are based on the entire FWD deflection bowl rather than one single deflection point.
(2) Use 3D-Move analysis software package to simulate field-measured FWD deflection bowls.
(3) Develop a scoring system to rank the strength of the pavement sections by relating developed deflection area parameters to field measured distress such as fatigue cracking and to remaining service life.

The findings of the proposed study will help the South-Central State DOTs and local highway agency officials to make more informed decisions about the most suitable maintenance and rehabilitation strategies for deteriorated flexible pavement structures.

METHODOLOGY

Nondestructive deflection measuring devices such as FWD apply an impulse or transient load that simulates truck loading to a large extent. It is obvious that strong pavements show small deflections compared to weak pavements. A wealth of FWD data is available in the Long-Term Pavement Performance (LTPP) data base, along with detailed information on material properties, layer thicknesses, and traffic data. LTPP is one of the largest pavement performance research programs, initiated in the year 1987, as a part of Strategic Highway Research Program (SHRP). The database includes around 2,500 pavement sections all over the USA and Canada.

3D Move analysis software utilizes a continuum-based finite-layer approach to compute pavement responses that has been released by University of Nevada, Reno (UNR), to analyze asphalt pavements under variety of loading conditions. Successful simulation of FWD deflection bowl utilizing the 3D Move software package would potentially save time and effort since FWD field tests are expensive to be conducted at network level. 3D-Move Analysis software package was utilized to simulate the entire FWD deflection bowl, and the simulated entire deflection bowls were utilized to develop deflection ratio and area parameters as tools for pavement structural condition rating.

FINDINGS

Comparison between measured FWD and simulated 3D-Move deflection bowls for the SHRP sections 1049 and 1116 at 4 different drop heights are shown in Figure 1. Figure 1 illustrates the capability of 3D-Move Analysis package to replicate the field measured FWD deflection bowls, which can be employed to limit the extensive FWD field testing.

In addition, the relationship between the measured and predicted values of the central deflection (D_0), that is one of the important parameters to assess structural condition of pavements, was studied. The R2 value was found to be 0.973, and that indicates the prediction ability of 3D-Move software package for the central deflection values.

The Deflection ratio, D_r, is considered one of the important parameters employed by different agencies. D_r is defined as the ratio of deflection measured at 250 mm (D_{250}) from the center of the load plate to the central deflection (D_0). In order to overcome the limitations of D_r, a new parameter is introduced, termed as Comprehensive Deflection ratio (CD_r). CD_r is the ratio of deflection measured at 600 mm from the load plate (D_{600}) to the central deflection (D_0). To overcome the limitations of utilizing deflections at only two points, the area ratio concept was primarily introduced. In addition, a new area ratio is developed to incorporate the entire deflection bowl, named Comprehensive Area Ratio (CA_r) and Normalized Comprehensive Area Ratio (CA_r').

The concept of CA_r is to divide the comprehensive area of the pavement profile by the comprehensive area of an imaginary rigid pavement section. A strong pavement section would cover more area than a weak pavement section and hence CA_r would be higher for a strong section and comparatively less for a weak section. For an extremely stiff pavement section, the CA_r value could be nearly 1.0 while a weak section may have a CA_r value of 0.1. Based on literature, it is known that area ratio parameter accounts only for the structural capacity of pavement sections above subgrade. Combining the area ratio and central deflection into a single parameter could account for the structural condition of the entire pavement structure, therefore, Normalized Comprehensive Area Ratio (CA_r') is introduced as shown in Equation 1.

$$CA_r' = (50 / D_0^2 * 1500) / \{((D_0 + D_{1500}) / 2) + \sum_{i=50}^{1450} Di\} \text{ ...... (1)}$$

Where; D_0 is the center deflection; D_{1500} is the deflection at offset 1500 mm from the load plate; and D_i is the deflection at offset i (mm) from the load plate.

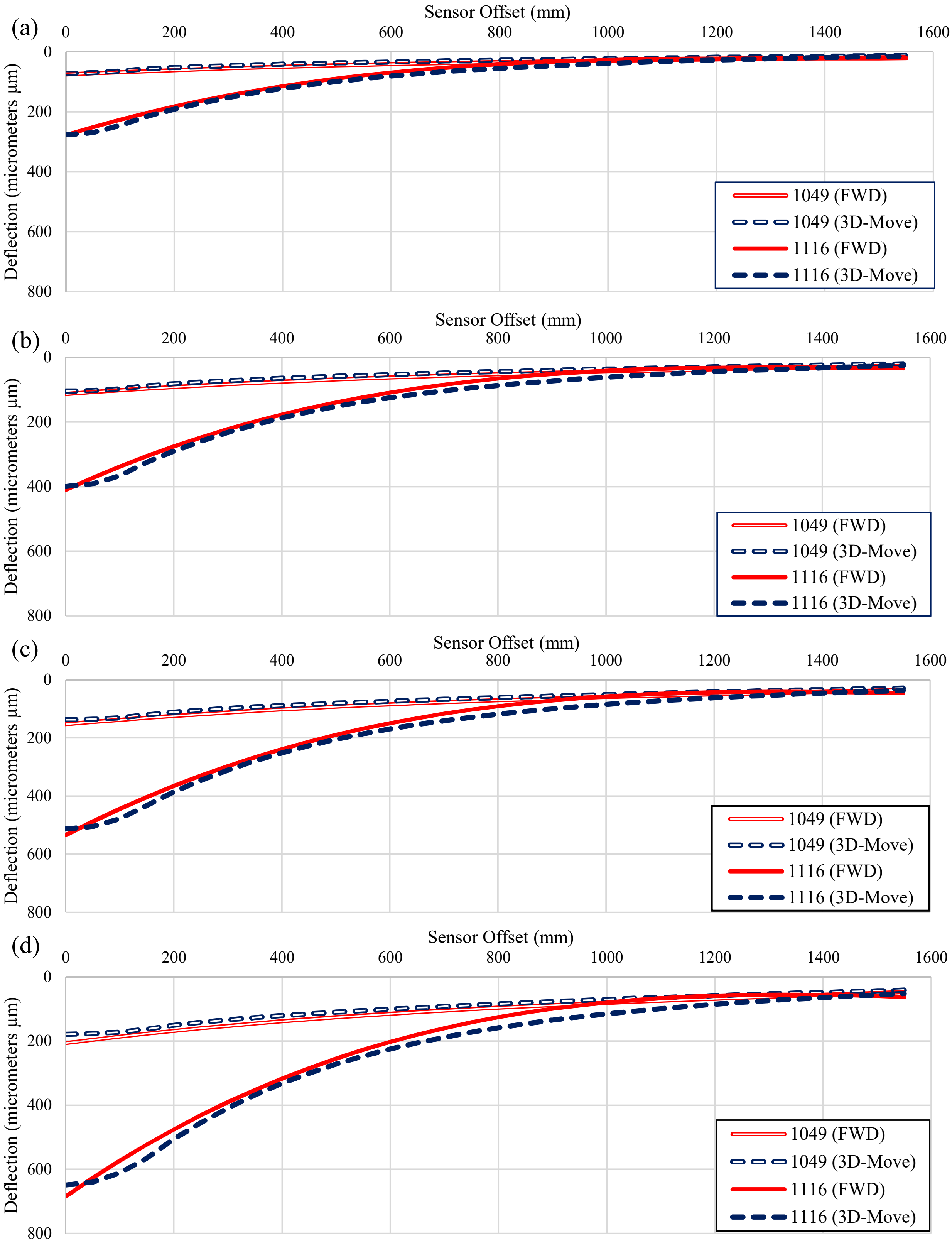

Figure 1 Measured FWD & 3D Move simulated deflection bowls for SHRP sections 1049 and 1116. (a) Drop Height 1, (b) Drop Height 2, (c) Drop Height 3, and (d) Drop Height 4.

A Strong correlation was observed between D_0 and CA_r', which proves that CAr' may be utilized as a structural accessibility parameter. However, pavement sections cannot be ranked solely depending on central deflection. In order to categorize and develop a scoring scale to rank pavement sections, the newly developed parameters were compared to the measured fatigue cracking recorded onthe pavement sections. Pavement sections with lesser fatigue area exhibited higher CA_r' whereas sections with higher fatigue area exhibited lesser CA_r'. CA_r' was found to be effective to represent the structural capacity of entire pavement structure, which can be observed in the comparison between pavement sections having different layer properties, as shown in Table 1.

Table 1. Comparison of pavement structural properties with respect to fatigue and CAr'.

SHRP ID	Pavement layer properties						CA_r'	Fatigue Area (%)	Pavement Classification
	Layer thicknesses (mm)			Layer moduli (MPa)					
	HMA	Base	Subbase	HMA	Base	Subbase			
1049	117	284	198	10,053	2,758	689	6.5	2	Good
1069	241	386	165	4,468	193	117	3.1	9	Fair
1116	117	277	0	3,351	262	0	1.2	26	Poor

CA_r' was well related to the tensile strain (ε) developed at the bottom of asphalt layer as well (Equation 2). The relationship represents that pavement sections experiencing lesser tensile strain would serve for higher number of load cycles until failure and pavement sections with higher tensile strain would handle significantly lesser number of load cycles before failure. Though pavement sections could be categorized based on their tensile strain, the number of load cycles to failure would serve the transportation agencies in a better way to plan the maintenance activities in a timely manner.

$$\varepsilon = 310.06 * CA_r'^{\,-1.219} \qquad \text{...... (2)}$$

$R^2 = 0.95$

The Remaining service life in terms of number of load repetitions to fatigue failure (N_f) was calculated utilizing the MEPDG equation. Calculated N_f was based on the elastic moduli of asphalt layer and the tensile strain at the bottom of HMA. Since CA_r' is well related to the tensile strain, it has a strong correlation with the remaining service life, as observed in the Figure 2. The relationship illustrates that the single, yet robust parameter CA_r', can be utilized to predict the remaining service life of any pavement section based on its deflection profile. Remaining service life can be assessed utilizing the relationship shown in Equation 3. Based on the relationship observed between CA_r' and measured fatigue as well as remaining service life, a scale was developed to classify pavement sections.

$$N_f = 553{,}694.910 * CA_r'^{\,3.110} \qquad \text{...... (3)}$$

$R^2 = 0.957$

Considering four drop heights during FWD testing (four load levels), four scales were developed to represent each load level. Table 2 shows the scale developed to categorize pavement sections as structurally good, fair, and poor. Therefore, CA_r' can be considered as a reliable parameter as it includes the entire deflection bowl rather than deflection at one point.

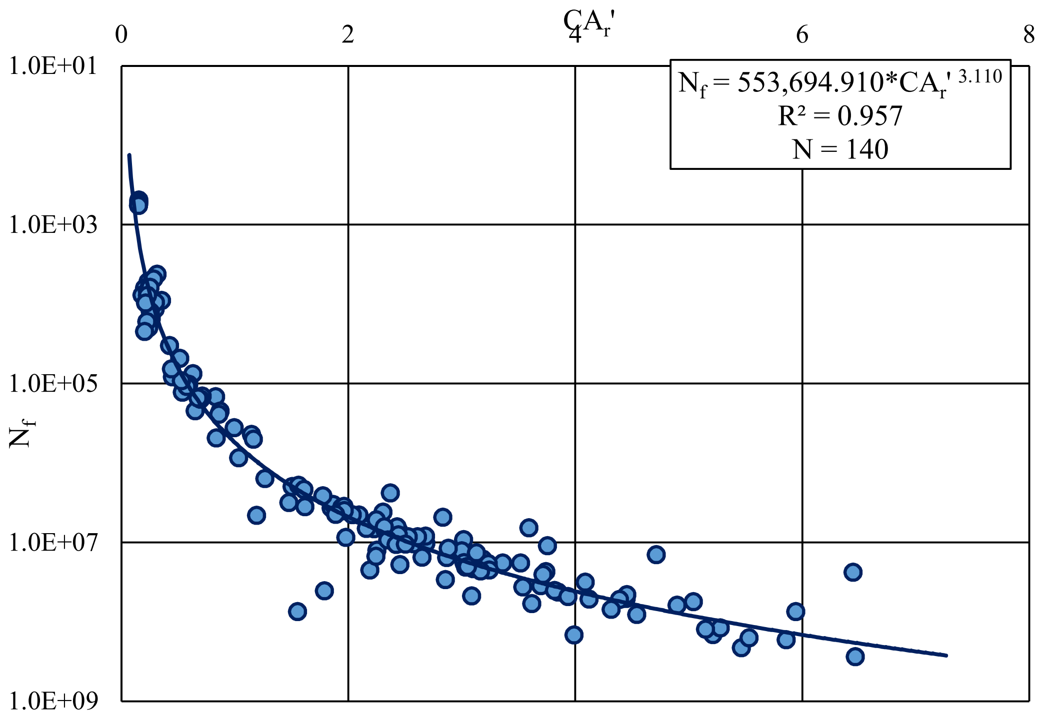

Figure 2. Relationship between Nf and CAr'

Table 2. Developed range of scale for CAr'.

Normalized Comprehensive Area Ratio, CA_r' ranges			
Target Load	Pavement structural capacity ranking		
	Good	Fair	Poor
27 kN (6,000 lbs)	> 4.0	2.0 - 4.0	< 2.0
40 kN (9,000 lbs)	> 3.0	1.5 - 3.0	< 1.5
53 kN (12,000 lbs)	> 2.0	1.0 - 2.0	< 1.0
71 kN (16,000 lbs)	> 1.8	0.8 - 1.8	< 0.8

CONCLUSION

Measured FWD deflection bowls were successfully simulated utilizing 3D Move analysis software package, which can limit the use of extensive FWD field testing. Normalized comprehensive area ratio (CA_r') was found to have a strong relationship with pavement critical responses such as central deflection (D_0) and tensile strain at the bottom of HMA (ε). Since strong relationship was observed between CA_r' and the tensile strain at the bottom of the asphalt layer, it is obvious that CA_r' must be effective to predict the remaining service life. Hence, CA_r' can be concluded as a robust, simple and practical method for the structural capacity evaluation of flexible pavements at the network level. Developed single and overall parameter, CA_r', would help the south-central state DOTs and local highway agency officials making more informed decisions about the most suitable maintenance and rehabilitation strategies.

REFERENCES

Coetzee, N. F., Van Wijk, A. J., & Maree, J. H. (1989). *Impact Deflection Measurements* Proceedings of the 5th Conference on Asphalt Pavements in Southern Africa, Swaziland.
Gedafa, D. S., Hossain, M., Miller, R., & Van, T. (2010). *Estimation of remaining service life of flexible pavements from surface deflections,* Journal of Transportation Engineering, 136(4), 342–352.
Haas, R., Hudson, R., & Tighe, S. (2001). *Maximizing customer benefits as the ultimate goal of pavement management,* 5th International Conference on Managing Pavements, TRB, Washington, DC.
Scullion T. (1988). *Incorporating a Structural Strength Index into the Texas Pavement Evaluation System*, Research Report 409 – 3F, Texas Transportation Institute.
Zhang, Z. E., *Development of a New Methodology for Characterizing Pavement Structural Condition for Network Level Applications*, Texas Dept. of Transportation, Austin, TX, 2003.
Saleh, M. (2015). *Utilization of the Deflectograph Data to Evaluate Pavement Structural Condition of the Highway Network*, DOI: 10.1080/14680629.2015.1064823.

Structural Health Monitoring using Magnetic Shape Memory Alloy Cables in Concrete

Allen Davis, Mirmilad Mirsayer, Emery Sheahan, and Darren Hartl

Texas A&M University

INTRODUCTION

Embedding shape memory alloy (SMA) wires in concrete components offers the potential to monitor their structural health via external magnetic field sensing. Currently, structural health monitoring (SHM) is dominated by acoustic emission and vibration-based methods. Thus, it is attractive to pursue alternative damage sensing techniques that may lower the cost or increase the accuracy of SHM. In this work, SHM via magnetic field detection applied to embedded magnetic SMAs (MSMAs) is demonstrated both experimentally and using computational models. A concrete beam containing iron-based MSMA wire is subjected to a 3-point bend test where structural damage is induced, thereby resulting in a localized phase change of the MSMA wire. Magnetic field lines passing through the embedded MSMA domain are altered by this phase change and can thus be used to detect damage within the structure.

MSMAs, known for their ability to change properties with their respective phase changes, can alter magnetic fields due to their change in magnetic permeability in the presence of internal stress. This use of magnetic sensing for non-destructive evaluation represents an inherently multidisciplinary research area with respect to both the computational and experimental domain. The analysis of phase transforming wires embedded in a concrete structure for the manipulation of a magnetic signal requires a strong understanding of the solid mechanics of the concrete-wire interface, the use of external magnetic sensing (and thus related work with metrology sensitivities, probe placement, and specimen size), and the ability to translate magnetic signals into internal stress fields.

Fortunately, a history of previous successes for each method exists individually. SMA wires have been embedded into concrete specimens for structural reinforcement and shown to improve the life of the structure [1], taking advantage of the super-elastic properties of MSMAs. Ferromagnetic SMAs, specifically FeMnAlNi (FMAN), have been developed with the strength required for structural reinforcement and a recoverable super elastic effect [2], and samples of these specimens have been produced by Karaman and coworkers. Embedded inductive sensors have been developed to monitor the corrosion of internal steel rebar [3], but this technique requires an applied electric current, and only shows the average corrosion between two points. Additional work on monitoring steel corrosion has proven magnetic sensing a viable method of non-destructive evaluation of similar structures, with obtained magnetic signals shown to be significantly strong as compared the background noise present in the system [4]. As for interpreting the detected magnetic fields, computational work has been previously done by Hartl and coworkers to transform signals generated from distributions of distinct embedded MSMA domains into internal continuous stress fields [5]. The purpose of the current work is the development of computational models and experimental work to integrate these previous and current developments into a robust model with the experimental results correlated to FEA models, leveraging previous FEA and experimental work on SMAs where possible.

The structural mechanics of the concrete-embedded wire system are modeled in Abaqus as an embedded wire in a concrete block. The model, created for both steel and MSMA wires, applies a load at the center of the block, inducing a crack which propagates through the block and wire.

As the crack nears the MSMA wire the stress on the wire increases, changing the local martensite volume fraction (MVF). Local changes in MVF are input into the COMSOL model to simulate external detection by magnetic sensing. The COMSOL model considers the local magnetic permeabilities of the embedded wire in performing a magneto-static analysis to determine the global magnetic field. With the global magnetic field calculated in COMSOL, a parametric study is then scripted using MATLAB to determine the change in magnetic field along the wire's length. The changes in magnetic field strength and MSMA phase transformation are compared to non-transformed portions of the wire. This model supports the feasibility of non-destructive evaluation for SHM using magnetic sensing and SMAs using a robust computational model to simulate the solid mechanics and magnetic sensing capabilities of the system.

METHODOLOGY

Structural Modeling

The Abaqus model is constructed as a concrete block with an embedded wire using C3D20R elements (a 20 node quadratic brick, reduced integration). The load conditions of a 3-point bend test are applied, with a crack introduced at the bottom of the block to specify the crack propagation's start. The MSMA wire is modeled using a user material subroutine to calculate the MVF as the stresses on the wire change due to the applied load and crack propagation. The crack propagates from the concrete block's bottom to top, around the wire and breaking the cohesion between wire and concrete near the crack. The Abaqus model calculates the stress in each time step, then determines the new MVF to input into the next time step.

The concrete's crack propagation utilizes the extended finite element method (XFEM) in Abaqus. The Abaqus model uses a traction-separation model to calculated the fracture. This model uses a scalar damage parameter D, which ranges from 0-1 [6]. This model requires the fracture energy of the material, which is derived from literature and experimental testing.

The Abaqus model utilizes a User Material Subroutine (UMAT) to characterize the wire's SMA behavior. The foundation and background for the constitutive model for the SMA structural response is provided elsewhere [7] and has been used to analyze a number of SMA applications [8-9].

Magneto-Static Modeling

The magnetic sensing and evaluation is modeled using COMSOL magneto-statics. This model demonstrates the sensing capabilities of an external magnet and sensor detecting an internal change in the MSMA wire, determining the change in detected magnetic field of the sensor. The model consists of an MSMA wire embedded in a concrete block, with a permanent magnet on one side of the concrete block generating a magnetic field. The magnetic sensor is simulated using a probe on the face of the concrete block opposite the magnet, while the permanent magnet is defined with a residual flux density of 1.2 T. This value matches the higher end of AlNiCo magnets, permanent magnets typically used for industrial applications and consumer products. The concrete specimen is a 150 mm by 50 mm by 50 mm block, the same size as the samples used in the 3-point bend tests and structural model. The magnet has a radius of 25 mm and thickness of 10 mm. The sensor is modeled as a point probe measuring the normal magnetic field strength, the same output as a Hall sensor. An air domain encompassing the entire model is required for flux conservation, with size studies performed to ensure the domain is sufficiently large.

FINDINGS

Structural Results

The Abaqus model evaluates the state of the MSMA wire as a crack propagates through the concrete block. The load applied to the concrete is transferred to the wire, particularly near the crack. The wire's stress instigates the SMA phase transformation, which is shown in Figure 1. The local transformation of the wire near the crack provides a simple input into the COMSOL model, due to the consistent MVF along the cross-section.

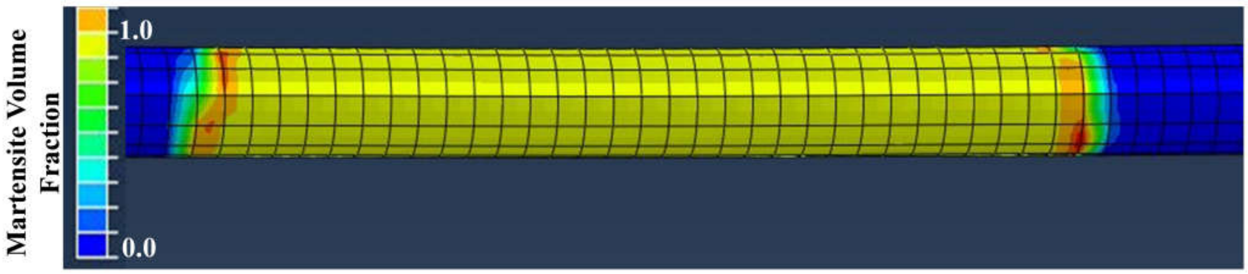

Figure 1. The MVF of the wire changes significantly near the crack, with approximately one cm of wire almost fully transformed.

Magnetic Sensing

Using the scripted search along the length of the concrete block for a single wire, the COMSOL model shows a distinct change in magnetic field near the phase transformation, as shown in Figure 2. This decrease in field strength very close to the phase transformation is due to the stronger magnetic field near the magnet edge, which are 0.025m away from the magnet's center. Braided cables show a similar result when detecting a phase transformation, but with a much larger change in magnitude due to the large cross-sectional area. Comparing the braided wire to a single wire with the same cross-sectional area, the braided cable shows a very similar recorded magnetic field strength compared to the single wire. Additionally, the increase in field strength presents a slightly more distinct profile over a slightly smaller area for the braided cable when compared to the single wire. When accounting for the cross-sectional area of the cable and wire, the effect of an identical phase transformation yields very similar results. The larger change in field strength in both of these tests as compared to the 1 mm radius single wire model shows the correlation between wire radius and magnetic sensitivity of the system, as the sevenfold increase in cross-sectional area increases the change in magnetic field strength from four percent to over 15 percent.

CONCLUSIONS

The Abaqus model shows how the solid mechanics of a crack propagating past an MSMA wire, and the resulting phase transformation. There is a significant transformation near the crack, in which over 1 cm of wire is transformed to martensite, while the surrounding wire's MVF quickly decreases at larger distances from the crack. This transformation is then input into COMSOL to simulate a non-destructive evaluation of the same wire using external magnetic sensing. As the permanent magnet and sensor are moved down the length of wire along the sides of the concrete block, the magnetic field changes near the phase transformation. For the single wire modeled in Abaqus, there is a 4 percent change in the magnetic field strength near the crack. Implementing a braided cable in place of a single wire does not create a significant change in recorded magnetic field strength when accounting for the change in cross-sectional area. However, that increase in cross-sectional area increases the maximum change in magnetic field strength from four percent to over 15 percent.

REFERENCES

[1]. Zafar, A. and Andrawes, B., \Experimental flexural behavior of sma-frp reinforced concrete beam," Frontiers of Structural and Civil Engineering 7, 341{355 (Dec. 2013).

[2]. Tseng, L. W., Ma, J., Wang, S. J., Karaman, I., Kaya, M., Luo, Z. P., and Chumlyakov, Y. I., \Superelastic response of a single crystalline femnalni shape memory alloy under tension and compression," Acta Materialia 89, 374{383 (May 2015).

[3]. Simonen, J. T., Andringa, M. M., Grizzle, K. M., Wood, S. L., and Neikirk, D. P., \Wireless sensors for monitoring corrosion in reinforced concrete members," 5391, 587{597, International Society for Optics and Photonics (July 2004).

[4]. Popovics, J. S., Gallo, G. E., Shelton, M., and Chapman, P. L., \A magnetic sensing approach to characterize corrosion in reinforced concrete," 6529, 65291A, International Society for Optics and Photonics (Apr. 2007).

[5]. Bielefeldt, B. R., Benzerga, A. A., and Hartl, D. J., \Analysis of shape memory alloy sensory particles for damage detection via substructure and continuum damage modeling," 9800, 98000B, International Society for Optics and Photonics (Apr. 2016).

[6]. Broekaart, D., \Modelling crack propagation using xfem," (Mar. 2017). https://info.simuleon.com/blog/modelling-crack-propagation-using-xfem.

[7]. Lagoudas, D., Hartl, D., Chemisky, Y., Machado, L., and Popov, P., \Constitutive model for the numerical analysis of phase transformation in polycrystalline shape memory alloys," International Journal of Plasticity 32-33, 155-183 (2012).

[8]. Hartl, D. and Lagoudas, D., \Characterization and 3-d modeling of ni60ti sma for actuation of a variable geometry jet engine chevron," Proceedings of the SPIE - The International Society for Optical Engineering 6529, 65293Z (12 pp.) (2007).

[9]. Peraza Hernandez, E., Hartl, D., and Malak, R., [Design and numerical analysis of an SMA mesh-based self-folding sheet], vol. 22 (Aug. 2013). DOI: 10.1088/0964-1726/22/9/094008.

Incentive Programs for Closure of Grade Crossings in The United States: A State-Of-The-Practice Synthesis

Julius Codjoe[1], Samira Soleimani[2], and Seth J. Ledet[3]

[1]ITS/Traffic Research Associate V, Louisiana Transportation Research Center
[2]Department of Geography & Anthropology, Louisiana State University
[3]Department of Civil and Environmental Engineering, Louisiana State University

INTRODUCTION

Considering the country's approximately 212,950 grade railroad crossings (including open crossings, reopened crossings, and new crossings) (1), the United States has always faced safety challenges involving collisions between trains and vehicles/ pedestrians. In addition to the loss of life and injuries resulting from these incidents, railroad administrators and state agencies incur massive financial burdens due to delays in services, and liability issues including damage to trains, tracks, and equipment. Some possible solutions to reduce the number of collisions at grade crossings are road active alarms, auditory alarms, in-vehicle alarms, visibility improvements, gates, corridors, grade separations, track relocation, grade crossing closures, and, crossing consolidation. It is usually difficult to prioritize which grade crossings to close or consolidate since every crossing has unique attributes. Moreover, residents are usually opposed to closing a crossing because they believe it will become a loss of property or it will inconvenience them (2).

The Federal Railroad Administration (FRA) has not mandated any state agency to offer specific incentive programs to its citizens for the purpose of closure or consolidation of grade crossings. Therefore, each state agency maintains its own programs. Primarily, these programs have been in the form of financial incentives which fund safety projects for the affected owners, and with each state agency having its own conditions attached. With limited state budgets, it is imperative that a state agency identifies the balance between the amount of available budget for incentives and the amount for its other programs. Therefore, each state has to continually evaluate its incentive programs to determine which ones offer the best value to its citizens. However, no such study to date synthesizes all of the current incentive programs provided by each state. Maintaining such a document will provide an easy and comprehensive means for state agencies and railroad entities to evaluate their programs in relation to other states nationwide. This study aims to contribute valuable information to the practice by offering state agencies and railroad entities a comprehensive reference document that lists the current incentive programs adopted by each state.

The remaining parts of this paper are organized as follows: a methodology section with a list of current incentive programs offered by each state based on the information retrieved from a questionnaire as well as online public resources; a summary and discussion of the study's findings; and finally a discussion of future work.

METHODOLOGY

In order to find out which incentive programs each state employs to reduce their number of at-grade railroad crossings, this study utilized a combination of public online resources, as well as a survey distributed among railroad crossing safety experts and personnel from state Departments of Transportation (DOT). The survey, designed with Qualtrics, included the following questions:

1. Some incentive programs for railroad closure/ consolidation are Cash Incentives, Nearby Roadway/Crossing Improvement, and Track Relocation programs. Does your state/ agency offer or administer an incentive program(s) for closure of at-_grade crossing?
2. Which type of incentive program(s) does your state/ agency offer or administer? Please provide any information on your program(s).
3. How long has your program(s) been in effect?
4. How effective is your incentive program(s) in achieving your goals of railroad closure/ consolidate?
5. In your view, what are the reasons for not having a very effective program(s)?

The survey was distributed to 240 railroad company experts, as well as 52 verified experts working in DOTs nationwide. Overall, there were 60 completed responses obtained, which included 33 responses from railroad companies, and 27 from state DOTs. The only states with no responses from either a railroad company or a state DOT were California, Arizona, Connecticut, Hawaii, Iowa, Maryland, Missouri, Nevada, New Hampshire, Rhode Island, Pennsylvania, and Vermont.

In the survey, experts could select any incentive program choices they used in their state or agency. However, 15 personnel from railroad agencies as well as 13 from DOTs, mentioned that they have no incentive programs for crossing closures. Based on the rest of responder's choice counts, 22 responders selected the cash incentive program, 12 selected the roadway/crossing improvement, 9 selected nearby crossing grade separation programs, and 3 selected track relocation programs. The responders could then rate the effectiveness of each program(s) they have selected and point out the main weakness within the program(s). Afterwards, the mean overall effectiveness of each program is calculated in Qualtrics data analysis section.

FINDINGS

Illustrated in Table 1 are the responses from the railroad companies from the various states regarding their existing incentive programs. The responses from DOTs are also shown in Table2, along with findings from the review of available online public resources.

The results show that approximately 53 percent of participants believe their states have a specific incentive program for consolidation or closure while the remaining 47 percent could not identify an existing incentive program. Illustrated in Figure 1 is the effectiveness of various incentive programs based on the responders' knowledge. The data analysis section of Qualtrics software provided the overall average effectiveness of each choices. Based on the choice counts, the most common incentive program is the cash incentive even though Figure 1 shows it is the least effective.

CONCLUSION

Prior to this research, a comprehensive study of all the states' incentive programs for crossing consolidation was mostly unknown. This research aims not only to attract attention to current incentive programs, but also to give individual states the opportunity to compare their processes with that of the rest of the nation.

Table 1 Existing incentive programs as reported by railway companies

Railroad Companies	Incentive Program(s)
Huntsville & Madison Railroad Authority (*Alabama*)	Cash Incentive
Alaska Railroad Corporation (Alaska)	No Answer
A&M Railroad (*Arkansas*)	No Incentive program
San Luis Central Railroad (*Colorado*)	No Incentive program
Colorado Public Utilities Commission (*Colorado*)	No Incentive program
Florida Central Railroad (*Florida*)	Nearby Crossing Improvement
Norfolk Southern (*Georgia*)	Cash Incentive, Nearby Crossing Improvement
Kankakee, Beavervill, and Southern RR (*Illinois*)	Cash Incentive, Road Improvement, Nearby Crossing Grade Separation, Nearby Crossing Improvement
Illinois Central Railroad Company (*Illinois*)	Cash Incentive, Finding alternative route to offset removal of an at-grade crossing
Norfolk Southern (*Indiana*)	Cash Incentive, Nearby Crossing Grade Separation
Delta Southern Railroad (*Louisiana*)	No Incentive program
Wacto Companies, LLC (*Louisiana*)	No Incentive program
Pinsly Railroad Company (*Massachusetts*)	No Incentive program
Cloquet Terminal Railroad (*Minnesota*)	No Incentive program
Mississippi Export RR (*Mississippi*)	An incentive program is available
BNSF Railway (*Mississippi*)	Road Improvement, Nearby Crossing Improvement
Norfolk Southern Railway (New Jersey)	No Incentive program
Santa Fe Southern Railroad (New Mexico)	No Incentive program
Western New York & Pennsylvania Railroad (New York)	No Incentive program
Ohio-Rail Corp. (Ohio)	No Incentive program
Ashland Railway Inc. (Ohio)	A combination of all incentive programs
CSX Transportation (Ohio)	Cash Incentive, Road Improvement, Nearby Crossing Improvement, Support for quiet zone establishment
Ohio Rail Development Commission (Ohio)	Cash Incentive, Road Improvement, Nearby Crossing Improvement, Track Relocation
Norfolk Southern Corporation (Ohio)	Cash Incentive, Road Improvement, Nearby Crossing Improvement, Nearby Crossing Grade Separation
Farmrail System (Oklahoma)	No Incentive program
Oregon Pacific Railroad (Oregon)	No Incentive program
West Tennessee Railroad (Tennessee)	No Incentive program
Fort Worth & Western Railroad (Texas)	Cash Incentive
Port & Pend Oreille dba Pend Oreille Valley Railroad (Washington)	No Incentive program
Watco Companies LLC (Wisconsin)	Cash Incentive

Table 2 Existing Incentive Programs per DOT Personnel, and Online Information Detailing Each State's Crossing Safety Program

State	DOT Survey results	Available Online Resources for Safety Programs
AR	*No Incentive programs*	State funds have only been used sparingly. When state funds are used, they come from the General Improvement Fund, whose rail funding depends on a separate contingency fund.
DE	*No Incentive programs*	The Delaware Capital Transportation Program is a six-year investment program that is annually updated to fund infrastructure projects throughout the state. Delaware also encourages private-public partnerships.
ID	*No Incentive programs*	The Idaho Transportation Board allocates $250,000 annually from the State Highway Distribution account for rail safety projects. Local funding mechanisms include tax increment financing, revenue anticipation bonds, and local option taxes.
IL	Cash Incentive, Road Improvement, Nearby Crossing Grade Separation, Nearby Crossing Improvement	The Grade Crossing Protection Fund (GCPF) was created by the General Assembly to assist local jurisdictions in paying for safety improvements at crossings. Each month $3.5 million in state motor fuel tax is transferred to the GCPF.
IN	Cash Incentive	INDOT offers incentive funding to communities who close grade crossings through the Grade Crossing Fund which provides up to $40,000 for safety improvement projects along grade crossings.
KS	Track Relocation, Nearby Crossing Improvement	The State funds a Highway-Rail Crossing Program that allocates $300,000 annually for crossing projects that are not eligible for federal aid. A 20% match is required to receive a grant.
ME	No Incentive programs	The State's Grade Crossing Safety Improvement Program funds safety projects at grade crossings. The program's funding is provided through a biennial legislative appropriations process.
MI	Cash Incentive, Track Relocation	The Crossing Surface Program funds 60% of the cost of a surface improvement. The Local Grade Crossing Program allows MDOT to pay cash incentives worth $150,000 to local authorities for crossing closures.
MN	Cash Incentive, Road Improvement, Nearby Crossing Improvement	MnDOT funds the Railroad-Highway Crossing Safety Improvement Program which applies federal and state funds for different crossing projects. The Antiquated Equipment Replacement Program uses $2 million of these funds to upgrade warning systems annually.

MS	Cash Incentive, Nearby Crossing Improvement	The State's Railroad Multimodal Transportation Improvement Program funds projects that improve the safety of publically owned railroads. The program receives 12% of the Multimodal Funds annually.
MT	Cash Incentive	-
NE	Cash Incentive, Road Improvement, Nearby Crossing Improvement, Nearby Crossing Grade Separation	The State Grade Crossing Protection Fund provides monetary incentives to local governments for crossing closures. $5,000 plus the cost of the closure will be paid for by the state and the Railroad Company.
NJ	Cash Incentive, Road Improvement, Nearby Crossing Improvement	The Rail Freight Assistance Program provides grants that cover 90% of the project cost. The rail line must continue service for at least five years following the upgrade.
NM	No Incentive programs	The State can fund rail safety improvements through Legislative Appropriations in which funds are granted through tax bond proceeds or from the General Fund.
NC	Cash Incentive, Road Improvement, Nearby Crossing Grade Separation, Nearby Crossing Improvement, Track Relocation	The Rail Industrial Access Program aids safety and construction projects by covering 50% of the costs. North Carolina Rail & Rail Crossing Safety Improvement Fund is allotted money through dividends made by the North Carolina Railroad Company.
ND	No Incentive programs	The NDDOT administers the Local Rail Freight Assistance loan fund. Loans may cover 80% of the cost with 0% - 4.5% interest. Applicants have a 15-year payback schedule.
OK	Nearby Crossing Improvement	The State plans to dedicate $100 million to rail crossing improvements to be used over the space of the upcoming years.
OR	No Incentive programs	Oregon's Grade Crossing Protection Account is accredited $300,000 through the State Highway Fund to aid grade crossing projects. ConnectOregon improves connections between intermodal transportations. It is funded through bonds and lottery proceeds and requires a 20% match.
SC	No Incentive programs	Most rail projects are privately funded by Rail Companies with help from federal program funding, as South Carolina does not have any dedicated funding sources.
SD	No Incentive programs	The South Dakota Railroad Trust Fund is set up to maintain and equip railroad infrastructure. This program may also be used to match Federal railroad funds.
UT	Ask for two closures to trade for the new one	The Spot Safety Improvement Program funds infrastructure projects that are expected to achieve a significant reduction in traffic fatalities

		and injuries. $2 million is available annually.
TN	Cash Incentive, Nearby Crossing Improvement, Nearby Crossing Improvement	The State relies on the federally funded Section 130 program to fund crossing projects and other safety improvements.
UT	Ask for two closures to trade for the new one	The Spot Safety Improvement Program funds infrastructure projects that are expected to achieve a significant reduction in traffic fatalities and injuries. $2 million is available annually.
VA	No Incentive programs	Rail Preservation Program funds projects that increase the safety and efficiency of short-lines. It is allocated $3 million annually and supports 70% of the project.
WV	No Incentive programs	The State Rail Authority receives state budget appropriations of roughly $7.7 million over five years to implement safety improvements along specific corridors.
WI	Cash Incentive	The Freight Railroad Preservation Program provides grants to local governments to improve their rail lines. These grants cover 80% of a project’s cost and are paid for by bonds.
WY	No Incentive programs	WYDOT has the legislative authority to maintain a Highway Crossing Protection Account within the State Highway Fund to administer safety projects along crossings.

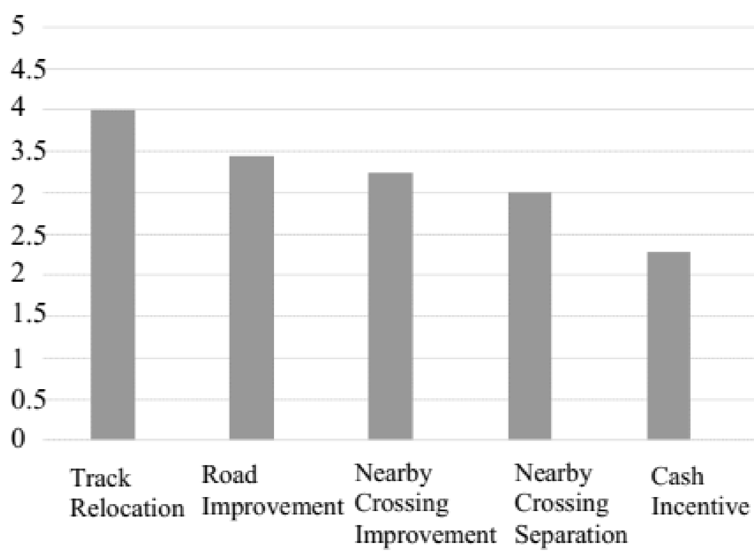

Figure 1 Efficiency of available incentive programs for railroad closure

The information gathered from online resources reveal that most incentive programs provide funding to cover a portion of a safety improvement project in regards to a railroad-highway crossing, with the applicant having to provide the remaining costs. Some programs also allow states to pay a required 10% match to gain federal funding for projects, as most states prioritize qualifying for federal funding before other sources of funding. States such as Michigan, Nebraska, and Texas have had success with providing incentive payments to local governments whenever the local government decides to voluntarily close a crossing. A percentage of states rely on one-time Legislative Appropriations to fund specific rail safety projects within a given year. To be able to support rail safety projects on the state and local level, states have also had success with regional funding mechanisms such as local sales tax and tax increment financing. Besides being funded either federally, by the state, or locally; safety projects can also be paid for by the railroad companies themselves. This can be seen in states such as Delaware where private-public partnerships have funded rail projects in the past.

Figure 1 shows that the track relocation program is the most effective but rarely utilized. This is evident in Table 2 where only four states reported using the track relocation program: Kansas, Ohio, North Carolina, and Michigan. The road improvement, nearby crossing improvement, and adjacent crossing grade separation programs have an effectiveness value of approximately 3.45, 3.25, and 3, respectively. The high cost of upgrade and renovation to infrastructures prevents the future success of any improvement-based incentive programs. Finally, the cash incentive program had the lowest effectiveness value with 2.29, even though this incentive program is the most popular one among states. Most of the existing incentive programs are not very useful due to the fact that communities are emotionally protective of redundant crossings and that local political pressure against the closure of a crossing is substantial. In addition to the most common incentive programs, the study discovered three other types of programs in Utah, Ohio, and Illinois that include compromising two closures in exchange for a new one, supporting a quiet zone establishment, and considering alternative routes to offset the removal of an at-grade crossing.

As a future goal, the authors are working to design a comprehensive consolidation model, which will consider various crossing characteristics. This will allow the research community to go one step further towards predicting the future conditions that a closed crossing will trigger on its environment. The urban planning of a city, social factors, land use management, infrastructure systems, accessibility, community cohesion, environmental management, crisis management, and economic condition of various facilities may be affected by a wrong choice of closure management. Such a model could predict the priority rating of each crossing for any safety improvement or closure program in the future.

REFERENCE

[1]. Research Information Management System (RIMS) Database. www.website.org. Accessed July 15, 2017.

[2]. Fakhrhosseini, S. Maryam, Myounghoon Jeon, Pasi Lautala, and David Nelson. An Investigation on Driver Behaviors and Eye-Movement Patterns at Grade Crossings Using a Driving Simulator. In 2015 Joint Rail Conference, pp. V001T06A012- V001T06A012. American Society of Mechanical Engineers. 2015.

[3]. De Gruyter, C., & Currie, G. Impacts of Rail-Road Crossings: International Synthesis and Research Gaps. In Transportation Research Board 95th Annual Meeting (No. 16- 1588). Iowa (Doctoral dissertation, Iowa State University). 2016.

[4]. US Department of Transportation, Federal Railroad Administration, Research Results, Crossing Consolidation Guidelines, Report # RR 09-12, July 2009.
[5]. Chadwick, S. G., Zhou, N., & Saat, M. R. Highway-rail grade crossing safety challenges for shared operations of high-speed passenger and heavy freight rail in the US. Safety Science, 68, 128-137. 2014.
[6]. Gabree, S. H., Chase, S., & Desilva, M. Effect of Dynamic Envelope Pavement Markings on Vehicle Driver Behavior at a Highway-Rail Grade Crossing. US Department of Transportation, Federal Railroad Administration, Office of Research and Development. 2014.
[7]. Larue, G. S., Kim, I., Rakotonirainy, A., Haworth, N. L., & Ferreira, L. Driver's behavioural changes with new intelligent transport system interventions at railway level crossings—A driving simulator study. Accident Analysis & Prevention, 81, 74-85. 2015.
[8]. Landry, S., Jeon, M., Lautala, P., & Nelson, D. Getting Active With Passive Crossings: Investigating the Use of Auditory Alerts for Highway-Rail Grade Crossings. In 2016 Joint Rail Conference (pp. V001T06A019-V001T06A019). American Society of Mechanical Engineers. April 2016.
[9]. Govoni, M., Guidi, F., Vitucci, E. M., Degli Esposti, V., Tartarini, G., & Dardari, D. UWB multistatic radars for obstacle detection and imaging in railroad crossing areas. In Proc. 12th Wksp. Positioning Navigation and Commun (WPNC). 2015.
[10]. Kumar, A., Das, A. K., Kumar, A., & Sahu, R. Automated Unmanned Railway Gate. Imperial Journal of Interdisciplinary Research, 3(4). 2017.
[11]. Rodriguez, A., Engineer, E. A., Brinckerhoff, P., & Engineer, S. S. Railroad-Highway Grade Crossing Analysis for Corridor Planning Projects. In Transportation Research Board 95th Annual Meeting (No. 16-4373). 2016.
[12]. Landry, Steven, Myounghoon Jeon, and Pasi Lautala. Effects of Driver Attention on Rail Crossing Safety And The Effects of Auditory Warnings and Driver Distraction on Rail Crossing Safety. No. NURail2012-MTU-R03. Michigan Technological University, 2016.
[13]. Johnson, P. M. An investigation of railroad-highway grade crossing consolidation rating in Iowa (Doctoral dissertation, Iowa State University). 2015.
[14]. Taylor, J., & Crawford, R. Prioritising road-rail level crossings for grade separation using a multi-criteria approach. In Australasian Transport Research Forum (ATRF), 32nd, 2009, Auckland, New Zealand (Vol. 32). 2009.
[15]. Hans, Z., Albrecht, C., Johnson, P. M., & Nlenanya, I. Development of Railroad Highway Grade Crossing Consolidation Rating Formula. 2015.
[16]. Arellano, J. R., Mindick-Walling, A., Thomas, A., & Rezvani, A. Z. Prioritization of Infrastructure of Investment for Rail Safety Projects: Corridor Level Approach (No. 17-04963). 2017.
[17]. Schrader, M., & Hoffpauer, J. Methodology for evaluating highway-railway grade separations. Transportation Research Record: Journal of the Transportation Research Board, (1754), 77-80. 2001.
[18]. Ćirović, Goran, and Dragan Pamučar. Decision support model for prioritizing railway level crossings for safety improvements: Application of the adaptive neuro-fuzzy system. Expert Systems with Applications 40, no. 6: 2208-2223. 2013.

[19]. Weissmann, A. J., Weissmann, J., Kunisetty, J. L., Warner, J., Park, E. S., Sunkari, S., ... & Venglar, S. Integrated Prioritization Method for Active and Passive Highway-Rail Crossings. 2013.
[20]. Austin, R. D., & Carson, J. L. An alternative accident prediction model for highway-rail interfaces. Accident Analysis & Prevention, 34(1),

Current Practices for Recruiting and Retaining Qualified Workers at State Transportation Agencies

Julia Hernandez[1], Kristal Metro[2], Christofer M. Harper[3], and Susan Bogus Halter[4]

[1]GRA, Bert S. Turner Department of Construction Management, Louisiana State University
[2]GRA, Department of Civil Engineering, University of New Mexico
[3]Assistant Professor, Bert S. Turner Department of Construction Management, Louisiana State University
[4]Professor, Department of Civil Engineering, University of New Mexico

INTRODUCTION

A safe, efficient, and effective transportation system is essential for the growth and stability of the nation's economy and the lifestyle of its inhabitants (Bertini, 2011). The effectiveness of the transportation infrastructure and service industry depends heavily on the ability to recruit and retain a highly skilled and qualified workforce. State departments of transportation (DOTs) currently face unprecedented challenges in recruiting and retaining the workforce necessary to function effectively (TRB, 2003). Many are the reasons for these challenges: demographic changes in the workforce; competitive labor market; new technologies; and demands on the transportation industry (Cronin et al., 2011).

The difference between older and younger generations has become a driving concern to human resource professionals as they prepare to manage the rapid demographic shifts expected in the transportation construction workforce (Gallagher & Villwock-Witte, 2016). According to the Transportation Research Board's 275 Report (2003), more than 50 percent of the state transportation agency workforce will be eligible to retire in the next 10 years, double the rate for the nation's entire workforce. As the retirement of the older generations increases, millennials are rapidly becoming the largest cohort within the transportation workforce (Gallagher & Villwock-Witte, 2016). The loss of experienced employees will result in core competency gaps needed for performance of certain job-related duties and responsibilities.

In addition to the demographic changes in the workplace, employee perceptions, values, and work ethics are also changing (TRB, 2003). Several studies consistently indicate that millennials place more value on work-life balance and leisure and seek more flexible and challenging work than their older generations counterparts (Jean, 2010). Conversely, millennials have the highest levels of job mobility of any generation (Gallagher & Villwock-Witte, 2016). Although the younger generation of workers "report higher levels of job satisfaction and less desire to leave their jobs" (Gallagher & Villwock-Witte, 2016, p. 44), they are willing to relocate across their workplace organization in search of professional development. Contrary to popular belief, millennials are interested in job security and stability. However, millennials are reluctant to work at state DOTs as these agencies are perceived as non-innovative and lacking interesting work.

State DOTs compete both with the private sector and with other public sector employers for transportation workers at all levels of experience (Gilliland, 2001). Transportation agencies offer employees stable work and a variety of benefit packages that include health, vacation and leave time, retirement, education opportunities, and training programs. However, recruitment and retention of qualified workers is challenging due to strong incentives offered in the private sector and other fields such as higher salaries and promotional opportunities (Cronin et al., 2011).

Transportation agencies typically offer lower salaries compared to the private sector, yet, DOTs can offer competitive benefits to offset the pay disparity (Anderson et al., 2010).

Recruitment and retention programs for professionals are essential to the success of a state DOT (TRB, 2003). Given the aforementioned workforce challenges, this research examined Region 6 state DOTs current and future transportation workforce issues, evaluated employee recruiting and retention strategies, and identified the practices that can have the potential for success and implementation in other DOTs. Region 6 includes the states of Texas, New Mexico, Arkansas, Oklahoma, and Louisiana.

To achieve and ensure this research complies with the need for transportation agency recruitment, the following research objectives have been established:

- Determine the best practices employed by transportation agencies that lead to recruitment of qualified transportation agency employees;
- Assess current best practices that are used to retain qualified and experienced transportation agency employees; and
- Identify potential institutional barriers that exist within transportation agencies that limit the recruitment and retention of high quality employees.

METHODOLOGY

The research completed to this point includes an in-depth literature review and interviews with DOT human resources staff. The literature review included collecting and reviewing pertinent journal articles, reports, DOT documents and previous research that reflects the practices used in transportation agencies relevant to recruiting, retaining, and promoting employees. The literature review provided the theoretical background for the study, as well as the basis for developing the coding structure to perform a content analysis of DOT human resource documents, reports, and training materials. The themes, concepts, and patterns obtained from the content analysis assisted in developing the DOT human resources (HR) staff interview questionnaire.

Before developing the qualitative content analysis, the information found in the literature was coded into manageable content categories. The coding structure was based on four areas: (1) recruiting, (2) retaining, (3) promoting, and (4) training. The predefined set of categories in the coding scheme allowed the authors to focus on and code for specific themes and patterns.

The content analysis was then completed using NVivo, a qualitative content analysis software program, to analyze and find insights in the collected literature and documents. After evaluating the data obtained, a semi-structured interview questionnaire was developed. The questionnaire was organized into four main sections: (1) general information of the interviewee, (2) recruiting strategies and incentives, (3) retention strategies and incentives, and (4) promotion programs and incentives.

Subsequently, in-depth interviews via conference call were conducted with each of the Region 6 DOTs HR departments. Each of the interview participants had at least 10 years of professional experience in employee recruitment, retention, training, compensation, and benefits at a state DOT. The subjects played a vital role in bringing their own knowledge and expertise to the research process. The interviewees consisted of the following participants:

- Participant 1 – HR Personnel Officer
- Participant 2 –Talent Acquisition Coordinator
- Participant 3 – HR Director
- Participant 4 – HR Director
- Participant 5 – HR Manager

- Participant 6 – Talent Manager
- Participant 7 – Talent Acquisition Coordinator
- Participant 8 – Recruitment specialist
- Participant 9 – Recruitment specialist

FINDINGS

Table 1 shows the findings from the interviews for recruiting practices at state DOTs in Region 6. First, all of the Region 6 DOTs noted difficulty in recruiting quality engineers and maintenance staff. This is a concern since a lot of the work that DOTs perform require engineers and maintenance personnel such as equipment operators. Then, four state DOTs offer tuition reimbursement to allow potential employees to further their education while working for the DOT. Reimbursing education is an incentive that works for position that require higher education knowledge. Next, three state DOTs purposefully recruit from historically-minority colleges and advertises positions to minorities and women to invoke a more diverse workforce of qualified individuals. Finally, all of the states except Louisiana are using social media and websites to advertise positions, which they believe will influence newer and younger generations of workers to consider a DOT job.

Table 1. Recruiting techniques

	Arkansas	Louisiana	New Mexico	Oklahoma	Texas
Difficult positions to fill	Engineers; Maintenance; IT	Engineers; Equipment operators	Engineers; Surveyors; Maintenance	Engineers; Equipment operators; Mechanics; GIS/ surveyors	Engineers; Supervisors; Inspectors
Strategies / Incentives	Assign a dollar value for the benefits package offered	Use of special entry-level pay rate; tuition assistance; flexible work schedule	Tuition assistance; Help obtain licenses/ certifications	Tuition assistance; Flexible work schedule; internships for college students; Helps obtain licenses/ certifications	Tuition assistance; work-life balance; wellness programs
Policies for recruiting minorities and females	Recruits from minority colleges; internships for minorities/ women	Recruits from minority colleges	Follows federal equal employment opportunities guidelines	Follows federal equal employment opportunities guidelines	Advertise position in minority/ women magazines
Advertising Positions	Workforce talent acquisition website; social media; newspapers; universities and colleges	Civil services websites; universities and colleges	NeoGov website; Social media; university and colleges; Other: Banners	Transit-website; social media; universities and colleges; Other: headhunters	social media; job fairs within the district; engineer magazines

Table 2. Retention techniques

	Arkansas	Louisiana	New Mexico	Oklahoma	Texas
High turnover positions	Engineers and techs; IT; Entry-level maintenance	Engineers and techs	Engineers; Surveyors; Maintenance	Engineers and techs; Maintenance	Inspectors; Pavement engineers; Maintenance
Strategies / Incentives	Performance-based pay; Bonuses	Education leave time; Annual DOT recognition program; Awards and bonuses	Bonuses; Pay raises based on performance reviews	Longevity bonuses; Employee appreciation days	Longevity bonuses
Professional development programs	Certification training available	Mentorship program; Critical task program that identifies specific tasks and work	Cross-training of staff to perform other duties when necessary	Certification training available; Helps staff develop a career progression plan	Mentoring program; Certification training; Helps staff develop a career progression plan

The next part of the interview focused on retention practices, or how DOTs keep quality employees at their DOT instead of leaving for somewhere else. Table 5 sums the findings from the content analysis. Of the information provided, the highlights include difficulties in keeping quality maintenance staff as two states (Oklahoma and Texas) mentioned that the DOTs have a hard time competing with the oil and gas industry. When the oil and gas industry is booming, many times these DOTs see an exodus of employees leaving for oil and gas companies, which can pay much higher salaries than a DOT can. However, when oil and gas is down, those same people do try to come back to the DOT. It is similar to a seasonal employee that goes where the work is at for work that will pay well. Furthermore, Arkansas stated that entry-level equipment operators are difficult to hold on to, as they people are brought on board, trained, obtain their commercial driver's license (CDL) to operate the maintenance machinery, which the DOT pays for, and then they leave for a private trucking or equipment operations firm that can pay twice as much an hour as the DOT.

Each region 6 DOT also mentioned difficulties keeping engineers and engineering technicians. Once an engineer gains experience at a DOT, and even sometimes gains their professional engineering license with support of the DOT, they find that private sector engineering firms will offer higher salaries and in some cases less responsibilities than a DOT. Therefore, engineers see more pay and less work, so they leave the DOT. In an ironic twist, a couple state DOTs mentioned that they still work with the same people, only these people work for the third-party engineering consultants that the DOT hires. As a summary to these two positions, the most common reason that each of these states mentioned as to why employees leave a DOT is low salary.

However, each of the five states interviewed did mention that their DOT is using specific incentives and professional development plans to entice employees to stay at their DOT. Pay raises and bonuses are based mainly on performance, although Oklahoma and Texas offer longevity bonuses and raises. Other incentives used are an annual DOT recognition program in Louisiana, which uses a week in May each year to celebrate the DOT and their employees, and Oklahoma DOT has employee appreciation days to recognize high functioning and high quality work.

CONCLUSION

State transportation agencies face complex workforce issues due to many factors such as the inability to compete salary wise with private sector firms. In conducting ten interviews with DOT human resources staff, the trials and tribulations of finding high quality employees, enticing them to come work for the DOT, and keeping the employees at the DOT long term is an uphill battle. Yet, DOTs are using new techniques and improved strategies to inform future generations of workers of the potentials they would have by working for at state transportation agency. The use of incentives such as quantifying the total amount of benefits along with a salary promotes that the DOT can pay similarly to private sector positions, just that more of their salary is tied up in a benefits package that private firms cannot offer. Also, DOTs are using the internet and social media to spread the word about their DOT to entice new generations such as millennials to work for the DOT.

For future research, the findings for this study are to be used to further a larger research project in affording specific strategies that can be formulated into a decision-support tool for DOTs to use in terms of recruiting and retaining quality employees. The decision-support tool will be dynamic and flow in various ways depending on the position being advertised and the person or persons that the DOT would like to hire and keep. DOTs are currently in need of a tool like this, which will help DOT human resources to be more effective and efficient in their job while bringing in employees that perform well and plan to stay with the DOT long term.

REFERENCES

Bertini, R. (2011). Transportation: Design, Build, and Manage the Future for America. *Community College Journal*, 81(3), 33-34.

Cronin, B., Anderson, L., Heinen, B., Blair Cronin, C., Fien-Helfman, D., & Venner, M. (2011). NCHRP Report 685: *Strategies to Attract and Retain a Capable Transportation Workforce*. Washington D.C.: Transportation Research Board.

Gallagher, S., & Villwock-Witte, N. (2016). Millennials in the Transportation Workforce. *Transportation Research Record*, 2552(1), 43.

Gilliland, C. A. W. (2001). *Managing change in state departments of transportation. Scan 5 of 8: Innovations in work force strategies* (No. NCHRP Project SP20-24 (14).

Jean M., T. (2010). A Review of the Empirical Evidence on Generational Differences in Work Attitudes. *Journal of Business and Psychology*, (2), 201.

Transportation Research Board. (2003). NCHRP Synthesis 323: *Recruiting and Retaining Individuals in State Transportation Agencies*. Washington, D.C.: The National Academies Press.

Transportation Research Board. (2003). TRB Special Report 275: *The Workforce Challenge: Recruiting, Training, and Retaining Qualified Workers for Transportation and Transit Agencies*. Washington, D.C.: The National Academies Press.

Sustainable and Equitable Financing for Pedestrian Infrastructure Maintenance and Reconstruction

Alexis Corning-Padilla and Gregory Rowangould
Department of Civil Engineering, University of New Mexico

INTRODUCTION

Cities across the country hold responsibility for maintaining streets and roadways. However, many cities, such as Albuquerque, New Mexico, place the responsibility of maintaining sidewalks on adjacent property owners (Shoup, 2009). Property owners are not only responsible for upkeep and maintenance of the sidewalks in front of their homes, they are also liable for paying any repairs that may be needed (Evans-Crowley, 2006).

For many cities, this type of sidewalk ordinance has been in effect for decades, and in some areas dating back to the late nineteenth century (Loukaitou-Sideris & Ehrenfeucht, 2009). The origins of adjacent property owner responsibility are unclear. The experience in Los Angeles, California, provides some clues. When its citizens began to advocate for sidewalks, adjacent property owners agreed they would pay for the construction because they wanted to be able to use the sidewalks for their own interests (Ehrenfeucht & Loukaitou-Sideris, 2007). As property owners were using sidewalks more for their own use, and were, in some cases, seeing them as a way to increase one's property value, they agreed to be responsible for maintenance and repairs (Loukaitou-Sideris & Ehrenfeucht, 2009). In other cities, such as Albuquerque, the requirement for adjacent property owners to pay for sidewalk repairs appears to have evolved from earlier sidewalk ordinances that required adjacent property owners to keep sidewalks clear of debris and snow (Messier, 2017; Roxbury, 1857).

Requiring individual property owners to inspect their sidewalks and contract out their repair when necessary is difficult to enforce and may partially explain why sidewalks in many communities are in poor condition. Furthermore, paying for sidewalk maintenance may not be possible for lower income households. Members of low income households and communities are also more likely to make trips by walking or by walking to public transportation and are therefore disproportionately impacted by relatively high sidewalk repair costs and poor sidewalk conditions (Grant, Edwards, Sveistrup, Andrew, & Egan, 2010).

Our research is focused on finding alternative means of paying for pedestrian infrastructure repairs that provide a sustainable source of revenue and more equitable outcomes. We collect data on the condition of sidewalks throughout the City of Albuquerque, New Mexico, estimate the cost of repairing sidewalks and maintaining them by neighborhood, and then evaluate the tax burden with respect to the social economic status of households and dependence on walking for transportation. While the project focuses on Albuquerque, we expect the results to be useful for cities across the country.

METHODOLOGY

Our study has three main tasks: collecting a sample of field data on sidewalk condition, estimating sidewalk condition and repair costs for each neighborhood in Albuquerque from our field data, and evaluating the distribution of sidewalk repair costs on households of various socioeconomic status and walking dependence under various funding methods.

Like most cities, Albuquerque does not have a program in place to collected data about sidewalk conditions and therefore our first task was to collect these data. Given budget and time constraints, we collecte sidewalk condition data from a sample of neighborhoods and a sample of streets from within the sampled neighborhoods. To determine an effective sampling method, preliminary sidewalk evaluations were completed for three neighborhoods in different areas of the city. This aim of our preliminary evaluation was determining how much of the existing sidewalks in Albuquerque would need to be evaluated to get a reasonable representation of the condition of sidewalks throughout the entire city. We observed that sidewalk conditions generally varied by neighborhood. There are about 250 defined neighborhoods within the city and it was not possible to gather data from each one due to time and resource constraints.

The three neighborhoods we initially evaluated varied in their socioeconomic status and urban form. One neighborhood represents a higher income, suburban neighborhood, another neighborhood is located near the University of New Mexico which is more centrally located and urban, and the third neighborhood is located in a lower income part of the city. Every sidewalk in these neighborhoods is evaluated for holes, cracks, and slab displacements that might hinder the use of the sidewalk. The evaluation criteria used is based on ADA Standards, which require sidewalks to be built and kept up to a standard that allows those with disabilities to use them. We then calculate defect rates for randomly selected intersections within each neighborhood and for varying distance from each intersection. By comparing the statistical data for each of these defect rates to defect rate from the complete inventory in each neighborhood, we determined how many intersections per neighborhood and how many feet in each direction at those intersections are required to get a reasonable estimate of sidewalk quality for each neighborhood.

Next, we evaluated sidewalks extending from randomly selected intersections in 50 randomly selected neighborhoods. Each defect is recorded in a GIS database and a defect rate is estimated for each neighborhood. A spatial interpolation model is then used to estimate defect rates for neighborhoods that were not sampled under the assumption that neighborhoods closer to each other are more similar. Unit repair costs obtained from the City of Albuquerque are then used to estimate the repair costs for the city's sidewalks as well as those in each neighborhood.

On-going work not yet completed will then evaluate the tax burden on each neighborhood and households of various socioeconomic status from alternative financing methods, including increments to the local portion of the gasoline excise tax, property tax, and the gross receipts tax (sales tax). Consumer expenditure survey data will be used for this analysis along with household travel survey data collected by the Mid Region Council of Governments. We will also evaluate how sidewalk quality varies across neighborhood level socioeconomic status and walking dependence to measure the equity impacts of the current ordinance. At this point we have just begun this analysis and show preliminary results below. We expect to present preliminary results of the complete study at the TranSET Conference.

FINDINGS

With the field work and preliminary spatial analysis phases of the project complete, we are now finishing spatial analysis to evaluate the distribution of sidewalk maintenance and repair costs across the city that will inform our financial modeling and equity analysis. Figure 1 shows the estimated defect rates across the city, with higher defect rates in the southwest region. Evaluating the association of defect rates with neighborhood level median household income from the U.S.

Census Bureau's American Community Survey indicates that sidewalks located in lower income neighborhoods have more defects than more recently built sidewalks which are predominantly located in more affluent neighborhoods (Figure 2). This result confirms what has been noted in other cities, that lower income neighborhoods have poorer quality sidewalks. The next steps of our analysis will evaluate equity of several alternative funding models that could raise enough revenue to repair and maintain sidewalks across the entire city. The ability of each funding mechanism to provide adequate funding over time will also be evaluated (e.g., increasing fuel economy and electric vehicles could quickly reduce the value of an incremented gas tax) as well as the tax burden across communities and households with different socioeconomic status.

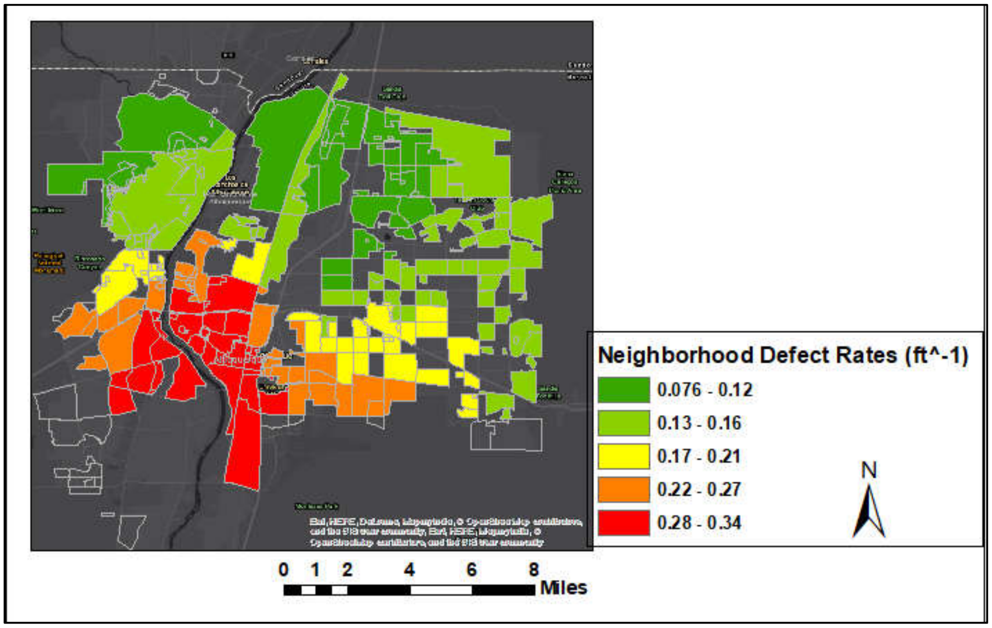

Figure 1: Sidewalk defect rates across city of Albuquerque.

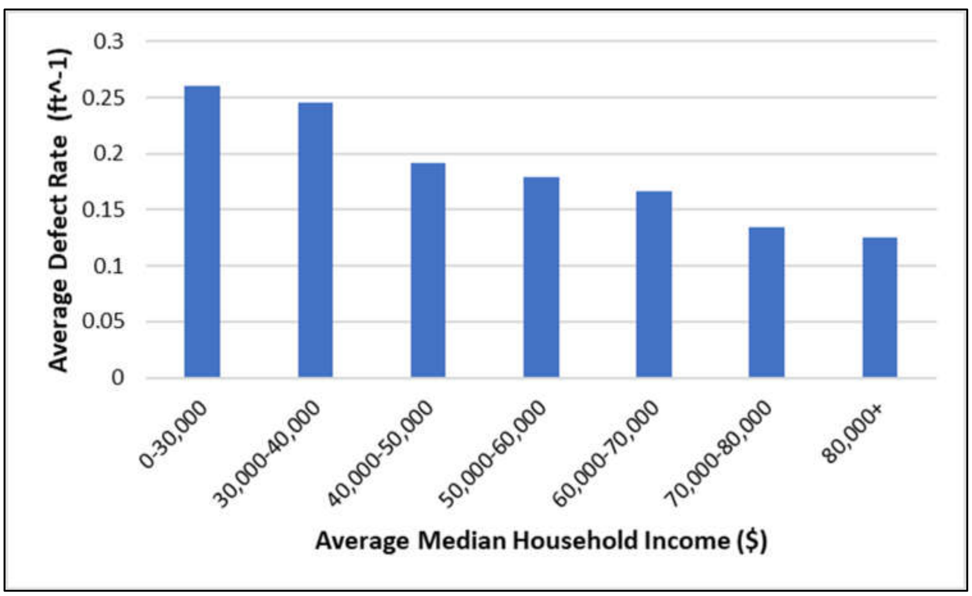

Figure 2: Average Defect Rate for Average Median Household Income categories in Albuquerque.

CONCLUSION

The goal of this project is to find a more robust solution to pay for sidewalk repairs without the burden to inspect and contract out repairs being placed on homeowners, which appears to be ineffective and contributing to an inequitable and unjust distribution of sidewalk quality. A more sustainable and equitable sidewalk financing model will not only help bring sidewalks up to ADA standards, increasing mobility for the disabled, but will also provide higher quality infrastructure that encourages walking and its many benefits. The final product of this research will be a white paper that aims to inform municipal leaders about alterative sidewalk financing models and their various benefits. We expect to present preliminary results for the entire study at the TranSET Annual Conference.

REFERENCES

Ehrenfeucht, R., & Loukaitou-Sideris, A. (2007). Constructing the sidewalks: municipal government and the production of public space in Los Angeles, California, 1880–1920. *Journal of Historical Geography*, *33*(1), 104–124.

Evans-Cowley, J. (2006). Sidewalk planning and policies in small cities. Journal of Urban Planning and Development, 132(2), 71–75.

Grant, T. L., Edwards, N., Sveistrup, H., Andrew, C., & Egan, M. (2010). Inequitable walking conditions among older people: examining the interrelationship of neighbourhood socio-economic status and urban form using a comparative case study. BMC Public Health, 10, 677. https://doi.org/10.1186/1471-2458-10-677

Loukaitou-Sideris, A., & Ehrenfeucht, R. (2009). *Sidewalks: Conflict and Negotiation Over Public Space*. MIT Press.

Messier, J. (2017, June 14). Former City of Albuquerque Planning Director, Personal Communication.

Roxbury (Boston, Mass.). *An ordinance to cause the removal of obstructions on the sidewalks caused by snow or ice.* Roxbury [Mass.], 1857. 3pp. *Sabin Americana*. Gale, Cengage Learning. University of New Mexico.

Shoup, D. (2009). Putting cities back on their feet. Journal of Urban Planning and Development, 136(3), 225–233.

Investigating Problem of Distracted Drivers on Louisiana Roadways

Xiaoduan Sun[1], M. Ashifur Rahman[2], Ming Sun[2], and Yi He[3]

[1]Professor, Department of Civil Engineering, University of Louisiana at Lafayette
[2]Ph.D. Candidate, Department of Civil Engineering, University of Louisiana at Lafayette
[3]Graduate Student, Department of Civil Engineering, University of Louisiana at Lafayette

INTRODUCTION

While the ongoing developments of autonomous vehicles show a great promise to reduce fatalities and injuries, the full implementation will take years to become a reality. Due to the escalating usage of cell phone and social networking, distracted driving is and will remain as one of the most serious problems faced by the Departments of Transportation (DOTs) and law enforcement agencies. Louisiana is one of the worst states in road safety performance in the U.S. while distracted driving remains a key contributing factor of road crashes in the state especially in urban areas. This study aims to investigate the scale of the problem in Louisiana, analyze characteristics of distracted drivers and how their behaviors affect roadway safety. To do that, the research team has collected the data including crash data, manually observed data of distracted driving behaviors, and in-vehicle video data.

The number of fatal crashes in the U.S. from cell phone distraction shows a general increasing trend over the last few years. The National Highway Traffic Safety Administration (NHTSA) reports that 660,000 Americans are using cell phones at any given moment *[1]*. In 2015, police reported distracted driving fatalities on Louisiana's highways represented 20.9 percent of all fatalities and 30 percent of serious injuries. A share of 55.3 percent of all injury crashes and 55.9 percent of total property damage only crashes occur on Louisiana roads due to distraction in driving *[2]*.

In addition to crash studies, methods of distracted driving detection and measurement have been studied. Typically, police and law enforcement officers identify distracted drivers, either from irregular movement of vehicles (e.g. failure to maintain consistent speed, abrupt lane movement, slow response to signals etc.), or from inattention of drivers (e.g. intermittently looking down, night time glow of the device, hand to ear with device in hand etc.) *[3]*. According to previous literature, impacts of distracted driving behaviors are measured either directly by on-road driving performance tests or by surrogate methods like driving simulators. Distracted driving effects are measured in the form of speed, headway, lane keeping, reaction time etc. Naturalistic Driving Study conducted by National Highway Traffic Safety Administration (NHTSA) investigated the association of distracted driving behaviors with crashes or near-crash incidents *[4]*. Louisiana was not part of the Naturalistic Driving Study, thus the results from that study may not accurately reflect the unique characteristics of our state drivers' behavior.

The research team studied the feasibility of using major sources of distracted driving related data, which are crash report, video recording, and manual observation. Crash report is an important resource for identification of factors related to distracted driving. The crash report also contains assigned police officer's narrative which includes circumstances associated with crash, officer's observations and opinions, statements of drivers, passengers, and possible witnesses. The actual field observation, the most conventional method for distracted driving identification, is underway. Plans have been undertaken for manual observation of distracted driving behaviors both at intersections and on segment. Analysis of in-vehicle video recordings is being conducted to identify distracted behaviors from the facial movements of selected drivers.

Results obtained so far is not conclusive, analysis from complete data collection is expected to deliver more confident results.

METHODOLOGY

The research team is exploring the crash investigation reports of distracted driving related crashes. Crashes with at least one distracted driver on all type of highways occurred between 2006 and 2015 are currently being studied. Preliminary analysis showed somewhat increasing trend of distracted driving crashes over the years. Conventional statistical methods and data mining algorithms will be used to predict distracted driving crashes.

Manual observation of visible distracted driving behaviors at selected intersections and on selected segments is currently underway. The project team has selected three segments and three intersections for observation. Graduate and undergraduate students are collecting data related to vehicle type, gender, age group and distraction type (i.e. hand-held cell phone, manipulation by texting or ear device). At intersection, drivers of stopped vehicles at red light are observed for potential distracted behavior. On segment, drivers passing a reference point during a certain time interval are observed. Data have been collected for a total of three hours at intersection and for four hours' observation on segment. Statistical analysis will continue to be performed on the collected data to identify vulnerable groups, inter-relationships among attributes, other significant patterns.

Analysis of driving behaviors from recorded videos of thirty-five drivers is ongoing with an aim to identify the combination of emotions that lead to distracted behaviors while driving. Mounted cameras were set up inside thirty-five vehicles to identify distracted driving behavior. High definition videos, separated in three-minute clips, were analyzed utilizing FaceReader software. The software recognizes emotions in the form of facial expressions based on the movement of eyes, mouth etc. Analysis of valence of emotions will be used to identify distracted driving behavior utilizing advanced data mining algorithms.

FINDINGS

Crash Analysis

A total of 157,155 crashes with at least one distracted driver occurred during 2006-2015 in Louisiana were identified for analysis. According to the crash reports, drivers were distracted by cell phone – 13.6%, other electronic device (pager, navigation device, etc.) – 3.3%, other inside the vehicle (e.g. talking with passenger) – 42.3%, other outside the vehicle (e.g. distracted by outside object) – 40.8%. Crash analysis by collision type shows majority of distracted behaviors result into rear end and single vehicle crashes (Figure 1). A more sophisticated statistical modeling for the prediction of distracted driving crash severity is in progress, results will be updated accordingly.

Crash rate is a normalized measurement which considers the length of roadways, and exposure (annual average daily traffic - AADT), and duration. While estimating distraction related crash rate, weighted AADT from length was calculated for each type of roadway. Urban roadways are more prone to distracted driving according to the estimation of crash rate in 100 million vehicle miles traveled (Table 1).

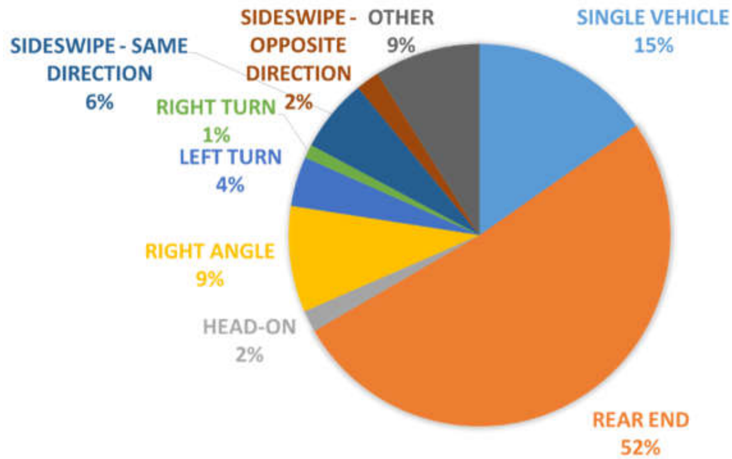

Figure 1: Distracted driving crashes on Louisiana roadways by collision type during 2006-2015

Table 1: Distracted driving crashes by roadway type in Louisiana in 2015

Roadway Type	Length (miles)	Crash rate (100 million VMT)
Urban 4-lane	187	951.7
Urban 2-lane continuous turn	59	796.1
Urban 4-lane continuous turn	229	707.9
Urban 6-lane	60	671.3
Urban 4-lane divided	578	480.6
Urban 2-lane	2,077	446.9
Urban 6-lane interstate	108	223.0
Urban other freeways	73	192.7
Rural 2-lane continuous turn	17	145.0
Rural 2-lane	11,668	139.6
Urban 4-lane interstate	301	115.2
Rural 4-lane	67	98.0
Rural 4-lane divided	643	72.2
Rural 4-lane continuous turn	48	71.5
Rural 6-lane interstate	31	43.5
Rural 4-lane interstate	497	39.5

Manual Observation

Distracted driving behaviors were categorized by the use of cell phones and other devices while driving – handheld use (talking), manipulating (texting, checking email, etc.), and hands-free use (including use of headphones). A total of 195 distracted drivers were identified from 1,429 observed drivers at the intersection – handheld use (19%), manipulating (70.8%), and hands-free use (10.3%). On the segment, 209 out of 946 total observed drivers were identified as distracted – handheld use (42.6%), manipulating (51.2%), and hands-free use (6.2%). Data collected from observations were analyzed to learn whether there is a significant relationship between any characteristics and distracted driving (Table 2). Chi-squared tests for independence were performed on several sets of variables involving gender, age group, vehicle type, and time of the day with binary variable (distracted or not distracted). The null hypothesis is formulated as – there is no relationship between distracted driving and any individual characteristic. Results are similar for both intersections and segments, if a level of significance of 0.05 is considered. Estimated p-value > 0.05 for gender indicates that there is no significant difference between male and female drivers, when distracted driving is concerned. Age group ($p < 0.05$) and vehicle type ($p < 0.05$) is not independent of distracted driving behavior both at intersection and on segment. A p-value higher than 0.05 indicates that we fail to identify any association between time of the day and distracted driving.

Table 2: Manual observation data at one intersection and on one segment

Characteristics	Variables	Frequency (Percentage) at Intersection			Frequency (Percentage) on Segment		
		Distracted	Not Distracted	Chi-squared p-value	Distracted	Not Distracted	Chi-squared p-value
Gender	Male	92 (14.1%)	559 (85.9%)	0.7003[a]	97 (19.8%)	394 (80.2%)	0.0767[a]
	Female	97 (13.8%)	605 (86.2%)		110 (24.6%)	338 (75.4%)	
	Unsure	6 (7.9%)	70 (92.1%)		2 (28.6%)	5 (71.4%)	
Age group	<30	88 (20.0%)	352 (80.0%)	<0.0001[b]	135 (25.5%)	394 (74.5%)	0.0109[b]
	30-60	91 (11.4%)	706 (88.6%)		68 (18.7%)	296 (81.3%)	
	>60	9 (7.5%)	111 (92.5%)		6 (12.0%)	44 (88.0%)	
	Unsure	7 (9.7%)	65 (90.3%)		0 (0.0%)	3 (100.0%)	
Vehicle Type	Car	123 (19.0%)	523 (81.0%)	<0.0001[c]	123 (24.5%)	379 (75.5%)	0.0483[c]
	Truck	28 (9.2%)	277 (90.8%)		27 (14.9%)	154 (85.1%)	
	SUV or van	42 (10.0%)	377 (90.0%)		57 (23.0%)	191 (77.0%)	
	Other	2 (3.4%)	57 (96.6%)		2 (13.3%)	13 (86.7%)	
Time	Morning	32 (18.8%)	138 (81.2%)	0.0910	-	-	0.6254[d]
	Noon	117 (12.6%)	813 (87.4%)		116 (22.7%)	395 (77.3%)	
	Afternoon	46 (14.0%)	283 (86.0%)		93 (21.4%)	342 (78.6%)	
Total		195 (13.6%)	1,234 (86.4%)		209 (22.1%)	737 (77.9%)	

Note: [a] Chi-square tests for gender dependence exclude unsure observations.
[b] Chi-square tests for dependence on age group exclude unsure observations.
[c] Chi-square tests for dependence on vehicle type exclude other vehicle type.
[d] Chi-square test for dependence on time of the day on segment doesn't include morning observations.

Video Recording Analysis

Face Capture technology captures facial expression and converts into digital form. FaceReader software, a specific type of Face Capture Program, recognizes gaze direction, head orientation, and personal characteristics to some extent. It measures valence of several emotions of the user as sad, happy, angry, surprised, or neutral and presents the emotions graphically. Facial expressions are coded to determine characteristics which distinguish distracted driving behaviors from non-distracted driving behaviors. A total of eighty-four valid video sections were analyzed. Few rules have been established based on valence of emotions to distinguish a driver talking on a cell phone and manipulating (e.g. texting) from non-distracted behaviors. A comprehensive analysis of the video and valence data from emotions is required to improve the accuracy of the rules.

CONCLUSION

Preliminary analysis of crash data shows that cell phone and outside distractive elements contribute most to distraction related crashes in Louisiana. Urban roadways are more prone to distracted driving related crashes than rural roadways. As the research work progresses, analysis results will be updated.

Analysis from manually observed data collected so far indicates gender and time of the day do not significantly impact distracted driving. Age group and vehicle type show association with distracted driving both at intersection and on segment. However, the results are only valid for one intersection and one segment. The overall result might change based on further data collection from two intersections and two segments.

In-vehicle video data analysis using FaceReader software requires iterative testing for more accurate combination of valence of emotions aiming at better prediction of distracted driving behavior.

REFERENCES

1. NHTSA Survey Finds 660,000 Drivers Using Cell Phones or Manipulating Electronic Devices While Driving At Any Given Daylight Moment (2013, April 5). Retrieved from https://www.transportation.gov/briefing-room/nhtsa-survey-finds-660000-drivers-using-cell-phones-or-manipulating-electronic-devices
2. Department of Transportation and Development, Louisiana (2017). *LADOTD Highway Crash List*. Retrieved from http://www8.dotd.la.gov/crash1/
3. Regan, M. A., Lee, J. D., & Young, K. (Eds.). (2008). *Driver distraction: Theory, effects, and mitigation*. CRC Press.
4. National Traffic Law Center. (2017, May). *Investigation and prosecution of distracted driving cases* (Report No. DOT HS 812 407). Washington, DC: National Highway Traffic Safety Administration.

Development of Field-Friendly Mechanical Characterization Method for Compacted Unbound Aggregates

Douglas D. Cortes and Paola Bandini

Department of Civil Engineering, New Mexico State University

INTRODUCTION

The evaluation of compacted unbound aggregate layers is perhaps the most common undertaking in transportation-related projects. The assessment of compaction compliance in engineered fills, subgrades, subbases, and bases in roadways and railways is central to ensure longevity of ground transportation infrastructure. In many cases, premature failures in roadways that originate in the unbound aggregate layers can be traced back to inadequate compaction. This is of course preventable provided the problem areas can be identified by a suitable field-test during construction.

Improving the in-situ mechanical characterization of compacted unbound aggregates in transportation infrastructure is a basic need in the transition from empirical to mechanistic design. The development and adoption of reliable automated test devices is expected to help engineers optimize their designs while maintaining adequate factors of safety. Furthermore, the same devices would allow highway inspectors and contractors to identify deficiencies in mechanical performance during construction which could prevent premature failure of pavement structures. As a result, the public can enjoy more affordable and longer lasting roads.

The most widely used method for compaction assessment during construction is the nuclear gauge density test. There are two primary issues with this device: it is radioactive, and it does not fully capture the mechanical performance of unbound aggregates. While the test itself is simple and robust, the complexity associated with the transportation and servicing of the radioactive device makes the test logistically and economically expensive. Furthermore, nuclear gauges were designed to extract density and moisture content. These parameters are the norm in practice for compaction quality control/quality assurance (QC/QA), but they do not provide the key mechanical properties needed for a mechanistic analysis of unbound pavement layers.

There are alternative devices available for field performance assessment; however, they are not necessarily field-friendly. Simple devices i.e., dynamic cone test and helical probe test, provide only index strengths, and require multiple people to operate, collect, and record data (Yokel and Mayne, 1988; Burnham and Johnson, 1993; Abu-Farsakh et al., 2004; Wu and Sargand, 2007). Since these devices do not produce direct measurements of mechanical properties, the analysis of results often involves the use of physically meaningless correlations, valid only for a very narrow range of materials and site conditions, see examples in Table 1.

More sophisticated methods, i.e., surface waves, require complex analysis and data post processing that make them unsuitable for field testing crews or applications that require decision-making in very short time frames such as field compaction (Rix and Leipski, 1991, Stokoe and Santamarina, 2000; Cosentini and Foti, 2014).

METHODOLOGY

The state-of-the-art in mechanical characterization of soils continues to make significant progress, and the gap with the state-of-the-practice in transportation geotechnics continues to widen. Despite efforts by FHWA and AASHTO to bring practice into the new millennium, it remains almost a half a century behind. New technologies continue to find resistance or serious challenges to adoption. The long-term objective of this project is to advance the state of the practice by developing a series of automated in-situ testing devices for the determination of mechanical properties of subgrade and base pavement layers.

Table 1. Examples of dynamic cone penetration (DCP) test correlations

Correlation	Reference
$Log(CBR_{lab}) = 2.465 - 1.12Log(PR)$	(Webster et al. 1992)
$CBR = \frac{5.1}{PR^{0.2} - 1.41}$	(Abu-Farsakh et al. 2004)
$M_R = 532.1 \cdot PR^{-0.492}$ ~ Fine-grained $M_R = 235.3 \cdot PR^{-0.475}$ ~ Coarse-grained	(George and Uddin 2000)
$\ln(M_{FWD}) = 2.35 + \frac{5.21}{\ln(PR)}$	(Abu-Farsakh et al. 2004)
$E_{back} = 338 \cdot (PR)^{-0.39}$	(George and Uddin 2000)

The first part of the project has been devoted to cataloguing available technologies for the determination of mechanical properties of compacted unbound aggregates. The research team carried out a critically assessment of the advantages and limitations of available devices, with the objective of eliminating technologies with inherent limitations. Thus, the remaining subset of technologies only share operational limitations. The researchers expect to find within this group of technologies a few that could be significantly improved through automation.

Recognizing that successful adoption of new testing equipment depends not only on the technical soundness of the device, the research team has set out to engage the primary end-users to seek an answer to the question: what does practice (i.e., state DOTs, contractors) look for in an in-situ test device? In other words, what makes the nuclear density gauge so popular, and why no other tests have been as widely adopted by state transportation agencies? Understanding the end-user priorities and engaging NMDOT in the development of rubrics for the evaluation of test methods should help further narrow down the group of test methods to those with the most likelihood of adoption.

FINDINGS

Unbound aggregate layers in well-designed pavement structures operate in the small strain regime. The maximum stress experienced by these layers occur during construction because, during service, the riding layer (asphalt concrete or Portland cement concrete) redistributes the load reducing the magnitude of the traffic induced stress. As a result, the key performance metric for unbound aggregate materials in pavement structures is the small-strain stiffness.

The most accurate small-strain stiffness measurements available are recovered using geophysical methods (i.e., surface waves). However, surface wave measurements require the density of the layer to be known, involve significant post processing, and can be affected by heterogeneities such as soil layers in subgrades and inadequately compacted bases and sub-bases. Penetration type tests are better at capturing changes in material properties with depth, but can only offer an indirect assessment of stiffness because the aggregates undergo large strains.

REFERENCES

Abu-Farsakh, M. Y., Alshibli, K., Nazzal, M., and Seyman, E. (2004). "Assessment of In-Situ Test Technology for Construction Control of Base Courses and Embankments ", Louisiana Transportation Research Center, Baton Rouge, LA 126.

Burnham, T., and Johnson, D. (1993). "In Situ Foundation Characterization Using the Dynamic Cone Penetrometer." Minnesota Department of Transportation St. Paul, MN, 32.

Cosentini R.M., and Foti S., 2014. "Evaluation of porosity and degree of saturation from seismic and electrical data," Géotechnique, Vol. 64, No. 4 (pp. 278-286).

George, K. P.; Uddin, W., 2000. "Subgrade Characterization for Highway Pavement Design"; Mississippi Department of Transportation Research Division: Jackson, MS, Dec 2000, p 245.

Rix, G.J., and Leipski, E.A., 1991. "Accuracy and resolution of surface wave inversion," In Recent Advances in Instrumentation, Data Acquisition and Testing in Soil Dynamics (pp. 17-32). ASCE.

Stokoe, K.H., and Santamarina, J.C., 2000. "Seismic-Wave-Based Testing in Geotechnical Engineering," In International Society for Rock Mechanics International Symposium, 19-24 November, Melbourne, Australia.

Webster, S. L.; Grau, R. H.; Williams, T. P., 1992. "Description and Application of Dual Mass Dynamic Cone Penetrometer"; U.S. Army Engineer Research and Development Center, Waterways Experiment Station: Vicksburg, MS.

Wu, S., and Sargand, S. (2007). "Use of Dynamic Cone Penetrometer in Subgrade and Base Acceptance." Ohio Department of Transportation, United States Department of Transportation, Federal Highway Administration.

Yokel, F. Y., and Mayne, P. W. (1988). "Helical Probe Tests: Initial Test Calibration." Geotechnical Testing Journal, 11(3), 179-186.

Environmentally-friendly and Sustainable Soil Stabilization for Transportation Infrastructure

Rinu Samuel[1], Oscar Huang[2], Aritra Banerjee[1], Miladin Radovic[2], and Anand Puppala[1]

[1]University of Texas at Arlington
[2]Texas A&M University

INTRODUCTION

Texas and its neighboring states have a prevalence of expansive clays, which are thought to be the primary cause of pavement distresses in these states (Puppala et al., 2006). As such, many low-volume roads in these areas are built on expansive clay subgrades. Expansive clays undergo volume change due to variations in its moisture content. An increase in moisture in the soil causes the clay to swell, while a decrease results in shrinkage. Swelling of expansive clay usually manifests itself in the form of heaves on pavements, while shrinking results in soil and pavement cracking, Figure 1. The weather conditions in Texas where wet periods are followed by hot dry conditions considerably aggravates the problem. These repetitive cycles of shrinking and swelling, impose additional stresses to the infrastructure as well.

Figure 1: Vertical Heaves Generated during Construction of US 67 near Midlothian (Harris et al., 2005).

Conventionally, the swell-shrink potential of expansive clays is mitigated with the mixing of chemical additives, such as different polymers, lime and ordinary Portland cements. While chemical stabilization methods are used extensively, they are highly prone to leaching and durability issues, which make them inept as long-term solutions. One of the major disadvantages of using calcium-based stabilizers, such as lime, is that they react with sulfate minerals resulting in disintegration of soils and subsequently loss of soil strength (Nair and Little, 2011). Furthermore, the production of additives demands high energy and generates substantial amounts of CO_2. As such, there is a need for environmentally friendly and sustainable means of soil stabilization for transportation infrastructure.

Alumino-silicate binders, known as Geopolymers, are proposed to be a sustainable and eco-friendly alternative to conventional chemical stabilization techniques (Davidovits 2005; Zhang et al. 2013; Sukmak et al. 2013). Geopolymers harden at ambient temperatures and in a relatively short amount of time (Lizcano et al., 2012) and can be created by curing activated solutions of various alumino-silicate sources including natural minerals (e.g. clay), their products (e.g. metakaolin), and waste materials (e.g. fly ash, furnace slag, etc.). Geopolymers are known for their high compressive strength and low shrinkage properties, and have been used in recent years as a sustainable alternative to ordinary Portland cements (OPC) in concrete structures, including pavements, bridges, etc. Geopolymers have a much lower carbon footprint than lime or OPC, and is therefore more environmentally friendly than other conventional additives used for soil stabilization nowadays. This eco-friendly nature of Geopolymers over conventional chemical stabilizers prompted the present research team to investigate the feasibility of Geopolymers for effective stabilization of pavement bases and subgrades.

The objective of this research is to develop an eco-friendly solution to provide resilient stabilized base and subgrade foundation support for pavements, using natural and waste materials that abound in the region to ensure extension of life of existing or new transportation infrastructure using innovative materials. The successful culmination of this research will aid in the design of durable and distress free pavement infrastructure in problematic soil conditions that prevail in Texas and its neighboring states. To this end, the scope of work includes a review of published literature on geopolymers, development and characterization of geopolymers, selection of base and subgrade materials for geopolymer treatment, comprehensive materials and engineering characterization of geopolymer treated soils, analysis of results, and sustainable and life cycle assessments.

METHODOLOGY

An important step in the process of this research is the acquisition and characterization of base and subgrade materials commonly available in Texas for the purpose of geopolymer treatment. The three types of soil that have been acquired are: high plasticity clay (CH), low plasticity clay (CL) and poorly graded sand (SP). The soils are characterized by laboratory index soil properties ranging from water content, specific gravity, particle-size analysis, Atterberg limits, and moisture-density relationships based on American Society for Testing and Materials (ASTM) testing procedures. Different geopolymer compositions will be selected for stabilizing these soil samples, which will be determined based on the viscosity of the selected geopolymer base and workability of the mixture. The three soils will be stabilized with different geopolymers at different dosage levels to optimize durability and mechanical properties. These variables will be established based on information from published literature on geopolymers and results from their material characterization and the soils selected to be treated. Engineering characterization studies will be performed to evaluate the enhancement in strength, stiffness and durability of the geopolymer stabilized soils. Stabilized bases and subgrades will then be subjected to unconfined compression strength (UCS), resilience modulus, and free vertical swell and linear shrinkage bar tests. All results will be analyzed to address the improvements in engineering properties from geopolymer treatments.

The geopolymers are made from high-purity activating aluminosilicate source (e.g. metakaolin) with sodium hydroxide and fumed silica solution. The additional aluminosilicate source is first mixed with clay, then mixed with the activator solution to form geopolymers to bind the clay particles as well as masonry sand (Figure 2). The goal is to be able to stabilize the soil with 10 percent or less by weight of geopolymers. In addition to the mentioned mechanical tests, the samples will also be examined with various material characterization techniques such as scanning electron microscopy (SEM), X-ray diffraction (XRD), and nuclear magnetic resonance (NMR). The purpose for these techniques is to get a better understanding of the composition-structure-property relationship for geopolymers as well as the interaction of soil and geopolymers. This will help accelerate the development of a working product.

Figure 2: Pure geopolymer (left) sample and samples of sand (center) and clay (right) stabilized with 10% (by volume) geopolymers after curing.

FINDINGS

So far, only preliminary experimental work has been carried out. The preliminary work focused on creating working samples with the proposed methodology. Therefore, we are still in the process of obtaining reportable results since the workable samples have only been synthesized recently and geopolymers also require around a month or so to cure to obtain the optimal properties.

CONCLUSION

It has been shown that geopolymers can be used to stabilize Texan soil. As more results are obtained from different characterization techniques, composition and/or process can be tailored to improve the properties, and eventually obtain the optimal properties. The limitation of this work is the timeline of the project which restricts findings for long term durability. However, this can be compensated by exposing the samples to aggressive environments as a way to accelerate the study and learn about the sample's long-term durability.

REFERENCES

Davidovits, J. (2005). Geopolymer, Green Chemistry and Sustainable Development Solutions: Proceedings of the World Congress Geopolymer 2005, Geopolymer Institute.

Harris, P., Von Holdt, J., and Scullicon, T. (2005). "Recommendations for stabilization of high sulfate soils in Texas." College Station, Texas, USA: Texas Transportation Institute, Report No 0-4240-3.

Lizcano, M., Gonzalez, A., Basu, S., Lozano, K. and Radovic, M. (2012). "Effects of Water Content and Chemical Composition on Structural Properties of Alkaline Activated Metakaolin-Based Geopolymers." *Journal of the American Ceramic Society* 95: 2169-2177.

Nair, S., and Little, D. (2011). "Mechanisms of distress associated with sulfate-induced heaving in limetreated soils." Transp. Res. Record: J. Trans. Res. Board, 2212(1): 82-90.

Olive, W.W., Chleborad, A.F., Frahme, C.W., Shlocker, Julius, Schneider, R.R., and Schuster, R.L. (1989). "Swelling clays map of the conterminous United States." Department of the Interior U.S. Geological Survey, Miscellaneous Investigations Series Map I-1940.

Puppala, A.J., Punthutaecha, K., and Vanapalli, S.K. (2006). “Soil water characteristic curves of stabilized expansive soils.” J Geotech Geoenviron Eng 132(6):736–750.
Sukmak, P., Horpibulsuk, S., and Shen, S.L. (2013). Strength development in clay–fly ash geopolymer, Construction and building Materials 40, 566-574.
Wanyan, Y., Abdallah, I., Nazarian, S., and Puppala, A. J. (2015). “Moisture content-based longitudinal cracking prediction and evaluation model for low-volume roads over expansive soils.” J. Mater. Civ. Eng., 10.1061/(ASCE)MT.1943-5533.0001217, 04014263.
Zhang, M., Guo, H., El-Korchi, T., Zhang, G., and Tao, M. (2103). Experimental feasibility study of geopolymer as the next-generation soil stabilizer, Construction and Building Materials 47 (2013) 1468-1478.
Zornberg, J.G., and Gupta, R. (2009). “Reinforcement of Pavements over Expansive Clay Subgrades.” Proceedings of the Seventeenth International Conference of Soil Mechanics and Geotechnical Engineering, Alexandria, Egypt, 5-9 October, pp. 765- 768.

Prediction and Rehabilitation of Highway Embankment Slope Failures in a Changing Climate

Navid H. Jafari[1], Jack Cadigan[2], Burak Boluk[3], Tejo V. Bheemasetti[4], and Anand J. Puppala[5]

[1]Assistant Professor, Department of Civil and Environmental Engineering, Louisiana State University
[2]GRA, Department of Civil and Environmental Engineering, Louisiana State University
[3]Ph.D. Student, Department of Civil Engineering, University of Texas at Arlington
[4]Post-Doctoral Fellow, Department of Civil Engineering, University of Texas at Arlington
[5]Professor, Department of Civil Engineering, University of Texas at Arlington

INTRODUCTION

In the direct aftermath of highway embankment slope failures, the preservation and resiliency of transportation infrastructure is extremely crucial for economic growth of the region and restoring daily mobility services. In the states of Texas and Louisiana, several highway embankment slope failures have occurred over the years resulting in high maintenance, expensive rehabilitation costs, and constrained mobility services. These failures are attributed to the presence of high-plasticity clays that undergo significant volumetric changes from seasonal climatic changes. In particular, weathering (i.e., wetting-drying) cycles results in desiccation cracks, which allow greater exposure of the embankment fill material to moisture from precipitation. As the moisture content of the clayey soil increases, the shear strength reduces to a fully softened shear strength, causing numerous, frequent shallow and medium slope failures that are oriented approximately parallel to the surface of the embankment. More importantly, the frequency of highway slope failures is anticipated to increase in the future because of increasing rainfall intensities and durations caused by longer drought-like conditions. Accordingly, there is an important need (1) to develop a predictive tool for identifying high-risk locations and (2) to determine cost-effective remedial methods. This research paper presents the methodology and preliminary findings for developing a predictive tool to identify high-risk slopes. To perform these studies, high to medium plasticity soils were collected from slope failures across different Texas and Louisiana regions which contain varying geological formations. Laboratory tests include physical index material characterization, fully softened shear strength (FSS), and soil water retention curves (SWRC). Inverse stability analyses were performed using the laboratory determined soil properties to evaluate the pore-water pressure that instigated the slope failures. The sections below present the methodologies, results, and preliminary conclusions.

METHODOLOGY

The main objective of this study is to (a) develop a framework that predicts which locations have a high risk of slope failure and demonstrate its functionality in Region 6, and (b) identify cost-effective rehabilitation techniques for repairing slides. Figure 1 presents the step-by-step approach to achieve the proposed objective. A systematic literature review is performed on the documented slope failures in Region 6 to understand the climatic and meteorological events during the service life, time required to mobilize FSS, and performance of rehabilitation methods. For each of soil sample collected from the field, Atterberg limits (PL, LL) and clay size fraction (CF) were measured in accordance with ASTM D4318 and D422 (ASTM 2008; ASTM 2017). Furthermore, Standard Proctor compaction tests determined the maximum dry density (MDD) and optimum moisture content (OMC) using ASTM D698-12 (ASTM 2012). Soils were classified based on the Unified Soil Classification System (USCS). The methodologies adopted for performing the FSS, unsaturated hydraulic conductivity and SWRC tests for Louisiana and Texas soils are provided herein.

Table 1. Steps to achieve the project objectives

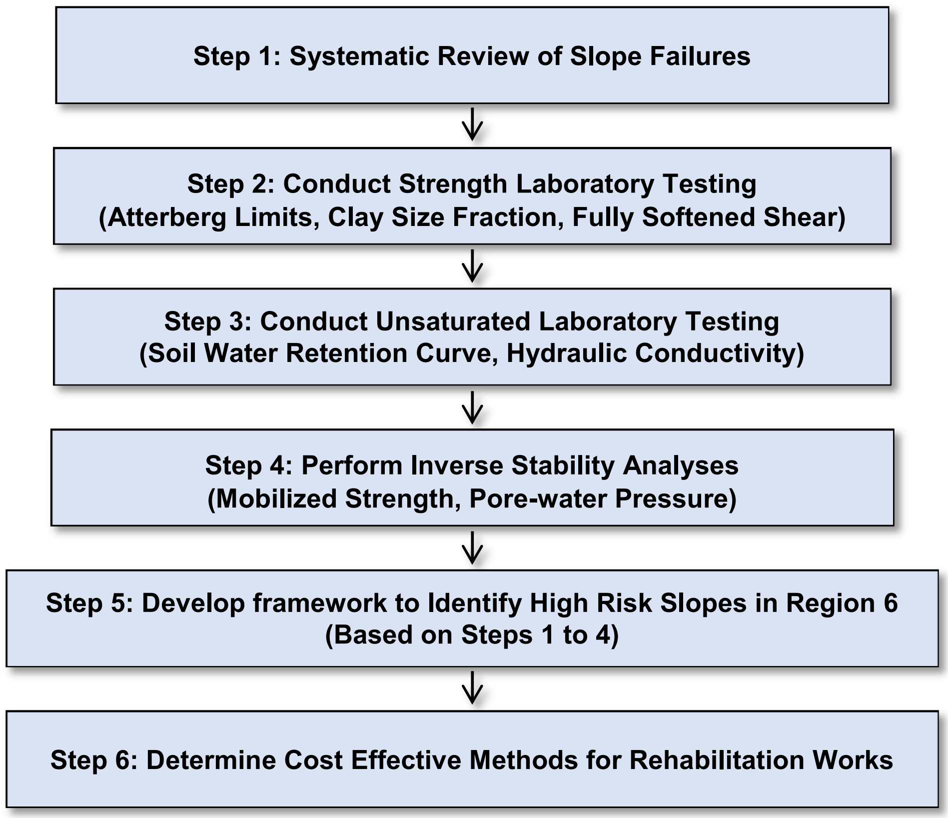

Fully Softened Shear Strength

Louisiana soils have yet to be evaluated for FSS, so this paper provides FSS envelopes for typical high plasticity soils found in the state. Three main correlations published in the literature to estimate the FSS envelope. The first correlation was proposed by Stark and Eid (1997), and subsequently augmented by Stark et al. (2005), Stark and Hussain (2013), and Gamez and Stark (2014). The other two correlations are presented by Mesri and Shahien (2003) and Wright (2005) using the data developed by Stark and Eid (1997). All three correlations were designed to estimate the effective normal stress-dependent FSS envelope identified by Stark and Eid (1997) using liquid limit, clay-size fraction, and plasticity index. A report by Burns et al. (1990) characterizing embankment failures in Louisiana up to 1990 by clay-size fraction, plasticity index, and liquid limit was digitized into a database. The database is being processed to develop FSS envelopes for Louisiana regions identified in the 1990 study.

To further characterize the FSS envelope for Louisiana soils, a modified Bromhead ring shear apparatus described in Stark and Eid (1993) which reduces the time required to establish a drained residual failure envelope is used in accordance with ASTM (2008a) to determine FSS envelopes for six case sites (3 in LA and 3 in TX). Soils from each site were air-dried, crushed with mortar and pestle, and processed through a U.S. standard No. 40 sieve. After processing, the soils were mixed to a water content near the liquid limit and placed in a climate-controlled room at 55°F with 95% relative humidity for approximately one week to hydrate.

Unsaturated Soil Properties

The soil water retention curve (SWRC) gives the relationship between matric soil suction and moisture content. To determine the unsaturated soil properties, SWRC tests need to be conducted. In the present study, drying path of SWRC was obtained using Tempe cell apparatus and filter paper technique (ASTMD5298-10). For the low suction value (less than 500 kPa), Tempe cell apparatus was used whereas the filter paper technique was used for high suction values. The required amount of air dried soil was, pulverized and passed through a US # 40 sieve. The soil samples were made at 95% of maximum dry density and at optimum moisture content value obtained from Standard Proctor test. The samples were compacted in static compaction machine. To ensure the uniform distribution of moisture throughout the sample, they were kept in a plastic bag in a humidity-controlled room for 48 hours.

Specimens were then confined in all the directions and were left submerged in the distilled water for at least 72 hours to obtain 100% degree of saturation. At the same time, the ceramic disc was saturated in Tempe cell at a pressure of 100 kPa for 24 hours. The Tempe cell apparatus uses the axis translation technique, and the matric suction is obtained by changing the air pressure. Once the air pressure is applied in the cell, the water presented in the pores is allowed to expel from the specimen. The expulsion will continue till the water and air phase reach the equilibrium. The matric suction is increased in steps and water content is calculated at every step by recording the amount of water coming out of sample. After reaching the equilibrium Filter paper water content can be measured. The water content of filter paper is the function of total soil suction. The matric suction can be obtained by utilizing related calibration curves. The unsaturated hydraulic conductivity will be obtained from SWRC curves using Van Gunechten model (1980).

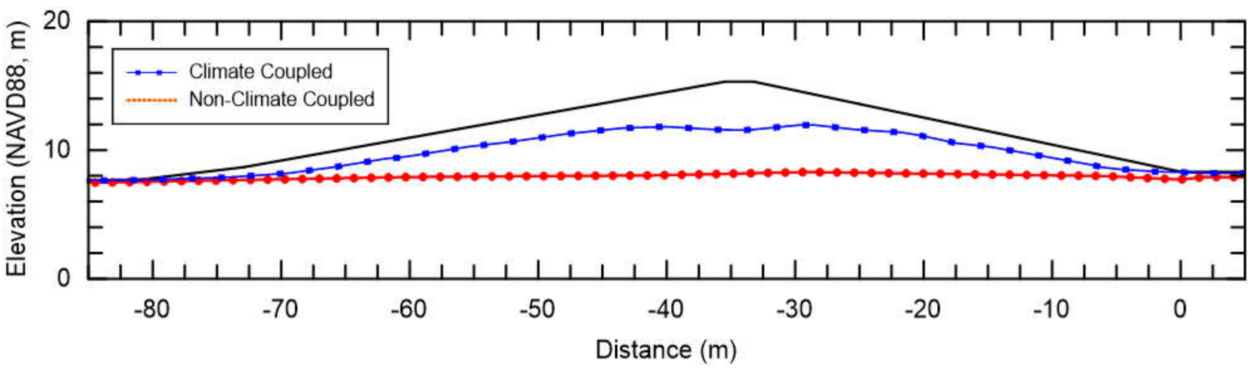

Figure 1. Wetting fronts through high plasticity embankment

FINDINGS AND DISCUSSION

Compilation of embankment failures in Louisiana has shown that the majority of failures occur in high plasticity clays with a large percentage of smectite (Burns et al. 1990). Soil testing is in progress on several Louisiana case studies, primarily located in LA DOTD District 62, along with several failures which occurred after Hurricane Harvey in the northwestern corner of the state near Lake Vernon. Preliminary findings of the coupled soil-atmosphere modeling indicate that an embankment remains saturated with moderate precipitation over a range of typical soil values for compacted clays. Figure 1 shows the wetting fronts of a high plasticity clay embankment from a coupled hydro-mechanical model and a non-coupled model.

Three different embankment slope failure test sites located in Texas were investigated. The soils retrieved from the field were tested for basic soil properties in the laboratory. Table 2 presents the test results. The Liquid Limit (LL) and Plastic Limit (PL) values ranged from 43 to 53 and 20.5 to 22.5, respectively. Based on USCS classification, the soils are high plastic soils with PI ranging from 21.5 to 30.5. The optimum moisture contents are 19, 20, and 22.5% corresponding to the maximum dry unit weight of 104, 98.5, 105 pcf for Site 1, Site 2, and Site 3 respectively.

Table 2. Physical properties of Texas soils

Soil Specimen	LL (%)	PL (%)	PI (%)	USCS	Max γ_d (pcf)	w_{opt} (%)
Site 1	43	21.5	21.5	CL	104	20
Site 2	53	22.5	30.5	CH	98.5	22.5
Site 3	46	20.5	25.5	CL	105	19

SWRC was conducted on soils collected from Sites 2 and 3 in Texas. Figure 2 shows the SWRC curves obtained from Tempe cell apparatus. The obtained results indicate that both soils have similar drying path of SWRC and air entry pressure value. For suction values lower than 100 psf, the change in water content is negligible. However, with an increase in suction level, the water content significantly drops to less than 10%. The high suction states represent the embankment soil conditions during summer season where the water content is less than 10% and the moisture content corresponding to low suction levels represent the conditions after a rainfall event. Further studies will be performed to correlate the water content, pore-water pressure, suction level, and FSS that provides information about the failure conditions at the slopes identified in Texas and Louisiana.

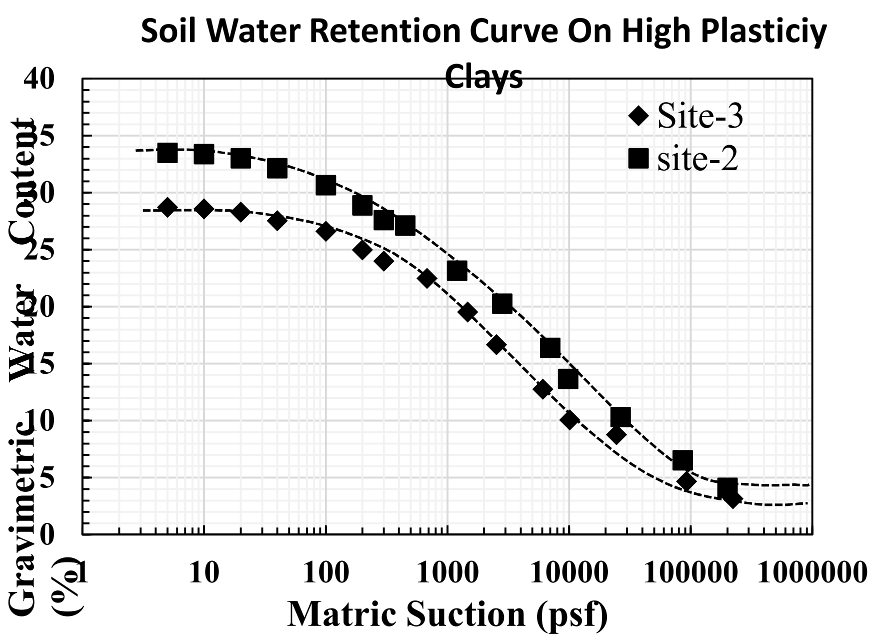

Figure 2. Soil Water Retention Curves for Texas Soils

REFERENCES

ASTM (2008). "Standard Test Method for Torsional Ring Shear Test to Determine Drained Fully Softened Shear Strength and Nonlinear Strength Envelope of Cohesive Soils (Using Normally Consolidated Specimen) for Slopes with No Preexisting Shear Surfaces."

ASTM (2012). "Standard Test Methods for Laboratory Compaction Characteristics of Soil Using Standard Effort ."

ASTM (2017). "Standard Test Methods for Liquid Limit, Plastic Limit, and Plasticity Index of Soils."

Burns, S. F., Hadley, W. O., Mutchler, J. W., Smith, S. M., Siddiqui, A., and Hernandez, M. (1990). "Development of Design Criteria for the Prevention of Slope Failures." Louisiana Transportation Research Center.

Cho, S. E. (2016). "Stability analysis of unsaturated soil slopes considering water-air flow caused by rainfall infiltration." *Engineering Geology*, 211, 184-197.

Collins, B. D., and Znidarcic, D. (2004). "Stability Analyses of Rainfall Induced Landslides." *Journal of Geotechnical and Geoenvironmental Engineering*, 130(4), 362-372.

Daniel, D. E., and Wu, Y. K. (1993). "Compacted Clay Liners and Covers for Arid Sites." *Journal of Geotechnical Engineering*, 119(2), 223-237.

Davies, O., Rouainia, M., Glendinning, S., Cash, M., and Trento, V. (2014). "Investigation of a pore pressure driven slope failure using a coupled hydro-mechanical model." *Engineering Geology*, 178, 70-81.

Gamez, J. A., and Stark, T. D. (2014). "Fully Softened Shear Strength at Low Stresses for Levee and Embankment Design." *Journal of Geotechnical and Geoenvironmental Engineering*, 140(9), 06014010.

Ng. C.W.W., and Menzies, B., (2007). "Advanced unsaturated soil mechanics and engineering."
Taylor and Francis, NY.

Oh, S., and Lu, N. (2015). "Slope stability analysis under unsaturated conditions: Case studies of rainfall-induced failure of cut slopes." *Engineering Geology*, 184, 96-103.

Qi, S., and Vanapalli, S. K. (2015). "Hydro-mechanical coupling effect on surficial layer stability of unsaturated expansive soil slopes." *Computers and Geotechnics*, 70, 68-82.

Stark, T., and Eid, H. (1993). "Modified Bromhead Ring Shear Apparatus."

Stark, T. D., Choi, H., and McCone, S. (2005). "Drained Shear Strength Parameters for Analysis of Landslides." *Journal of Geotechnical and Geoenvironmental Engineering*, 131(5), 575-588.

Stark, T. D., and Hussain, M. (2013). "Empirical Correlations: Drained Shear Strength for Slope Stability Analyses." *Journal of Geotechnical and Geoenvironmental Engineering*, 139(6), 853-862.

Sun, D.-m., Li, X.-m., Feng, P., and Zang, Y.-g. (2016). "Stability analysis of unsaturated soil slope during rainfall infiltration using coupled liquid-gas-solid three-phase model." *Water Science and Engineering*, 9(3), 183-194.

Van Genuchten, M. T. (1980). A closed-form equation for predicting the hydraulic conductivity of unsaturated soils 1. Soil science society of America journal, 44(5), 892-898.

Yang, K.-H., Uzuoka, R., Thuo, J. N. a. a., Lin, G.-L., and Nakai, Y. (2017). "Coupled hydro-mechanical analysis of two unstable unsaturated slopes subject to rainfall infiltration." *Engineering Geology*, 216, 13-30.

Understanding the Influence of Subsurface Geologic Faulting on Transportation Infrastructure, Southeast Louisiana

Chris S. Young[1], Elizabeth C. McDade[2], Nancye H. Dawers[1], and David B. Culpepper[2]

[1]Tulane University
[2]The Culpepper Group, LLC

INTRODUCTION

The influence of active subsurface geological faulting on transportation infrastructure in southeastern Louisiana is insufficiently documented. This is in part due to limitations of mapping the effects of surface faults in poorly consolidated sediments and submerged wetlands. Additional limitations are the knowledge gaps created by the proprietary nature of subsurface data owned by the oil and gas industry, as well as considerable amounts of privately owned land in coastal Louisiana, including large tracts of land owned by commercial interests.

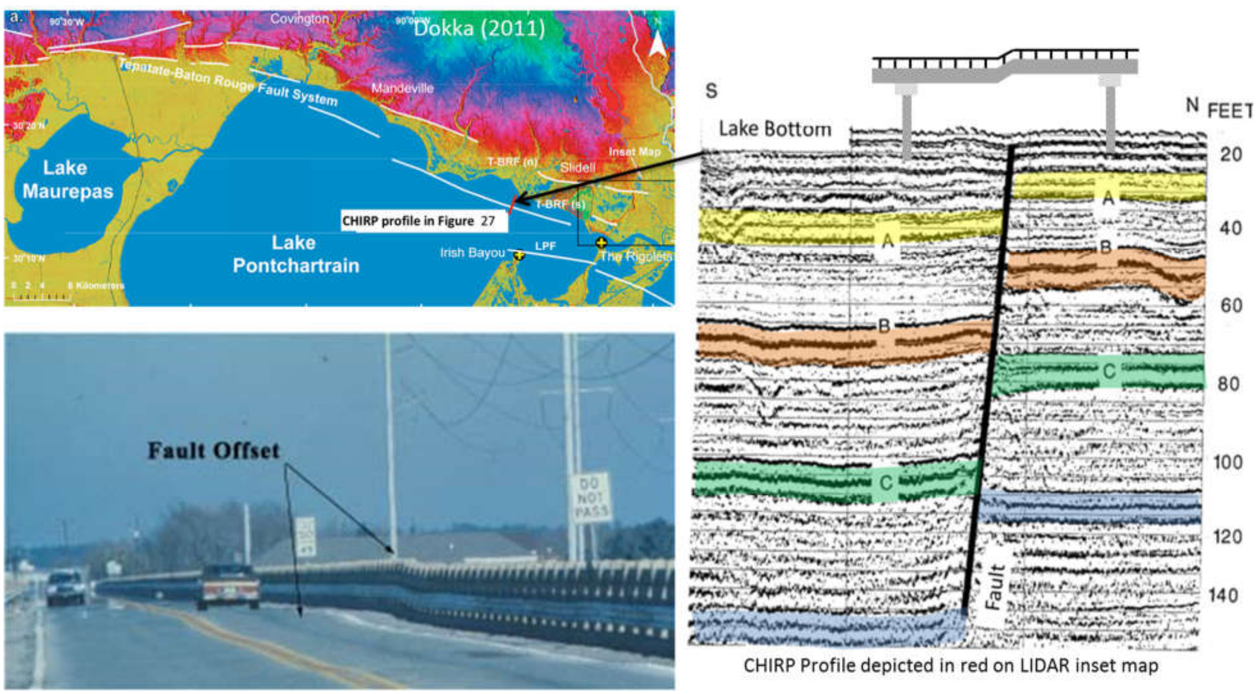

Lopez, J.A., Penland, S. and Williams, J. (1997)

Figure 1: Compilation of figures showing the location of a fault known in the geologic community as the Goose Point fault in Lake Pontchartrain, an extension of the Tepetate-Baton Rouge fault trend whose various segments are shown as white lines on the LIDAR image in the upper left. Lopez et al. 1997 demonstrated that movement on the fault over a 40 year period caused the deformation seen in the Highway 11 bridge near the Northshore entrance. The figure on the right half is a high-resolution 2D CHIRP line that shows the near-surface with clarity. Layers labelled A, B, C were connected and horizontal at the time each was deposited.

Figure 1 shows the effect of more than 40 years' movement on a well-known fault in Lake Pontchartrain, shown here on a shallow high-resolution 2D CHIRP line. The offset seen across the fault plane shows that, for instance, layer C has been offset by about 25 ft at only 75 ft depth. Precise age dating of correlative near-surface layers using radiometric methods allows for calculation of rates of differential movement across the fault. It is important to note that the optimally oriented CHIRP line was acquired after deep 2D seismic data revealed the fault's presence. As Louisiana moves forward in designing and maintaining transportation infrastructure for the future, a continued lack of understanding of the causes of subsidence and surface failure could lead to inappropriate mitigation and rehabilitation measures and create expensive problems that could have been anticipated.

Fortunately, because of its century-long-history of oil & gas exploration, Louisiana does have a wealth of oil & gas industry 3D and 2D seismic reflection data that can provide the foundation for fault trace maps to be created and refined. Because of recent efforts by the New Orleans Geological Society and a number of energy-sector companies, we have access to 3D datasets in a number of areas within the coastal zone. Our coupled TranSET and DOTD LTRC projects aim to compile available fault locations from the 3D and older 2D industry data that we have access to with existing public domain resources to form a foundation for more detailed work. This project is the first of its kind in Louisiana, and with the exception of the Houston area, active fault systems of the Gulf Coast region have largely been ignored in infrastructure planning. This research will contribute to both theory and practice in terms of the planning and adaptive maintenance of transportation infrastructure in southeastern Louisiana.

METHODOLOGY

Our study area, outlined in black in Figure 2, extends from north of Baton Rouge eastward to the Mississippi state line, and southward encompassing all of the onshore area through the Mississippi River's mouth and westward to just west of Houma. The western boundary generally parallels the Atchafalaya River basin NW to SE between Baton Rouge and Lafayette. This area (almost 11,000 sq. miles) contains the major fault systems affecting the Mississippi River delta plain, including the Denham Springs and Baton Rouge fault zones in the north, the Golden Meadow fault zone in the south, and numerous smaller faults in the area south of the river. We have liaised with DOTD personnel to identify key areas of DOTD transportation infrastructure, which include the LA 1 corridor from Golden Meadow to Port Fourchon, LA 23 from the Mid-Barataria area to the Birdsfoot, plus roadways in St. Bernard Parish and interstate highways surrounding the Pontchartrain basin.

We are using GIS methods and ArcMap to create layers of geological information and infrastructure. Data sources we have incorporated to date include geospatial data that delineates the coverage of available oil and gas industry 3D and 2D seismic within southeastern Louisiana. This allowed us to create a layer showing data gaps where high-quality 3D data is not available (3D data gap). Surface fault trace maps from literature sources of a variety of vintages and qualities are being georeferenced to form overlays in Arc-GIS. Compiled fault trace locations from three university-led projects using academically- licensed 3D data form yet another layer. These data are located area in the Golden Meadow to Leeville area (in collaboration with Prof. Rui Zhang, University of Louisiana – Lafayette), Lake Borgne and Lake Pontchartrain areas (in collaboration with Prof. Mark Kulp, University of New Orleans) and the Montegut/Chauvin area (PI Dawers, Tulane University). We are considering the best way to display the fault traces in Arc-GIS and cataloging descriptive metadata to indicate the reliability and resolution of the various data sources

When imported into an Arc-GIS system, surface fault traces will be linear, and their locations can be compared to maps of DOTD managed infrastructure and differentiated from other surface deformation effects such as sediment compaction or fluid withdrawal that would be expected to have very different areal extent. Determination of the cause of surface deformation is necessary so that appropriate design and repair measures can be employed. Once the location and rate of movement of fault zones are delineated, mitigating and rehabilitating actions can be discussed and implemented where warranted. Education of DOTD and LTRC personnel on where and how faults move in south Louisiana is an ultimate goal of this project. When this project is complete, we expect it to be the most comprehensive dataset of its type, and that it will be an essential addition to managing infrastructure in south Louisiana for the next 50 years and more because of the long-acting nature of faults and their movement over time.

FINDINGS

Figure 2A depicts our study area outlined in black with DOTD managed roads and highways; commercially available 3D seismic data is shown in pink and 3D data gap areas in pale yellow. Almost 60% of the study area is covered by 3D, and in the west and south, fully 75% of the study area affected by the most active regional fault zones has 3D coverage. The three university-led projects using academically- licensed 3D data [Golden Meadow-Leeville (ULL), Montegut/Chauvin (Tulane), Lake Borgne (UNO)] are areas of special focus and will provide the most complete picture of near-surface fault effects when this study is complete. In these areas, some funding is available for a full appraisal of fault effects that can be used as a protocol for future work in south Louisiana. The process includes 1) identification of key infrastructure likely to be affected by active faulting, 2) identification and interpretation of 3D and/or 2D seismic data as available, 3) acquisition of appropriately placed sediment borings for near-surface sediment characterization, 4) radiometric dating of correlative horizons so that rates of differential movement across the faults can be calculated.

Ongoing tasks of this project are projecting fault traces in the main study areas, followed by acquisition of high-resolution seismic in the field and collection of sediment cores. Key transportation infrastructure locations in these focused study areas include LA1 and the New Orleans land bridge area including I-10, US Highway 11 and Highway 90 in New Orleans East and Slidell.

As one might expect due to the source, 2D data density is greatest where 3D data is also available in the western and southern parts of the study area due to the concentration of oil & gas development in these areas. It is apparent that 2D data will be especially important to verify faulting in Lake Pontchartrain, in the New Orleans land bridge area between New Orleans East and Slidell, and along the Mississippi River near the proposed Mid-Barataria Sediment Diversion and LA 23.

CONCLUSION

Oil and gas exploration in southern Louisiana has been supported by 2D and 3D seismic reflection data that images the subsurface. This data has shown that in some places, subsurface geologic faults extend to the surface and are active today, potentially deforming the surface and causing an unstable foundation for important transportation infrastructure. Documenting where the faults are, and how they might interact with important transportation infrastructure can be greatly improved when 2D and 3D seismic data interpretation is included as a preliminary step for further geotechnical work. Historical geologic literature with mapped surface impacting faults can also be incorporated into an Arc-GIS system to permit additional examination of the geologic framework. It is expected that this synthesis of the state of knowledge of fault locations in southeast Louisiana will be a useful tool to quickly determine whether DOTD transportation infrastructure is likely to be impacted by active faulting. When confirmed by near-surface investigative procedures such as those employed by the University-led projects, greatly improved temporal and geospatial resolution of differential movement across faults will be the result.

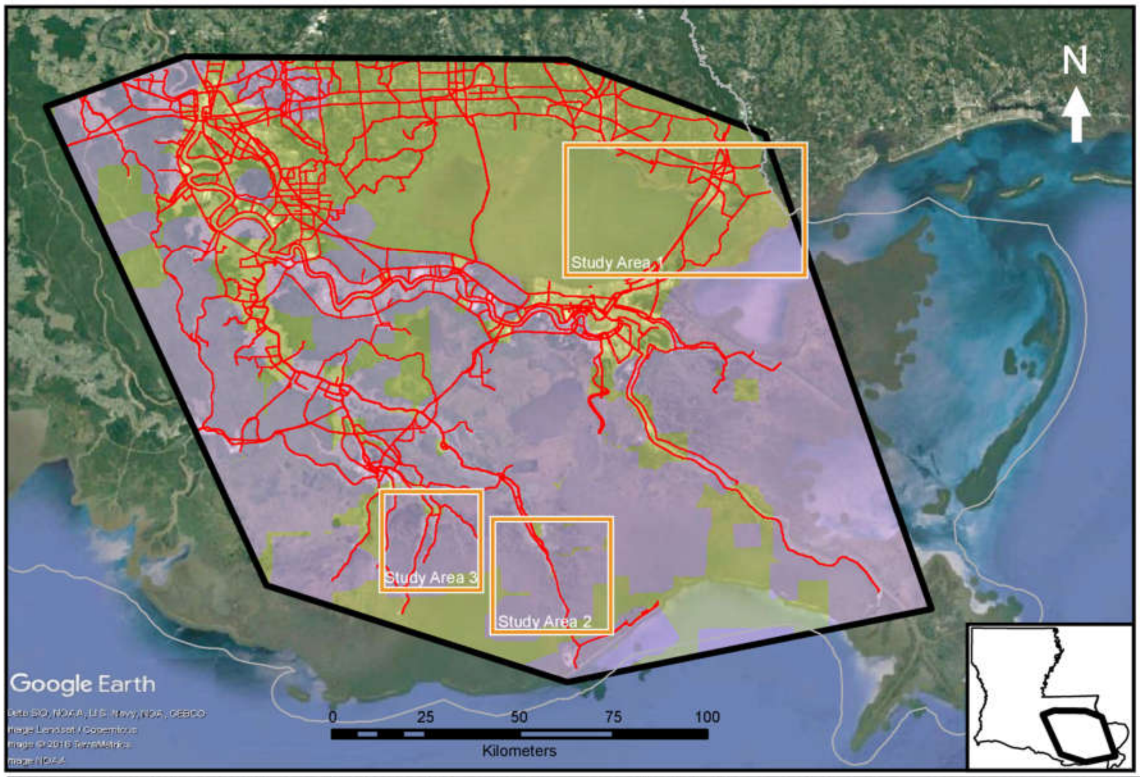

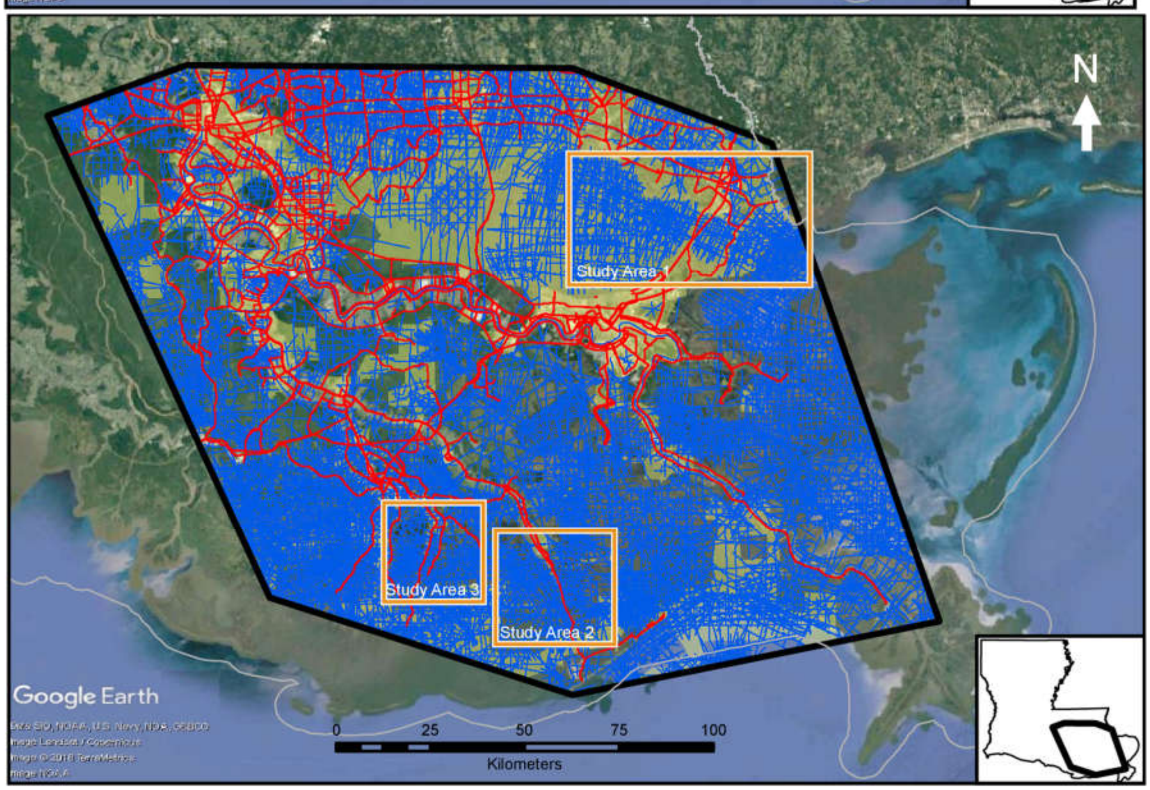

Figure 2: Google Earth satellite image of LTRC DOTD/TranSet UTC study area outlined in black in southeastern Louisiana. The study area touches 21 parishes, spans 103 mi north to south, 114 mi east to west, and encompasses a total area of 10,655 mi^2. Roads and highways are colored red, areas containing 3D seismic data are shaded pink. Areas with no 3D available are shaded yellow (3D data gap). On Figure 1B, an additional layer shows 2D seismic shown as blue lines. The 3D seismic data layer is a composite of existing 3D surveys from SEI, SEITEL, and Schlumberger. 3D seismic coverage consists of 285 surveys that cover a total of 11572 mi^2 and 58% of the study area. Three university-led projects using Academically-Licensed 3D Data [Golden Meadow-Leeville (ULL), Montegut/Chauvin (Tulane), Lake Borgne (UNO)] Are Outlined In Yellow.

REFERENCES

R. K. Dokka, Modern day tectonic subsidence in coastal Louisiana, *Geology* **34(4)** 281-284 (2006) doi:10.1130/G22264.

R. K. Dokka, The role of deep processes in late 20th century subsidence in New Orleans and coastal areas of southern Louisiana and Mississippi, *J. Geophys. Res.,* **116**, (2011) B0643, doi:10.1029/2010JB008008.

Lopez, S. Penland, J. Williams, Confirmation of active geologic faults in Lake Pontchartrain in southeast Louisiana, *Trans. Gulf Coast Assoc. of Geol. Soc.***47,** 299-303 (2008).

Integrated Health Monitoring and Reinforcement of Transportation Structures with Optimized Low-Cost Multifunctional Braided Cables

H. Ozcan[1], J. Ma[2], I. Karaman[1,2]

[1]Department of Mechanical Engineering, Texas A&M University
[2]Department of Materials Science and Engineering, Texas A&M University

INTRODUCTION

To enhance the longevity and performance of next generation structures, high performance material and systems should be integrated with health monitoring systems that can obtain real time data on the condition of structures and identify defects in a timely fashion. Smart materials that can serve multiple functions enables simplified designs, reduced material use, and less manufacturing complexity. A particularly appealing and interesting class of smart materials is shape memory alloys (SMAs). Superelastic SMAs can produce large recoverable deformations triggered by change in stress, and have been considered in a range of civil engineering applications such as bracing systems, connectors, and concrete reinforcement due to their superelastic response, which provides a restoring force to the structure after deformation. This response has been shown to limit the damage sustained by the structure from adverse event such as earthquakes by controlling the deformation and crack growth. Currently, the most widespread SMA candidate for such applications is the NiTi-based alloy also known as “Nitinol”. While it shows excellent superelastic properties, the high cost due to inherent materials cost, difficulty in processing and fabrication, and limited in supply severely limit its application in large - scale applications in transportation projects. This, there exists a need for an alternative to NiTi (Figure 1) that is cost effective, easily processed, and show comparable superelastic response.

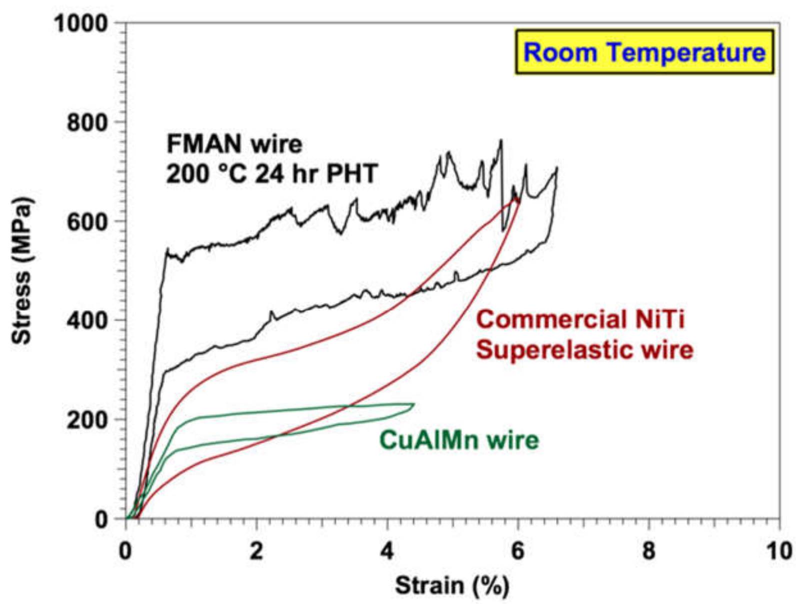

Figure 1: Comparison of the superelastic response of a FMAN wire with wires made of a conventional NiTi and CuAlMn alloys

In recent years, a FeMnAlNi SMA showing large full recoverable superelasticity and high strength was engineered that could address this need. This Fe-SMA contains inexpensive alloy elements and does not require high vacuum during melting required for titanium-based alloys like NiTi. Furthermore, the Fe-SMA shows an interesting meta-magnetic shape memory response, where the magnetic characteristics of the alloy change significantly between the austenite and martensite phases. The result is a change in the induced magnetization of the material during phase transformation, for example from applied stress, which can be easily detected using commercial magnetometers. This property can be harnessed to create a method to monitor the stresses and strains on structural systems with Fe - SMAs remotely and in a non-destructive fashion. The combination of these properties enable a new kind of structural health monitoring framework where the structural and sensing elements are integrated and quantitative information could be collected in real - time with simple instruments. In the current project, we combine materials design, microstructural engineering, modeling, and component level (concrete composite) testing to demonstrate the capability of a self-sensing structural system based on the Fe-SMA system.

METHODOLOGY

We have developed series of thermomechanical processing techniques that allow us to obtain high strength FeMnAlNi superelastic wires transforming at room temperature with a high superelastic strain (Figure 1). These thermomechanical processes are divided into three important steps. First step includes drawing FeMnAlNi wires at room temperature successfully. Second step is to ensure proper microstructure that will provide desired mechanical properties, as well as high superelastic strain. Last step is controlling superelastic stress levels by controlling nano-precipitate size in the microstructure. Finally, these materials are manufactured into large-dimension cable braids that would be suitable for the scale of transportation-related applications. The Cable braiding setup includes a rotating shaft in the middle with seven wire guides. This part is flexible and can be changed to different cable configurations. Individual wires are going to be fed to this rotating shaft and the shaft is attached to motor.

FINDINGS

Fe-based shape memory alloys usually suffer from large elastic and transformation strain anisotropy. This leads to high internal stresses between grains with large orientation mismatches during martensitic transformation. Additionally, limited number of martensite variants in Fe-based systems inhibits strain accommodation at the grain boundaries and intergranular fracture occurs before the transformation is complete. Therefore, it is necessary to eliminate grain boundary constraints, triple junctions to obtain good superelasticity. In order to eliminate these constraints, grain size of the material has to be coarse, perpendicular to the wire axis and span the cross section of the wire. We have developed a simple technique to obtain large grain size through abnormal grain growth. In this method, material has to be repeatedly cycled between single phase and two phase regions in the phase diagram. In order to promote abnormal grain growth in the wires, we subjected cyclic heat treatments between 1200 °C (single phase region) and room temperature (two phase region) for five times under high purity argon atmosphere. In each cycle wires are kept in the furnace for 0.5h and subsequently air cooled. Finally, wires are solution heat treated at 1300 °C for 30 min and quenched in water. Resulting wires with bamboo-like grains that span the entire width is shown in Figure 2.

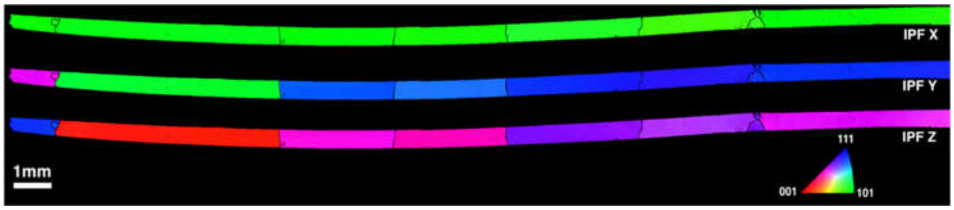

Figure 2: Electron backscatter diffraction orientation mapping of a Fe-34%Mn-15%Al-7.5%Ni (at. %) superelastic wire aged at 200 °C for 24h after tensile superelastic test (the superelastic response is shown in Fig. 1a). The colors represent the crystal directions parallel to the drawing direction (IPFX) and the transverse direction (IPFY) and the normal direction (IPFZ), given in the stenographic triangle.

In order to produce braided cables with different cable configuration, we first need to able to produce wires with greater length. A prototype setup to accomplish this has been designed and fabricated. This system includes a high temperature furnace with atmosphere controlled since all previous heat treatments are performed under high purity argon atmosphere. A spool of wire is fed through a quartz tube and heat treated wire is going to be collected by spool which is located at the bottom of the furnace. Induction coils wrapped around the quartz tube heat the wires to a desired temperature. Each spool is attached to a motor and the speed at which the wire is fed through the heating zone is used to adjust the heat treatment duration. This feature will enable us to change some heat treatment parameters such as duration of the heat treatment. After wires are heat treated inside the quartz tube, air cooling is conducted by removing it from the heating zone.

In cable development, a method has been successfully demonstrated that allows for the fabrication of large diameter wires and strands from the Fe-SMA. Additionally, a method for the fabricating braided cables from Fe-SMA wires has been identified and a design has been created. Prototype design for the braiding weave was created to show a 1x7 wire pattern as shown in Figure 3. The PIs have established an industrial collaboration with Fort Wayne Metals, one of the leading metal cable and braided structure producers in the United States.

(a) (b)

Figure 3: a) Three different braiding patterns made from braiding setup, and b) close-up of a single wire

CONCLUSIONS

We have shown through a combined design of the micro and macro-structure of the material, the Fe-SMA alloy system can be adopted into a self-sensing structural framework. We further show that such a system can be potentially used in real-life transportation projects by creating braided cable structures with large dimensions and determining acceptable sensing conditions. The developed multifunctional composites will potentially transform the design, construction, and rehabilitation of infrastructure systems. They will improve safety by increasing structural performance and enabling damage detection; enhance durability by limiting progressive damage; increase sustainability by extending service life; and improve resiliency by providing re-centering capabilities. Additionally, the project defines a viable path for technology transfer by establishing substantive partnerships with commercial alloy manufacturers such as Fort Wayne Metals, one of the leading metal cable and braided structure producers in the United States, and cultivate the awareness and expertise in the technology through workforce development and outreach activities.

Coastal Bridges under Hurricane Stresses along the Texas and Louisiana Coast

Adolfo Matamoros and Firat Testik
University of Texas at San Antonio

RESEARCH FOCUS AND OPPORTUNITY BEING ADDRESSED

The societal cost of natural disasters can be significantly decreased through planning for resilience instead of accepting the risk and repairing the damage. For example, Padgett et al. (2009) indicate the cost of repairing and replacing bridges damaged during hurricane Katrina exceeded 1 billion dollars, and their review of the damage reports showed that this cost could have been significantly reduced by implementing relatively simple mitigation measures.

The most severe damage consisted of superstructure collapse due unseating of the deck, which was induced by the combined actions of storm surge and hydrodynamic forces from waves. This type of failure was observed both in bridges with integral and non-integral supports, which shows that in some instances uplift forces were large enough to exceed the weight of the superstructure and cause failure of the connection at the support. Studies that document damage from major hurricanes provide a valuable source of information to study the risk to bridge infrastructure due to hurricanes. While empirical observations are useful, there is a need to develop scientific models capable of simulating fluid-structure interaction under the combined actions of storm surge and waves, so the risk can be quantified through a scientific rather than empirical approach.

PROJECT IMPACT

The research addresses a knowledge gap by developing a new model to simulate complex interactions between bridges, storm surge, and waves. A model of this type will permit studying the effect of hydrodynamic forces characteristic of the Texas-Louisiana Gulf coast, which will help identify bridge structures with the greatest risk of collapse due to unseating during hurricanes.

SUMMARY

A high-resolution FE model was created to simulate the hydrodynamic forces caused by waves impacting on bridge girders. The model relied on Coupled Eulerian-Lagrangian techniques (CEL) where solids are simulated with Lagrangian meshes while fluids are simulated using Eulerian meshes (Figure. 1).

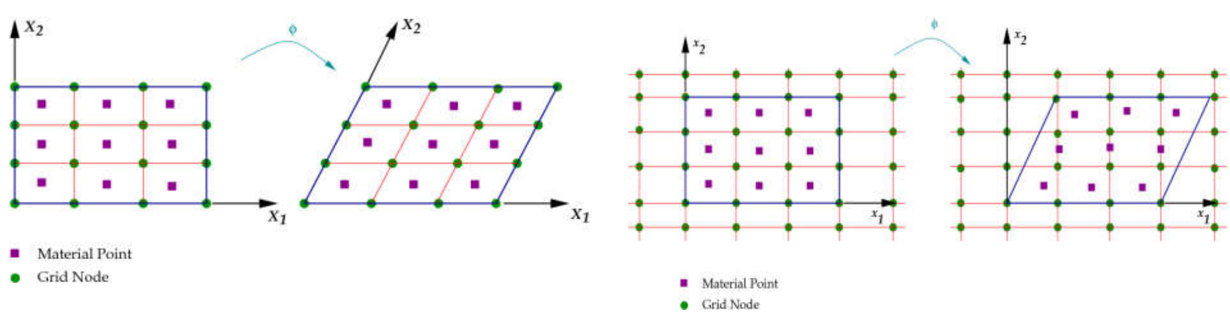

a) Lagrangian Mesh b) Eulerian Mesh

Figure 1. Eulerian and Lagrangian meshes

Lagrangian meshes are attached to material points, and as materials deform, the mesh deforms with them (Figure. 1a). Eulerian meshes remain the same as the material flows (or deforms) within the mesh. The extent of deformation in this case is measured when the material particle flows across an element node (it acts as a background grid).

Results from the simulations are shown in Figure 2. A wave is simulated by inducing an initial velocity in the fluid, at the edges of the domain. Variations in wave properties (wavelength and amplitude) are introduced by adjustments in the boundary conditions of the fluid domain. The model is being validated by calculating buoyancy forces induced by simple variations in fluid height, and by comparing hydrodynamic forces with existing data sets and classical solutions.

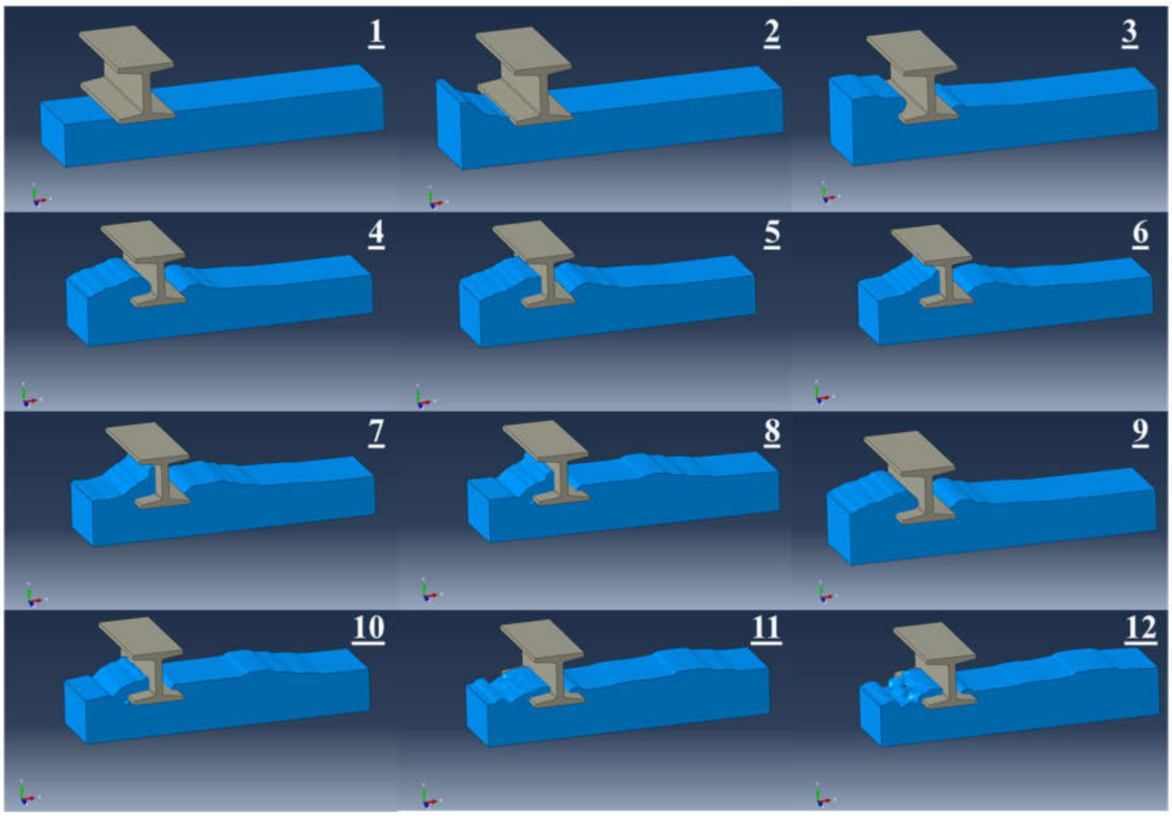

Figure 2. Modeling of a wave impacting a bridge girder

Design Considerations in the Use of Unmanned Aerial Vehicles for the Purpose of Bridge Inspection

Paul J. Darby
Department of Electrical and Computer Engineering, University of Louisiana at Lafayette

INTRODUCTION

The practical scope herein included data gathering, and analysis pursuant to provide recommendations for two instrumented Unmanned Aerial Vehicles (UAVs) for demonstration to determine their application, feasibility, suitability, practicality, and effectiveness in bridge inspection. When considering the practical application of Unmanned Aerial Vehicles (UAVs) to the task of bridge inspection, many factors may be considered in the design of practical UAVs and associated instrumentation. The *problem and objective* in this study, is not to determine ways to fully replace the bridge engineers or inspectors, but instead to achieve a system design to assist and even augment those persons where possible, achieving a more practical and safe interim solution, which can evolve with technological improvements and changes in the case of UAVs, instrumentation, knowledge in the inspection of bridges, and bridge design itself. While UAV demos have not taken place as of yet, the research done thus far is revealing interesting opportunities for improvement of both commercial off the shelf (COTS) and custom UAVs and Instrumentation, to better meet the needs of bridge inspection and to better assist the needs of bridge inspection engineers in this process.

BRIEF REVIEW OF THE PERTINENT LITERATURE

Sources especially useful to the team in considering the instrumentation to be carried by UAVs, included the Bridge Inspector's Reference Manual, the Unmanned Aerial Vehicle Bridge Inspection Demonstration Project, by the Minnesota Dept. of Transportation, and papers on Crack Detection in Concrete, to name a few [1] [3] [4]. With respect to the available functionality in the field of UAVs, interviews with both a commercial UAV pilot and the Input from hobbyists consultants, as well as numerous hobbyists literature sources, proved to be invaluable [6 through 29].

BRIEF DESCRIPTION OF METHODS

The method of initial investigative research within the project has followed four steps:

1) Step 1: Gaining a useful knowledge of the conventional bridge inspection process, i.e. what human bridge inspectors look for and related ergonomics.
2) Step 2: Gaining knowledge pertaining to projects similar to our UAV Bridge Inspection Project.
3) Step 3: Survey of instrumentation functionality, suitable for use in bridge inspection using UAVs.
4) Step 4: Survey of UAV functionality, suitable for use in bridge inspection.

THE MAIN RESULTS OF THE WORK

Thus far, this includes specialized design adaptations to UAV and Instrument hardware and software to allow application of this technology toward practically assisting bridge inspectors in their work, to offer scheduling, economic and safety benefits.

IMPORTANCE OF THIS WORK

The research is important in contributing primarily to potential enhancements to the *practice* of bridge inspection through UAV technology. We feel that the application of UAVs, and broadly defined intelligent instrumentation, to assist in bridge inspection offers substantial economic and safety benefits, but to be accepted it must be seen by bridge inspectors, and the employing organizational entity as useful, practical and offering the aforementioned economic and safety benefits.

METHODOLOGY

The primary theme driving our methodology is “mission success.” Here the mission is defined as the design of a UAV-centered system to assist bridge inspectors and bridge engineers in the meaningful, economical, and practical inspection of bridges. The following were important premises to our methodology:

1) *Small Budget Limitation* - With respect to the potential costs of professional-grade UAVs, utilized by for example, the State of Minnesota, in its bridge inspection demo, with costs up to $140,000 [2][29], our entire budget for UAVs and instrumentation to be utilized in our demo is only $6,000. This required our team to be highly innovative in its design considerations for the mission, to achieve mission success on a budget.
2) *Practicality Focus Group, Design Team and Interviews* – We surmised that the research goal is to determine if bridge inspection by UAV’s can provide practical assistance to bridge inspectors and economic and safety benefits to the organizational entity employing this technology, e.g. State of Louisiana. Hence, in addition to a literature search to learn the science and technology associated with bridge inspection [1] [2] [3] [4] [5] both currently and to understand the potential evolution of the technology, the PI formed a project team combining expertise from physics, engineering, computing, and UAV hobbyists, and the team conducted interviews with bridge inspectors and engineers with the LADOTD, as well as a commercial UAV pilot with Aerobotics Inc [27][28]. The team served as both a focus group and design team. The aim was not only to assess the potential capabilities of UAV and instrument technology, but also to determine its current limitations or weaknesses with respect to bridge inspection, and to make recommendations in the course of this research to strengthen the application of UAVs to bridge inspection.
3) *Reliability to ensure Mission Success* – UAV technology is still quite new requiring a combination of traditional research methods and new ones. Our team felt it was important that all avenues to ensure practical results having credibility in the bridge inspection community were taken. Hence, our methodology employed *characterization experiments* with UAVs, the *experience of actual UAV hobbyists, consultation with a commercial UAV pilot*, and *thought experiments* covering the use of UAVs and instruments in bridge inspection. Our methodology further considered UAV experience, extrapolated from actual hobbyists flight experience, in order to practically consider design alternatives and tradeoffs to ensure high mission reliability.

4) *Maximization of Software use to add Value where feasible* – The great effort to get a UAV in the air and to reliably trace the bridge in order to gather inspection data, should not be wasted. Instruments carried aloft by the UAV are only as good as their ability to collect meaningful data. Hence, the team felt that every effort should be made to maximize the use of intelligent software so as to optimize the UAV flight time and engineering time in the collection, safe storage, transmittal, pre-analysis, concurrent analysis, and post analysis of data. If this capability is not "off the shelf available'" then it is recommended as a research and development goal finding of this project.

FINDINGS

While the current state of Unmanned Aerial Vehicle (UAV) and Instrumentation technology is impressive, UAVs and the Instruments they can carry, are not naturally suited to bridge inspection. The team found that all "Off the Shelf" Commercial UAVs and Instruments must be adapted or modified in order to be suitable practically for bridge inspection. In some cases, especially with an economically restricted budget, it may be necessary to construct a do it yourself (diy) UAV and even to construct instruments and fixtures with which to attach them to the UAV. A brief abridged summary of important decisions and findings pertaining to the appropriate design of the UAV bridge inspection system are included below:

1) *The Design should be limited to Small Inexpensive UAVs*, so as to live within our modest budget, and to demonstrate that bridge inspections can be economically assisted through UAVs, 2) *The Design should seek to use adaptable lightweight off the shelf or custom built instruments*, to maximize flight time and to adapt instruments to bridge inspection, 3) *The design should plan to have separate inspection flights, each with a single instrument*, so as to maximize flight time given to each bridge inspection pass, and to minimize the cost of a single mishap, where instruments may be lost, 4*) UAVs and gimbal arrangement will need to be adapted for inspecting beneath the bridge deck*, i.e. to include top mounted and upward-looking camera gimbals, upward-looking spot lights to provide a visual light source, and visual location software to allow the UAV's self-location when GPS is lost beneath the bridge deck, 5) *The UAV will require special modifications so as to allow it to survive the environment in and around the bridge*, including a pressurized gas canister inflated parachute and floats to slow the UAV's fall and to stop it from sinking into the water beneath the bridge, should an emergency occur, 6*) Since wind speed and turbulence near and around the bridge can be gusty and significantly greater than at ground level, the UAV flight controller should be equipped with high-speed orientation compensation to face the UAV into the wind*, and an automatically adjusting gimbal, to ensure a low wind profile, while maintaining the gathering of visual data, to name a few.

Other Important Findings include:

- UAV Aircraft Carrier - i.e. a small remotely controllable boat beneath the bridge to serve as a landing craft, to store freshly charged batteries, and to serve as a visual location reference point in case of loss of GPS signal.
- Ceiling Distance Control and Obstacle Avoidance – the UAV tends to get pulled toward a physical ceiling if it comes to close when flying. In the case of flying beneath the bridge deck, an active self-limiting distance control is in order to prevent crashes.
- Waterproofing – of UAV components is an area requiring some practical research.

- Use of 3D Printed Components – is important as it allows customization of both the UAV, instruments and instrument attachments, as well as the economic replacement when such custom components become damaged.
- UAV Onboard Computer Programmed with Bridge Components – A UAV could be programmed with a list of bridges and their components data, e.g. from the bridge truss, deck, beams, piles, etc., and their previous conditions, to allow the UAV to focus its inspection on needed areas and to do comparisons with new inspection data, enhancing the inspection process.
- Video of bridge deflection with dynamic vehicle load.
- Software to search-identify - the most important inspection images out of thousands for the engineer to view.
- Fault-tolerant UAV design - with multiple UAVs that are able to coordinate activities, e.g. for location, recovery of downed UAV, etc.
- More practical research needed to enhance concrete crack detection with instrumented UAVs.

CONCLUSION:

From the findings herein, we can infer that a) commercial off-the-shelf UAVs and instruments require customization to be adequate to the task of bridge inspection. Hence, whether we pursue a do it yourself UAV, or utilize off-the-shelf components, a significant degree of customization will be required, b) a number of logistical difficulties, namely involving FAA regulations and the need for a UAV pilot's license, as well as weather and safety factors, make extensive proof testing in the actual environment slow going, however, the work herein provides a platform of practical improved UAV-Instrumentation design recommendations upon which theories can be tested through experimentation.

REFERENCES

[1] Bridge Inspector's Reference Manual, Publication No. FHWA NHI 12-049, December, 2012, Federal Highway Administration, Bridges & Structures, website: www.fhwa.dot.gov/bridge/nbis.cfm, Information, direct website: www.fhwa.dot.gov/bridge/nbis/pubs/nhi12049.pdf.

[2] B. Lovelace, Principal Investigator, "Unmanned Aerial Vehicle Bridge Inspection Demonstration Project," Minnesota Dept. of Transportation, Research Services & Library, Office of Transportation Management, July 2015, website: http://www.dot.state.mn.us/research/TS/2015/201540.pdf

[3] A. Mohan, and S. Poobal, "Crack Detection using image processing: A critical review and analysis, Alexandria University, Alexandria Engineering Journal, website: https://ac.els-cdn.com/S1110016817300236/1-s2.0-S1110016817300236-main.pdf?_tid=7802e9a0-0098-11e8-9714-00000aab0f27&acdnat=1516751736_2224f2c544f958f3deba328f19ff0d51

[4] F. Pereira, C. Pereira, "Embedded Image Processing Systems for Automatic Recognition of Cracks using UAVs," ScienceDirect, IFAC –PapersOnLine 48-10 (20150 016-021, website: https://ac.els-cdn.com/S2405896315009684/1-s2.0-S2405896315009684-main.pdf?_tid=64ca798a-0097-11e8-b135-00000aab0f26&acdnat=1516751275_740952005b041775a2ad46aa62bd2e8d

[5] B. Milovanovic, and I. Pecur, “Review of Active IR Thermography for Detection and Characterization of Defects in Reinforced Concrete,” Journal of Imaging, 2016, 2, 11, doi:10.3390/jimaging2020011, website: https://www.mdpi.com/journal/jimaging
[6] “Drones The Complete Manual Third Edition,” 2017, Future Publishing Ltd, Richmond House, 33 Richmond Hill, Bournemouth, Dorset BH26EZ, website: http://www.futurepic.com
[7] “2017 Best Camera Drones Buying Guide,” website: http://m-campaign.dji.com/event/views/drone/index.html
[8] Team Rotordrone, “Nine Great Camera Drones,” A guide for the aerial photographer and videographer,” Rotor Drone Magazine, Vol. 4, No. 5, Sept. /Oct. 2017, pp. 40-48.
[9] “Drone Cam,” The Drone Book, 2017, Future Publishing Ltd, Richmond House, 33 Richmond Hill, Bournemouth, Dorset BH26EZ, website: http://www.futurepic.com, p. 8
[10] “Getting Started with Your Drone,” The Drone Book, 2017, Future Publishing Ltd, Richmond House, 33 Richmond Hill, Bournemouth, Dorset BH26EZ, website: http://www.futurepic.com, p. 20
[11] “Essential Drone Accessories,” The Drone Book, 2017, Future Publishing Ltd, Richmond House, 33 Richmond Hill, Bournemouth, Dorset BH26EZ, website: http://www.futurepic.com, p. 32
[12] “Top 10 Drones,” The Drone Book, 2017, Future Publishing Ltd, Richmond House, 33 Richmond Hill, Bournemouth, Dorset BH26EZ, website: http://www.futurepic.com, p. 34
[13] “Building Your own Drone,” The Drone Book, 2017, Future Publishing Ltd, Richmond House, 33 Richmond Hill, Bournemouth, Dorset BH26EZ, website: http://www.futurepic.com, p. 46
[14] “How Not to Get Into Trouble,” The Drone Book, 2017, Future Publishing Ltd, Richmond House, 33 Richmond Hill, Bournemouth, Dorset BH26EZ, website: http://www.futurepic.com, p. 52
[15] “Photographic Filming,” The Drone Book, 2017, Future Publishing Ltd, Richmond House, 33 Richmond Hill, Bournemouth, Dorset BH26EZ, website: http://www.futurepic.com, p. 64
[16] “Explore with Your Drone,” The Drone Book, 2017, Future Publishing Ltd, Richmond House, 33 Richmond Hill, Bournemouth, Dorset BH26EZ, website: http://www.futurepic.com, p. 70
[17] “Getting Started with FPV,” The Drone Book, 2017, Future Publishing Ltd, Richmond House, 33 Richmond Hill, Bournemouth, Dorset BH26EZ, website: http://www.futurepic.com, p. 76
[18] “10 Amazing Ways Drones are Changing the World,” The Drone Book, 2017, Future Publishing Ltd, Richmond House, 33 Richmond Hill, Bournemouth, Dorset BH26EZ, website: http://www.futurepic.com, p. 90
[19] “Deliveries, Errands, & More,” The Drone Book, 2017, Future Publishing Ltd, Richmond House, 33 Richmond Hill, Bournemouth, Dorset BH26EZ, website: http://www.futurepic.com, p. 106
[20] “Mapping the World,” The Drone Book, 2017, Future Publishing Ltd, Richmond House, 33 Richmond Hill, Bournemouth, Dorset BH26EZ, website: http://www.futurepic.com, p. 126
[21] “Program a Raspberry Pi Quadcopter,” The Drone Book, 2017, Future Publishing Ltd, Richmond House, 33 Richmond Hill, Bournemouth, Dorset BH26EZ, website: http://www.futurepic.com, p. 142

[22] "Program a Drone's Flight Path," The Drone Book, 2017, Future Publishing Ltd, Richmond House, 33 Richmond Hill, Bournemouth, Dorset BH26EZ, website: http://www.futurepic.com, p. 148
[23] "Underwater PI Drone," The Drone Book, 2017, Future Publishing Ltd, Richmond House, 33 Richmond Hill, Bournemouth, Dorset BH26EZ, website: http://www.futurepic.com, p. 156
[24] PB_DronesandQuadcopters-10-2016-single, website: https://www.droneflyers.com/wp-content/uploads/2016/10/PB_DronesandQuadcopters_10-2016-single-1.pdf
[25] J. Baichtal, "Building Your Own Drones – A beginner's Guide to Drones, UAVs, and ROVs," Que Publishing, 2016, Aug 2015, Chapter 4
[26] "Drones The Complete Manual Third Edition," 2017, Future Publishing Ltd, Richmond House, 33 Richmond Hill, Bournemouth, Dorset BH26EZ, website: http://www.futurepic.com
[27] J. Begnaud, LA Dept. of Transportation and Development, Interview, Aug. 2017
[28] D. Bartels, Aerobotics Inc., Interview, Aug. 2017.
[29] Minnesota Dept. of Transportation, Email questionnaire, Aug. 2017.

Cost-Effective Methods to Retrofit Metal Culverts Using Composites

Rahulreddy Chennareddy[1], Susan Bogus Halter[2], and Mahmoud Reda Taha[2]

[1]Doctoral Student, Department of Civil Engineering, University of New Mexico
[2]Professor, Department of Civil Engineering, University of New Mexico

INTRODUCTION

Metal culverts are serving as a major water conveyance structures in highway design since the mid 1950's. Corrosion of metal culverts has excessively lowered their life expectancy from 50 years to 30 years and significantly affected their serviceability [1]. A study by the Transportation Research Board (TRB) in 2004 indicated that failure of metal culverts has been significantly increasing all over the country. Failure of metal culverts is a relatively expensive event. The high cost of rebuilding metal culverts is not only related to materials and construction cost, but also to costs associated with closure of and traffic delay [2]. Retrofit of existing culverts would be preferable than replacing them because of the complexity associated with un-backfilling, deconstruction, reconstruction and re-backfilling. A common current technique to retrofit metal culverts is to apply a metal liner inside the culvert and apply shotcrete lining to the surface [2]. The challenge in that approach is the new metal liner is still prone to corrosion and shotcrete loses cross-section due to water flow abrasion. There is an urgent need to develop cost-effective strategies to retrofit corroding metal culverts. The proposed technique shall be corrosion free and shall also require minimal maintenance.

Fiber reinforced polymers (FRP) are polymeric matrix typically polyester, vinyl ester, and epoxy reinforced with fibers being glass, carbon, basalt or aramid fibers. A detailed review of FRP materials for structures can be found elsewhere [3]. With improved manufacturing techniques, glass fiber reinforced polymers (GFRP) have emerged as a desirable material for structural applications. GFRP is essentially corrosion free. This makes GFRP a preferred material over steel under harsh service environments. We propose to use GFRP pipe section that is slide to fit inside the metal culvert to a method to retrofit current corroded metal culverts. The proposed technique shall alter life expectancy of retrofitted metal culverts to exceed 70 years post rehabilitation. We show a method of fit in a GFRP profile liner into an existing metal culvert and using a nano-modified polymer grout to achieve a composite action between the existing metal culvert and the new GFRP liner.

METHODOLOGY

First, bond strength tests were conducted between GFRP and steel using a double lap joint test method. The tests were conducted using 5.6 kip MTS Bionex servo hydraulic test system with a crosshead displacement rate of 0.02 in/min as shown in the Figure 1. Second, a full scale GFRP pipe with an outer diameter of 15 in, length of 90 in and a thickness 0.5in has been acquired. The GFRP pipe has been fabricated using filament wounding technique using an amine based epoxy as the matrix for GFRP section. A corrugated metal pipe with an outer diameter of 18 in, length of 90 in, and a thickness of 0.25 in has also been acquired. The composite GFRP pipe has been fit into the metal corrugated pipe. To enable composite action between the metal pipe and the GFRP pipe, an epoxy grout was used to bond the GFRP pipe to the steel section. The epoxy used for the grout is a two-component epoxy system supplied by U.S. Composite, Palm Beach, FL was used. The primary component is a low viscous liquid epoxy resin 100% reactive based on Bisphenol-A containing EPOTUF®37-058, which is C12-C14 glycidyl ether. The second component is an epoxy-hardener consisting Aliphatic Amine EPOTUF®37-614. The resin to hardener mix ratio is 2:1 by weight of the epoxy. A threepoint bending test was conducted to test the composite action between the metal culvert and the GFRP pipe. The fit-in GFRP-steel composite pipe section is shown in Figure 2.

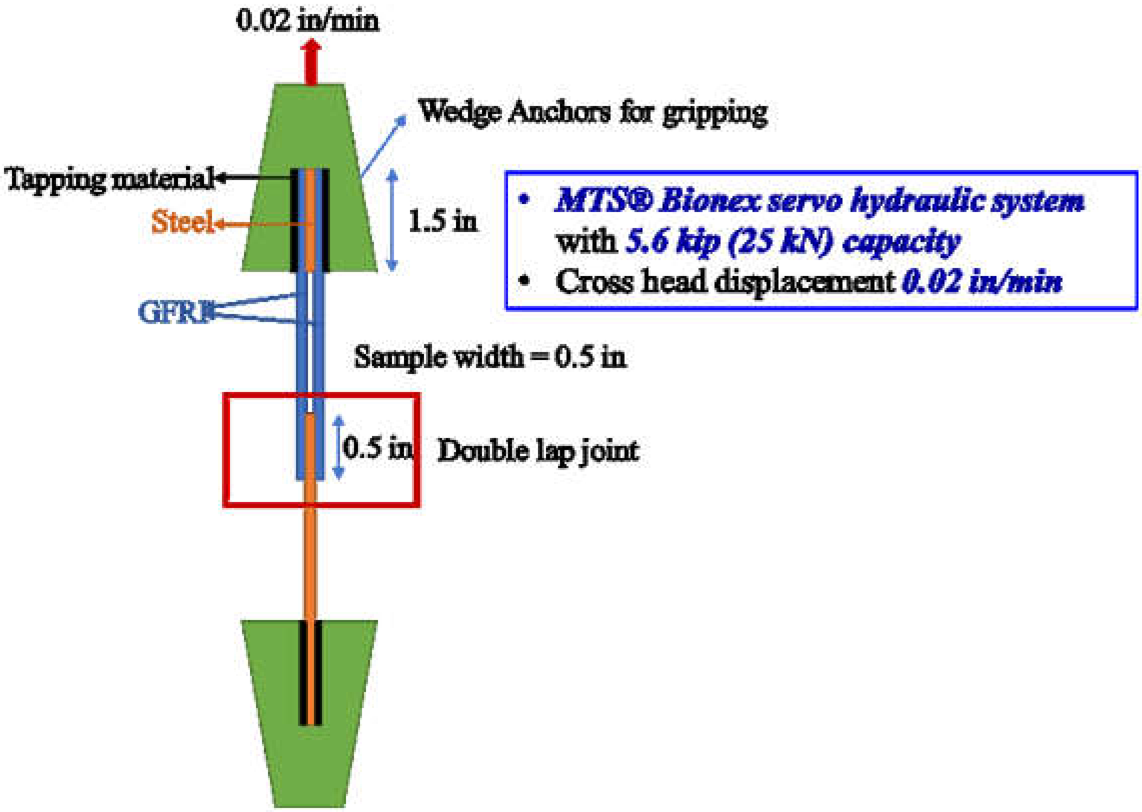

Figure 1: Schematic showing the shear test setup used for determining the bond strength between steel and GFRP

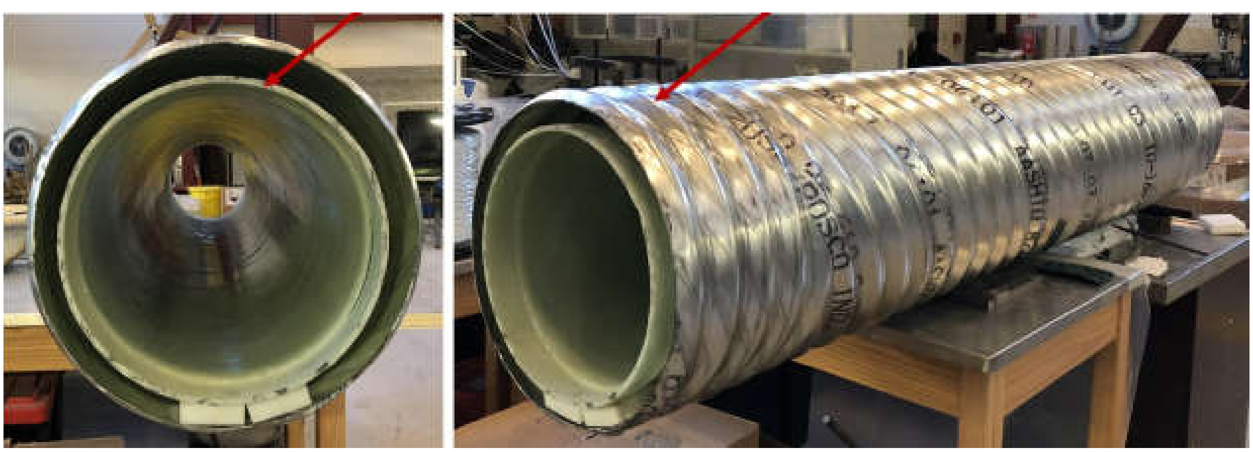

Figure 2: GFRP pipe section as a fit-in liner for the corrugated metal pipe simulating the technique to be used in the field for retrofit of corroded metal culverts

FINDINGS

We have conducted double lap shear test to determine the bond strength between GFRP and steel using epoxy. It is to be noted that the bond shear strength and shear modulus are critical parameters for developing the composite action of the metal culvert and the GFRP material.

The experimental results are presented in Table. 1. The results show that sufficient bond between GFRP and metal surface is accomplished and thus a composite action between the two sections can be developed.

Table 1: Double lap joint bond test results

	Bond shear strength	**Shear Modulus**
Sample	MPa	MPa
1	25.6	203.8
2	24.9	135.5
3	27.6	201.9
4	24.1	205.3
5	25.3	121.4
Mean	25.5	173.6
St. dev.	1.3	41.5

A methodology to completely rehabilitate an existing corroded corrugated metal culvert has been developed by fitting in a GFRP pipe section and the gap between GFRP pipe and the corrugated metal pipe is filled using an epoxy. Testing of the composite GFRP-steel pipe under 3-point bending is on-going.

CONCLUSIONS

A comprehensive culvert rehabilitation technique with an expected life of 75 years is being developed using as fit in GFRP pipe liner slide inside corroded metal culvert. Bond shear strength between GFRP and steel has been determined to be sufficient to achieve composite action. Further testing is underway to show the capacity of the new composite section to be used for retrofitting corroded metal culverts.

REFERENCES

[1]. Perrin Jr, J., C.S. Jhaveri, and J. Perrin Jr. *The economic costs of culvert failures*. In *Prepared for TRB 2004 Annual Meeting, Washington DC*. 2004.

[2]. Wyant, D., *Assessment and Rehabilitation of Existing Culverts. NCHRP Synthesis of Highway Practice No. 303.* Transportation Research Board, Washington DC, 2002.

[3]. Bakis, C., et al., *Fiber-reinforced polymer composites for construction-state-of-the-art review.* Journal of Composites for Construction, 2002. **6**(2): p. 73-87.

Multi-hazard Risk Analysis of Bridges Considering Climate Change

Omid Khandel[1] and Mohamed Soliman[2]

[1]Doctoral Student, School of Civil & Environmental Engineering, Oklahoma State University, Stillwater, OK 74078
[2]Assistant Professor, School of Civil & Environmental Engineering, Oklahoma State University, Stillwater, OK 74078

INTRODUCTION

Bridges are vulnerable to continues deterioration due to various mechanical and environmental stressors. Hydraulic-related hazards (e.g., flood and scour), environmental conditions, and seismic events (e.g., earthquake) are recognized as the most significant sources that may threat the safety of bridges. In the United States, more than 50% of bridges failures are attributed to hydraulic stressors (Cook et al. 2015). In addition, the annual direct cost of corrosion damage of highway bridges in the U.S. is estimated at $8.3 billion (about 0.1% of the Nation's gross domestic product, GDP), while the indirect cost (e.g., traffic delays) is estimated to be 10 times of that value (Koch et al. 2002). Furthermore, analysis of bridge failures between 1980 to 2012 indicates that earthquake events are among the hazards that lead to most losses (Lee et al. 2013). The significance of each of these deterioration mechanisms and the possibility of occurrence of two or more of these hazards requires performing multi-hazard analysis in order to assess bridge failure risk. This paper focuses on multi-hazard risk assessment for bridges under flood, earthquake, and corrosion effects.

Hydraulic-related hazards have been identified as the most probable causes of bridge failure in the U.S. (AASHTO 2010; Briaud et al. 2013). This type of failures depends on precipitation patterns and flood events at the bridge location. In this context, the National Oceanic and Atmospheric Administration (NOAA) reported an average increase of 612% in the number of floods in the United States since the 1960s; future increase in this percentage is also possible and expected (NOAA 2015). This increase in flood frequency and intensity, which may be attributed to climate change, can unfavorably affect the safety of Nation's bridges. Subsequently, our transportation systems and the communities which they serve may experience overwhelming consequences due to the impact of climate change. As an indication on the severity of this problem, the 2015 flooding in Texas and Oklahoma led to at least five reported complete or partial bridge failures, 31 deaths, and more than $2.5 billion in economic losses to the region (Fechter 2015; Danner and Fuller 2015; Smith et al. 2017). As a result, bridge design and management approaches should consider climate change in quantifying the future flood hazard.

Prediction of future temperature, precipitation, regional moisture, rainfall, and river streamflow is subjected to significant uncertainty due to climate change. Traditional design methods relying on return periods (i.e., 50, 100, or 500 year floods) may not be provide reliable results. Accordingly, in order to improve future predictions, more advanced computational tools such as global climate modeling should be adopted. Global Climate Models (GCMs) provide a numerical representation of chemical, physical, and biological aspects of global climate system. Downscaling methods should next be used for deriving regional climate information from the adopted global scale data. For the proper implementation of these models, different types of GCMs, scenarios of future greenhouse gas (GHG) emission, and downscaling methods should be considered.

Over the past decades, researchers have introduced methodologies to quantify the risk of bridge failure under flood and flood induced scour. Some of these methodologies consider the uncertainties associated with the flood and scour prediction through probabilistic analysis. Banerjee & Ganesh Prasad (2013) and Ganesh Prasad & Banerjee (2013) proposed a multi-hazard risk assessment framework considering bridges under scour and seismic loading. In both of these studies, fragility curves considering the flood, scour, and earthquake loadings for different damage states have been established. The structural analysis and flood prediction in these studies have been performed using finite element modeling and return period methodology, respectively. In another effort, Dong and Frangopol (2016) presented an approach to quantify the risk of bridge failure and bridge resilience under multi-hazard exposure. Their study quantified the bridge risk under 100, 200, and 500 years flood hazard; however, no future climate prediction was included. In addition, Zhu & Frangopol (2016a, b) presented a multi-hazard risk assessment framework considering bridges under scour and traffic loading. A time dependent risk analysis by modeling the closure of bridge lanes have been utilized in their study. Although, both types of human-made and natural hazards (traffic and scour loads) were considered in their study, the effect of climate change was also not included.

The review of the literature reveals that significant effort has been devoted to probabilistic analysis of the bridges under flood, flood-induced scour, and the combined effects of these stressors. However, less effort has been directed to properly integrate the effect of climate change using global climate models into probabilistic risk analysis. This paper addresses this knowledge gap by presenting a probabilistic framework for quantifying the multi-hazard risk of bridge failure considering climate change. Downscaled climate data adopted from global climate models are employed to predict the future streamflow and temperature profiles at a given location. Seismic hazard analysis is performed by considering both human induced and natural earthquake hazards. The proposed framework is illustrated on an existing bridge in Oklahoma.

METHODOLOGY AND FINDINGS

Global climate models and their downscaled regional projections can help achieving more reliable flood and scour prediction. Various scenarios of GCMs, future greenhouse gas (GHG) emissions, and downscaling methods should be considered to account for uncertainties associated with this flood prediction technique. The Couple Model Inter-comparison Project Phase 5 (CMIP5) GCMs with more than 50 different GCMs, varied based on their atmospheric horizontal resolution, is able to project the past and future climate data (Taylor et al. 2012). In addition, the uncertainties in GHG emissions can be considered by using different representative concentration pathway (RCPs) scenarios. RCP values represent the change in balance of radiation between incoming and outgoing solar and infrared radiation in Watt/meter^2 of earth surface (Stocker et al. 2013). Apart from the effects on flood and scour prediction, climate change can also alter the corrosion propagation rate in structural components. This impact is due to the change in carbon dioxide concentration, temperature, and humidity at the location of interest. Particularly, when the temperature profile increases, the material diffusivity and, consequently, the corrosion rate in reinforcement also increases (Stewart, et al. 2012). In this paper, refined precipitation and temperature data for the time period of 1960 to 2100 with Daily Bias Correction Constructed Analogs (BCCA) downscaling method are adopted (Brekke et al. 2013). These datasets are used to perform flood prediction and corrosion assessment.

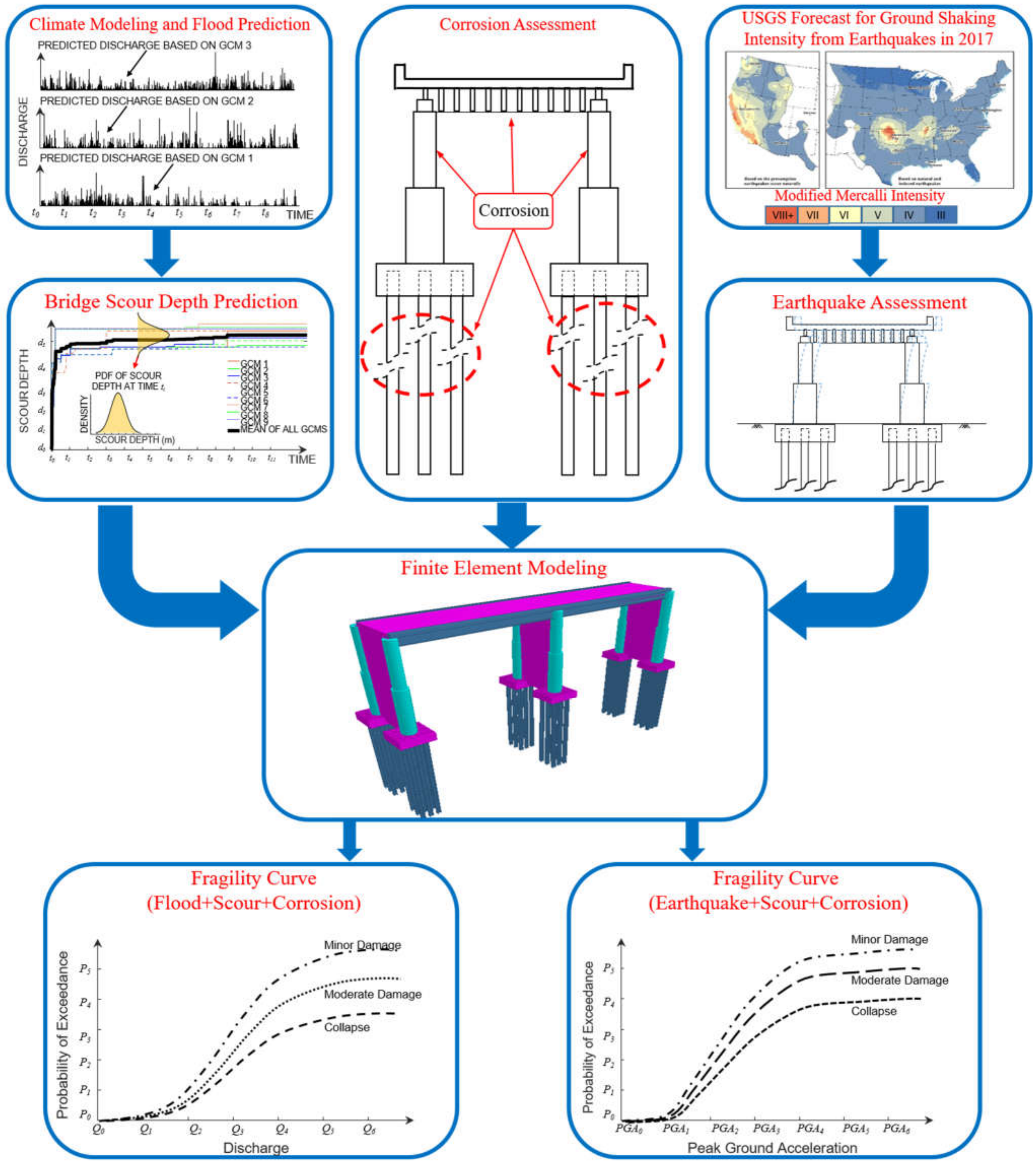

Figure 1. Layout of the proposed framework for multi-hazard risk analysis

Results of short-term and long-term earthquake hazard forecasts for central and eastern U.S. are adopted from United States Geological Survey database (USGS 2017; Petersen et al. 2017) and integrated into the proposed framework. Unlike the U.S. Geological Survey (USGS) National Seismic Hazard Model Project (NSHMP), the short-term maps consider both natural and human induced earthquakes. Due to deep wastewater disposal, the number and intensity of human induced earthquakes have increased significantly in central and eastern United States. Particularly in Oklahoma, seismicity rates have increased considerably since 2009 (Elsworth, 2013). Based on Petersen et al. (2017), the seismic hazard for 1% probability of exceedance in one year extended to 0.6g in northern Oklahoma and southern Kansas. This value is three times the 2014 NHSMP predictions. In addition, the chance of having a damaging earthquake (i.e., earthquakes with Modified Mercalli Intensity VI or greater) in these regions is predicted to be 5-12 % per year, which is comparable to the chance of having a natural earthquake in some regions in California.

In this study, three GCMs that are appropriate for southern Oklahoma, along with three RCP values, are used to predict the future climate trends. The predicted temperature, streamflow, and time-dependent scour depths based on nine climate scenarios are integrated in a probabilistic framework to perform multi-hazard analysis considering flood, scour, corrosion and seismic hazards. A layout of this framework is shown in Figure 1. The resulting flood and temperature prediction profiles, as well as earthquake forecasts, are next used to assess the structural performance using finite element analysis. In addition, Monte Carlo simulation technique is used to quantify the probabilistic descriptors of bridge resistance. This process results in establishing long-term risk profiles considering flood, scour, corrosion, and earthquake.

CONCLUSIONS

This paper presented a probabilistic framework for risk analysis of bridges susceptible to damage due to floods, flood-induced scour, earthquake, and corrosive environment. The framework predicts the probability of failure considering the effects of climate change using downscaled data adopted from global climate models. Human-induced and natural earthquake hazards are included through USGS hazard maps. The proposed framework can establish risk profiles which can depict the performance of the structure as a function of streamflow or peak ground acceleration.

REFERENCES

AASHTO. (2010). American association of state highway and transportation officials (LRFD) bridge design specifications. 5th Ed., *Washington, DC*.

Banerjee, S., & Ganesh Prasad, G. (2013). Seismic risk assessment of reinforced concrete bridges in flood-prone regions. *Structure and Infrastructure Engineering*, *9*(9), 952-968.

Brekke, L., Thrasher, B. L., Maurer, E. P., and Pruitt, T. (2013). Downscaled CMIP3 and CMIP5 climate and hydrology projections: Release of downscaled CMIP5 climate projections, comparison with preceding information, and summary of user needs. *US Dept. of the Interior, Bureau of Reclamation, Technical Services Center, Denver*.

Briaud, J. L., Gardoni, P., & Yao, C. (2013). Statistical, risk, and reliability analyses of bridge scour. *Journal of Geotechnical and Geoenvironmental Engineering*, *140*(2), 04013011.

Cook, W., Barr, P.J., & Halling, M.W. (2015). Bridge failure rate. *Journal of Performance of Constructed Facilities, 29*(3), 04014080.

Danner, C., & Fuller, J., (2015). Texas and Oklahoma begin cleaning up after devastating floods. Retrieved from: http://nymag.com/daily/intelligencer/2015/05/floods-devastate-texas-and-oklahoma.html

Ellsworth, W. L. (2013). Injection-induced earthquakes. *Science*, *341*(6142), 1225942.

Fechter, J. (2015). TXDoT: Two bridges completely wrecked in Central Texas floods, others damaged. Retrieved from: http://www.mysanantonio.com/news/local/article/TXDoT-Two-bridges-wrecked-in-the-Central-Texas-6294892.php#photo-8045574

Ganesh Prasad, G., & Banerjee, S. (2013). The impact of flood-induced scour on seismic fragility characteristics of bridges. *Journal of Earthquake Engineering*, *17*(6), 803-828.

Koch, G. H., Brongers, M. P., Thompson, N. G., Virmani, Y. P., & Payer, J. H. (2002). *Corrosion cost and preventive strategies in the United States* (No. FHWA-RD-01-156,).

Lee, G. C., Mohan, S. B., Huang, C., & Fard, B. N. (2013). A Study of US Bridge Failures (1980-2012) 13-0008. pdf.

NOAA (2015). Nuisance flooding, an increasing problem as coastal sea levels rise, National Oceanic and Atmospheric Administration, http://www.noaanews.noaa.gov/stories2014/20140728_nuisanceflooding.html

Petersen, M. D., Mueller, C. S., Moschetti, M. P., Hoover, S. M., Shumway, A. M., McNamara, D. E., ... & Rubinstein, J. L. (2017). 2017 one-year seismic-hazard forecast for the Central and Eastern United States from induced and natural earthquakes. *Seismological Research Letters*, *88*(3), 772-783.

Smith, A., Lott, N., Houston, T., Shein, K., Crouch, J., & Enloe, J. (2017). US billion-dollar weather & climate disasters: 1980-2017. *NOAA National Centers for Environmental Information*. https://www.ncdc.noaa.gov/billions/events.pdf.

Stewart, M. G., Wang, X., and Nguyen, M. N. (2012). Climate change adaptation for corrosion control of concrete infrastructure. *Structural Safety*, *35*, 29-39.

Stocker, T., Qin, D., Plattner, G., Tignor, M., Allen, S., Boschung, J., Nauels, A., Xia, Y., Bex, B. & Midgley, B. (2013). IPCC, The physical science basis. Contribution of working group I to the fifth assessment report of the intergovernmental panel on climate change.

Taylor, K. E., Stouffer, R. J., & Meehl, G. A. (2012). An overview of CMIP5 and the experiment design. *Bulletin of the American Meteorological Society*, *93*(4), 485-498.

USGS (2017). United State Geological Survey, Earthquake Hazard Program, https://earthquake.usgs.gov/hazards/

Zhu, B., & Frangopol, D. M. (2016a). Time-variant risk assessment of bridges with partially and fully closed lanes due to traffic loading and scour. *Journal of Bridge Engineering*, *21*(6), 04016021

Zhu, B., & Frangopol, D. M. (2016b). Time-dependent risk assessment of bridges based on cumulative-time failure probability. *Journal of Bridge Engineering*, *21*(12), 06016009.

Use of Nanoclays as Alternatives of Polymers Toward Improving Performance of Asphalt Binders

M M Tariq Morshed[1], Mohammad Nazmul Hassan[1], and Zahid Hossain[2]

[1]GRA, Department of Civil Engineering, Arkansas State University
[2]Associate Professor, Department of Civil Engineering, Arkansas State University

INTRODUCTION

The main goal of this study is to assess the feasibility of the use of nanoclay as an alternative of commonly used polymers such as styrene-butadiene-styrene (SBS) and styrene-butadiene-rubber (SBR), which are used to modify performance grade (PG) binders. Neat binders are usually modified by SBS and SBR to sustain increased load and extreme temperature events. Such modifications increase the overall cost of the binder. Alternatively, nanoclay is economical and naturally abundant. It is expected that the use of nanoclay instead polymers will significantly reduce the cost of asphalt binders.

Applications of nanoclays in asphalt pavements are relatively new. It gained huge interest since the "NSF Workshop on Nanomodification of Cementitious Materials" in 2006 (Birgisson, 2006). Different types of polymer were applied to prepare polymer modified asphalt, but a very little number become satisfactory based on the performance and the cost (Polacco et al. 2006). Many researchers have incorporated nanoparticles effectively. Ghile (2005) used Cloisite and conducted mechanical tests. The result presented that nanoclay modification enhances mechanical properties such as creep and fatigue resistance. Nanoclay works as filler reinforcements. Polacco et al. (2008) also examined the polymer modified asphalts to find out the effect of the addition of clay. You et al. (2011) studied two types of nanoclays (Nanoclays A and B) and performance grade binder PG 58-22 in Michigan. Hossain et al. (2014) evaluated the viscosity and rutting properties of nanoclay-modified asphalt binders. Jahromi and Khodaii (2012) studied two types of nanoclays, namely, Cloisite 15A and Nanofill 15. It was reported that nanoclay increased rutting resistance and stiffness. Yu et al. (2007) reported that montmorillonite modified asphalts had higher viscoelastic properties and rutting resistance. Zapién-Castillo et al. (2016) investigated nanocomposite styrene-ethylene–butylene-styrene (SEBS) Cloisite 15A-modified asphalt binders, and they reported favorable test results.

In this study, three types of nanoclay and two types of neat binders were selected for laboratory investigation. A blending protocol has been developed to mix the nanoclay with asphalt binder. Rotational Viscosity (RV), Dynamic Shear Rheometer (DSR) and Atomic Force Microscope (AFM) were used to evaluate the properties of modified asphalt binder. Other Superpave tests such as Bending Beam Rheometer (BBR), Rolling Thin Film Oven (RTFO), Pressure Aging Vessel (PAV) and Texas boiling test, sessile drop test, Tensile Strength Ratio (TSR), creep resistance will be conducted throughout the duration of the project. Chemical analysis was conducted for determining the chemical constituents in the neat binders. The research team is now working to analyze the results obtained from the chemical analysis. From RV tests it was found that the viscosity values of the modified asphalt binders were significantly higher than those of neat binders. The highest viscosity was found for 2% Cloisite 10A. The viscosity of 2% Cloisite 10A-modified binder was about 248% of that of the neat binder. In the case of nanoclay-modified binders, the complex shear modulus (G^*) increased, but the phase angle (δ) decreased. Therefore, rutting factor ($G^*/\sin\delta$) increased for modified binders and maximum rutting resistance was observed for binder modified with 1% Cloisite 11B. Morphological and nanomechanical properties were observed from the AFM analysis. Adhesion and deformation values decreased for modified asphalt binders. The minimum adhesion and deformation values were found for asphalt binder samples modified with 1% Cloisite 10A. It may be said that nanoclay has a great possibility to become an alternative modifier and more investigation is required to establish this idea.

METHODOLOGY

After conducting a thorough literature review, unmodified PG 64-22 asphalt binders were collected from two different sources. One source was Ergon at Memphis and another source was Marathon at Catlessburg. Three different types of organically treated nanoclays, namely, Cloisite 10A, Cloisite 11B, and Cloisite 15A, were collected from Southern Clay Products Inc. Based on the existing literature and manufacture's recommendations, nanoclays at 1%, 2% and 3% by weight of asphalt were selected for blending with unaged asphalt binders. After different trials of temperature, time and rotational speed, a blending protocol was developed. Nanoclays were then blended with the unaged asphalt binders using a high shear mixer. The viscosity of the control and nanoclay-modified asphalt binder were evaluated with the help of a Brookfield Rotation Viscometer. Viscosity tests were conducted from 135ºC to 180ºC in 15ºC interval following AASHTO T 316. For characterizing the viscous and elastic behavior of neat binder and blended asphalt, dynamic shear rheometer (DSR) test was performed according to AASHTO T 315. The equation derived from NCHRP Project was used to calculate viscosities and A-VTS parameters from complex shear modulus and phase angle (Bari and Witczak 2007; NCHRP 2004). An AFM is being used to evaluate morphological and nanomechanical properties of neat and modified asphalt binder. Research team is now working to conduct SARA analysis for modified binders. RTFO and PAV will be used to simulate short term and long term aging condition. BBR, TSR, sessile drop, Texas boiling test and creep resistance at low temperature will be conducted. Moreover, Life Cycle Cost (LCC) analysis will be performed to evaluate the most economic option.

FINDINGS

Blending Protocol

Nanoclays were blended with the unaged asphalt binders using a high shear mixer. Nine different trials were conducted using different time (2h, 3h, and 4h), rpm (1500 and 2000) and temperature (150ºC and 160ºC). RV, DSR, and AFM tests were accomplished for every trial. From DSR test, complex shear modulus and phase angle were calculated, and rutting factor ($G^*/\sin\delta$) versus temperature charts were plotted. From AFM test, the morphology, adhesion, DMT modulus and deformation values of the samples were observed and compared. From the output of these tests, a blending protocol (2h time, 2000 rpm and 150ºC) was established to mix nanoclays with asphalt binders.

Rotational Viscosity

When nanoclays were mixed with the neat binder, the viscosity of the blended asphalt binder is increased. Viscosity (mPa.s) in log scale versus temperature in degree Celsius was plotted (Figure 1). For 1%, 2% and 3% Cloisite 10A blended asphalt binders, the viscosity values at 135ºC are increased by 171%, 248%, and 144%, respectively. At the same temperature, 176%, 166%, and 158% increases in viscosity are observed when 1%, 2% and 3% Cloisite 11B are mixed with the neat binder. Similarly, with the addition of 1%, 2% and 3% Cloisite 15A, the viscosity is increased by 166%, 186%, and 152%, respectively compared to the neat binder.

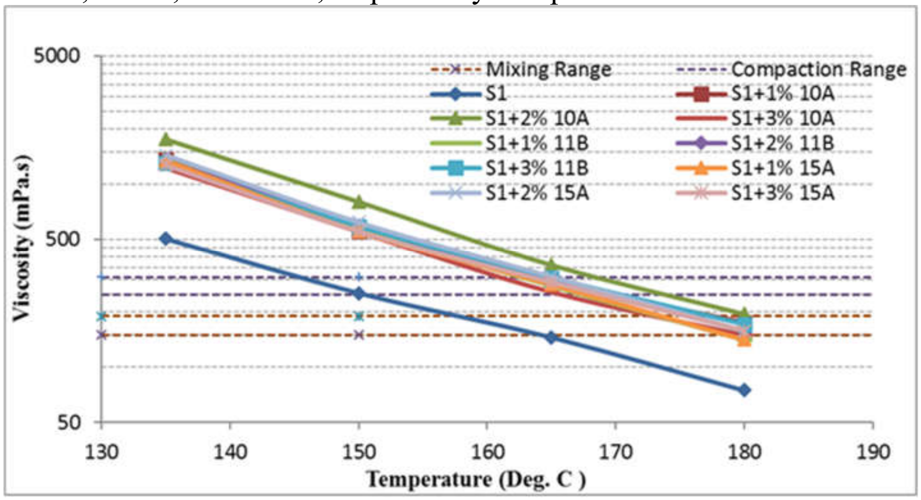

Figure 1 Viscosity (mPa.s) in Log Scale vs Temperature in degree Celsius

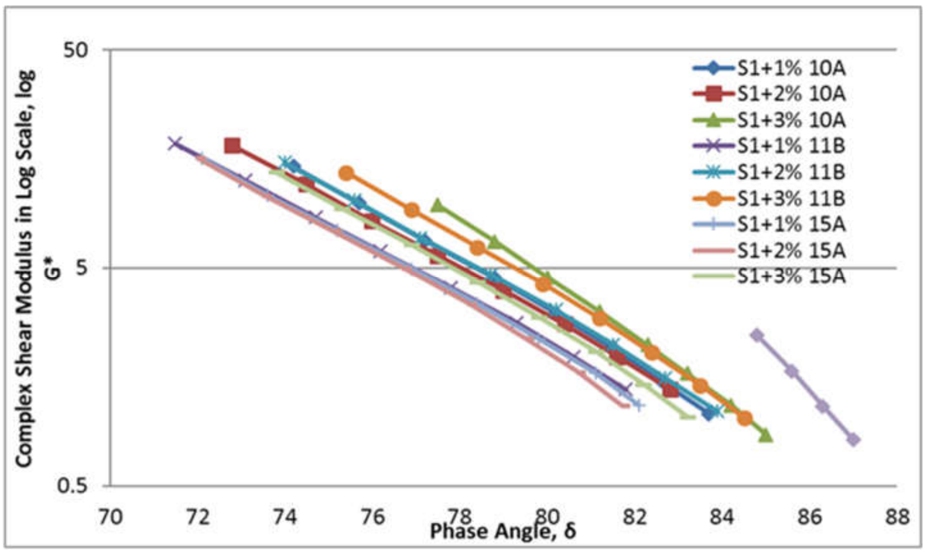

Figure 2 Complex Shear Modulus (G*) in Log Scale vs Phase Angle (δ) Known as Black Curve

Dynamic Shear Rheometer (DSR)

The G* (in log scale) versus δ, known as the black curve, was plotted (Figure 2). It is observed that the black curves for modified asphalt binders have shifted from position of the neat binder to left. The G* values for nanoclay-modified asphalt binders increased and δ values decreased with respect to those of the neat asphalt binder. At 64ºC, the maximum G* and the minimum δ are found when asphalt binder blended with 1% Cloisite 11B. G* and δ values were also used to evaluate A-VTS parameters shown in Table 1. The viscosity parameter "A" value for nanoclay modified asphalt binder is decreased from that of the neat binder. The absolute value of another viscosity parameter "VTS" is also decreased from that of the neat binder. Therefore, the nanoclay-modified asphalt binder is less temperature susceptible compared to the neat binder. Rutting factor (G*/ sinδ) was also increased for modified binders and maximum rutting resistance was observed for binder modified with 1% Cloisite 11B.

Table 1 A-VTS Parameter for Unmodified and Modified Asphalt Binders

Sample ID	A	VTS
S1 (Neat Binder)	23.76	-8.41
S1+1% 10A	21.68	-7.62
S1+2% 10A	20.56	-7.21
S1+3% 10A	20.82	-7.32
S1+1% 11B	20.94	-7.34
S1+2% 11B	21.65	-7.6
S1+3% 11B	21.5	-7.55
S1+1% 15A	21.55	-7.57
S1+2% 15A	21.51	-7.55
S1+3% 15A	20.82	-7.32

Table 2 Value of the Morphological and Nanomechanical Properties

Sample ID	Average Value of Height Sensor (nm)	Average Value of DMT Modulus (MPa)	Average Value of Adhesion (nN)	Average Value of Deformation (nm)
S1 (Neat Binder)	7.79	3221	362	5.41
S1+1% 10A	7.32	755	73.7	1.94
S1+2% 10A	13.5	1768	222	2.8
S1+3% 10A	6.52	2937	305	5.37
S1+1% 11B	13.7	625	136	4.2
S1+2% 11B	8.36	682	102	3.19
S1+3% 11B	9.32	2081	196	4.41
S1+1% 15A	6.5	694	176	4.21
S1+2% 15A	9.46	1522	163	4.05
S1+3% 15A	15.8	1234	261	3.55

Atomic Force Microscope (AFM)

Morphological and nanomechanical properties such as DMT modulus, adhesion, and deformation parameters were measured for unmodified and nanoclay-modified asphalt binders and test data is shown in Table 2. Height sensor value was found the maximum for asphalt binder modified by 3% Cloisite 15A and minimum for asphalt binder modified by 1% Cloisite 15A. The DMT modulus was found to decrease for nanoclay-modified asphalt binders. Adhesion and deformation values were also found to decrease for modified asphalt binders. The minimum adhesion and deformation values were found for asphalt binder samples modified with 1% Cloisite 10A.

CONCLUSIONS

In this study, nanoclay modified asphalt binders were tested in the laboratory. The viscosity and mechanical properties of the asphalt binder were improved successfully. Rutting resistance increased significantly due to the addition of nanoclay, but the adhesion and deformation values decreased. Based on the results, it may be said that nanoclay has a great chance to become an alternative polymer. But, further test results are required to establish this idea. The research team plans to conduct BBR, TSR, sessile drop test, Texas boiling test and creep resistance to characterize the performance of the blended asphalt binders.

REFERENCES

Bjorn Birgisson (2006) “Workshop on Nanomodification of Cementitious Materials.” *NSF Program for Mechanics of Materials and Str and Structural and Architectural E.* Program Reference Codes:1057, 7237, 9237, CVIS, Program Element Codes: 1630, 1637.

Polacco, G., Stastna, J., Biondi, D., and Zanzotto, L., (2006) “Relation between polymer architecture and nonlinear viscoelastic behavior of modified asphalts.” *Curr Opin Colloid Interface Science 11(4)*, 230–45.

Ghile, D. B., (2005) “Effects of nanoclay modification on rheology of bitumen and on performance of asphalt mixtures.” *Delft University of Technology.*

Polacco, G., Filippi, S., Stastna, J., Biondi, D., and Zanzotto, L., (2008) “Rheological properties of asphalt/SBS/clay blends.” *Eur Polym J;44:35,* 12–21.

You, Z., Mills-Beale, J., Foley, J. M., Roy, S., Odegard, G. M., Dai Q., and Goh, S. W., (2011), “Nanoclay-modified asphalt materials: Preparation and characterization.” *Construction and Building Materials 25*, 1072-1078.

Hossain, Z., Zaman, M., Saha, M. C., and Hawa, T., (2014) “Evaluation of Viscosity and Rutting Properties of Nanoclay-Modified Asphalt Binders.” *Geo-Congress 2014 Technical Papers: Geo-Characterization and Modeling for Sustainability.* 3695-3702.

Jahromi, S. G., and Khodaii, A., (2009) “Effects of nanoclay on rheological properties of bitumen binder.” *Construction and Building Materials 23*, 2894-2904.

Yu, J., Zeng, X., Wu, S., Wang, L., and Liu, G., (2007) “Preparation and properties of montmorillonite modified asphalts.” *Materials Science and Engineering A 447,* 233–238.

Zapién-Castillo, S., Rivera-Armenta, J. L., Chávez-Cinco, M. Y., Salazar-Cruz, B., A., and Mendoza-Martínez, A. M., (2016) “Physical and rheological properties of asphalt modified with SEBS/montmorillonite nanocomposite.” *Construction and Building Materials 106.* 349–356.

NCHRP Project 1-37A. (2004). "Guide for Mechanistic-Empirical Design of New and Rehabilitated Pavement structures." *Final Report, National Cooperative Research Program (NCHRP)*, Washington D.C.

Evaluation of Polymer Degradation Due to Aging in Asphalt Binder and Determination of Polymer Content in Asphalt Emulsion Using an Extensional Deformation Test

Roksana Hossain, Waleed Mohammed Omer, and Nazimuddin M. Wasiuddin
Department of Civil Engineering, Louisiana Tech University

INTRODUCTION

Applications of polymer modified asphalt binders (PMAB) and polymer modified asphalt emulsions (PMAE) on pavements construction have become very popular in this era. The addition of a small amount of polymers such as polyolefins (polyethylene, ethylene/propylene diene copolymer, chlorinated polyethylene), ethylene/vinyl acetate (EVA) copolymers, poly phosphoric acid and SBS (styrene– butadiene–styrene) triblock copolymer can improve the physical and rheological properties of asphalt for road construction (Morrison et al., 1994; Lu and Isacsson, 2001). However, during the service life of the pavement, different types of environmental factors, traffic loads and oxidation due to aging deteriorate the pavement (Petersen, 1998).

Hao et al. (2017) investigated the rheological behaviour of various polymer modified asphalts and its' properties before and after aging, using rheological master curves and Gel Permeation Chromatography (GPC). The GPC test was performed to obtain the average molecular weight (Mw) of the polymer and the distribution of asphaltenes and maltenes. It was observed from the master curve of phase angle, δ that after long term aging, δ of all samples were almost equal to the δ obtained from the original binder which means polymer effect is gone after long term aging. From the aging index values, it was found that R-value and Normalized R-value increased with aging where cross-over modulus decreased with aging which clearly indicates that aging degree was deeper.

Cortizo et al. (2004) investigated SBS modified asphalt under different aging condition. The free radical reactions produce chain scission and radical addition to some asphalt components during the polymer degradation due to aging. This phenomenon is verified by the size exclusion chromatography and infrared spectroscopy analysis. Chromatographic profiles of SBS modified asphalt have shown that the second average molecular weight of fraction (F_2) decreased by 10% and the elution volume remain stable after aging. In contrast, the first average molecular weight of fraction (F_1) slightly increased and the elution volume slightly decreased after aging. It is the clear consequence of polymer degradation, and oxidation of asphalt binder.

Chen et al. (2012) performed Composite Specimen Interface Cracking (CSIC) test on polymer modified asphalt emulsion under repeated tensile loading and monitored the damage development rate. The results clearly indicated that the polymer modification significantly improves reflective cracking resistance. Zhang et al. (2011) performed penetration test, softening point test and ductility tests on SBR latex modified asphalt emulsion (MAE) with different percent of polymer. Tests were performed for every 1% in the range between 1% and 8%, the results did not show any linear correlation with respect to polymer percent increment for all the performed tests.

However, Sentmanat (2004) developed the dual wind-up extensional rheometer SER, that achieved a truly uniform extensional deformation. This fixture can convert a conventional rotational rheometer host system into a universal testing station capable of performing extensional melt rheology experiments, all within the controlled environment of the host systems' environmental chamber. Mohammed and Wasiuddin (2018) recommended a novel test method using the DSR-based SER extensional rheometer test. To this end, this study has been initiated to determine the polymer degradation in the PMAB after short term and long term aging by analyzing the rheological extensional deformation parameters of the PMAB. Additionally, the study investigates the correlation between the polymer content in the PMAE and the rheological extensional deformation parameters.

Objectives

The main objectives of this study are to investigate the polymer degradation due to aging in PMAB and to correlate the extensional deformation parameters with the percent of polymer content in the PMAE. The specific objectives are as follows:

1. Develop a sample preparation procedure and modify the sample geometry recommended by Mohammed and Wasiuddin (2018).
2. Investigate the effect of the short term and long term aging on the rheological extensional deformation parameters: first peak elongation force (F_1), second peak elongation force (F_2) and second peak elongation force over first peak elongation force (F_2/F_1).
3. To investigate the correlation between the polymer percent in the PMAE and the force parameter F_2.

METHODOLOGY

PMAB PG 76-22 and latex modified cationic asphalt emulsions were used in this study. For short term aging PMAB PG 76-22 samples were aged by rolling thin film oven (RTFO) method. As for long term aging, samples were aged using the pressure aging vessel (PAV) method. To improve the thickness accuracy, numerous samples were made using different sample preparation approaches. Tests were performed using an Xpansion Instruments SER Universal Testing Platform model SER3-G on a DSR model AR 2000ex host system. In order to investigate the effect of aging on the PMAB, 24 extensional deformation tests were performed on Original, RTFO and PAV aged samples at three different temperatures: 0ºC, 4ºC and 12ºC. The dimensions of the specimens were (W= 1 mm x T= 0.72 mm) as shown in Table 1.

For PMAE binder, the residues were recovered from the emulsions using residue by evaporation of emulsified asphalt "ASTM D6934 – 08". The optimum polymer percent recommended by the manufacturer was 4%. In order to investigate the effect of the polymer percent content on the extensional deformation parameters, 1.5% above and 1.5% below the optimum percent were chosen along with the optimum percent to be tested. 12 extensional deformation tests were performed at 4ºC, three replicates for each of the polymer percentages. All the specimens' dimensions were (W= 3 mm x T= 0.72 mm) as shown in Table 1.

Table 1. Summary of Materials and Experimental Plan.

Sample Type	Sample Geometry			No. of samples	Temperature	Polymer Percent
	W mm (+/- 0.25)	T mm (+/-0.06)	A mm^2 (+/- 0.39)			
PMAB	1.0	0.72	0.72	24	0°C, 4°C and 12°C	
PMAE	3	0.72	2.16	12	4°C	0%, 2.5%, 4%, 5.5%

Sample Preparation

Samples were prepared by following the sample preparation method proposed by Mohammed and Wasiuddin (2018).

Test Procedure

Measurements were performed on a Universal Testing Platform model SER3-G manufactured by Xpansion Instruments LLC connected to DSR model AR2000ex with an environmental chamber. The sample was loaded and secured at each end by clamps and then the chamber was closed. An ultra-thin double-sided adhesion tape with thickness of 0.1 mm was placed into the drum prior to the sample loading to prevent sample from slipping. Then the sample was loaded in the SER. As for the test parameter, the environmental chamber was set to 0 ºC, 4ºC and 12 ºC respectively for PMAB and 4ºC for PMAE. The soak time was 600s, and the wait for temperature option was activated to ensure temperature equilibrium. Solid density was set to 1.0 g/cm^3. For conducting experiment on PMAB final strain was 3.7 rad and for PMAE the final strain was 3.4 rad, with strain rate of 0.1 s^{-1}. For more accurate detecting of the results, fast sampling option was activated. Upon test completion, sample was removed immediately.

RESULT AND DISCUSSION

First and Second Peak Elongation Forces

Polymer modified binder is a non-homogeneous material. In the elongation force vs. step time graph, the first peak, F_1 indicates the original asphalt binder property and the second peak, F_2 is related to the polymer characteristics and polymer content as no second is observed in non-modified binder.

PMAB Original and Aged Parameters

The ratio F_2/F_1 vs temperature is shown in Figure 1. $F_2/F_1$is a very distinctive parameter of the original and aged PMAB, as the polymer is degraded with aging, F_2/F_1 decreases. It is clearly observed that RTFO aging reduces $F_2/F_1$and PAV aging further reduces F_2/F_1. Therefore, through this study it is recommended that this parameter can be used to determine aging susceptibility of polymer in an asphalt binder.

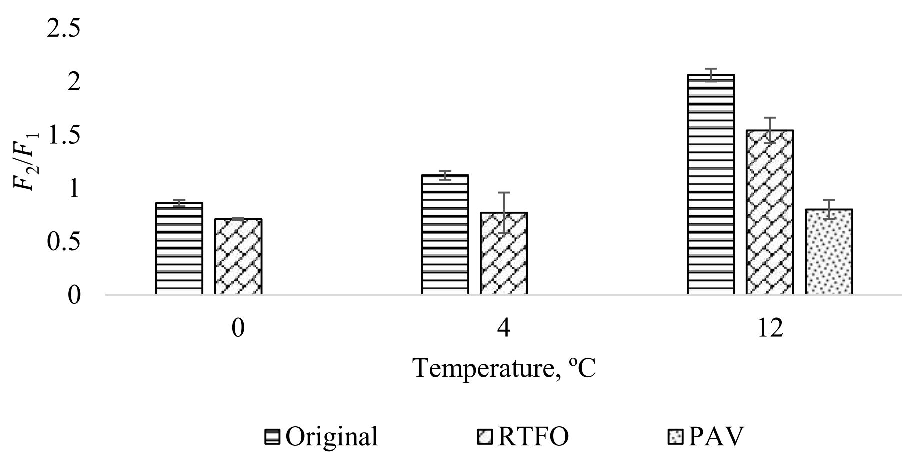

Figure 1. Ratio of Average Second Peak Elongation Force over Average First Peak Elongation Force vs. Temperature

Polymer Percent Content Parameters

PMAEs with four different percentages of polymer were tested to establish a correlation between the polymer percent in the PMAE and the investigated parameter. The investigated parameter was F_2. As mentioned earlier, the four-different percent of polymer were 0%, 2.5%, 4%, and 5.5%. Figure 2 indicates the second peak elongation force, F_2 vs percent of polymer for four different polymer percent. It can be observed that with the increment of the polymer percentage, F_2 increases, that is due to the improvement in the PMAE because of the polymer additives. For 0%, F_2 is equal to 0 N. For 2.5% F_2 is equal to 2.43 N and for 4% F_2 is equal to 3.25 N and for 5.5% F_2 is equal to 5.17 N. In which it is linearly increasing with $R^2 = 0.98$.

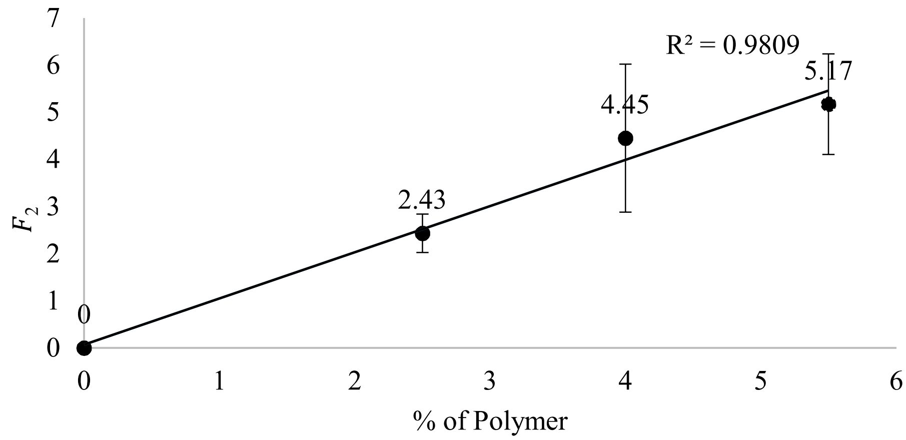

Figure 2. F_2 vs % of polymer

CONCLUSION

The main objective of this study is to investigate the degradation of polymer in PMAB due to short term and long term aging and the potential of SER fixture for detecting the percent of polymer content in PMAE. The sample preparation procedure recommended by Mohammed and Wasiuddin (2018) was used in this study. In order to perform the tests on an aged binder, the sample geometry used in this study is 1 mm x 0.72 mm instead of 9 mm x 0.72 mm recommended by Mohammed and Wasiuddin (2018) for PMAB. Similarly, for PMAE the geometry used is 3 mm x 0.72 mm to perform the tests on emulsions with different percentages of polymer.

The analysis indicates that, F_2/F_1 decreases with aging which clearly indicates the degradation of the polymer. F_2/F_1 is recommended as a polymer degradation parameter due to aging. All three testing temperatures used in this study exhibited reduction in F_2/F_1 due to RTFO aging and further reduction due to PAV aging.

A detailed analysis indicates that, F_2 has a linear correlation with the percent of the polymer in the PMAE with R^2 value equal to 0.98.

REFERENCE

Chen J. C., Lio M. C., and Shian M. S. (2002). Asphalt Modified by Styrene Butadiene-Styrene Triblock Copolymer: Morphology and Model. *Journal of Materials in Civil Engineering*, 14 (2), 224-229.

Chen Y., Tebaldi G., Roque R., nad Lopp G. (2012). Effects of Poplymer Modified Asphalt Emulsion (PMAE) on Pavement Reflective Cracking Performance. *7th RILEM International Conference on Craking in Pavements*, 4, 879-888.

Cortizo M.S., Larsen D.O., Bianchetto H., and Alessandrini J.L. (2004). Effect of the thermal degradation of SBS copolymers during the ageing of modified asphalts. *Polymer Degradation and Stability,* 86, 275-282.

Hao G., Huang W., Yuan J., Tang N., and Xiao F. (2017). Effect of aging on chemical and rheological properties of SBS modified asphalt with different compositions. *Construction and Building Materials*, 156, 902–910.

Lu X. and Isacsson U. (2001). Modification of road bitumens with thermoplastic polymers. *Polym Testing*, 20(1), 77-86.

Morrison G. R., Lee J. K. and Hesp S. A. M. (1994). Chlorinated polyolefins for asphalt binder modification. *J Appl. Polym. Sci*, 54(2), 231-40.

Mohammed, W. B. O., and Wasiuddin, N. M. (2018). Development of a Novel and DSR Based Extensional Deformation Test Replacing Force Ductility Test (AASHTO 300). *Presentation on TRB's 97th Annual Meeting*.

Petersen, J.C. (1998). Sequential mechanism for the oxidation of petroleum asphalt. *Pet. Sci. Technol*., 16, 1023–1059.

Sentmant, M. L. (2004). Miniature universal platform: from extensional melt rheology to solid state deformation behavior. *Journal of Rheologica Acta*, 43 (6), 657-669.

Zhang, Q., Fan, W., Wang, and T., Nan, G. (2011). Studies on the temperature performance of SBR modified asphalt emulsion. *International Conference on Electric Technology and Civil Engineering (ICETCE),* China, 730-733.

Evaluation of Effects of Moisture on Asphalt Pavements

Sumon Roy[1] and Zahid Hossain[2]

[1]GRA, Department of Civil Engineering, Arkansas State University
[2]Associate Professor, Department of Civil Engineering, Arkansas State University

INTRODUCTION

Moisture damage is one of the major concerns to the Department of Transportations (DOTs) and other agencies since it prematurely deteriorates the performance and durability of asphalt pavements. The mechanism that causes stripping related moisture damage in asphalt concrete (AC) is very complex. It may be due to the failure of the bond between the asphalt binder and the aggregate (adhesive failure) or failure within binder itself (cohesive failure) (Little & Jones 2003, Zollinger 2005, and Santucci 2010). Over 50 years, a numerous research studies have been conducted to identify and describe the root causes of moisture damage (Scherocman et al. 1985, Little & Jones 2003, Hicks et al. 2003, Lu 2003, Santucci 2010, Sebaaly et al. 2010, Taylor & Khosla 1983, Fromm 1974, Tarrer & Wagh 1991 and Scott 1978) and developed test methods for predicting sensitivity of AC pavements. Among these tests, the Texas Boiling, Indirect Tensile Strength (ITS), and Hamburg Wheel Test (HWT) methods are widely used by most of the agencies. However, Arkansas Department of Transportation is the only state agency that still uses the Retained Stability test, which is based on the Marshall technique. Thus, ARDOT is in need of having an effective tool to predict moisture susceptibility of AC pavements in Arkansas. Furthermore, these traditional tests do not have a scientific rigor. On the other hand, an atomic level understanding of the moisture damage phenomenon and its mechanisms will give a better understanding of the issue. The main objective of this study is to develop a simple and cost effective test method to evaluate moisture damage potential of asphalt mixture using the surface chemistries and molecular level properties as well as aggregate-binder compatibility. Specific objectives of this study are to i) determine the stripping resistance of aggregate-binder systems using surface chemistries and atomic level material properties; ii) quantify moisture damage of asphalt mixture samples using conventional mechanistic-empirical test procedures; iii) find the most effective test method to evaluate moisture susceptibility on the basis of materials' surface chemistries, mechanistic and field performance data, and iv) provide recommendations to ARDOT for possible revision of asphalt mixture test specification (Article 404.04 Quality Control of Asphalt Mixtures).

To accomplish the aforementioned objectives, two methods (Texas Boiling test and the static contact angle measurements) for determining the moisture susceptibility were applied in this study. The percentage retention of asphalt binders was measured visually under the boiling temperature with the presence of water in Texas Boiling test while the aggregate-binder compatibility was measured through the measurement of the static contact angles. Also, the determination of molecular level properties of asphalt binders has been started using the Atomic Force Microscope (AFM). According to multiple researchers, the AFM can be used to investigate the surface morphology and the micromechanical properties of the asphalt binders (Hossain et al. 2016, Masson et al. 2006, Fischer et al. 2013, Nahar et al. 2014, Rashid & Hossain 2016, Dourado et al. 2012, Rashid et al. 2017). These researchers described three distinct phases such as Catana or dispersed phase, Peri-phase or interstitial phase, and Para-phase or matrix to characterize the morphological clusters, which were also used in this study. Findings of this study will provide insight into the moisture sensitivity and help find the most effective test method to quantify moisture damage potentials of asphalt binders for conditions prevailing in Arkansas.

METHODOLOGY

To achieve the goals of this study, a comprehensive literature review was conducted related to moisture damage in asphalt binders. After reviewing the literature, a detailed test plan was prepared to be followed throughout the completion of the project. The required asphalt binder samples were collected from two different crude sources (Canadian crude: Ergon Asphalt and Emulsions, Inc. Memphis, TN and Arabian crude: Marathon Petroleum Corporation, Catlettsburg, KY). The moisture sensitivity tests such as static contact angle measurements and Texas Boiling tests were conducted for this study. A guideline was followed to conduct the Texas Boiling test, which is provided by the Texas Transportation Institute (TTI). In this test, the stripping of asphalt binders was measured on the basis of visual observation (Table 1). On the other hand, an Optical Contact Analyzer (OCA) device was used in this study to measure the contact angles of asphalt binders and aggregates (Figure 1). In addition, the determination of nanomechanical properties of asphalt binders using AFM has started for this study. The AFM tests were conducted on the dry and wet conditioned binder samples to capture the topography of surface of the asphalt binders as well as mechanical properties at molecular level. In AFM tests, the Peak-Force Quantitative Nanomechanical Mapping (PFQNM) techniques of AFM were used. The scan parameters that used in AFM test are: scan size of 10 um x 10 um, scan rate of 0.502 Hz, samples/lines of 512. After conducting AFM scan (Figure 2), surface morphology and mechanical properties of asphalt binder are quantified using NanoScope Analyses 1.5 (Table 2).

FINDINGS

Texas Boiling Tests: The summary of boiling tests results showed in Table 1. From Table 1, it is found that PG 64-22 binders for both sources showed lower percentage of asphalt retention after the boiling test compared to any other binder used in this study. Conversely, the higher asphalt retention rates were found for SBS modified binders of both sources, which is also higher than the PPA-modified binder's values. Interestingly, the PPA-modified binder from Source 1 exhibited less stripping resistance than the PPA-modified binder from Source 2.

Static Contact Angles Measurements: The average contact angles of the asphalt binder samples from sources 1 and 2 are presented in Figure 1. From Fig. 1, it is observed that water showed the highest contact angles compared to other probe liquids (ethylene glycol and formamide). From the compatibility analysis, it can be concluded that the PPA-modified asphalt binders from source 1 displayed lower adhesion energy in the dry condition but higher adhesion energy in the wet condition. On the other hand, the opposite phenomenon was found in source 2 binder samples.

AFM Test Results: The AFM maps are analyzed using NanoScope Analyses for characterizing the surface morphology as well as mechanical properties (DMT modulus, adhesion force, deformation, and dissipation) (Table 1). The effects of moisture on the wet-conditioned binder samples are clearly evident in the morphological images and nanomechanical properties. From figure 2(a), it is observed three distinct phases, several larger and few smaller bees, and a uniform distribution of "bee" structures are over the entire scan area. However, these bees are eliminated by some hilly areas in the wet conditioned sample as presented in Figure 2(f). The decrease in average roughness values (from 5.45 nm to 1.57 nm) was also noticed in the wet conditioned samples. The roughness of dispersed and interstitial area was found to be decreased by approximately 50% after water immersion whereas no significant change in the matrix area.

The effect of moisture changes the modulus and adhesion force values significantly in wet binder samples. Under the wet condition, modulus values reduced significantly from 536 MPa to 271 MPa, which is 50% reduction from the dry samples. Further, the variation of adhesion values in the wet samples was considerably lower compared to the dry samples (from 85 nN to 20 nN). AFM test results showed that about 76% higher adhesion values in the dry sample. Similar, decreasing trends are also observed in deformation and dissipation values for all wet-conditioned samples. The deformation and dissipation values were reduced from 1.73 nm to 0.43 nm (75% reduction) and from 139967 eV to 3208eV (77% reduction), respectively. However, the reduction in adhesion value was found to be higher compared to all other mechanical properties. From this finding, it can be concluded that moisture damage due to adhesive failure will be observed in the neat asphalt binder.

Table 1 Summary of Texas Boiling Test

Asphalt Binder Designation	Binder Sample Source	Percentage of Asphalt Retained (%)
PG 64-22	1	50
	2	55
PG 70-22 (PPA-modified)	1	60
	2	65
PG 70-22 (SBS-modified)	1	70
	2	70
Note: PG: Performance Grade; Binder Sample Source 1: Canadian crude: Ergon Asphalt and Emulsions, Inc. Memphis, TN; Source 2: Arabian crude: Marathon Petroleum Corporation, Catlettsburg, KY; PPA: Polyphosphoric Acid, SBS: Styrene Butadiene Styrene.		

Table 2 Summary of the Mechanical Properties of Asphalt Binder

Sample Condition	Mechanical Properties				
	Analysis Parameters	DMT Modulus (Mpa)	Adhesion (nN)	Deformation (nm)	Dissipation (eV)
Dry	Average of the entire specimen	536.33	84.67	1.73	13996.67
	Dispersed and Interstitial phase	250-842	18-172	0.521-3.1	3228-28655
	Matrix Phase	78.9-324	13-94	0.274-1.33	2242-12333
Wet	Average of the entire specimen	271.73	20.16	0.43	3208.33
	Dispersed and Interstitial phase	55.6-630	4.29-51.8	0.127-1.02	1052-9552
	Matrix Phase	53.1-339	2.1-19.4	0.116-0.565	369-2105

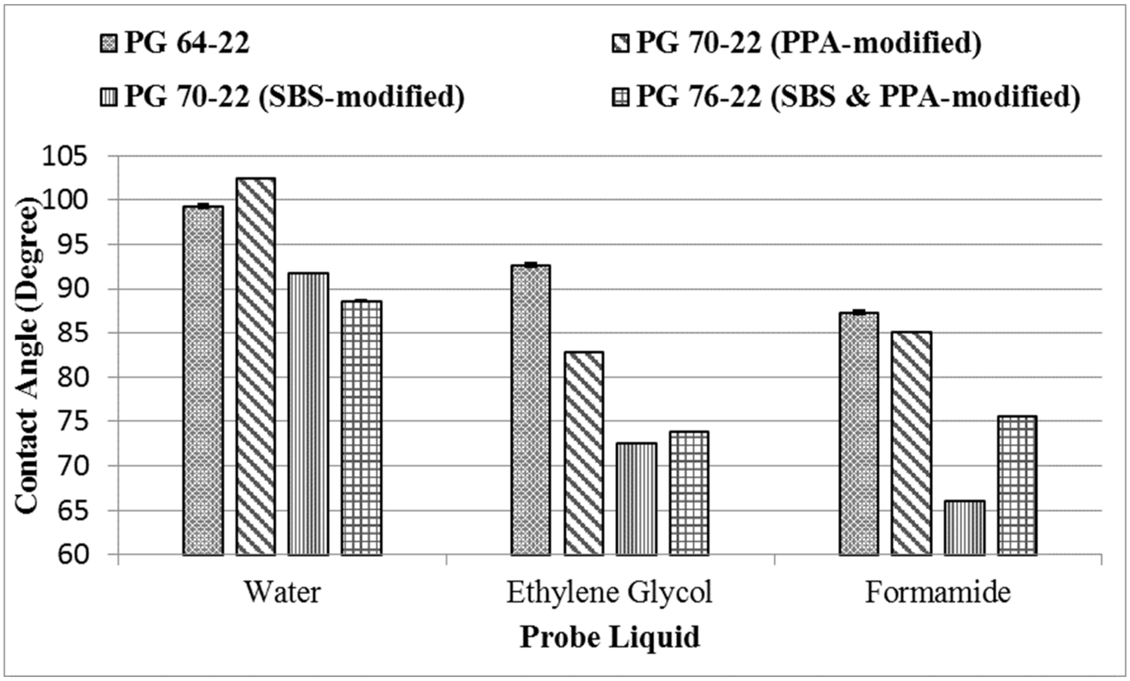

(a)

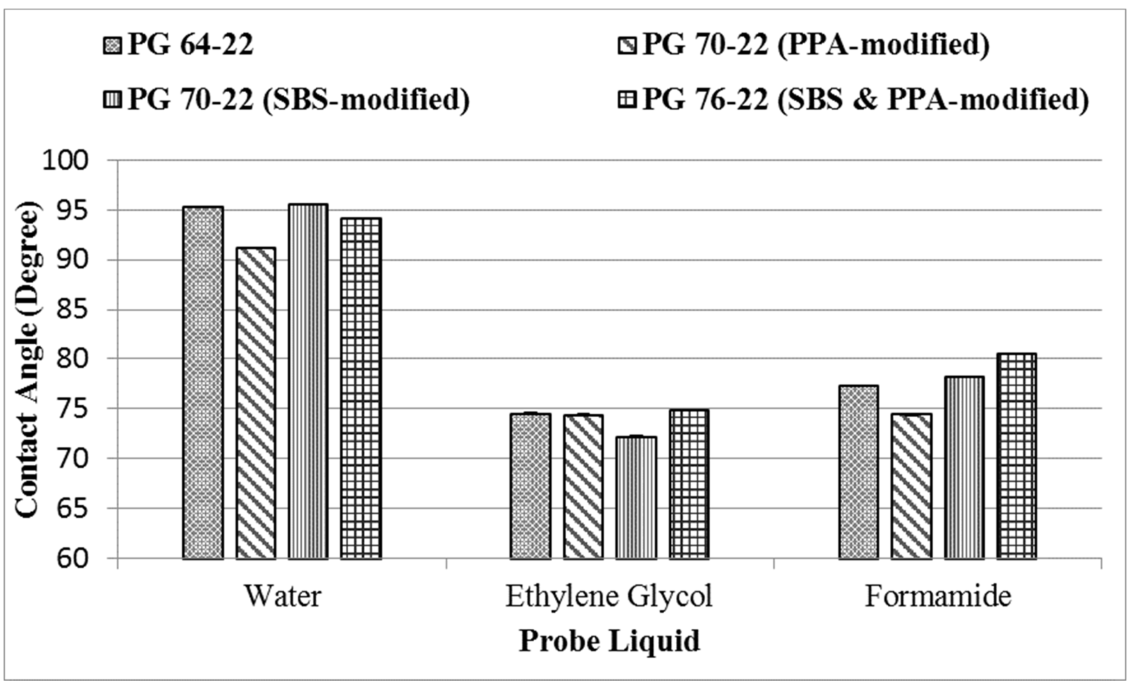

(b)

Figure 1 Contact Angles of Asphalt Sample Binders (a) Source 1 and (b) Source 2

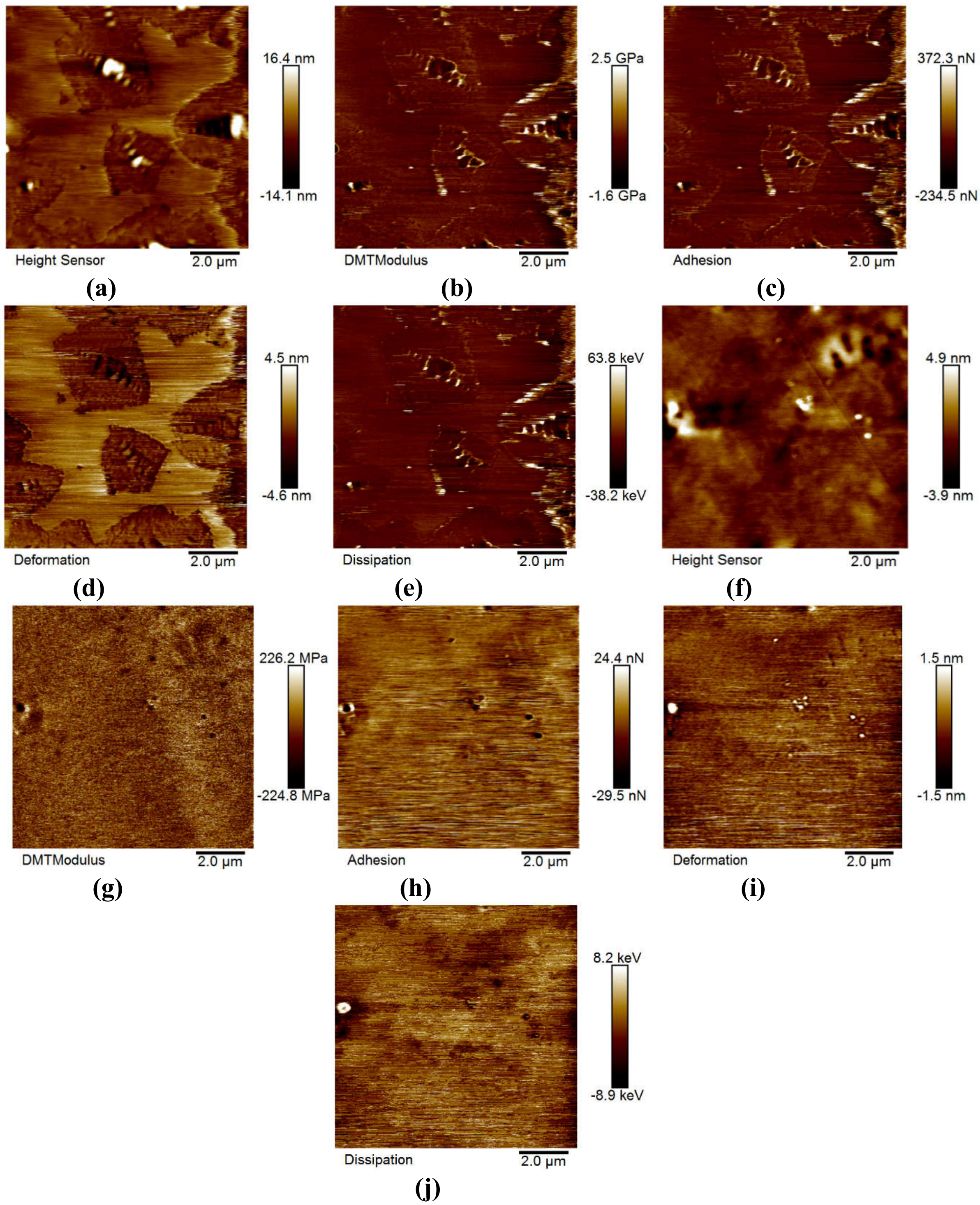

Figure 2 AFM-based Maps of Asphalt Binder (a)-(c): Dry Condition and (f)-(j): Wet Condition; here: (a & f) Morphology, (b & g) DMT Modulus, (c & h) Adhesion, (d & i) Deformation, and (e & j) Dissipation.

CONCLUSION

Based on the Texas boiling tests results, the percentage of asphalt retention for SBS-modified binder is better than the PPA-modified PG 70-22 binders, which is furtherly better than the base binder (PG 64-22). Compatibility analysis of asphalt binders shows higher adhesion energy in wet condition and lower adhesion energy in dry condition for PPA-modified asphalt binders for source 1. However, the opposite trend was noticed in case of source 2 binders. The evaluation of moisture on the binder properties at the molecular level were investigated using AFM. The topographic image revealed that surface of the binder samples is significantly changed due to the effect of water. In another word, it can be concluded that moisture changed the morphology of the asphalt binder surface. Furthermore, the effect of moisture also observed in all mechanistic data. The findings of this study are expected to help to have a better understanding of the effects of water in asphalts at the molecular level, and thereby help pavement professionals and engineers to use a proper binder for roadway construction as well as to develop a suitable test to quantify moisture damage potentials.

REFERANCES

Dourado, E.R., Simao, R.A., and Leite, L.F.M. (2012). "Mechanical properties of asphalt binders evaluated by atomic force microscopy". Journal of Microscopy, Vol. 245, No. 2, pp. 119-128.

Fromm, H.J. (1974). "The Mechanisms of Asphalt Stripping from Aggregate Surfaces", Proceedings, Association of Asphalt Paving Technologists, Vol. 43.

Fischer, H., Stadler, H., and Erina, N. (2013). "Quantitative temperature-depending mapping of mechanical properties of bitumen at the nanoscale using the AFM operated with PeakForce TappingTM mode". Journal of Microscopy, Vol. 250, No. 3, pp. 210-217.

Hicks, R.G., Santucci, L. and Aschenbrener, T. (2003). "Introduction and Seminar Objectives," Topic 1, National Seminar on Moisture Sensitivity of Asphalt Pavements, TRB Miscellaneous Report ISBN 0-309-09450-X, February 4-6, 2003.

Hossain, Z., Rashid, F., Mahmud, I., and Rahaman, M. (2016) Morphological and Nanomechanical Characterization of Industrial and Agricultural Waste-Modified Asphalt Binders. International Journal of Geomechanics, Vol. 17, No. 3, https://doi.org/10.1061/(ASCE)GM.1943-5622.0000767.

Little, D.N. and Jones, D.R. (2003). "Chemical and Mechanical Processes of Moisture Damage in Hot-Mix Asphalt Pavements," Topic 2, National Seminar on Moisture Sensitivity of Asphalt Pavements, TRB Miscellaneous Report, ISBN 0-309-09450-X, February 4-6, 2003, pp. 37 -70.

Lu, Q. (2003). "Investigation of Conditions for Moisture Damage in Asphalt Concrete and Appropriate Laboratory Test Methods," Proposal for doctoral thesis. Department of Civil and Environmental Engineering, University of California, Berkeley.

Masson, J.F., Leblond, V., and Margeson, J. (2006). "Bitumen morphologies by phase-detection atomic force microscopy". Journal of Microscopy, Vol. 221, No. 1, pp. 17-29.

Nahar, S.N., Schmets, A.J.M., Schitter, G., and Scarpas, A. (2014). "Quantitative nanomechanical property mapping of bitumen micro-phases by peak-force atomic force microscopy". Presented at 12th ISAP Conference on 30 Asphalt Pavements, Raleigh, N.C.

Rashid, A.F., and Hossain, Z. (2016). "Morphological and nanomechanical analyses of ground tire rubber-modified asphalts". Innovative Infrastructure Solutions, Vol. 1, No. 1, pp. 36.

Rashid, F., Hossain, Z., and Bhasin, A. (2017). "Nanomechanistic properties of reclaimed asphalt pavement modified asphalt binders using an atomic force microscope". International Journal of Pavement Engineering, pp. 1-9.

Santucci, L. (2010). "Minimizing Moisture Damage in Asphalt Pavements." Pavement Technology Update, University of California Pavement Research Center, Transfer Program, Vol. 2, No. 2, pp. 1-12.

Scherocman, J.A.o, Proctor, J.J., and Morris, W.J. (1985). "Prevention of Moisture Damage in Asphalt Concrete Pavement," Journal of the Canadian Technical Asphalt Association, Vol. 30, pp. 102-121.
Scott, J.A.N. (1978). "Adhesion and Disbonding Mechanisms of Asphalt Used in Highway Construction and Maintenance". Proceedings, Association of Asphalt Paving Technologists, Vol. 47.
Sebaaly, P.E., Elie, H., Dallas, L., Sivakulan, S., Thileepan, S., and Kamilla, V. (2010). "Evaluating the Impact of Lime on Pavement Performance," University of Nevada, Reno.
Tarrer, A.R. and Wagh, V. (1991). "The Effect of the Physical and Chemical Characteristics of the Aggregate on Bonding," SHRP-A-403, Strategic Highway Research Program, National Research Council.
Taylor, M.A., and Khosla, N.P. (1983). "Stripping of Asphalt Pavements: State of the Art," Transportation Research Record: Journal of the Transportation Research Board, No. 911, pp. 150-158.
Zollinger, C.J. (2005). "Application of Surface Energy Measurements to Evaluate Moisture Susceptibility of Asphalt and Aggregates". Master's Thesis, Texas A & M University. Retrieved from: http://oaktrust.library.tamu.edu/handle/1969.1/2320. Accessed on January 22, 2018.

Enhancing the Durability and the Service Life of Asphalt Pavements through Innovative Light-Induced Self-Healing Material

Sharareh Shirzad[1], Marwa M. Hassan[2], Max A. Aguirre[1], Samuel Cooper[3], Jr., Ioan Negulescu[4], and Louay N. Mohammad[5]

1GRA, Department of Construction Management, Louisiana State University
2Professor, Department of Construction Management, Louisiana State University
3Director, Louisiana Transportation Research Center
4Professor, Department of Chemistry, Louisiana State University
5Professor, Department of Civil and Environmental Engineering, Louisiana State University

INTRODUCTION

Asphalt pavement is the most common type of pavement all around the world; 90% of 5.2 million km of European roads and 92% of 4 million km North American roads are paved with asphalt materials [1]. Acquisition, processing and transportation of the material used in asphalt pavements construction, maintenance and rehabilitation, leads to significant energy consumption and Co2 emissions. In addition, frequent rehabilitation of asphalt pavements results in a large amount of excessively aged waste, which should be landfilled. With the increase in demand for roads and highway construction, asphalt pavement industry facing the challenge of increase in virgin material consumption, and therefore, issues with negative environmental and economic impacts. The use of recycled materials such as Recycled Asphalt Shingles (RAS) and/or Reclaimed Asphalt Pavement (RAP) as a partial replacement of virgin materials can significantly reduce the use of virgin materials, negative social impacts, and negative environmental effects of asphalt pavement reconstruction. However, the main challenge with this solution is that the asphalt binder in the recycled materials has been subjected to severe oxidation, thus is a hardened and brittle binder, which can increase crack susceptibility and consequently affect the performance of asphalt pavements. These issue limits the incorporation of high percentages of recycled asphalt material in asphalt pavement construction.

During the last decade, polymers were used as asphalt modifier to increase pavements resistance to rutting, fatigue and thermal cracking, decrease stripping and temperature susceptibility, and to improve its elastic recovery [2]. In addition, asphalt binder has the self-healing ability, which can be defined as the ability to recover its original properties. In asphalt pavements, self-healing properties can be used for repairing the damaged area by closing the cracks, stopping crack propagation, and eventually enhancing the performance of asphalt pavement. Using a similar approach, this study evaluated the application of a new generation of UV light induced self-healing polymers in asphalt binder; with the aim to enhance elastic recovery of the binder and increase the self-healing capabilities of asphalt mixtures at the same time. The propagation of micro-cracks due to aging and excessive loading cause the chemical breakage of polymer bonds and consequently produce free radicals. The produced free radicals would subsequently recombine through UV light exposure and close the micro-cracks [3]. Improved performance of asphalt pavement, through the use of self-healing polymer can lead to significant increase in the percentage of recycled asphalt material incorporation in asphalt pavement construction.

In order to achieve this goal, five main objectives were introduced; (1) Develop an optimized synthesis procedure for the production of UV light induced self-healing polymers; (2)

Examine the thermal stability of the produced polymer; (3) Evaluate the effect of self-healing polymer on the rheological properties of the binder; (4) Evaluate the effect of self-healing polymer on the mix mechanical properties; and (5) Evaluate the effect of UV light induced polymer on self-healing capabilities of asphalt mixture.

METHODOLOGY

Light activated self-healing polymer used in this study is introduced by Ghosh et al [3]. UV light-activated, self-healing polyurethane, used in this study, oxetane substituted chiton polyurethane (OXE-CHI-PUR), was introduced by Ghosh et al. (4). Self-healing polymer has three main components, which were selected based on their functionality. Chitosan was selected to provide UV light sensitivity, oxetane was chosen to provide a constraint in the four-member ring, and PUR was selected to provide mechanical integrity as well as network heterogeneity, and to facilitate the cleavage of the oxetane ring. This novel polymer has the ability to self-repair upon exposure to UV light, through the remodeling of damaged network. During the micro-crack appearance in asphalt pavement containing light-activated self-healing polymer, different chemical bonds in OXE-CHI-PUR will be broken. Consequently, a breakage of the bonds generates unstable, free radicals. These radicals will recombine through UV light exposure; during the recombination, the radicals will repair damaged areas of the asphalt binder [4].

After production of the self-healing polymer in the material laboratory, they were characterized by comparing obtained Fourier Transform Infrared (FT-IR) spectra of CHI with OXE-CHI, as well as HDI with OXE-CHI-PUR. Later, thermal stability of self-healing polymer was examined using Thermogravimetric Analysis (TGA). Self-healing polymer requires a certain thermal stability to withstand high temperature of asphalt pavement mixing process.

In order to evaluate the effect of self-healing polymer on the performance of asphalt binder, three different percentage of self-healing polymer were added to two different binders (64-22 M and 70-22 M), with or without recycled asphalt materials (RAP/RAS). 32 different binder blends were prepared and tested using fundamental rheological tests such as rotational viscometer, the dynamic shear rheometer, bending beam rheometer and multiple stress creep recovery. In addition, Superpave Performance Grade (PG) was used to compare results of the modified binder blends to the unmodified binder. RAS was added to the blends by 5% weight of the binder and RAP by 20% weight of the binder. In order to gain comprehensive understanding of effect of self-healing polymer, tests were repeated after 1 hour and 48 hours of UV light exposure. Result from rheological binder testing was used to determine the optimum percentage and type of self-healing polymer for asphalt mixture testing.

Mechanical properties of asphalt mixture containing recycled asphalt material (RAS/RAP) and optimum percentage of self-healing polymer was evaluated using semi-circular bending (SCB) test and loaded wheel tracking test (LWT). SCB was performed to examine samples resistance to fatigue cracking at intermediate temperature, while LWT evaluated rutting susceptibility of mixture at high temperature. Next, samples were prepared for evaluation of the structural behavior of asphalt beams with and without self-healing polymers. To achieve this goal, a three-point bending test setup was used to measure the flexural strength of the asphalt beams at room temperature for different types of asphalt mixtures before and after healing. Slab specimens was compacted and rectangular specimens with dimensions of 40 mm × 40 mm × 160 mm was cut from slab samples. Undamaged or initial stiffness of the beams was measured as the slope of the load-deflection curve in the linear region. The stiffness of the beams was re-measured after creating the cracks and was referenced as the damaged stiffness or day 0 stiffness. Finally, the beam stiffness was measured after 6 days of healing. A relative comparison of initial stiffness, day 0 stiffness, and day 6 stiffness will be used to evaluate self-healing progress in the beams. In addition, the healing of cracks was monitored in the different mixtures, various cracks with varying widths, using light microscopy and image analysis. Images was captured and analyzed at day 0, day 1, day 2, day 3 and day 6.

FINDINGS

Fourier Transform Infrared (FT-IR) Spectroscopy

The reaction of OXE with CHI in the oxetane-substituted chitosan (OXE-CHI) and the reaction of OXE-CHI with HDI and PEG in OXE-CHI-PUR were confirmed using the FTIR spectra obtained for CHI and OXE-CHI, spectra obtained for OXE-CHI and OXE-CHI-PUR, respectively.

Thermal Stability

Based on result obtained from the Thermogravimetric Analysis of produced OXE-CHI-PUR cross-linked networks, the weight loss of sample was less than 10% in the first 200ºC.

Effect of Light Activated Self-Healing Polymer on Rheological Properties of Asphalt Binder

Rotational Viscometer (RV)

The measurements from RV showed that the addition of self-healing polymer reduced the viscosity of the binder blends containing recycled asphalt material (RAP/RAS). However, the viscosity of the unmodified binder was not completely recovered.

Dynamic Shear Rheometer (DSR)

DSR results, the G*/sinδ value of the unmodified binder increased due to the addition of recycled asphalt material (RAP/RAS). When 1% self-healing polymer was added to the blend containing an unmodified binder and RAS, the G*/sinδ value decreased. However, the blends containing 3% and 5% self-healing polymer exhibited a higher G*/sinδ value, compared to the blend with 1% self-healing polymer.

Bending Beam Rheometer (BBR)

BBR result shows that the addition of recycled asphalt material (RAP/RAS) caused an increase in the stiffness and a decrease in the m-value of the binder blends. Furthermore, an increase in the stiffness and a decrease in the m-value of the binder blends were observed as the result of self-healing polymer modification.

Performance Grade (PG)

The final performance grade result shows that the addition of recycled asphalt material (RAP/RAS) caused an increase in the high temperature grade of the binder blend, which is an indication of a stiffer binder. Furthermore, changes in high temperature grade and low temperature grade caused by addition of recycled asphalt material (RAP/RAS) and self-healing polymer were not significant enough to alter the low temperature grade of the binder blends.

Results from tests performed on binder blends exposed to UV light demonstrate an increase in the continuous high temperature grade of the blends with the increase in the duration of UV exposure. Furthermore, delta Tc was calculated for all binder blends as the difference between the critical stiffness temperature and the m-value critical temperature. As a result of recycled asphalt material (RAP/RAS) addition, delta Tc was increased, however, the addition of self-healing polymer decreased delta Tc. These values were further reduced with UV light exposure.

Multiple Stress Creep Recovery (MSCR)

The percent recovery and the non-recoverable creep compliance (Jnr) of the samples, measured by MSCR, increased for 64-22 M binder blends by increasing the percentage of self-healing polymers. However, these value were decrease for 70-22 M binder blends with the addition of self-healing polymer.

CONCLUSIONS

An innovative, light-activated, self-healing polymer was synthesized in the laboratory by means of a photocatalytic-based chemical method. The synthetic degree of produced self-healing polymers was confirmed, using FT-IR spectroscopy, while the thermal stability was analyzed by means of TGA. In addition, performing rheological tests on prepared binder blends showed that viscosity of blends increased by addition of recycled asphalt material. However, binder blends viscosity decreased with self-healing polymer incorporation. Furthermore, an increase in G* and G*/sinδ and a decrease in δ of binder blends was observed with self-healing polymer incorporation when compared to the binder blends containing only recycled asphalt material. Performance grading results showed an increase in high temperature grade of the binder blends containing recycled asphalt material and binder blends containing both recycled asphalt material and self-healing polymer. However, the low-temperature grade was the same for all tested binder blends. Delta Tc showed an improvement in low service temperature performance for samples exposed to UV light, with binder blend containing 5% self-healing polymers showing the best results. Finally, based on the results from the MSCR test, a binder blend with 64-22 M binder, containing recycled asphalt material and 5% self-healing polymer, showed the highest percent recovery among the tested binder blends, indicating that this binder blend showed the most desirable characteristics against rutting.

REFERENCES

[1] Thives. L. P., Ghisi, E. (2017). “Asphalt mixtures emission and energy consumption: A review.” Renewable and Sustainable Energy Reviews 72 473–484.

[2] Yildirim, Y. (2007). Polymer modified asphalt binders. Construction and Building Materials 21 66–72.

[3] Ghosh, B., CHellappan, V., Urban, W. M. (2011). Self-healing inside a scratch of oxetane-substituted chitosan-polyurethane networks. Journal of materials chemistry, 21, 14473.

Development of a Self-healing and Rejuvenating Mechanism for Asphalt Mixtures containing Recycled Materials

Max A. Aguirre[1], Marwa M. Hassan[2], Sharareh Shirzad[1], Samuel Cooper, Jr.[3], Ioan Negulescu[4], and Louay N. Mohammad[5]

1GRA, Department of Construction Management, Louisiana State University
2Professor, Department of Construction Management, Louisiana State University
3Director, Louisiana Transportation Research Center
4Professor, Department of Chemistry, Louisiana State University
5Professor, Department of Civil and Environmental Engineering, Louisiana State University

INTRODUCTION

Self-healing products such as hollow-fibers filled with an asphalt rejuvenator present an emerging technology that would enhance an asphalt mixtures resistance to cracking damage. Also, the development of polymer fibers containing a rejuvenator type product would promote the use of recycled materials by restoring the properties of the aged binder and improving the properties of HMA resulting in an enhancement in pavement performance. The main objectives of this project were to develop a synthesis procedure for the production of sodium-alginate fibers containing an asphalt rejuvenator; evaluate the thermal stability and the resistance to mixing processes of the fibers; evaluate the rheological properties of asphalt binder blends with and without sodium-alginate fibers; and assess the performance of HMA mixtures containing sodium-alginate fibers against distresses such as fatigue cracking, low-temperature cracking and permanent deformation.

Self-healing concept in asphalt pavement has been evaluated in different studies by encapsulating a rejuvenator product and dispersing them into a new HMA mixture. Single-walled and double-walled microcapsules containing a rejuvenator product has been successfully developed in previous studies *(1-2)*. In addition, Aguirre at al. evaluated the healing efficiency of microcapsules containing an asphalt rejuvenator by quantifying the healing progress of cracked HMA specimens as a function of time *(3)*. Another promising self-healing product is the develop of hollow fibers containing an asphalt rejuvenator. Sodium-alginate fibers containing o-dichlorobenzene (DCB) have been successfully synthesized via wet-spinning showing a good thermal stability and high tensile strength of the developed fibers, which may offer the possibility to incorporate them as self-healing products in asphalt pavement applications *(4)*.

METHODOLOGY

Fiber's Synthesis and Properties

The synthesis procedure to produce hollow-fibers containing a rejuvenator product was adapted from Mookhoek et al. *(4)*. The hollow-fibers were synthesized via wet-spinning process from an oil-in-water emulsion containing the shell material and the core material. Sodium alginate was selected as the shell material because it provides suitable properties such as water solubility, fast coagulation in the presence of divalent ions, and adequate mechanical properties *(5)*. The morphology of the produced fibers was evaluating by using a Scanning Electron Microscope (SEM-FEI Quanta 3D FEG Dual Beam SEM/FIB).

Optimization of Production Parameters for Fiber Synthesis

A variation in the production parameters of the hollow-fibers was evaluated to determine their effects in the thermal stability and tensile strength of the fibers in order to assess their resistance to HMA production parameters. The optimization process was performed with the variation of the following production parameters: percentage of emulsifier (i.e. PEMA), percentage of plasticizer (i.e., ethylene glycol) and the ratio rejuvenator to shell. The thermal variation of each fibers type was evaluated by performing a Thermogravimetric Analysis (TGA) with a rate of 10.00°C/min from room temperature (i.e., 25°C) to 600°C. In addition, the ultimate tensile strength (UTS) of the developed fibers was tested in tension using a force testing system with a 50 N load cell at a crosshead speed of 5.0 mm/s.

Evaluation of the Rheological Properties of Asphalt Binder Blends with Fibers

Seven different binder blends including a conventional virgin binder PG 64-22 and six binder blends with 5% of extracted binder from RAS and 20% RAP by weight of virgin binder with 5% fibers were prepared. Another set of binder blends with a PG 70-22 binder as a based binder were prepared.

Performance Grading (PG Grading)

The rheological properties of the different asphalt binder blends were characterized using fundamental rheological tests and by comparing the Superpave Performance Grade (PG) of the modified blends to the conventional asphalt binder in accordance to AASHTO M 320-09 *(6).*

Multiple Stress Creep Recovery (MSCR)

The rutting resistance of the asphalt blends was characterized by conducting the Multiple Stress Creep Recovery (MSCR) test. The MSCR was performed in accordance to AASHTO TP 70 *(7)*.

Frequency Sweep Test

The Complex Shear Modulus, G*, of the different asphalt binder blends were obtained by performing a frequency sweep tests at temperatures ranging from 4.4°C to 54.4°C and frequencies between 0.1 to 100 radians/second. This dynamic test consisted of applying a sinusoidal strain to the specimen and the resulting stress is measured as a function of frequency in the dynamic mechanical analysis.

Effects of Sodium-Alginate Fibers in HMA Mixture

A level 2 Superpave HMA mixtures were designed and prepared in accordance with AASHTO R 35-17 (8) and AASHTO M 323-12 *(9)*. The optimum asphalt content for each Superpave mixture was determined according to volumetric (air voids = 3% to 5%, voids in mineral aggregates ≥ 13%, and voids filled with asphalt = 68% to 78%), and densification requirements (%Gmm at Ninitial ≤ 89%, and %Gmm at Nfinal ≤ 98%).

HMA Mixture Performance Tests

Two fundamental tests (SCB and TSRST) and a simulative test (HWTD) were conducted to characterize the performance of asphalt mixtures. Cylindrical specimens were fabricated using a Superpave gyratory compactor (SGC), except for TSRST. The laboratory TSRST specimens were compacted into a rectangular slab, 260.8 mm wide by 320.3 mm long by 50 mm thick, using a kneading compactor. After compaction, the required beam specimens for the TSRST were obtained by sawing the rectangular slab to the required dimensions. The target air voids for all specimens prepared in this study was 7.0 ± 0.5%.

FINDINGS

Sodium-Alginate Fibers with Rejuvn8

Thermogravimetric Analysis (TGA)

The evaluated parameter in TGA was the percentage weight retained at 163°C. TGA results showed that the increase in the emulsifier content from 30 to 50% had a negative impact on the percentage weight retained of the developed fibers. It was also observed that the addition of a plasticizer at a dosage rate of 10% and 40% had a positive effect in the percentage weight retained compared to a dosage rate of 20 and 30%. Lastly, increasing the rejuvenator to shell material ratio resulted in the highest percentage weight retained.

Tensile Strength

Tensile strength was measured to evaluate the fibers resistance to breakage during the mixing process. Ten fibers from three different batches for each developed fiber were tested. A minimum value of 12 MPa for tensile strength was determined to be required to avoid disintegration of the fibers during a HMA mixing process. The UTS test results suggest that the addition of a plasticizer at a dosage rate from 10% to 40% improved the tensile strength of fibers as it increased from 11.4 MPa to 28.4 MPa.

Optimum Preparation Procedure for Sodium-alginate Fibers Containing Rejuvn8

Based on the TGA and UTS test results, a rejuvenator to shell material ratio of 1:1.5, a 30% emulsifier content, and 40% plasticizer content were selected as the optimum production parameters for the fiber synthesis.

Effects of Fibers on the Binder Rheological Properties

Based on DSR test results at high-temperature, the addition of fibers was counteracting the negative effects of adding aged binder from a recycled material as a decrease in $G^*/\sin\delta$ for both unaged and short-term aged binder blends was observed. For intermediate temperature and long-term aging condition, a lower failed temperature with the addition of fibers was obtained, which suggests a better performance against fatigue cracking. Furthermore, the addition of fibers resulted in an improved performance in the BBR test where a reduction in the stiffness and an increased in the m-value was observed compared to the control blend.

MSCR test results showed that the addition of recycled material and developed fibers positively improved the rutting resistance compared to virgin binders as the non-recoverable creep compliance (J_{nr}) decreased at both stress levels. In addition, the highest percent recoveries were observed in the binder blends with 20% extracted binder from RAP for both PG 64-22 and PG 70-22.

Lastly, the improvements against permanent deformation in the binder blends observed in the MSCR tests results were confirmed in the frequency sweeps as it was possible to observe higher G^* values at low-frequencies rates in the blends with recycled materials compared to both virgin binders.

Performance of HMA Mixtures with Sodium-Alginate Fibers

The results from the HWTD test showed that the addition of recycled materials improved the performance of HMA mixture against permanent deformation. Also, it was possible to observe that the addition of fibers did not positively or negatively affect the performance against permanent deformation compared to mixtures with recycled materials.

The intermediate fracture properties of the HMA mixtures was negatively affected by the addition of recycled materials compared to the control mixture. However, the addition of 5% fibers improved the intermediate fracture properties by showing an increased in the critical release strain energy value based on the SCB test results.

Finally, the TSRST test results showed an improvement in the failure temperature of the HMA mixtures with the addition of the developed fibers. In addition, a higher failure load was also observed in the mixtures containing fibers.

CONCLUSION

A suitable sodium-alginate fiber containing a rejuvenator to resist a HMA mixing process was developed by performing an optimization process of different production parameters. The fibers prepared with a rejuvenator to shell material of 1:1.5, an emulsifier content of 30%, and a plasticizer content of 40% were selected as the optimum fibers based on TGA and UTS test results. In addition, the Continuous PG grading results shows that a decreased in both high-temperature grading and low-temperature grading was observed with the addition of the developed fibers. Furthermore, the addition of recycled material and fibers enhanced the rutting resistance of binder blends compared to the control blend based on the J_{nr} values in the MSCR test. The enhancement observed in the MSCR test results for the binder blends was confirmed in the frequency sweet test results. A similar behavior was observed in the mixture testing where the addition of recycled materials improved the permanent deformation of the evaluated mixtures based on the HWTD test results. The SCB test results showed an improvement in the critical strain release energy value in the mixtures with recycled materials with the addition of the developed fibers. Finally, the addition of fibers to HMA mixtures resulted in the coldest failure temperature and highest failure load in TSRST test.

REFERENCES

1. Aguirre, M. A., M. M. Hassan, S. Shirzad, W. H. Daly and L. Mohammad. (2016). *Micro-encapsulation of asphalt rejuvenators using Melamine-Formaldehyde*. Construction and Building Materials, vol. 114, pp. 29-39.
2. Shirzad, S., M. M. Hassan, M. A. Aguirre, L. N. Mohammad and W. H. Daly. (2016). *Evaluation of sunflower Oil as a Rejuvenator and Its Microencapsulation as a Healing Agent*. J. Mater. Civil. Eng.
3. Aguirre M. A., M. M. Hassan, S. Shirzad, L. N. Mohammad, S. Cooper and I. I. Negulescu. (2017). *Laboratory Testing of Self-Healing Microcapsules in Asphalt Mixtures Prepared with Recycled Asphalt Shingles*. Journal of Materials in Civil Engineering.
4. Mookhoek, S. D., H. R. Fischer and S. van der Zwaag. (2012). *Alginate fibres containing discrete liquid filled vacuoles for controlled delivery*. Composites Part A: Applied Science and Manufacturing, vol. 43, no. 12, pp. 2176-2182.
5. McDowell, R. H. (1977). *Properties of alginates*. London (UK): Alginate Industries.
6. AASHTO. (2015). *Standard specification for performance-graded for asphalt binder*. AASHTO M320, Washington, DC.
7. AASHTO. (2013). *Standard Method of Test for Multiple Stress Creep Recovery (MSCR) Test of Asphalt Binder Using a Dynamic Shear Rheometer (DSR)*. AASHTO TP 70, Washington, DC.
8. AASHTO. (2017). *Standard Practice for Superpave Volumetric Design for Asphalt Mixtures*. AASHTO R 35, Washington, DC.

9. AASHTO. (2012). *Standard Specifications for Superpave Volumetric Mix Design*. AASHTO M 323, Washington, DC.

Use Ultra-High-Performance Fiber-Reinforced Concrete (UHP-FRC) for Fast and Sustainable Repair of Pavement

Ashish Karmacharya[1] and Shih-Ho Chao[2]

[1]Graduate Student, Department of Civil Engineering, the University of Texas at Arlington
[2]Professor, Department of Civil Engineering, the University of Texas at Arlington

INTRODUCTION

Statistical data shows that in industrially developed countries about 50 percent of total construction costs are related to repair, replacement, and maintenance of existing structures that have deteriorated or been damaged by environmental stress, structural loading, or other effects (Metha and Monteiro, 2006). The durability issues of infrastructure can lead to a significantly higher life-cycle cost in comparison to the initial construction cost. Fast transportation infrastructure deterioration can be caused by climate change, overloaded and increasing traffic, and other environmental loads. For example, climate change such as summer heatwaves, droughts, and flooding can have major impacts on the pavement maintenance and rehabilitation costs. These extreme events are likely to occur in greater frequency and intensity in the future as the global temperature continues to rise. Rainfall changes can alter moisture balances and influence pavement deterioration. In addition, temperature can affect the aging of bitumen resulting in an increase in cracking of the pavement surface, with a consequent loss of waterproofing. The result is that surface water can enter the pavement causing rapid loss of surface condition. Changes in temperature and rainfall patterns can interact where higher temperatures increase cracking. Recent statistics indicates that annual pavement maintenance and rehabilitation budget is estimated to increase by around 30% (considering both the influences of climate change and transport demand changes). Deficiencies in conventional concrete and its subsequent impact on the environment calls for a much durable material that will last longer under environmental stress, thereby contributing to the conservation of natural resources and the protection of the ecosystem.

This project offers a new methodology which will enable the transportation infrastructure to use an advanced fiber-reinforced concrete material, ultra-high-performance fiber-reinforced concrete (UHP-FRC), which will delay or prevent the deterioration of transportation infrastructure when subjected to traffic and environmental loadings. The major problem of concrete is the considerable deterioration and consequent repair work needed due to its brittleness and limited durability. The consequence of concrete deterioration and short service life requires frequent repair and eventual replacement, which consumes more natural resources.

UHP-FRC is a new generation of fiber-reinforced concrete which has ultra-high compressive strength (18–30 ksi; 10 to 12 ksi after 24 hours.) and ductility. A concrete with only ultra-high compressive strength is not suitable for structural application, even reinforced with mild reinforcing steel, as the very brittle nature can cause potential issues such as abrupt unpredictable failures and a minimum capability of stress redistribution. UHP-FRC was developed by changing the porous nature of conventional concrete through reducing dimensions of microcracking (or defects) in the concrete. This is achieved in UHP-FRC through a very low water to cementitious materials ratio (0.18 to 0.25) and a dense particle packing (Aghdasi et al., 2016), which leads to almost no shrinkage or creep, making it very suitable for concrete members under long-term compression. The consequences of a very dense microstructure and low-water ratio results in enhanced compressive strength and delayed liquid ingress. Furthermore, the addition of steel or synthetic fibers improves the brittle nature of concrete by increasing the tensile cracking resistance, post-cracking strength, ductility, and energy absorption capacity. In terms of corrosion resistance, research has indicated that UHP-FRC has a much greater durability than conventional concrete due to its very dense microstructure. This dense microstructure impedes the conductive chloride ions from coming into direct contact with the steel reinforcing bars, which protects the reinforcing bars from corrosion. **Table 1** provides a comparison between typical conventional concrete and UHP-FRC.

Table 1. Comparison of typical conventional concrete and UHP-FRC (all data from UT Arlington research except Rapid Chloride Penetration Test)

Properties of Concrete	Conventional Concrete	UHP-FRC
Ultimate Compressive Strength	< 8,000 psi (55 MPa)	18,000 to 30,000 psi (124 to 207 MPa)
Early (24-hour) compressive strength	< 3000 psi (21 MPa)	10,000 – 12,000 psi (69 to 83 MPa)
Flexural Strength	< 670 psi (4.6 MPa)	2,500 to 6,000 psi (17 to 41 MPa)
Shear strength	< 180 psi (1.2 MPa)	> 600 psi (4.1 MPa)
Direct Tension	< 450 psi (3 MPa)	up to 1,450 psi (10 MPa)
Rapid Chloride Penetration Test*	2000-4000 Coulombs passed	Negligible (< 100 Coulombs passed)
Ductility	Negligible	High ductility
Ultimate Compressive Strain, ε_{cu}	0.003	0.015 to 0.03
Confining	Negligible	High confining capability

* Ahlborn et al. 2011

Currently adding an overlay in pavement and bridge deck is the majority transportation infrastructure applications of UHP-FRC (Khayat and Valipour, 2014). Log Cezsoski Bridge in Slovenia is an example which used UHP-FRC overlay in bridge deck (Sajna et al., 2012). UHP-FRC overlay shows greater bond strength between the substrate concrete and the UHP-FRC overlay than that of the substrate concrete. UHP-FRC also exhibits significant increase in flexural strength and toughness, post cracking tensile capacity, high resistance to environmental and chemical attack, and negligible permeability. UHP-FRC was used successfully in a pilot project for the repair and upgrade of an existing reinforced concrete motorway bridge in a high level road network in Austria (Hadl, Pietra, Hoang, Pilch and Tue, 2015). Toppings and deck panels using UHP-FRC was employed in the rehabilitation of orthrotropic bridge deck, in Netherlands (Buitelaar, 2004). However, no literature has shown that UHP-FRC was used for pavement repair.

This research will address the strong need to develop fast and sustainable repair UHP-FRC materials for pavement repair that can be easily cast onsite without special treatments such as heat, pressure, and vacuum thereby avoiding any major changes to current concrete production practice to accelerate the use of UHP-FRC materials. Taking advantage of the early strength and durability of UHP-FRC, this research aims at investigating the viability of UHP-FRC in fast repair of pavement. Pavement repair in partial depth patches and full depth patches will be carried out using UHP-FRC. This research also investigates a new type UHP-FRC pavement without dowel bars.

METHODOLOGY

Two tasks have been carried out in the experimental programs: 1) material development for suitable pavement UHP-FRC mixtures including mixtures with steel or synthetic fibers. The procedure is similar to that used by Aghdasi et al. (2016). Four UHP-FRC mix designs have been investigated and their compressive stress-stain data were collected. We tried to vary the composition of fiber combinations and mix components to obtain the optimized UHP-FRC mixtures. 2) interface strength testing using slant shear test (SST). The interface shear strength between existing concrete and repairing concrete, including early interface shear strength (24 hours) and short-term interface shear strength (7-day) have been investigated by using SST. SST is a simple testing method (ASTM, 2013) commonly used to investigate the bond performance between two different concrete (Santos, 2009). A roughened surface without dowel bars was investigated to compare with common practice where dowel bar was inserted in a saw-cut (relatively smooth) interface to provide interface shear resistance (**Figure 1**). A specimen 150 mm x 150 mm (5.9 in. x 5.9 in.) cross section with a total height of 560 mm (22 in.) is used for the test. A bond interface angle of 30 degrees with the vertical, longitudinal axis of the specimen, was selected as per the guidelines of ASTM C882/C882M (ASTM, 2013).

(a)

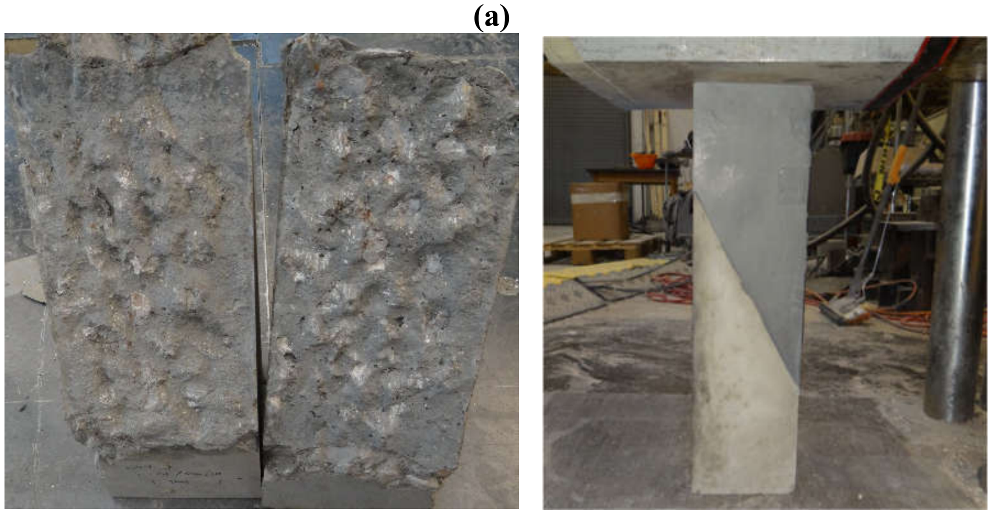

(b) **(c)**

Figure 1: (a) smoothened surface (rebar is not shown) and actual saw-cut concrete pavement; (b) roughened surface; (c) slant shear test

FINDINGS

Table 2 summarizes the preliminary results comparing the interface shear strength from roughened surface (without interface shear reinforcement) and smooth surface (with No. 4 interface shear reinforcement). The smooth surface is similar to those saw-cut surface for pavement repair. Only plain concrete was used in this phase. It is seen that, generally, the roughened surface provides greater strength than the smooth surface with dowel bar either after 24-hour or 7-day of casting. **Figure 2** indicates that the interface shear reinforcement (dowel bar) did not carry much of the load until certain slip had occurred. This is seen from the very small strain (0.0005 << yielding strain of 0.002). This shows that majority of the load was actually carried by the concrete interface rather than the dowel bar. The strain in the rebar increased significantly after the interface of concrete started to degrade. This study shows that it is possible to use a roughened surface without a post-installed dowel bars to reduce the labor work and repair time. The roughened surface could be created by a jack hammer or other tools.

Table 2. Preliminary results comparing the interface shear strength from roughened surface (without interface shear reinforcement) and smooth surface (with interface shear reinforcement). Plain concrete only

Specimen Top Half	Days	Surface preparation	Shear stress (psi)	Peak Longitudinal Load (kips)	Average shear stress (psi)
PC	1	Roughened	616	50	616
	7	Roughened	780	63	780
PC with #4 rebar	1	Smooth	550	36	443
	7	Smooth	738	59	738

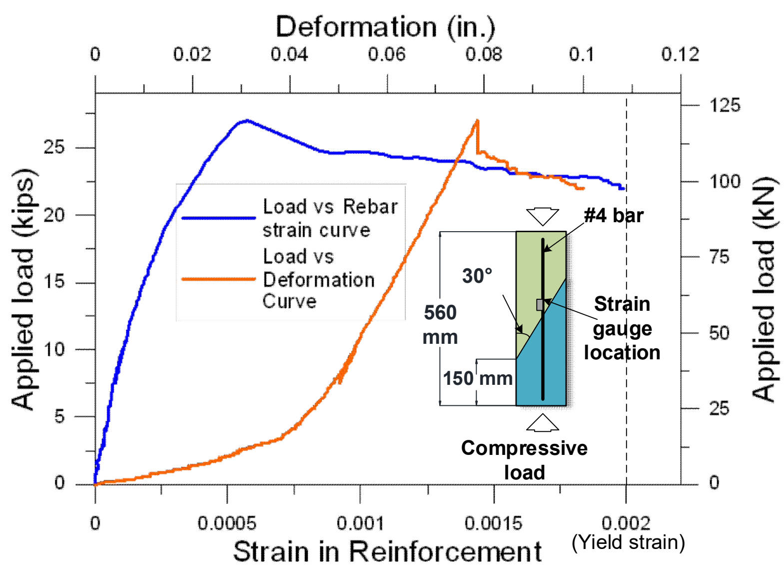

Figure 2: Applied load versus deformation and applied load versus strain in the embedded No. 4 interface shear reinforcement

CONCLUSION

Several UHP-FRC mixtures with either steel or synthetic fibers for pavement repair were developed in this study. In addition, interface shear strength test using slant shear test (SST) shows that it is possible two use a roughened surface to replace saw-cut surface with dowel bars. Combining the high early strength and durability of UHP-FRC and the elimination of dowel bars, the results from this project could result in direct benefits to society through short- and long-term cost savings by extending the lifetimes of pavement and reducing the construction, repair, and maintenance costs. Ongoing research of this project will provide more information on the strength and performance of UHP-FRC repaired pavement.

REFERENCES

Aghdasi, P., Heid A. E., and Chao, S.-H. (2016), "Developing Ultra-High-Performance Fiber-Reinforced Concrete for Large-Scale Structural Applications," ACI Materials Journal, V. 113, No. 5, September-October 2016, pp. 559-570.

Ahlborn, T., Harris, D., Misson, D., and Peuse, E. (2011), “Characterization of Strength and Durability of Ultra-High-Performance Concrete Under Variable Curing Conditions,” Transportation Research Record: Journal of the Transportation Research Board, No. 2251, Transportation Research Board of the National Academies, Washington, D.C., 2011, pp. 68–75. DOI: 10.3141/2251-07.

ASTM. (2013), Standard Test Method for Bond Strength of Epoxy-Resin Systems Used with Concrete by Slant Shear, C882/C882M − 13a, ASTM International, 4 pp.

Buitelaar, P., “Heavy Reinforced Ultra-High-Performance Concrete,” Proceedings of the International Symposium on Ultra High Performance Concrete, Ed., Schmidt, M., Fehling, E., and Geisenhanslüke, C., Kassel University Press, Kassel, Germany, 2004, pp. 25–35.

Hadl, P., Pietra R. D., Hoang, K. H., Pilch, E., Tue, N. V. (2015), “Anwendung von UHPC als direkt befahrener Aufbeton bei der Integralisierung eines bestehenden Brückenbauwerks in Österreich”, Ernst & Sohn Verlag für Architektur und technische Wissenschaften GmbH & Co. KG, Berlin. Beton- und Stahlbetonbau 110 (2015), Heft 2.

Khayat, K. H. and Valipour, M. (2014), “Design of Ultra High Performance Concrete as an Overlay in Pavements and Bridge Decks,” Center for Transportation Infrastructure and Safety/NUTC program, Missouri University of Science and Technology, funded by U.S. Department of Transportation Research and Innovative Technology Administration, 2014.

Metra, P. K. and Monteiro, P. J. M. (2006). Concrete—Microstructure, Properties, and Materials, third edition, McGraw-Hill.

Sajna, A., Denarié, E., and Bras, V. (2012). “Assessment of a UHPFRC Based Bridge Rehabilitation in Slovenia, Two Years After Application,” Proceedings of Hipermat 2012 3rd International Symposium on UHPC and Nanotechnology for High Performance Construction Materials, Ed., Schmidt, M., Fehling, E., Glotzbach, C., Fröhlich, S., and Piotrowski, S., Kassel University Press, Kassel, Germany, 2012, pp. 937–944.

Santos, P.M.D. (2009). Assessment of the Shear Strength between Concrete Layers, Ph.D. Dissertation, University of Coimbra, July, 2009. 338 pp.

Deterministic and Probabilistic Modelling Framework of Electrochemical/Corrosion Behavior of Reinforced Concrete Specimens Exposed in Marine Environments

Changkyu Kim[1], Ahmad Karayan[1], Doeun Choe[2], Pedro Castro[3], Ayman Okeil[4], Mahmoud Taha[5], and Homero Castaneda[1]

[1] Texas A&M National Corrosion and Materials Reliability Laboratory, Texas A&M University
[2]Department of Civil and Environmental Engineering, Prairie View A&M University
[3]Applied Physics, CINVESTAV, Merida Mexico
[4]Deptartment of Civil and Environmental Engineering, Louisiana State University
[5]Department of Civil Engineering, University of New Mexico

INTRODUCTION

In modern society, Reinforced concrete (RC) bridges in the US are critical components in transportation networks, which are required to be maintained through proper inspection, as their durability and reliability are highly affected by corrosion-induced deterioration. Some inspection processes, tools, and control action practices (control and prevention) can be inadequate to provide sufficient information that can be used for addressing corrosion-induced damage. Since it does not include mathematical and reliability modeling tools and control actions based on quantitative testing and monitoring to analyze the extent of damage where corrosion may be occurring and actions should be taken. The corrosion process consists of two steps: initiation and propagation. During this processes each stage can be determined depending on the material properties, environmental conditions, and the geometry of the structures. Coastal environments significantly impact the corrosion process by accelerating the mechanism due to the combination of factors activating the passivated rebar. The chloride content and accumulation within the concrete structure has been one of the critical factors for corrosion activation. While the chloride content can be an indirect measure for corrosion, there are some parameters affecting the dissolution process that can be used to estimate degradation processes in concrete structures. The initial approach will be taken based on the classical model including the error function by the solution of Fick's law with correction factors based on the experimental data to estimate the reliability. The current results will allow generating a second approach that considers the interfacial processes occurring at the rebar/concrete interface. Both approaches will be used to compare the outcome of a reliability model.

The final goal is to develop a comprehensive framework for corrosion damage management of RC structures. This will provide an effective approach to monitoring and quantifying the evolution of damage, assessment of structural integrity as well as providing efficient and cost-effective maintenance/repair strategies by incorporating the corrosion damage to the structural design process.

METHODOLOGY

This work aims to analize, through deterministic modelling, the electrochemical behavior at the initiation stage, of small specimens exposed in different locations along the Gulf of Mexico coast. Marine environments have a detrimental effects on RC structures, affecting the durability and reliability of the infrastructures. Exposure to the environment and the continuous transport of aggressive agents promote the activation of the metallic surface, having an initiation and propagation process. There is widely available information regarding the corrosion process that has been obtained through different techniques and exposure conditions. However, there are factors that could affect the data when the measurements are taken within long periods between them, and this may affect the interpretation of corrosion stages. Understanding the initial corrosion stage and its relation with the aggressive environments will provide a general view to propose corrosion control actions.

The long term exposed reinforced concrete samples designed and casted included typical fine and coarse aggregate and ordinary Portland cement. One parameter critical for the corrosion activity is the mixes water/cement ratios, the samples considered: 0.46, 0.50, 0.53, 0.70, and 0.76. Another concrete fabrication property is the curing time; we have results for 1, 3, and 7 days. The long term concrete cylinders have been in the coastal environment for 25 years close to the shore at the north coast of the Yucatan Peninsula, Gulf of Mexico. The experimental-theoretical approach gives a better understanding of how concrete properties and exposure conditions influence the realibility of reinforced concrete structures when they are exposed to a corrosive environment. In this project the samples are under no load conditions, the theretical framework includes coastal environments influence the corrosion process due to the combination of factors activating the passivated rebar and depredating the composite asset. The chloride content and accumulation within the concrete structure has been one of the critical factors for corrosion activation. While the chloride content can be an indirect measure for corrosion, there are some parameters affecting the dissolution process that can be used as parameters to build a reliability model.

FINDINGS

At this stage we presented different reinforced concrete cylinders, 7.5 cm in diameter by 15.0 cm in length, with a reinforcing steel bar (9.5 mm nominal diameter and 20.0 cm long), placed in the center of the cylinder were tested by using an electrochemical equipment (Figure 1 and 2). The experimental-theoretical approachimproves the understanding and the prediction of the corrosion process. The impacts of material and exposure conditions to the material durability are quantified for RC structures subject to marine atmospheric enviroment.

Figures 1 and 2 present the corrosion current density (i_{corr}) evolution for the long term exposure samples with different casted water to cement (w/c) ratio measured for 1 and 7 days of curing, respectively. For samples cured for 1 day (Fig. 1), all samples show an increase of corrosion current density over time, and it indicates an increase of corrosion rate. Results shows differences in samples with higher w/c ratio tend to have higher corrosion current density during the first 50 months of exposure. After the 50 months, there is an increased varaibility for the same magnitude. During the first 50 months, there was a trend that higher i_{corr} value was observed in higher w/c ratio samples while lower i_{corr} value in lower w/c ratios. However, the corrosion current density values of higher w/c ratio became lower after 50 months. In specific, after 50 months, the samples with the lower w/c ratio becomes more active as indicated by higher i_{corr} values. For the intial time periods, most samples are in the passive condition ($i_{corr} < 0.1$ μA/cm^2), and then corrosion activity becomes more active as indicated by an increase of i_{corr} after 10 months, except for the samples with the lower two w/c ratios as they shows extended passive conditions until 20 months for each 1-day-cured and 7-day-cured samples. After 20 months, a trend of increasing corrosion rate was observed, especially the corrosion rates for all 1-day-cured samples were high ($i_{corr} > 1$ μA/cm^2). Similarly, all these behaviors are also observed for samples cured for 7 days (Fig. 2). No significant effects between 1 and 7 days of curing on corrosion behavior were observed. The corrosion resistant was controled by the w/c ratio. The results may indicate that the impacts of w/c on the corrosion process is more siginicant compare to those of the concrete curing time. Further observation on various curing time will improve the understanding of this parameter. Large uncertainties were observed during the test.

Probabilistic modeling was used to quatify the uncertianties inherent in the corrosion proces of concrete materials including environmental and material condition. It is well-known that large uncertainties exists in the concrete materials, environmental conditions, and the corrosion process. The impact of the each uncertainties hinders the prediciton of the reliability of RC structures. This research utilizes the probabilistic methods to identify and predict the uncertainties involved in the system, and allows to provides the reliability prediction. Bayesian methodology will be applied for the evidence-based model using the experimental data. The impacts of each parameters including material properties, environmental conditions, and the structural geometries will be invetigated considering the uncertainties within the system.

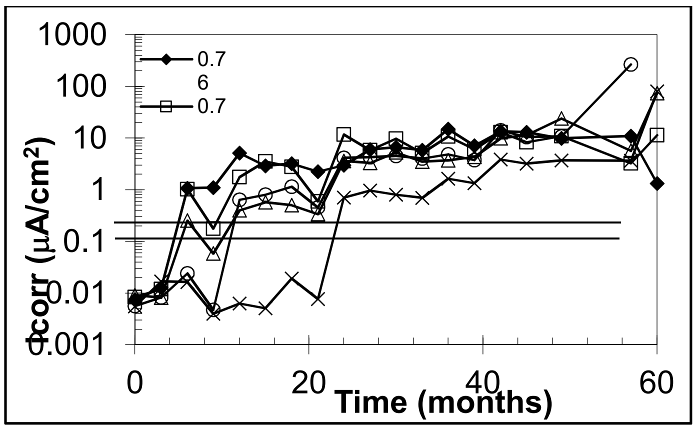

Figure 1. i_{corr} evolution of 1-day-cured samples over time with various w/c ratios.

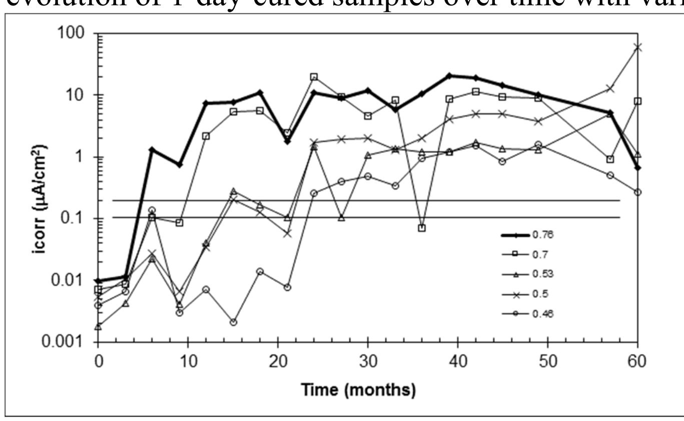

Figure 2. i_{corr} evolution of 7-days-cured samples over time with various w/c ratios.

CONCLUSIONS

No significant impacts of the concrete curing time (1 and 7 days) on the short-term corrosion behaviors were observed. Rather, the corrosion behaviors were controlled by the w/c ratio. However, the large uncertainties during the corrosion process hinders the proper analyses of the impacts. The probabilistic modeling will improve the understanding of the parameter sensitivities and help identifying the significant parameters. The long-term samples will be used to calibrate the two different approaches for corrosion based reliability model. And the short-term samples will be used to increase the robustness of the model as the increased number of parameters could be used for robust reliability and integrity modeling. The project includes the structural aspects of the RC components by using load data from the literature. Additionally, the project will also establish monitoring techniques to obtain the real-time data for the components of reinforced concrete bridges.

REFERENCES

P. Castro-Borges, L. Veleva, M- Balancán –Zapata, J. M. Mendoza-Rangel, L. A. Juárez, “Effect of environmental changes on chemical and electrochemical parameters in reinforced concrete. The case of a tropical marine atmosphere”, Int J Electrochem Sci, Vol 8, Mayo 2013, pp. 6204-6211 , ISSN 1452-3981, FI JCR 3.7 (2011)

P. Castro-Borges, M. Balancán Zapata, A. López González, “Analysis of tools to evaluate chloride threshold for corrosion onset of reinforced concrete in tropical marine environment of Yucatán, México”, Journal of Chemistry, Vol 2013, Article ID 208619, 8 p, 2013, FI JCR 0.5 en 2011.

K. Tuutti, “Corrosion of steel in concrete,” Research Report 4, CIB, Stockholm, Sweden, 1982.

High School Students Building and Using Sensors Towards Smart Management of Transportation Systems

Fernando Moreu[1], Christopher Lippitt[2], Rhytham Soni[3], Ali Ozdagli[4], Bideng Liu[5], Xiaomeng Li[3], Emmanuel Ayorinde[6], and Su Zhang[7]

[1]Assistant Professor, Department of Civil Engineering, University of New Mexico
[2]Associate Professor, Department of Geography and Environmental Studies, University of New Mexico
[3]GRA, Department of Civil Engineering, University of New Mexico
[4]Post-doc Fellow, Department of Civil Engineering, University of New Mexico
[5]Visiting Professor, Department of Civil Engineering, University of New Mexico
[6]Undergraduate Research Assistant, Department of Mechanical Engineering, University of New Mexico
[7]Senior Research Engineer, Earth Data Analysis Center, University of New Mexico

INTRODUCTION

The transportation infrastructure in United States has grown rapidly in the recent years, with huge investments being made for its future development and maintenance works *(1)*. The current America's infrastructure report card scores a D+, which shows a massive need of improvement and subsistence of the existing infrastructure *(2)*. However, the U.S. is facing a shortage of skilled transportation engineers. Therefore, there is an immense demand for training future transportation engineers in the U. S. *(3)*. There are many ongoing researches in the field of smart technologies in the development and maintenance of the transportation systems *(4)*.

Civil infrastructure is critical to any country's economy *(5)*. Infrastructure assets are expensive to maintain as they have long service life *(6)*. As time passes, the performance of infrastructure assets deteriorates *(7)*. Currently, there is a vast infrastructure investment gap in the United States *(8)*, which requires a pragmatic use of the investment on infrastructure. Using low cost sensors for monitoring structures can benefit the decisions on the distribution of limited resources for maintenance and construction projects, and ultimately, improve the U.S. economy *(9)*. UNM Summer Transportation Institute organized a series of workshops for the high school students in summer 2017. One of the workshops is the Smart Transportation Systems that was focused to encourage students from high schools to seek a career in Transportation in University. In the educational program, Arduino Microcontrollers coupled with an accelerometer were used as a sensing tool to measure vibrations to monitor the Structure. The current traditional sensors used for dynamic health monitoring costs around 60 times more than the Arduino microcontroller boards *(10),* which shows the economic potential of using the low-cost sensors.

METHODOLOGY

Hardware of Arduino

Arduino is an open-source electronic prototyping platform that enables users to create interactive electronic objects. It consists of a physical board where all the connections of the accelerometer and the Arduino microcontroller is created using the header pins and the jumper cables. Arduino Integrated Development Environment (IDE) can be used to design and upload a program that gives acceleration values as its output data using a computer code used for Arduino programming *(11)*.

Accelerometer MMA 8452Q

Accelerometers are devices that measure accelerations, (i.e. the rate of change of velocity of an object). They can measure both static forces (e.g., gravity) and the dynamic forces (e.g., vibrations in a structure). Accelerometers either consists of capacitive plates internally connected to a miniscule spring or piezoelectric materials. As the plates move internally, they develop a capacitance between them due to the sensing of accelerations. These changes in the capacitance are used to measure the accelerations. For piezoelectric materials, the mechanical stresses developed due to change in accelerations or gravity or any movement of the sensor is converted into electrical energy to determine the accelerations *(12)*. The parts of the chip, that are used to connect with the Arduino circuit board. The accelerometer MMA 8452Q can be connected to the Arduino circuit using either a breadboard or prototype shield (*13*). Arduino IDE is a software that Arduino uses, where we can write programs or codes to upload on the Arduino's microcontroller board to acquire the data used for post processing in SHM (14). Figure 1 shows the setup of the Arduino with the accelerometer in a casing that can be applied on the structure for measuring accelerations.

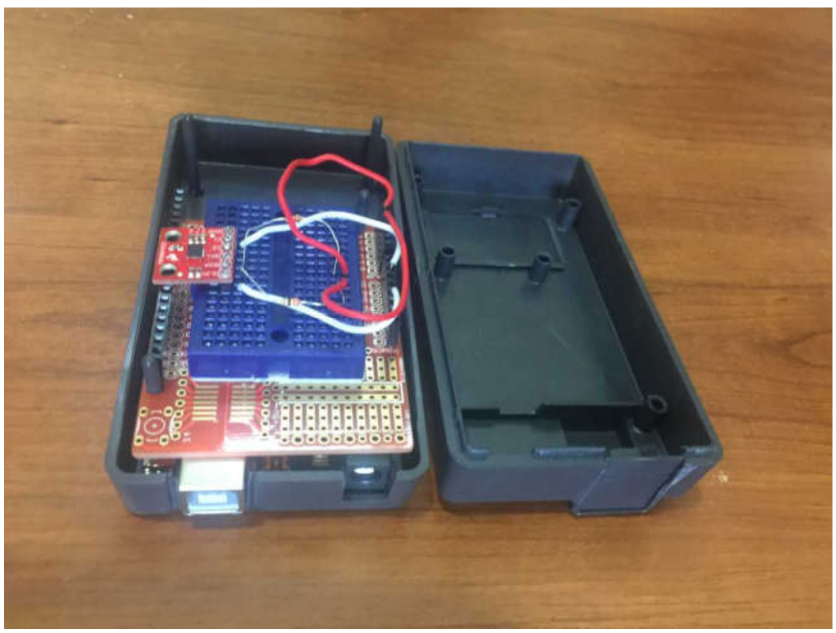

Figure 1 Arduino prototype sensor.

Program

Day 1

On day 1, there were brief seminars on various topics related to smart transportation systems by different presenters from the professionals in the industry and academics.

Smart Cities: maintenance and transit

This presentation was provided by Philo Shelton, who is the director of the Los Alamos County Engineering. He discussed the technology on Automatic Vehicle Location (AVL) systems and how the data obtained is used to manage bus schedules, collect ridership data, miles traveled and various applications of these data. These data can be used to assist a transit dispatcher to connect buses with customers, or real-time arrival prediction models that use the data to develop real time arrival schedule for their bus route. This is then transmitted over a mobile application where the customer can receive these real-time predictions at their transit stop.

a.2 Smart Inspections

This presentation was provided by Bideng Liu. He talked about the monitoring of structures from time to time, proper maintenance, and possible measures that should be taken to prevent catastrophic failure of the structure. He explains the importance of smart inspections especially in regions highly susceptible to Earthquakes. He explains the importance of smart inspections especially in regions highly susceptible to earthquakes. He describes the current methods employed in today's world and what future technologies will be involved in these methods.

Remote Sensing and Drones

This presentation was provided by Dr. Su Zhang. He presented the use of drones for remotely sensing the damages of the critical infrastructure for post disaster response. This technology can be highly useful where traditional data acquisition systems cannot be employed due to limited accessibility in a post disaster scenario. The drones with a consumer-level camera can be to detect fine-scale damages to transportation infrastructure in a safe and rapid manner.

Prestressed Concrete

This presentation was provided by Dr. Islam Mantawy, who is a visiting faculty at UNM for prestressed concrete. He explains what prestressed concrete is, how the concept of pre-stressing steel was developed basic understanding of the subject. The use of prestressed concrete in transportation structures was also discussed. The use of high tensioned and low-relaxation cables in concrete beams that provide pre-stressing effect to carry the load on the beam was discussed.

Figure 2 Mentors supervising the high school students.

Day 2

On day 2, the high school students were provided with all the parts and tools to build their own Arduino sensors with the assistance of the mentors and step by step guidance. They were supervised by the mentors to follow the procedures to build the Arduino sensor. The construction of the sensor involves making connections between the accelerometer chip and the Arduino board using prototype shield and jumper wires as explained earlier. Figure 2 shows the high school students building their own sensors by following the instructions given by one of their mentors, while other mentors supervise the students building the sensors to help them while they build it.

FINDINGS

After building their self-built Arduino sensors, the high school students tested their setup successfully with the Arduino IDE software. Subsequently, they tested their sensors at the Tramway to Sandia Peak to monitor the Structural behavior of the tramway car. At the tramway, the high school students attended a tour into the operating room to watch how the tramway car is operated. They learned the speed at which the tramway car runs while going upwards and while going downwards, the maximum overturning force of pylons, that must be kept under control always. After knowing the interesting facts and the technical background of tramway, the high school students perform the experiment on the tramway car with their self-built Arduino sensors.

The mentors instructed the high school students how to perform their experiment. The students placed their sensors on the floor of the tramway car to enable the capture of the movements of the whole car in all the directions, including longitudinal direction (the direction the Tramway car moves forward, the transverse direction (the direction perpendicular to the longitudinal direction), and the gravity direction, (the vertical direction). There are 2 pylons along the path of the tramway car from the foothill to the peak. These were the critical locations as when the tramway car passes the pylon, it creates oscillations of the tramway car. The students collected the data along the journey and especially when the tramway car passes the Pylon to compare their results. The vibration is little until the tramway car passed the pylon whereto the speed of the tramway car was reduced to control the dynamic load that could develop on the pylon. The tramway car developed oscillations on the sideways which could be felt or sensed. The data was acquired during the entire journey in the Sandia Peak. After the onward journey to the top of the Sandia Peak was completed, the collected data were processed and analyzed. By the end of the trip, the students were able to interpret the results themselves. The data in the tramway car was collected via the Arduino IDE 1.8.3 software and then visualized using the Fast Fourier Transformation (FFT) in MATLAB. The FFT is used to convert any time history data into Frequency Domain analysis. The tramway car while passing the pylon was swaying around 2 to 4 times every second in both longitudinal and the transverse directions (*15*).

CONCLUSIONS AND FUTURE WORK

This project was intended to develop high school students' interest in building low-cost sensors for SHM. This project has successfully motivated high schoolers. The workshop organized by UNM Summer Transportation Institute have broadened their perception about the engineering discipline, while the tramway field experiment has guided them in expanding their curiosity about pursuing a career in science and engineering. Such programs can be repeated to yield Future Transportation Engineers for the United States *(16)*.

REFERENCES

1. 2013-AAR_spending-Graphic-Fact-Sheet.Pdf. https://www.aar.org/Fact%20Sheets/Safety/2013-AAR_spending-graphic-fact-sheet.pdf. Accessed Jul. 23, 2017.

2. ASCE's 2017 Infrastructure Report Card | GPA: D+. *ASCE's 2017 Infrastructure Report Card*. http://www.infrastructurereportcard.org.
3. Cronin, B. E. *Attracting, Recruiting, and Retaining Skilled Staff for Transportation System Operations and Management*. Transportation Research Board, 2012.
4. Recent-R-D-Activities-on-Structural-Health-Monitoring-in-Korea.Pdf. https://www.researchgate.net/profile/Jeong-Tae_Kim/publication/301623488_Recent_RD_activities_on_structural_health_monitoring_in_Korea/links/589072abaca272bc14be3af8/Recent-R-D-activities-on-structural-health-monitoring-in-Korea.pdf. Accessed Jul. 23, 2017.
5. Economic Impact. ASCE's 2017 Infrastructure Report Card.
6. Ang, A. H.-S., D. M. Frangopol, and H.-N. Cho. *Life-Cycle Cost and Performance of Civil Infrastructure Systems*. Routledge, 2007.
7. *Read "Accelerated Aging of Materials and Structures: The Effects of Long-Term Elevated-Temperature Exposure" at NAP.Edu*.
8. ASCE-Failure-to-Act-2016-FINAL.Pdf. https://www.infrastructurereportcard.org/wp-content/uploads/2016/10/ASCE-Failure-to-Act-2016-FINAL.pdf. Accessed Jul. 25, 2017.
9. Building Smart Infrastructure Sensors. https://phys.org/news/2016-09-smart-infrastructure-sensors.html.
10. Application of Low-Cost Sensors for Estimation of Reference-Free Displacements Under Dynamic Loading for Railroad Bridges Safety. *ResearchGate*. https://www.researchgate.net/publication/311169069_Application_of_Low-Cost_Sensors_for_Estimation_of_Reference-Free_Displacements_Under_Dynamic_Loading_for_Railroad_Bridges_Safety.
11. What Is an Arduino? - Learn.Sparkfun.Com. https://learn.sparkfun.com/tutorials/what-is-an-arduino. Accessed Jul. 20, 2017.
12. Piezoelectric Accelerometer - Wikipedia. https://en.wikipedia.org/wiki/Piezoelectric_accelerometer. Accessed Jul. 23, 2017.
13. Fritzing. http://fritzing.org/.
14. Arduino - Environment. https://www.arduino.cc/en/Guide/Environment. Accessed Jul. 23, 2017.
15. StreamGate.Pdf. http://digitool.library.mcgill.ca/webclient/StreamGate?folder_id=0&dvs=1500766271165~192. Accessed Jul. 23, 2017.
16. P.e, S. S. N., and K. F. Boakye. An Overview and Preliminary Assessment of a Summer Transportation Engineering Education Program (STEEP) for Ninth Graders. Presented at the 2016 ASEE Annual Conference & Exposition, 2016.

Development of A Thermal Energy Harvester for Powering Structural health Monitoring Systems in Remote Areas

Utpal Datta[1], Andrew Ortega[1], Samer Dessouky[2] and A. T. Papagiannakis[2] and Aydin Karsilayan[3]

[1]Graduate Student, University of Texas at San Antonio
[2]Professor, Department of Civil and Environmental Engineering, University of Texas at San Antonio
[3]Professor, Department of Electrical Engineering Texas A&M University

INTRODUCTION

Sustainable source of energy is one of the great challenges in generating clean power. There are several energy resources available for this purpose, such as photovoltaic, wind and geothermal. An emerging technology for sustainable energy harvesting is thermoelectricity, whereby temperature gradients in a structure are used to directly power thermoelectric generators (TEGs). For example, in South Texas, the asphalt pavement surface temperature in the summer is as high as 55°C due to solar radiation while Soil temperatures below the pavement, are roughly constant (i.e., 27°C to 33°C) at relatively shallow depths (150 mm). In such cases, there is around 20ºC of thermal gradient available throughout most of the year. This thermal gradient can be used to drive TEG (typically 5mm in thickness) to produce electricity. This study describes the development of prototype using TEG to harvest this thermal energy and convert it into electric power. The objective of this study is to design a prototype that optimizes the temperature gradients available for thermoelectric power generation and evaluate the prototype under laboratory and field conditions.

METHODOLOGY

A thermal energy harvesting prototype was assembled to collect the wasted heat from pavement surface and transfer it to a thermoelectric generator module (TEG) embedded in nearby soil. The thermoelectric energy harvesting prototype consists of four basic components (Figure 1):

- A thermal isolated copper plate (Z-shape and L-shape)
- A thin square TEG sandwiched between the copper plate and bottom heat sink,
- A heat sink connected to the bottom of the TEG.

The copper plate allows transferring the heat from top of pavement surface down to the top of TEG module, while the heat sink provides a relatively constant temperature over time, while dissipating the heat that gets conveyed across the TEG. The prototype efficiency depends largely on the performance of the thermal harvester. The more temperature gradient (ΔT) it ensures; the more output electrical power is produced. To maximize the prototype efficiency several models of thermal harvester were analyzed through finite element (FE) analysis. Finally, from the output of the FE an optimum model was selected for laboratory testing. Two heat conductors metal plates were examined, the Z-shape and L-shape (Figure 1)

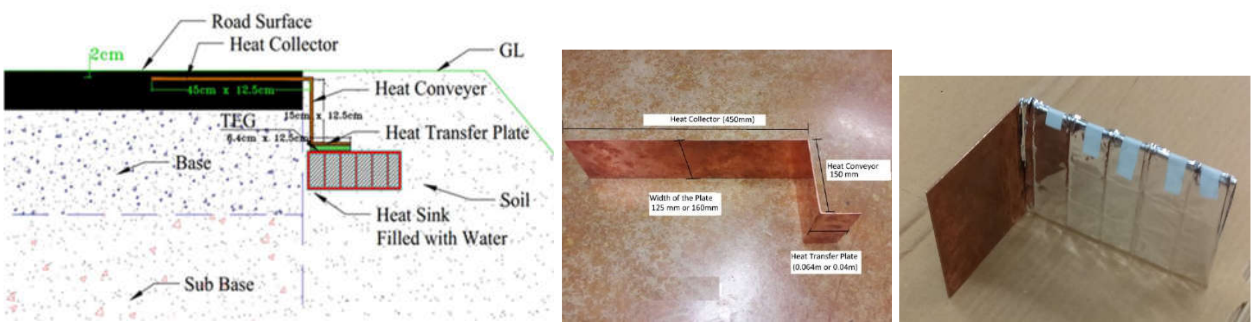

Figure 1. Schematic of the harvester prototype (left), Z-shape heat conductor (middle) and isolated L-shape heat conductor (right)

The TEG produces power in response to temperature gradients at both of its top and bottom surfaces, referred to as the "Seebeck effect". There are four engineering parameters which define the performance of a TEG:

1) ΔT: Temperature gradient (difference), between the hot and cold side of the TEG;
2) V: Voltage generated by TEG due to temperature gradient;
3) I_L: electric current drawn by the TEG and
4) P_L: output power produced by the TEG.

The generated voltage is given by:

$$V = N(0.0002 \times 1.004^{\Delta T}) \times \Delta T \tag{1}$$

where N is the total number of thermoelectric elements (e.g. 574 for a 64mm x64mm module or 254 for a 40mmx40mm module; twice the number of thermocouples), and $\Delta T = T_{Hot} - T_{Cold}$, where T_{Hot} is the heat flux temperature of the hot side and T_{Cold} is the cold side surface temperature *(7)*. To maximize the output voltage and power, an external resistant is used with the TEG. When an external resistance, R_L, is applied to the TEG, the output voltage that appears across that load, VL, is less than V and is a function of the external and the internal resistance R_{int} of the TEG. The output voltage, current and power are given by:

$$V_L = \frac{V\,R_L}{(R_L + R_{int})} \tag{2}$$

$$I_L = \frac{V_L}{R_L} \tag{3}$$

$$P_L = V_L I_L \tag{4}$$

FINDINGS

The aim of the FE analysis, conducted using ABAQUS, was to study the optimum design materials and dimensions of the thermoelectric prototype. In order to get the maximum possible temperature gradient and output power from the prototype, some key parameters were examined, i.e., effective materials for the harvester components, design depth of the TEG, dimensions of the heat transfer plate as well as number of TEG units to be used. Prior to the FE analysis, the pavement temperature profile was analyzed by TEMPS software to numerically quantify the thermal gradient available in pavement to effectively operate an energy harvesting prototype. For this analysis, weather data in South Texas used from LTPP program. The FE model in Figure 6b consists of a Z-shape metal plate with thermal boundary conditions of 50°C at top left side (e.g., pavement). A one-dimensional steady state flow analysis was conducted to determine the temperature at the bottom right side (soil) of the model. The FE analysis indicates that the thermal gradient (ΔT) for 50mm depth is 7^0C. At depth 180mm the gradient reaches its maximum value (ΔT=13^0C) and with further increasing of depth the gradient decreases (at 225mm ΔT= 8°C and at 300mm ΔT=6°C). Hence the optimum design depth is suggested at 180mm (Figure 2).

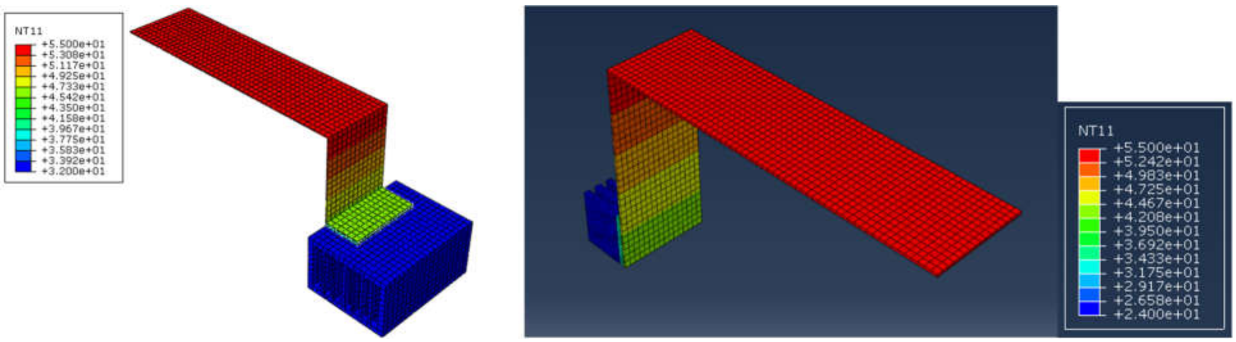

Figure 2: Finite Element analysis results for Z-shape and L-shape prototypes.

The laboratory testing involved the evaluation of the several prototypes represented by a heated water tub. The soil condition temperature was controlled by the heat sink filled with water at room temperature. The heat conducting plate was fully inserted into the heated water tub. Temperature data was collected by the four-channel data logger and the output voltage, current and power were measured by a power meter. The lab tests were conducted at three water tub temperatures of 45, 50 and 55°C and heat sink temperature (represents soil temperature) ranges from 26-29°C. Upon reaching thermal stabilization in the prototype, data showed that the imposed temperature gradient was in the range of 23-33°C and the output (recoverable) temperature gradient for the two-TEG prototype was measured to be between 10-14°C, yielding a power output of 15-23mWatt (Figure 3).

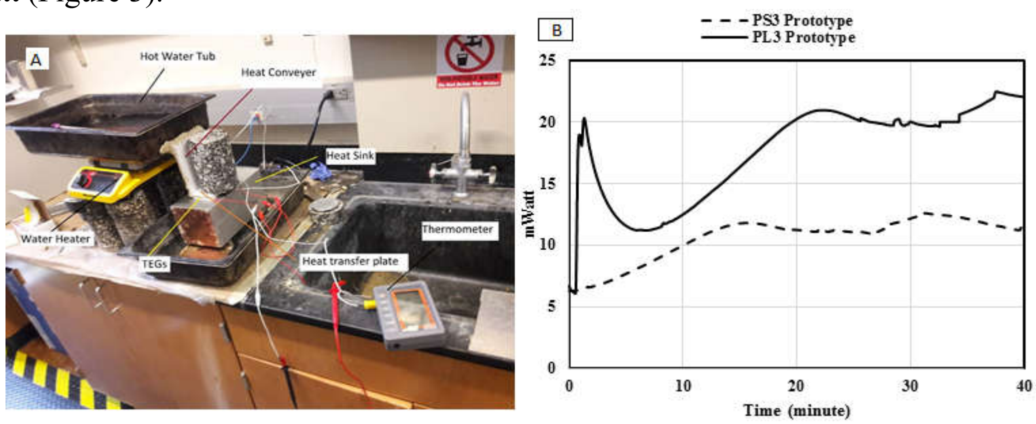

Figure 3. Laboratory setup and LED light demo from the prototype.

CONCLUSION

The prototype is capable of generating an average of 10 mWatt continuously over a period of 8 hours a day. The produced power may look very small for conventional electronic devices.

But it can be used for powering pavement health monitoring (strain gauge, pressure sensors etc. which consumes power as low as 3mW (2)) and roadway communication devices especially in off-grid areas where it will cost millions of dollar to power these devices from on-grid electricity. It can be an alternate source of self-powered electronic road signs or markings and street illuminating with LED (each with 1mW for eight hours from a single day power accumulation) in remote areas. It is worth mentioned that the developed thermal energy harvesting prototypes are not obtrusive and they do not interfere with the traffic.

Use of Rice Hull Ash (RHA) As A Sustainable Source of Construction Materials

Kazi Tamzidul Islam[1], Mohammad Badrul Ahsan[2], and Zahid Hossain[3]

[1]GRA, Department of Civil Engineering, Arkansas State University
[2]Graduate Transportation Associate, Tennessee Department of Transportation (TDOT)
[3]Associate Professor, Department of Civil Engineering, Arkansas State University

INTRODUCTION

With the rapid increase of urbanization in all over the world, construction projects are highest in number. Each year the need for construction materials has increased drastically. To fill up the ongoing need the natural sources of construction materials are facing a hard time. These all circumstances concluded the modern technology to bring up with modern and sustainable means of construction. Different cost-effective technologies, blended Portland cement, and modified concrete have been used to reduce the impact on the environment. Rice husk is a by-product of the rice industry, which is obtained during the process of milling rice. In 2009, about 678 million tons of rice was produced in the whole world [1]. Typically, 20% of total volume of the paddy becomes rice husk (RH) [1]. From the industrial and agricultural point of view, rice husk is considered as a waste material. However, because of its high energy capacity (3200 kcal/kg), a significant amount of rice husk has been used as a biofuel [2, 3]. After the incineration process, about 20% of rice husk's weight remains as rice husk ash (RHA) which is considered as a waste material [4, 5]. RHA is considered as a mineral admixture for cement and cementitious products [4, 6]. In addition, most of the properties and behavior of blended cementitious product vary with the source of RHA [5, 7]. It is reported that the minerals in RHA bring some favorable influences on the strength and durability of concrete [1]. The combustion process of RH produces a secondary Calcium-Silicate-Hydrate (C-S-H) gel, which is responsible for the pozzolanic activity, and the particle sizes influence the physical activity of the hydration process [1].

This paper mainly investigates the use of RHA as a supplementary cementitious material in a proportion of ordinary Portland cement (OPC) to produce concrete. Different proportions of RHA have been used to study selected chemical, physical and strength properties of concrete. Three different sizes of RHA (RHA1: 600 µm, RHA2: 150 µm, and RHA3: 44 µm) were selected in this study. In addition, two different supplementary cementitious material (SCM) materials, namely Class C fly ash (CFA) and silica fume (SF), were also added to compare their performance properties with RHA-modified concrete. All types of RHA and SCM materials were added in a certain proportion with cement. Laboratory tests on fresh concrete as well as mechanical properties of hardened concrete were conducted. Alkali-silica reaction (ASR) and deicing chemicals tests on the concrete surface were conducted to find out the durability of modified concrete.

In the case of compressive strength, it was found that the smallest RHA (44 µm) showed the highest increase compared to the control sample. A similar trend was found for the tensile and flexural strengths. The coarser RHA were found to be ineffective in mitigating ASR expansion. On the other hand, finer RHA lessens the expansion. Even for the deicing durability test, finer RHA showed less deterioration compared to the control sample. Considering the significant changes in all the mechanical and other properties, 10% replacement level of RHA can be defined as the optimum level of utilization.

METHODOLOGY:

Throughout the experimental phase of this study, work RHA, CFA, and SF modified concrete were prepared and properties of modified concrete with different pozzolanic materials were compared. A selected mix design with same coarse aggregate (CA) and fine aggregate (FA) samples and Type-I cement were maintained throughout the study. All types of RHA (RHA-1, RHA-2, and RHA-3) and CFA, SF sample were collected from suppliers approved by the Arkansas Department of Transportation (ARDOT). According to AASHTO M 321-04 and ASTM C 618 specifications, the physical and chemical data of RHA, CFA, and SF were compared. ASTM standard sieves were used to determine the grain size of RHA. As the concrete strength is highly affected by the particle surface area, specific surface area (SSA) of RHA, CFA, and SF were determined by the BET (Brunauer, Emmett, and Teller) method which aims to follow the physical adsorption of gas molecules on a solid surface theory on measuring the specific surface area (SSA). Using nitrogen gas as adsorbate [8], the multi-point BET mode of a NOVA 2200e analyzer was used in the determination of SSA. At the beginning of concrete mix design, all physical properties of CA and FA were determined by using appropriate ASTM standards. Afterwards, fresh concrete properties such as slump (ASTM C143), unit weight (ASTM C127), air content (ASTM C128) were determined. Concrete cylinders and beams were cast according to ASTM C31 and ASTM C293 specification respectively. Concrete cylinder samples were tested under a compression machine according to ASTM C 39. Splitting tensile strength (ASTM C496), flexural strength (ASTM C293), modulus of elasticity and Poisson's ratio (ASTM C469) tests were performed on the hardened concrete. Mortar bars were prepared to conduct ASR test (ASTM C1567) and durability test under deicing chemicals (ASTM C672). Finally, Analysis of Variance (ANOVA) method was used to perform statistical analyses of the experimental data.

FINDINGS

From the measured BET data (SSA of RHA3 as 27.4 m^2/g, that of RHA2 as 29.1 m^2/g, and that of RHA3 as 30.4 m^2/g), it was found that finer RHA exhibits higher surface area. For Type-I OPC, CFA and SF the SSAs were measured as 47.178 m^2/g, 42.270 m^2/g, and 19.31 m^2/g, respectively. As particle size affects the pozzolanic activity, the development of strength properties of concrete is directly related to the particle size [9, 10]. In the measurement of workability of concrete, finer RHA modified concrete showed less slump value than the coarser RHA-modified concrete. So, finer RHA in concrete needs more water.

The compressive strength of concrete is being considered as the primary quality of concrete. From Figure 1, it is shown that RHA1 (600 µm) and RHA2 (150 µm) modified concrete showed less compressive strength at 28 days compare to the control sample. On the other hand, RHA3 (44 µm) modified concrete showing more compressive strength values compared to the control sample. Here 10% replacement of cement showed a greater increase in strength than 20% cement replacement. For the other two SCM materials, CFA and SF both showed higher compressive strength than the control sample.

Table 1 shows the bending resistance of modified concrete. The modified concrete sample followed a similar trend of the other parameters such as the compressive strength. RHA3 (44 µm) and CFA-modified concrete showed a significant increase in flexural strength compared to the control sample. On the other hand, SF (10%-3.45 MPa, 20%-2.69 MPa) showed less compressive strength than that of the control sample (4.17 MPa).

ASR data (Table 2) showed that RHA (600 µm) did not meet the ASTM specification. RHA (150 µm) was under the recommended of ASTM C1567 specification limit but it expands more than the control sample. On the contrary, RHA (44 μm) mortar bar expand less than the ASTM specification as well as the control sample. Both Class C fly ash (CFA) and silica fume (SF) mitigate mortar bar expansion in a similar way.

Figure 2 shows effects of deicing chemicals on mortar bars for 10 continuous freeze and thaw cycles. RHA1 (600 μm) showed severe surface damage, compare to that RHA2 (150 μm) showed moderate damage. RHA3 (44 μm), CFA and SF modified mortar bar showed the lowest damage among all samples.

Table 1: Flexural Strength of Modified Concrete.

Type of RHA/Fly Ash	Percentage of replacement	Measured in the Laboratory (MPa)	Estimated from ACI formula: $f_r=0.7\sqrt{f_c}$ (MPa)
Control	0%	4.17	3.74
RHA(600 μm)	10%	3.14	2.79
	20%	2.69	2.51
RHA(150 μm)	10%	3.62	2.97
	20%	2.79	2.55
RHA(44 μm)	10%	4.72	3.82
	20%	4.41	3.77
CFA	10%	5.03	3.93
	20%	4.76	3.87
SF	10%	3.45	4.29
	20%	2.69	4.22

Table 2: Effect of Alkali-silica Reaction on Mortar Bars.

Types of SCM	(%) Expansion			
	4 Days	8 Days	12 Days	14 Days
Control	0.0016	0.049	0.095	0.129
10%-600 RHA	0.0006	0.011	0.0228	0.024
20%-600 RHA	0.00012	0.0254	0.052	0.078
10%-150 RHA	0.08	0.1	0.13	0.18
20%-150 RHA	0.11	0.15	0.19	0.22
10%-44 RHA	0.1	0.13	0.19	0.26
20%-44 RHA	0.15	0.18	0.24	0.33
10%-CFA	0	0.001	0.00125	0.0018
20%-CFA	0	0.001	0.00155	0.0022
10%-SF	0.1247	0.1497	0.1500	0.1681
20%-SF	0.0447	0.0497	0.0514	0.0667

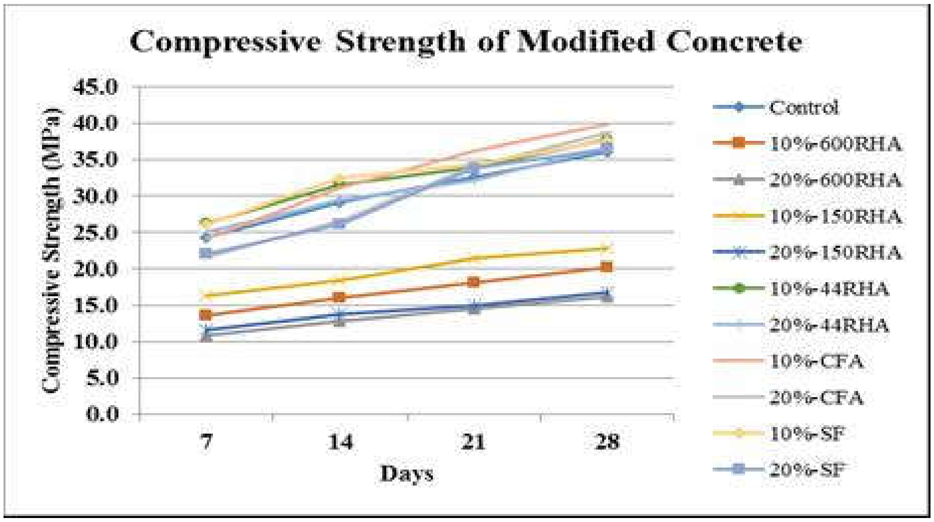

Figure 1: Effect of Different Cementitious Material in Concrete Strength.

Figure 2: Effect of deicing chemical before and after 10 freeze thaw cycles: (a) Control, (b) RHA (600 µm), (c) RHA (150 µm), (d) RHA (44 µm), e) CFA, an (d) SF.

CONCLUSION

In the process of finding out the alternative cementitious materials, RHA was incorporated with cement in producing concrete. To predict the behavior of RHA-modified concrete field, a number of physical, chemical and mechanical tests were performed. It has suspected that the amount of carbon present in the RHA hinders the process of getting strength of concrete and 10% replacement of finer RHA with cement increase the compressive strength. A similar trend was found for Class C Fly Ash (CFA) and silica fume (SF). Other mechanical properties such as flexural strength, modulus of elasticity, Poisson's ratio also get increment with 10% replacement of the finest RHA. From the durability test, it was also observed that finest RHA, CFA, and SF modified concretes are more durable than the ordinary concrete. After all the test data it can be concluded that fine RHA (44 μm), can be used to produce durable concrete. The results of this study are expected to help the concrete industry to apply it in the practical field.

REFERENCES

[1] Gemma Rodriguez de sensale, Antonio B.Ribeiro,Goncalves. Effect of rice-husk ash on durability of cementitious materials.Cement and Concrete Composites 32(9):718-725 ·October 2010

[2] Zerbino R, Giaccio G, Isaia GC. Concrete incorporating rick-husk ash without processing. Constr Build Mater 2011;25(1):371-8

[3] Gonvalves MRF, Bergmann CP. Thermal insulators made with rice husk ashes:production and correlation between properties and microstructure. Constr Build Mater 2007;21(12):2059-65

[4] P.K. Mehta, The chemistry and technology of cements made from rice husk ash, [in] Proceeding of UNIDO/ESCAP/RCTT Workshop on Rice Husk Ash Cement, Peshawar, Pakistan, Regional Centre for Technology Transfer, Banghalore, 1979, p.113.

[5] Malhotra VM, Mehta PK. Pozzolanic and cementitious materials. In:Advances in concrete technology, 1. Canada: Gordon and Breach Publ.;1996

[6] RILEM. Committee 73-SBC final report: siliceous by-products for use in concrete. Mater Struct 1988;21(121):69-80

[7] James J, Rao MS. Reactivity of rice husk ash. Cem Concr Res 1986;16:296-302

[8] Mohamed, R. M., Mkhalid, I. A., and Barakat, M. A. (2015). Rice husk ash as a renewable source for the production of zeolite NaY and its characterization. Arabian, Journal of Chemistry, 8(1), 48-53

[9] Cordeiro, G. C., Toledo Filho, R. D., Tavares, L. M., Fairbairn, E. D. M. R., & Hempel, S. (2011). Influence of particle size and specific surface area on the pozzolanic activity of residual rice husk ash. Cement and Concrete Composites, 33(5), 529-534.

[10] Givi, A. N., Rashid, S. A., Aziz, F. N. A., and Salleh, M. A. M. (2010). Contribution of rice husk ash to the properties of mortar and concrete: a review. Journal of American Science, 6(3), 157-165.

Low Fiber Content PVA-ECC for Transportation Infrastructure

Gabriel Arce[1], Hassan Noorvand[2], Marwa Hassan[3], and Tyson Rupnow[4]

[1]Post-Doctoral Associate, Department of Construction Management, Louisiana State University
[2]GRA, Department of Construction Management, Louisiana State University
[3]Professor, Department of Construction Management, Louisiana State University
[4]Associate Director, Louisiana Transportation and Research Center

INTRODUCTION

Concrete has proven itself through time as an outstanding construction material; yet, it is not elusive to well documented weaknesses. Concrete is brittle (approximately 0.01% strain capacity in tension) and possess a low tensile strength (between 1/9 to 1/14 of its compressive strength), which allow for the occurrence and propagation of cracks (due to load or changing environmental conditions) *(1)*. Moreover, the occurrence of cracks in concrete is highly related to deterioration and failure of concrete pavements and overlay systems; hence, improvements of these properties are of particular interest for the transportation sector.

Adding fibers to concrete is a well-established practice to mitigate the brittle behavior of concrete by limiting crack growth and propagation. Yet, traditional fiber reinforced concrete (FRC) produces rather marginal improvements in ductility and tensile strength. Furthermore, FRC continues to exhibit a strain-softening phenomenon after first cracking (single localized crack growth associated with a decrease in load carrying capacity) under tensile or flexural stresses. For these reasons, high performance fiber reinforced cementitious composites (HPFRCC) have been introduced as a superior alternative to mitigate concrete brittleness and its weak behavior under tensile stresses. In contrast to FRC, HPRFRCC exhibit a strain-hardening performance after first cracking under tensile or flexural loading. Strain-hardening occurs due to inelastic deformation of the composite through the formation of multiple micro-cracks *(2)*.

ECC is a relatively new class of high performance fiber reinforced cementitious composites (HPFRCC), which are designed and optimized based on micromechanical principles. In contrast to traditional HPFRCC, ECC can exhibit a high tensile ductility of 100 to 500 times that of concrete (1 to 5% strain capacity in tension) at low fiber contents (usually between 1 to 2% volume fraction) *(2–5)*. This makes ECC practical to be implemented in the field using existing equipment and techniques as well as significantly more cost-effective than early versions of HPFRCC. Moreover, ECC also exhibit enhanced tensile and flexural strength as well as a superior performance against major type of concrete deterioration including corrosion, freeze-thaw, sulfate attack, and alkali silica reaction *(4, 6, 7)*. In addition, ECC possess well documented self-healing characteristics because of the micro-size cracks that can take place in these materials (usually less than 60 μm), in contrast to macro-cracks produced in traditional concrete, which allows for autogenous healing mechanisms of cementitious materials to be effective *(8)*.

Due to its superior mechanical properties, ECC is a promising material for the transportation sector as it could be successfully implemented for repair and new construction of pavements. For instance, its high tensile ductility can allow for reflective cracking suppression through a crack arrest mechanism in overlay applications *(9)*. Moreover, the removal of joints in rigid pavements and overlay system is also possible due to the enhanced ductility of ECC, eliminating one important deterioration mechanism in concrete pavements *(10)*. Furthermore, ECCs exhibit a superior fatigue resistance and flexural strength that can allow for a significant enhancement of transportation infrastructure durability *(11)*.

The objective of this study is to investigate the influence of material selection (aggregate type) and mix proportioning (different levels of cement replacement with fly ash) on the mechanical properties of PVA-ECC with low fiber content (1.75% volume fraction). High replacement of cement with fly ash, utilization of coarse sand, partial replacement of sand with crumb rubber and low fiber content were investigated for cost-effectiveness, practicality, and greenness of the composite.

METHODOLOGY

Test Materials

Locally available materials where utilized to produce ECC: Ordinary Portland Cement (OPC) Type I, Class F Fly Ash (FA), crumb rubber with maximum particle size of 177 µm, and coarse and fine river sands with a maximum particle size of 1.18 mm (1.96 fineness modulus) and 0.6 mm (1.75 fineness modulus), respectively. Chemical compositions of cement and fly ash are presented in Table 1. Fibers utilized throughout the investigation were REC15 polyvinyl alcohol (PVA) fibers supplied by Kuraray Co. Ltd in Japan. Table 2 present the properties of the PVA fibers utilized. Moreover, a polycarboxylate-based high range water reducer (HRWR) was utilized as admixture.

Table 1 Chemical Composition of Cement and Fly Ash (Weight %)

Material	SiO_2	Al_2O_3	Fe_2O_3	CaO	MgO	SO_3	K_2O	TiO_2	Na_2O
Cement	19.24	4.75	3.35	65.81	2.20	3.61	0.54	0.21	-
Fly ash	62.08	18.56	8.22	5.69	1.69	0.37	1.42	1.03	0.35

Table 2 PVA Fibers Properties

Fiber type	Length (mm)	Diameter (µm)	Young's Modulus (GPa)	Tensile Strength (MPa)	Elongation (%)
REC 15	12	39	40	1456	5.7

Table 3 ECC Mix Design Proportions by Weight

Mix ID	Proportions by Weight									
	Cement	Fly Ash	Water	Sand	HRWR[1] (%)	W/B	S/B	FA/C	Fibers (Vol%)	CR (%)[2]
M-1.6	1	1.6	0.71	0.94	0.32	0.27	0.36	1.6	1.75	0
M-2.2	1	2.2	0.87	1.16	0.29	0.27	0.36	2.2	1.75	0
M-3.0	1	3.0	1.09	1.45	0.23	0.27	0.36	3.0	1.75	0
MR-1.2	1	1.2	0.60	0.80	0.32	0.27	0.36	1.2	1.75	20
MR-1.6	1	1.6	0.71	0.94	0.29	0.27	0.36	1.6	1.75	20
MR-2.2	1	2.2	0.87	1.16	0.27	0.27	0.36	2.2	1.75	20

[1] %HRWR dosage by weight of cement [2] % of sand replacement with crumb rubber by volume

PVA-ECC Specimen Preparation

Three cylindrical and prismatic specimens were cast and demolded after 24 hours, and subsequently allowed to cure for 28 days in a moist room (23 ± 2 °C, > 95% Relative Humidity [RH]) according to ASTM C192 *(12)*.Two experimental series of ECC specimens were produced, regular ECC and crumb rubber ECC, where three levels of cement replacement with Fly Ash (by weight) were evaluated for each experimental series (62%. 69% and 75% for regular ECC series and 55%, 62%, 69% for crumb rubber ECC series). In crumb rubber ECC experimental series a

20% of sand was replaced with crumb rubber (by volume). Furthermore, water to binder ratio (W/B) as well sand to binder ratio (S/B) were kept constant throughout this investigation for comparative purposes. The details of the different mix proportions are summarized in Table 3.

For the mixing procedure, dry powder components (cement and fly ash) were mixed in a Hobart mixer for 3 minutes. Then, sand and crumb rubber (crumb rubber experimental series) were combined with the dry powders and mixed for three additional minutes. Subsequently, water and HRWR were added and mixed for three more minutes. Finally, PVA fibers were introduced slowly to the wet mix (for 3 min) and mixed for an additional 7 minutes.

ECC Testing

Compressive strength of ECC mix designs was evaluated according to ASTM C 39 on 101.6 x 203.2 mm (4 in x 8 in) cylindrical specimens *(13)*. Moreover, third-point bending test according to ASTM C 1609 was performed to assess flexural performance of ECC mixtures on 101.6 x 101.6 x 355.6 mm (4 x 4 x 14 in) prismatic specimens *(14)*.

FINDINGS

Compressive Strength

As shown in Figure 1 Increasing contents of cement replacement with fly ash produced lower compressive strengths in ECC materials studied, proportionally. This behavior was attributed to the high contents of fly ash and low water to binder ratio (W/B=0.27) utilized in ECC mixes which likely limited the secondary hydration reaction of fly ash making it to partially act as a filler *(15)*. Moreover, another important factor influencing compressive strength of ECC was the addition of crumb rubber. Due to the defect-like behavior of crumb rubber in the cementitious matrix its implementation in ECC mixes produced a significant reduction in compressive strength. Furthermore, while less impactful than fly ash increments and crumb rubber addition, the fine sand utilized in this study produced lower compressive strengths than coarse sand.

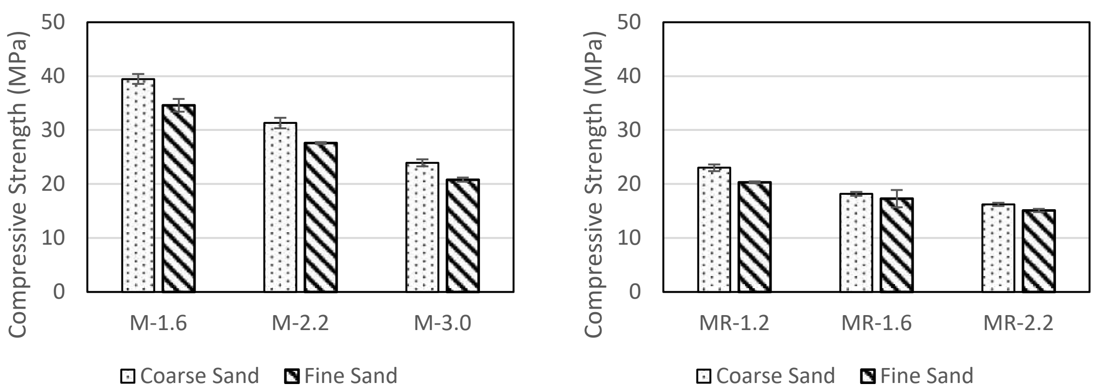

(a) **(b)**

Figure 1 Compressive Strength (a) Regular ECC (b) Crumb Rubber ECC

Flexural Performance

As it can be observed in Figures 2 and 3, all mixes evaluated in this study presented significant amounts of deformation capacity typical of ECC materials. Yet, material selection (crumb rubber addition, as well as coarse and fine sand utilization) and mix proportioning (increasing contents of fly ash) had a profound impact in the ductility and strength of the composites (as shown in Figures 4 and 5).

Deformation capacity of ECC mixes was dramatically improved (up to 121%) by the implementation of crumb rubber. However, a moderate reduction in flexural strength (up to 28%) was also reported. In addition, ductility of ECC mixes was also substantially improved (up to 152%) by increasing contents of fly ash (except for M-3.0 compared to M-2.2 for fine sand specimens, yet not statistically significant). However, reductions in flexural strength of up to 26% were also noticed. For both, crumb rubber and fly ash, improvement in ductility are attributed to an increase in the complementary energy of the fiber bridging relation J'_b and a reduction in the crack tip toughness of the cementitious matrix J_{tip} produced by these materials (which increased $J'_b/\, J_{tip}$ strain hardening performance indicator) *(16)*. Moreover, strength reduction was linked to a decrease in the fiber bridging capacity σ_0 *(16)*. In addition, the utilization of different types of sands did also affect the flexural performance of ECC specimens; yet, to a lesser degree than crumb rubber and fly ash. Finer sand generally produced a reduction in flexural strength (except for MR-2.2 where coarse and fine sand produced equivalent flexural strengths) and an increase in ductility (except for M-3.0 and MR-1.2 were fine sand specimens exhibited slightly lower deflection at peak strength, yet not statistically significant). Increments in deformation capacity with finer sand were attributed to a better fiber dispersion allowed by fine aggregate particles as well as a reduction in the cementitious matrix crack tip toughness J_{tip} due to a lower aggregate interlock (leading to a larger $J'_b/\, J_{tip}$ performance index) *(17)*.

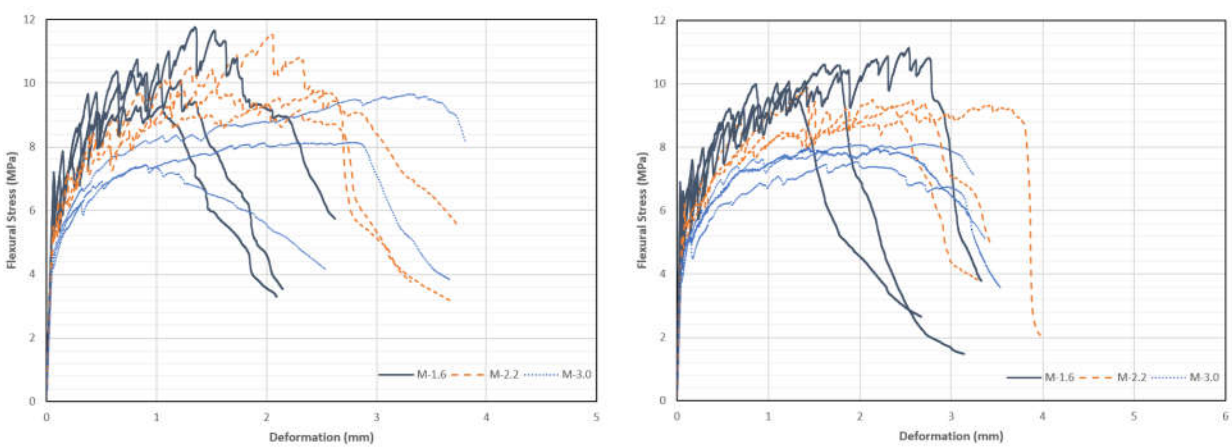

(a) (b)

Figure 2 Regular ECC Flexural Stress vs. Deformation Curves (Regular ECC series) (a) Coarse Sand (b) Fine Sand

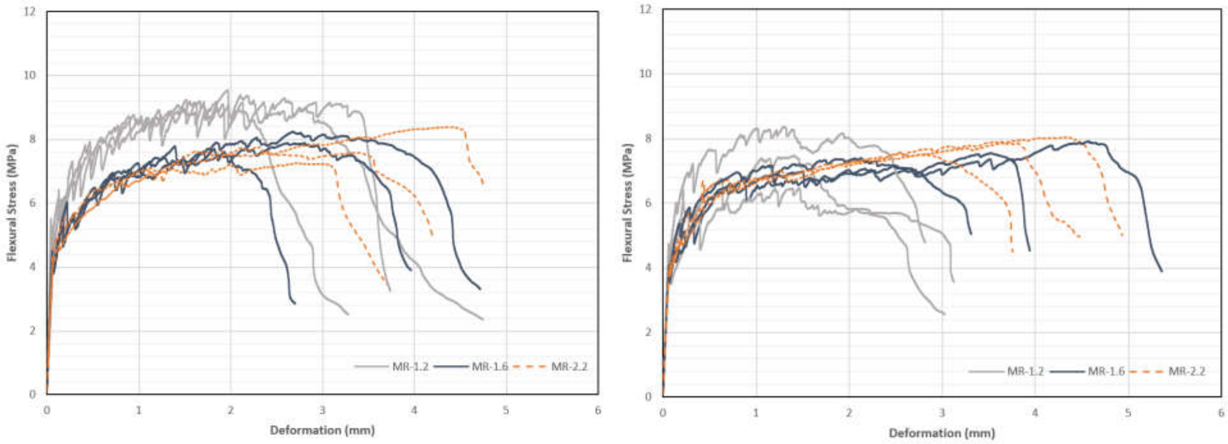

(a) (b)

Figure 3 Crumb Rubber ECC Flexural Stress vs. Deformation Curves (a) Coarse Sand (b) Fine Sand

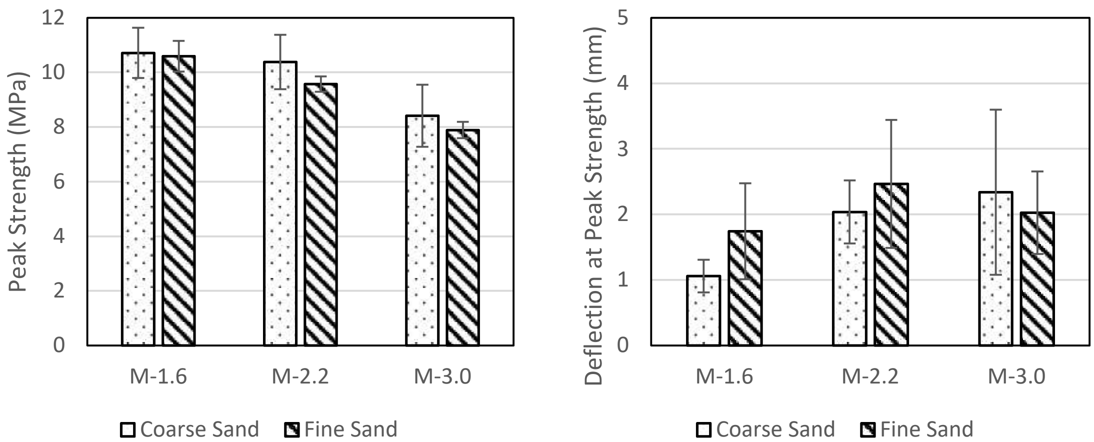

(a) (b)

Figure 4 Regular ECC Flexural Performance (a) Peak Strength (b) Deflection at Peak Strength

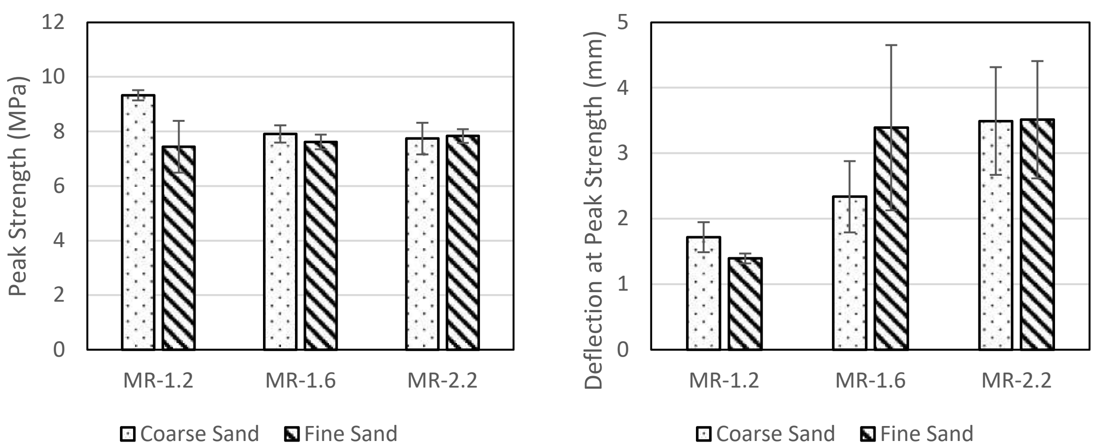

(a) (b)

Figure 5 Crumb Rubber ECC Flexural Performance (a) Peak Strength (b) Deflection at Peak Strength

CONCLUSIONS

The production of PVA-ECC materials with low fiber content (1.75% volume fraction) was successfully achieved for all mix designs presented in this study. However, future research should be directed in mitigating excessive compressive strength decrease due to crumb rubber addition (by the evaluation of different dosages of crumb rubber and mixture proportions). Furthermore, mechanical properties of low fiber content PVA-ECC should be evaluated at later ages than 28 days to guaranty that ductility is preserved in the long term due to the possibility of significant cementitious matrix strengthening (due to high contents of fly ash).

REFERENCES

1. Mindess, S., F. J. Young, and D. Darwin. *Concrete*. Prentice Hall, 2003.
2. Yang, E. Designing Added Functions in Engineered Cementitious Composites. 2008, p. 276.
3. Li, V. C. On engineered cementitious composites (ECC). A review of the material and its applications. *Journal of Advanced Concrete Technology*, Vol. 1, No. 3, 2003, pp. 215–230.
4. Li, V. C. Engineered Cementitious Composites (ECC) – Material , Structural , and Durability Performance. *Concrete Construction Engineering Handbook*, 2008, p. 78.
5. Fischer, G., and V. C. Li. Effect of fiber reinforcement on the response of structural members. *Engineering Fracture Mechanics*, Vol. 74, No. 1–2, 2007, pp. 258–272.
6. Sahmaran, M., and V. C. Li. Suppressing Alkali-Silica Expansion. *Concrete International*, No. May, 2016, pp. 47–52.
7. Liu, H., Q. Zhang, V. Li, H. Su, and C. Gu. Durability study on engineered cementitious composites (ECC) under sulfate and chloride environment. *Construction and Building Materials*, Vol. 133, 2017, pp. 171–181.
8. Şahmaran, M., G. Yildirim, R. Noori, E. Ozbay, and M. Lachemi. Repeatability and Pervasiveness of Self-Healing in Engineered Cementitious Composites. *ACI Materials Journal*, Vol. 112, No. 4, 2015, pp. 513–522.
9. Zhang, J., and V. C. Li. Monotonic and fatigue performance in bending of fiber-reinforced engineered cementitious composite in overlay system. *Cement and Concrete Research*, Vol. 32, No. 3, 2002, pp. 415–423.
10. Zhang, Z., Q. Zhang, S. Qian, and V. C. Li. Low E Modulus Early Strength Engineered Cementitious Composites Material. *Transportation Research Record: Journal of the Transportation Research Board*, Vol. 2481, 2015, pp. 41–47.
11. Zhang, Z., J. Hu, and H. Ma. Feasibility study of ECC with self-healing capacity applied on the long-span steel bridge deck overlay. *International Journal of Pavement Engineering*, Vol. 8436, No. September, 2017, pp. 1–10.
12. ASTM Standard C 192. *Standard Practice for Making and Curing Concrete Test Specimens in the Laboratory*. ASTM International, West Conshohocken, PA, 2002.
13. ASTM Standard C 39. *Standard Test Method for Compressive Strength of Cylindrical Concrete Specimens*. ASTM International, West Conshohocken, PA, 2003.
14. ASTM Standard C 1609. *Standard Test Method for Flexural Performance of Fiber-Reinforced Concrete (Using Beam With Third-Point Loading)*. 2005.
15. Yang, E. H., Y. Yang, and V. C. Li. Use of high volumes of fly ash to improve ECC mechanical properties and material greenness. *ACI Materials Journal*, Vol. 104, No. 6,

2007, pp. 620–628.
16. Ma, H., S. Qian, Z. Zhang, Z. Lin, and V. C. Li. Tailoring Engineered Cementitious Composites with local ingredients. *Construction and Building Materials*, Vol. 101, 2015, pp. 584–595.
17. Sahmaran, M., M. Lachemi, K. M. A. Hossain, R. Ranade, and V. C. Li. Influence of aggregate type and size on ductility and mechanical properties of engineered cementitious composites. *ACI Materials Journal*, Vol. 106, No. 3, 2009, pp. 308–316.

UHPC Overlays on Concrete Bridge Decks

William Toledo[1], Ahmed Al-Basha[2], Craig M. Newtson[3], and Brad D. Weldon[4]

[1]GRA, Department of Civil Engineering, New Mexico State University
[2]Ph.D. Student, Department of Civil Engineering, New Mexico State University
[3]Professor, Department of Civil Engineering, New Mexico State University
[4]Associate Professor, Department of Civil Engineering, New Mexico State University

INTRODUCTION

A major problem in transportation infrastructure is degradation of concrete bridge decks because they are exposed to both weather and sources of wear. Degradation of bridge decks can expose steel reinforcement, disrupt rideability, and jeopardize skid resistance. Overlaying a concrete bridge deck with a new wearing surface is a common alternative to full-depth reconstruction of the deck. Common bridge deck overlay materials include asphalt concrete, latex-modified concrete, low-slump dense concrete, and polymer modified concrete. Each of these overlay materials have drawbacks associated with their use.

Ultra-high performance concrete (UHPC) is an attractive overlay alternative because of its durability and strength properties. The excellent durability of UHPC has the potential to improve the service life of an overlay as well as the underlying bridge deck. The objective of this study is to investigate the potential of using UHPC produced with local materials as an overlay material for existing concrete bridge decks.

To assess the potential of UHPC as an overlay material, the investigation must focus on the strength of the bond between the UHPC and the normal strength concrete (NSC) substrate. In a study, conducted by Harris et al. (2011), the bond strength of slant-shear specimens were tested using four different surface roughness values. The four surface roughnesses were smooth, low roughness, high roughness, and shear key. To quantify the degree of roughness ASTM 965-96 was implemented. The high roughness and shear key yielded greater bond strengths and produced failure in the substrate as expected (Harris et al. 2011). The high roughness was produced with transverse grooves measuring 5 mm (0.20 in.) in depth (Harris et al. 2011). Surface preparation was also emphasized in a study performed by Silfwerbrand and Paulsson (1998). In their study, methods to enhance the bonding of the substrate and overlay materials were analyzed. Sufficient bond was achieved when the substrate surface was textured and cleaned of any rubble (Silfwerbrand and Paulsson 1998).

METHODOLOGY

All of the UHPC for this research was produced with cement, fly ash, and aggregates local to central New Mexico. Silica fume, high-range water reducing admixture, and steel fibers were obtained from local suppliers since there were no local producers for these materials. Each batch of UHPC was tested for workability by conducting slump and spread tests for every batch. Following the workability tests, UHPC was cast into 100x100 mm (3.94x3.94 in.) cubes for compressive strength testing.

Effectiveness of an overlay depends primarily on the bond strength between the overlay material and the existing concrete deck, shrinkage of the overlay material, and cracking properties of the overlay material. Slant-shear, split cylinder, and split prism specimens that consisted of one-half UHPC and one-half NSC substrate material were produced to measure the bond strength between the UHPC and NSC. NSC with a water-to-cement ratio of 0.45 was used to form the substrate material. The substrate was stored in a wet room for 28 days and then textured using a handheld power grinder to a depth of 1-2 mm (.04 -.08 in.) to mimic surface preparation of concrete bridge decks. Bonding agents were not used because the nano-scale particles in the UHPC were expected to provide sufficient bond with the substrate concrete (Muñoz 2012).

Shrinkage of the UHPC overlay material is being assessed in both the fluid and solid states. Early-age shrinkage (fluid state to an age of seven days) was studied by measuring UHPC shrinkage in a 152x152x609 mm (6x6x24 in.) beam mold with two linearly variable displacement transducers (LVDTs). The LVDTs measured displacements of metal hangers embedded 25 mm (1 in.) into the UHPC as the specimen experienced shrinkage. Shrinkage of the specimen was recorded for seven days at 15 second increments.

Ongoing work includes longer term monitoring of shrinkage in prismatic UHPC specimens and larger scale testing of shrinkage and thermal gradient effects in NSC slabs with UHPC overlays.

FINDINGS

A UHPC mixture with a 28-day compressive strength of 17,220 psi (118.8 MPa) was used for the slant-shear, split cylinder, and split prism tests. Table 1 presents sample results from the slant-shear tests along with the shear stress and normal stress calculated at failure. Initial attempts at surface preparation by grinding resulted in over- and under-textured surfaces according to ASTM E965. Using ASTM E965 the under-textured surface had an average depth of 0.054 mm (0.2 in) and the over-textured surface had an averaged depth greater than 2 mm (0.08 in).

Table 3. Slant Shear test results.

Slant Shear Test Results						
Cylinder size	**Specimen**	**Force [lbf]**	**Strength [ksi]**	**Shear Stress [ksi]**	**Normal Stress [ksi]**	**Failure**
6 by 12 inch Over Textured	1	184900	6.54	2.83	1.64	Bond Failure
	2	206060	7.29	3.16	1.82	Substrate Failure
	3	166640	5.89	2.55	1.47	Bond Failure
	4	208690	7.38	3.2	1.85	Substrate Failure
	5	205890	7.28	3.15	1.82	Substrate Failure
	6	221400	7.83	3.39	1.96	Substrate Failure
6 by 12 inch Slightly Textured	1	84010	2.97	1.29	0.74	Bond Failure
	2	67530	2.39	1.03	0.60	Bond Failure
	3	88240	3.12	1.35	0.78	Bond Failure
	4	53530	1.89	0.82	0.47	Bond Failure
	5	93210	3.3	1.43	0.83	Bond Failure
	6	86860	3.07	1.33	0.77	Bond Failure

According to the American Concrete Institute's Guide for Selection of Materials for the Repair of Concrete, a 7-day bond shear strength must be greater than 6.9 MPa (1000 psi) to be acceptable. According to this criteria, even the under-textured specimens provided adequate bond strength.

Table 2 presents initial results from split prism tests. For this test, under-textured 102x102x76 mm (4x4x3 in.) prisms were tested. A minimum bond strength of 1.0 MPa (150 psi) is required at 7 days. Again, acceptable results were achieved with under-textured specimens.

Table 4. Split prism test results.

Split Prism Test Results				
Prism size	**Specimen**	**Force [lbf]**	**Strength [psi]**	**Failure**
4x4x3 in. Under Textured	1	4140	165	Bond Failure
	2	5790	230	Bond Failure
	3	6330	252	Bond Failure
	4	5460	217	Bond Failure
	5	4520	180	Bond Failure
	6	5730	228	Bond Failure

Figure 1 presents shrinkage results for a 6x6x24 inch (152x152x609 mm) UHPC beam specimen. Total shrinkage during the seven day test was nearly1800 microstrain. This strain level is consistent with other tests conducted on UHPC specimens (Allena 2010).

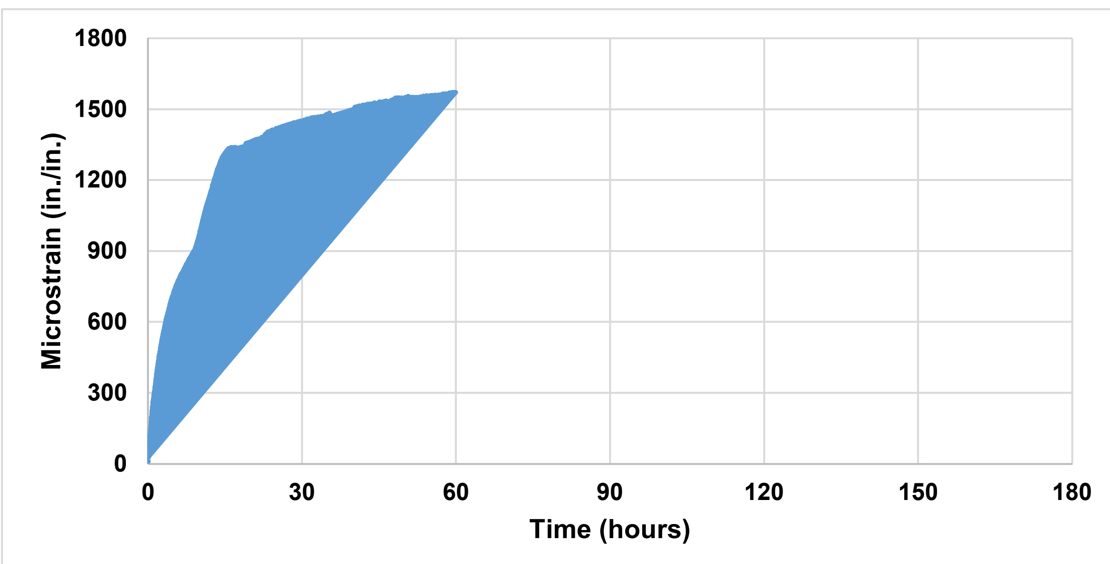

Figure 2. Early-age shrinkage results for UHPC.

CONCLUSION

Slant-shear and split prisms tests have shown that the bond strength of the UHPC overlay material and NSC substrate depend greatly on the surface preparation of the substrate. Bonding agents were not required to bond UHPC overlay to the substrate material because nano-scale particles in the UHPC provided sufficient bond for marginally textured surfaces as long as they were clean.

Early-age shrinkage testing has shown that the UHPC used in this study experienced less shrinkage in the first 24 hours than in previous research by Allena (2010), but had greater long-term shrinkage.

Surface preparation to ensure bond between the substrate and overlay material produced roughness depths that were less than and greater than the acceptable range of 1-2 mm (0.04 – 0.08 in). However, even the under-textured specimens produced adequate bond strength.

Based on the preliminary results of this study, UHPC appears to have the potential to be used as an overlay material as long it has proper workability and the substrate surface is adequately prepared.

REFERENCES

Allena, S. (2010). "Ultra-High Strength Concrete using Local Materials." Ph.D. dissertation, New Mexico State University.

Harris, D., Sarkar, J., and Ahlborn, T. (2011). "Characterization of Interface Bond of Ultra-High-Performance Concrete Bridge Deck Overlays." *Transportation Research Record: Journal of the Transportation Research Board*, 2240(2240), 40–49.

Muñoz, M. Á. C. (2012). "Compatibility of ultra high performance concrete as repair material : bond characterization with concrete under different loading scenarios." Michigan Technological University.

Silfwerbrand, J., and Paulsson, J. (1998). "Better Bonding of Bridge Deck Overlays." *The Swedish experience*, 56–61.

Characterizing and Understanding Self-Healing Microcapsules Embedded in Reinforced Concrete Structures Exposed to Corrosive Environments

Reece Goldsberry[1], Melvin McElwee[2], Jose Milla[3], Ahmad Ivan Karayan[4], Marwa Hassan[5], and Homero Castaneda[6]

[1]GRA, Department of Materials Science and Engineering, Texas A&M University
[2]GRA, Department of Construction Management, Louisiana State University
[3]Research Associate IV, Department of Construction Management, Louisiana State University
[4]Postdoctoral Researcher, Department of Materials Science and Engineering, Texas A&M University
[5]Professor, Department of Construction Management, Louisiana State University
[6]Associate Professor, Department of Materials Science and Engineering, Texas A&M University

INTRODUCTION

Steel reinforcement in concrete is generally in a passive state due to the surface oxide layer in a highly alkaline environment. However, such passive layer may be deteriorated by the ingress of aggressive agents (e.g., chlorides ions) and thus lead to the corrosion of the steel reinforcement. In order to minimize corrosion, researchers have proposed embedding microencapsulated corrosion inhibitors in concrete. Zuo et al. (2017) prepared polymer/metal hydroxide microcapsules that steadily released the encapsulated materials over time. Using calcium hydroxide and barium hydroxide as corrosion inhibitors, the results showed the microcapsules successfully delayed the decline on the pH values of concrete, thus decreasing the corrosion rate of rebar. Dong et al. (2014) prepared polystyrene microcapsules containing sodium monofluorophosphate. The results showed strong corrosion inhibition in a simulated concrete environment, measured with an Electrochemical impedance spectroscopy (EIS) technique. In this study, microencapsulated corrosion inhibitors embedded in concrete will be tested for their efficiency to mitigate corrosion in rebar and thus extend the durability of reinforced concrete structures. Two corrosion inhibition mechanisms are proposed, where (a) calcium nitrate microcapsules rupture during a cracking event and thereby release the core material; and (b) triethanolamine microcapsules that release the core material due to pH changes in the local environment. The compounds are reportedly known to retard the corrosion of steel, and will be encapsulated in polymeric shells and mixed into concrete at different concentrations (0.25%, 0.50%, and 2.00% by weight of cement).

METHODOLOGY

Microcapsule Preparation

The microencapsulation procedure for calcium nitrate was adapted from a previous study (Milla et al. 2017). The process is based on a water-in-oil suspension polymerization reaction of polyurea- formaldehyde. The suspension polymerization reaction was enabled by heating at an elevated temperature (40 °C) in the presence of an acid catalyst (sulfonic acid) for 2 hours. The sulfonic acid concentration used was of 0.25% by wt. of organic solvent. Once the microcapsules were synthesized, they were washed with a 1% sodium bicarbonate solution. The microcapsules were then recovered through a vacuum filtration. On the other hand, the encapsulation procedure for triethanolamine was adapted from Choi et al. (2012, 2013).

Concrete Mix Design

A water-cement ratio of 0.42 was selected through preliminary laboratory tests. The maximum aggregate size was 19 mm for the coarse aggregate, and 4.76 mm for the fine aggregate, respectively. The microcapsules were embedded at varying concentrations (0.25%, 0.50%, and 2.00%) by weight of cement to determine the minimal dosage required to mitigate corrosion considerably. A superplasticizer was added to increase workability to the concrete mix design. A defoaming agent was also introduced to counter the increases in air voids caused by the addition of microcapsules in concrete.

Concrete Testing

Concrete cylinders were made for compressive strength (ASTM C39), and surface resistivity tests (AASHTO TP 95), while concrete beams were made for corrosion testing (ASTM G109). The concrete samples were cast and cured in laboratory settings per ASTM C192 guidelines. A total of three 100 mm x 200 mm cylinders and three 150 mm x 150 mm x 280 mm beams were poured per specimen group. Table 1 shows characteristics of the specimens used in this study. Two control beams were included in the experimental matrix, since the calcium nitrate samples needed to be cracked to rupture the capsules and release the core material, while the triethanolamine samples do not require cracking to release the core material. All beam specimens associated with calcium nitrate were subjected to a 3-point loading system, where a slow strain rate (0.005 in/s) was applied until a crack was induced. The crack sizes induced ranged from 0.2 – 0.45 mm.

Table 1. Description of specimen groups.

Sample	Corrosion Inhibitor	Microcapsule Concentration
Control CN	Control for Calcium Nitrate	0.00 %
Control TEA	Control for Triethanolamine	0.00%
CN-0.25	Calcium Nitrate	0.25 %
CN-0.50	Calcium Nitrate	0.50 %
CN-2.00	Calcium Nitrate	2.00 %
TEA-0.25	Triethanolamine	0.25 %
TEA-0.50	Triethanolamine	0.50 %
TEA-2.00	Triethanolamine	2.00 %

Corrosion Characterization

This work presents the interfacial characterization of corrosion-inhibiting agents by exposing the concrete specimens to continuous ponding and wet/dry cycles. The corrosion tests for both exposures consist of electrochemical impedance spectroscopy (EIS), open circuit potential (OCP) and potential difference

The EIS was performed in the frequency range from 10k – 0.01 Hz with the amplitude of 10 mV. The traditional three-electrode configuration was used for EIS testing that consist of working electrode (anodic rebar), saturated calomel electrode (SCE) as the reference electrode, and platinum mesh wire as the counter electrode. The polarization resistance (Rp) from EIS was used to calculate the instantaneous corrosion rate. The OCP of anodic rebar was measured against

SCE. The voltage drops across a resistor of 100 Ω (potential difference measurement) was monitored allowing macrocell corrosion current between the top bar (anode) and bottom one (cathode) to be determined using Ohm's law.

For the continuous ponding, all the corrosion tests were performed every week for 85 days. However, in the first ten days, the measurement was taken every 2 days, In the wet/dry cycles, the ponding well was filled with a 3 wt.% NaCl solution and the specimens were alternately exposed to 2-week periods with solution then 2 weeks without solution. the corrosion testing was conducted at the beginning of the second week of ponding.

RESULTS

Concrete Testing

The compressive strength results indicate that for the calcium nitrate specimens, an increase in microcapsule concentration has a negative impact on strength, where the highest microcapsule concentration (2% by wt. of cement) resulted in an 18% strength reduction. Furthermore, the surface resistivity tests showed that the addition of microcapsules dropped the chloride permeability level from 'Low' to 'Moderate' for the tested mix design. The triethanolamine specimens are expected to be tested shortly.

A statistical test using Fisher's least squares difference (LSD) was used to determine if the addition of microcapsules had a significant effect on the compressive strength of concrete. The analysis shows that the control specimen group is significantly different from those samples admixed with microcapsules at 0.5% and 2.0%. Even though the defoaming agent was shown to improve dispersibility of the microcapsules in water, it is possible that with the defoamer concentration used it was still insufficient to adequately disperse the capsules throughout the concrete matrix. Thus, any clusters of microcapsules would weaken the cementitious matrix and increase the variability of the compressive strength considerably with respect to the control specimens.

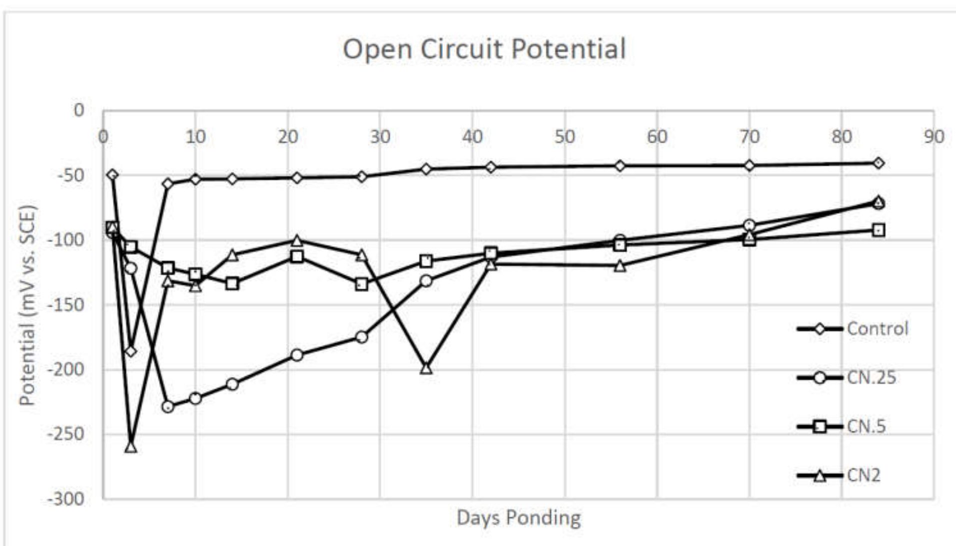

Figure 1. Open circuit potential measured for 85 days during the continuous ponding.

Corrosion Testing

The values of OCP measured for 85 days are presented in Figure 1. In general, all the samples show a corrosion activation in the first week of continuous ponding, as suggested by a sharp decrease in OCP in the first ten days. This phenomenon can be related to the chloride ingress through a diffusion that reached rebar. During this period, localized corrosion occured on rebar. However, since the continuous ponding does not result in a significant increase in the chloride accumulation on rebar, localized corrosion tends to cease, then repassivation occurs. This repassivation is evident by an increase in OCP in the noble direction from day 10 – 85. The highest activation was found on the CN2 (2% microcapsules). This is even higher than the control sample. This may suggest a high concentration of microcapsule is detrimental to corrosion resistance of rebar. Our wet/dry cycle testing is underway. In this wet/dry cycle testing, the triethanolamine samples were included.

CONCLUSIONS

The use of microcapsules containing calcium nitrate tetrahydrate as a corrosion inhibitor was explored in this study. The concentration of microcapsules added had a significant effect on the compressive strength of concrete when added at 0.5% and 2.0% by weight of cement, leading up to 18% strength reduction.

Surface resistivity tests also indicated that a slight increase in chloride penetrability was attributed to the addition of microcapsules.

From the OCP results, it is clear that there was a passivation-activation-repassivation process during the continuous ponding. The activation during the first ten days might be associated with the maximum chloride accumulation on rebar during this period. After ten days of ponding, the OCP increased significantly which indicated repassivation process. The highest magnitude of activation was found in the sample that had the highest microcapsule concentrations (2%).

REFERENCES

Zuo, J., Zhan, J., Dong, B., Luo, C., Qiuhong, L., Chen, D. (2017). “Preparation of metal hydroxide microcapsules and the effect on pH value of concrete”. *Construction and Building Materials*, 155, 323- 331.

Dong, B., Wang, Y., Ding, W., Li, S., Han, N., Xing, F., Lu, Y. (2014). “Electrochemical impedance study on steel corrosion in the simulated concrete system with a novel self-healing microcapsule”, *Construction and Building Materials,* 56, 1-6.

Milla, J, Hassan, M. M., Rupnow, T. (2017). Evaluation of Self-Healing Concrete with Microencapsulated Calcium Nitrate. *Journal of Materials in Civil Engineering,* 29 (12).

H. Jamil, A. Shriri, R. Boulif, M. Montemor, M. Ferreira, Corrosion behaviour of reinforcing steel exposed to an amino alcohol based corrosion inhibitor, Cement and Concrete Composites, 27 (2005) 671-678.

F. Tittarelli, G. Moriconi, The effect of silane-based hydrophobic admixture on corrosion of reinforcing steel in concrete, Cement and Concrete Research, 38 (2008) 1354-1357.

N.S. Berke, D.F. Shen, K.M. Sundberg, Comparison of the Linear Polarisation Resistance Technique to the Macrocell Corrosion Technique. , in: N.S. Berke, V. Chaker, D. Whiting (Eds.) Corrosion rates of Steel in Concrete, ASTM STP 1065, ASTM, Philadelphia, PA, 1990, pp. 38–51.

The Influence of Osmotic Pressure On the Deformation of Concrete Exposed to Sulfate Solution

Syeda F. Rahman[1] and Zachary C. Grasley[2]

[1]Postdoctoral fellow, The University of Texas at Austin
[2]Professor, Texas A&M University

INTRODUCTION

According to the nation's existing highway and transit condition and performance report published by the Federal Highway Administration (FHWA), over $35 billion was spent in 2012 in replacing and rehabilitating the existing pavements and bridges [1]. Even though the concrete structures are built conforming the building codes and recommendations, much of the rehabilitation is due to the material deterioration exposed to aggressive environments. Sulfate attack is known to be the most widespread form of chemical degradation of concrete that appears in regions where concrete is exposed to soil or water containing sulfates. External sulfate attack, due to its complicated nature, has led to numerous researches, both experimental and theoretical, Experimental determination of concrete susceptibility to sulfate attack involves long term immersion of concrete specimens in sulfate solution. While these tests that require months to perform, manifest damage in the form of large expansion, field investigations indicate evidence of high stresses at surface leading to cracks or softening and disintegration of the cement matrix. Moreover, the alternative recommended accelerated tests do not mimic the field conditions. Based on the previously performed experimental studies, the current design code prescribes a maximum allowable limit for the tricalcium aluminate phase in cement to mitigate the problem. This limit prohibits practitioners from using local raw materials and researchers from engineering binders with broad chemical and physical properties. Little data are available for modern materials for which increasing substitution of cement is utilized to reduce energy consumption and environmental emission. In addition, the mechanism and distress type caused by different sulfate solutions containing Na, Mg, Ca, K, and Fe are not fully known. For example, cement with low tricalcium aluminate, as prescribed by the design code to withstand damage caused by the sodium sulfate solution, may prove detrimental when exposed to magnesium sulfate or sulfuric acid [2].

Due to the complex nature of sulfate attack and varied effects caused by different sulfate bearing solutions, several models were developed in the past focusing on the volumetric expansion of concrete [3], crystallization pressure generated by the crystal growth in the pore network [4], and poroelastic damage based on the reactive diffusion model [5]. However, none of these models account for the osmotic suction caused by the gradient in the solute concentration in the pore solution. Therefore, the objective of this paper is to assess the effect of osmotic suction on the stress and strains developed in concrete exposed to sulfate solution.

The osmotic suction can be defined as the difference in pressures exerted by solutes on either side of a semi permeable membrane due to spatial gradient in the solute concentration [6]. While, osmotic suction is recognized to initiate damage in organic coatings on concrete substrates in the form of delamination, folding, and blisters [7], its effect on the deformation of concrete structures subject to sulfate solution is not known. In order to determine the effect of osmotic suction on concrete deformation, the proposed work utilizes poroelasticity [8] to develop a coupled linear elastic model that accounts for the difference in pore pressure driven by the spatial gradient in solute concentration. A cylindrical concrete specimen saturated with pure water is assumed to subject to sulfate solution of a given concentration. It is assumed that the diffusion of solute in the pore solution is much slower than the advection of water molecules so that there is no expansive agent formed in the pore network. The model shows that high tensile stresses can be exerted at the concrete boundary due to the spatial gradient in the sulfate concentration across the radial position. It is believed that such a mechanistic model incorporating the effect of the osmotic suction in concrete deformation will allow engineers to understand the underlying mechanism dictating the damage evolution process by short term sulfate exposure, where the sulfate ions have not diffused through the pore network to react with the hydrated products and precipitate as expansive agents.

METHODOLOGY

For modeling purpose, it is assumed that a cylindrical concrete specimen, completely saturated with pure water, is immersed in a sulfate solution bath with known solute concentration. The pore pressure at the boundary is calculated from the water activity of the solution bath. As we are focusing on osmotic effects, the concrete specimen is approximated to transport solvent more rapidly than the solute. For simplicity, we thus consider transport of solvent only.

The governing equations associated with the mass balance and linear momentum balance for an elastic porous material are used. In absence of inertia and body forces, the conservation of linear momentum provides

$$\mathrm{div}\underline{\underline{T}} = 0, \tag{1}$$

where $\underline{\underline{T}}$ represents the externally applied total Cauchy stress tensor and is expressed (for a linearly isotropic material) as

$$\underline{\underline{T}} = 2G\left[\underline{\underline{\varepsilon}} + \frac{\nu}{1-2\nu}\mathrm{tr}\left(\underline{\underline{\varepsilon}}\right)\underline{\underline{I}}\right] - 3K\varepsilon_f\,\underline{\underline{I}}\ . \tag{2}$$

Here, $\underline{\underline{\varepsilon}}$ is the infinitesimal strain tensor, G is the shear modulus of the porous body, K is the bulk modulus of the porous body, ν is the Poisson's ratio of the porous body, and $\underline{\underline{I}}$ is the identity tensor. For a poroelastic material with invariant porosity upon pressurization, the free strain ε_f can be denoted as

$$\varepsilon_f = \frac{b\,p^L}{3K}\ , \tag{3}$$

where

$$b = 1 - \frac{K}{K_s}, \tag{4}$$

is Biot's coefficient and K_s is the bulk modulus of the solid phase comprising the skeleton of the porous body. The liquid pressure, p^L, can be determined using the mass balance equation,

$$\frac{1}{\rho^L}\frac{dm_w}{dt} = \frac{k}{\eta^L}\mathrm{div}(\mathrm{grad}p^L), \tag{5}$$

where ρ^L is the undeformed density of the liquid phase, k is the intrinsic permeability with dimensions of length squared, η^L is the viscosity of the pore liquid, and m_w stands for the total mass of water per unit initial volume of the porous material. The simulated specimen is immersed in the solution bath at stress free condition. The boundary pressure is determined using the following expression

$$p^L_{osmotic} = -\rho^L \frac{R\theta}{M^L} \ln\left(a^L\right), \quad (6)$$

obtained from [6]. Here, R is the universal gas constant, θ is the temperature, M^L is the molar mass of the solvent water, and a^L is the activity coefficient of the solvent water. Coupled equations (1) and (5) are solved simultaneously using the NDSolve function in *Mathematica* to determine the unknowns, $\underline{\underline{T}}$ and p^L.

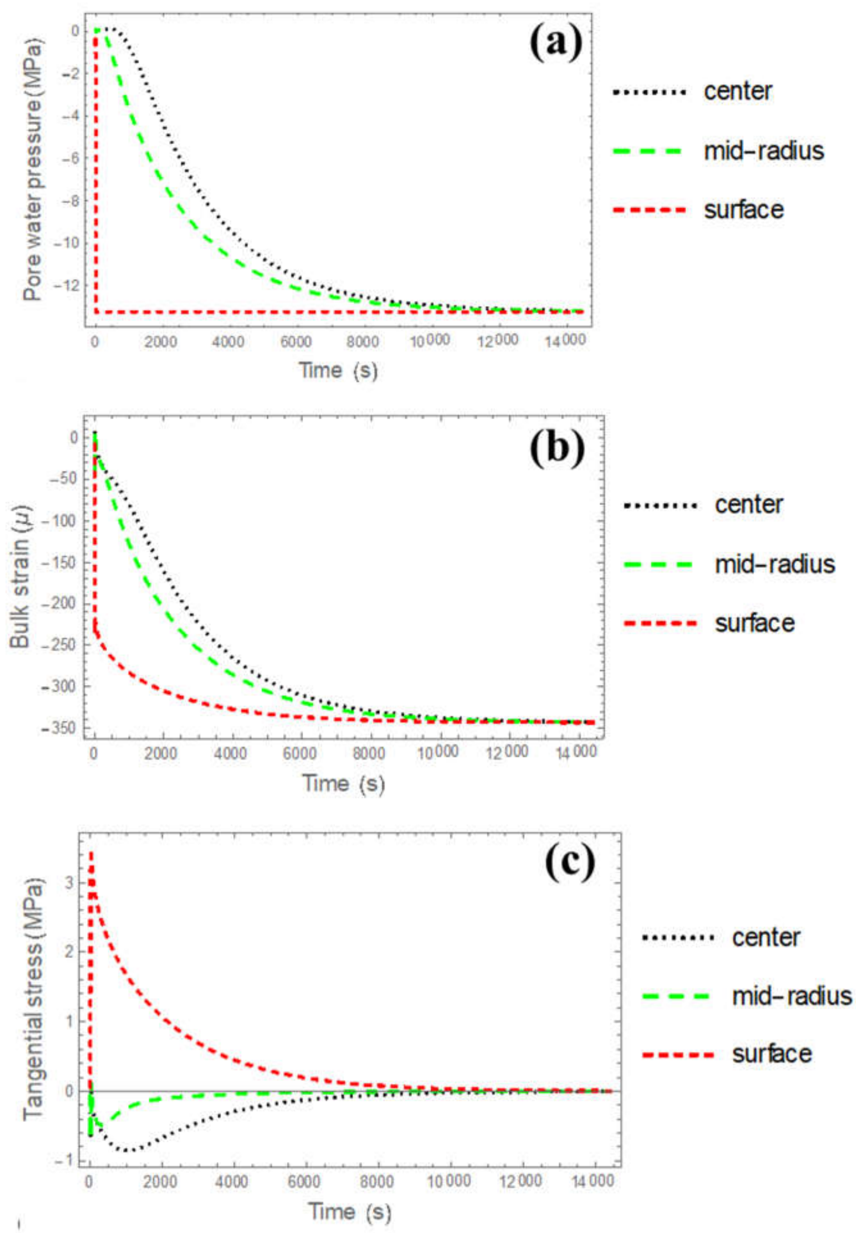

Figure 1 (a) Osmotic pore pressure, (b) bulk strain, and (c) tangential stress developed in a cylindrical concrete specimen exposed to 6% Na_2SO_4 solution

FINDINGS

The simulated pore pressure, bulk strain, tangential stresses for a 6 in diameter cylinder are plotted in Figure 1. The following materials properties are assumed:, $k = 1\times10^{-19}\,\mathrm{m}^2$, $K_s = 25.4\times10^3\,\mathrm{MPa}$, and $K = 11.1\,\mathrm{GPa}$ with a porosity of 0.2. The concrete specimen is assumed to be immersed in 3 mol/kg Na_2SO_4 solution. The corresponding water activity coefficient is obtained to be 0.9 [9], which according to equation (6), gives the boundary pressure of $-13.24\,\mathrm{MPa}$. As the specimen contains no solute in the pore solution, a sudden exposure to the solution creates spatial gradient in the solute concentration. As a result, high osmotic suction is developed at the boundary, which draws solvent molecules (water) from the specimen center to surface. Since concrete is a weakly permeable material, water takes a long time to drain to the surface to equilibrate with the boundary pressure (Figure 1 (a)). As a result, the boundary contracts more than the center that exhibits higher pressure than the surface (Figure 1 (b)). This differential strain across the radial direction develops instantaneous high tensile tangential stresses at the boundary as shown in Figure 1 (c). This high stress has a potential to create micro-cracks at the concrete surface, which may exacerbate the problem when the expansive agents are precipitated in the pore network accompanied by the diffusion of sulfate ions and may lead to peeling or flaking of materials.

CONCLUSION

It is found that differential strain caused by high pressure gradient can exert instantaneous tensile tangential stress at the concrete boundary when it is exposed to sulfate solution. This pressure gradient can be attributed to osmotic suction caused by the spatial gradient in solute concentration, which draws liquid water from low solute concentration to high solute concentration. As a result, a high differential in the volumetric strain can be observed, which in turn can cause tensile tangential stress at the material surface. When this tensile stress exceeds the tensile strength of the material, it can create spalling or flaking at the surface.

In light of the simulated results, it is expected that the osmotic suction plays an important role in the deformation of concrete exposed to sulfate solution, and needs to be incorporated in the diffusion-binding-mechanical model to accurately predict concrete deformation and damage potential. The present work captures the short term advection of the solvent only and does not include the diffusion of solutes and the subsequent reaction with the hydrated product and crystallization. It is believed that the incorporation of osmotic pressure in a coupled chemo-poro-mechanical model will help engineers understand the mechanism of concrete deformation (both expansion due to crystallization and spalling at the surface) exposed to sulfate solution.

REFERENCES

1. *2015 Status of the Nation's Highways, Bridges, and Transit: Conditions & Performance*. 1/30/2017]; Available from: https://www.fhwa.dot.gov/policy/2015cpr/es.cfm#6h.
2. Santhanam, M., M.D. Cohen, and J. Olek, *Sulfate attack research — whither now?* Cement and Concrete Research, 2001. **31**(6): p. 845-851.
3. Tixier, R. and B. Mobasher, *Modeling of Damage in Cement-Based Materials Subjected to External Sulfate Attack. I: Formulation.* Journal of Materials in Civil Engineering, 2003. **15**(4): p. 305-313.

4. Bary, B., *Simplified coupled chemo-mechanical modeling of cement pastes behavior subjected to combined leaching and external sulfate attack.* International Journal for Numerical and Analytical Methods in Geomechanics, 2008. **32**(14): p. 1791-1816.
5. Cefis, N. and C. Comi, *Chemo-mechanical modelling of the external sulfate attack in concrete.* Cement and Concrete Research, 2017. **93**: p. 57-70.
6. Grasley, Z.C. and K.R. Rajagopal, *Revisiting total, matric, and osmotic suction in partially saturated geomaterials.* Zeitschrift für angewandte Mathematik und Physik, 2011. **63**(2): p. 373-394.
7. Günter, M. and H.K. Hilsdorf, *Stresses Due to Physical and Chemical Actions in Polymer Coatings on a Concrete Substrate*, in *Adhesion between polymers and concrete / Adhésion entre polymères et béton: Bonding · Protection · Repair / Revêtement · Protection · Réparation*, H.R. Sasse, Editor. 1986, Springer US: Boston, MA. p. 8-21.
8. Biot, M.A., *Theory of Propagation of Elastic Waves in a Fluid-Saturated Porous Solid. I. Low-Frequency Range.* Journal of the Acoustical Society of America, 1956. **28**(2): p. 168-178.
9. Guendouzi, M.E., A. Mounir, and A. Dinane, *Water activity, osmotic and activity coefficients of aqueous solutions of Li2SO4, Na2SO4, K2SO4, (NH4)2SO4, MgSO4, MnSO4, NiSO4, CuSO4, and ZnSO4 at T=298.15K.* The Journal of Chemical Thermodynamics, 2003. **35**(2): p. 209-220.